Environmental creep mechanisms in glass/polyester composites.

White, Roger John

Award date:
1985

Awarding institution:
University of Bath

ENVIRONMENTAL CREEP MECHANISMS IN GLASS/POLYESTER COMPOSITES

Submitted by

Roger John White

For the degree of Ph. D.
of the University of Bath

RJ White

R.J. WHITE

MAY 1985

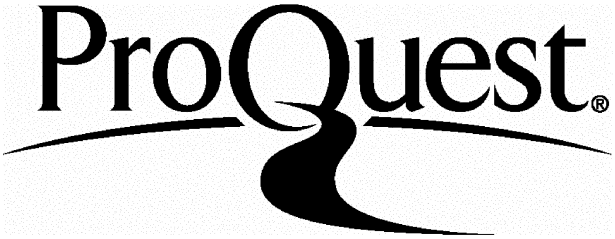

ABSTRACT

A previous study, looking at the creep-rupture behaviour of mixed reinforcement GRP when immersed in water, had discovered that at low loads, behaviour became temperature sensitive. Since the recorded time to failure of a sample was reduced at elevated temperatures, from that predicted by a linear extrapolation of the short term creep-rupture results, this deviation caused problems in the accurate prediction of long-term design stresses. In order to improve the accuracy of long term design predictions, it was decided to study the mechanisms of creep in GRP that initiates time dependent failure. From this, it was hoped that accurate design criteria suitable for predicting GRP response over a 30 year design life from short term creep tests, could be developed. This thesis reports the results obtained from such a study.

A series of creep tests were performed on mixed reinforcement GRP samples at several stress levels, both in air, and in room temperature distilled water, using a microcomputer based data collection system. In conjunction with this work, damage development in samples,due to combinations of water uptake and creep loading, was followed, using both scanning electron, and optical, microscopy. Moisture uptake measurements were undertaken under a series of load/temperature regimes, and fibre/matrix debonding followed using photographic techniques. In this way, water absorption, both in terms of uptake rate, and location within a sample, could be characterised. Tensile tests were also performed to determine the standard mechanical properties of the mixed reinforcement GRP used.

It was found that a critical damage state was created at loads in excess of 50% of ultimate, but not below. This took the form of between 2 and 8 neighbouring filament breaks in the longitudinal woven rovings at weave cross-over points, producing microcracks in the reinforcement. The creation of this multi-filament fracture damage during primary creep,was considered to be necessary for time dependent failure to occur in air. Secondary creep strain was found to increase in discrete steps, both in air and water. This was attributed to the formation of transverse cracks in the longitudinal woven

rovings, propogating from the above critical damage.

In water, diffusion was found to be non-Fickian. Moisture uptake increased with increases in applied load and temperature. Water was seen to accumulate at weave cross-over points when immersed under load. This led to stress-enhanced fibre corrosion in these regions, weakening the reinforcement, and reducing the failure time from that expected at the same load level in air. The localised nature of moisture degradation was thought to result in the formation of critical fibre damage at loads below 50% of ultimate, when immersed in water.

Two design criteria based on the observed creep mechanisms, have been developed for GRP that predict response when loaded in either air, or water. Both predict the existence of creep-rupture limits at low loads.

ACKNOWLEDGEMENTS

The author would like to thank the following people for their help and assistance in producing this thesis:-

Mr.M.G. Phillips, for his supervision and guidance throughout the project.

The Polymer Engineering Directorate, for funding the project.

Mr. S. Bowman, for designing and building the strain monitor used.

The CEGB, Scientific Services, Bedminster Down, Bristol, for the use of data and samples taken from programmes funded by them.

Scott Bader Ltd., for kindly supplying the resins used.

The Department of Metallurgy and Materials Science, University of Liverpool, for kindly supplying the creep-monitor software adapted for use in this work.

The Science and Engineering Research Council, for use of the scanning electron microscopes funded by them.

The technicians in the School of Materials Science for their general support.

Mrs. S. Wood, for typing this thesis.

Wendy, for proof reading the draught thesis, and general moral support.

Mum and Dad, without whose assistance over the last 7 years, this thesis would not have been possible.

INDEX

PART ONE

LITERATURE REVIEW

CHAPTER 1

INTRODUCTION

Glass fibre reinforced plastics have been in existence for several decades, their earliest commercial application being the manufacture of aircraft radomes in the last war (1). From this highly specialised application, many other applications for this material have been developed. The first G.R.P. boats were produced in 1946 from fine woven glass fabrics in a polyester matrix. With the introduction of chopped strand mat in 1947, many previously prohibitively expensive applications became viable. By 1949, translucent GRP panels were introduced to the building industry, and by the mid 1950s, some car body panels and lorry cabs were being made from reinforced plastics. Mild steel was replaced in these cases because of the superior corrosion resistance of GRP.

A very important industrial application for GRP is in the transport and storage of corrosive liquids. Reinforced plastic piping has been used by the chemical industry for several years, as a replacement for the expensive grades of stainless steel previously used. The electricity generation industry is also now looking at the advantages of using GRP in cooling water systems. The CEGB has several coastal power stations where sea water is used as the coolant. Operating temperatures for these circuits are of the order of 40°C, causing highly corrosive conditions within steel piping, valves, water boxes etc., even when top grade stainless steels are selected for the job. As a result, plant shutdowns are fairly frequent, pushing up production costs. By replacing steel with GRP, cost reductions due to the lower maintenance required, would be achieved. Considerable effort has recently been expended on developing practical replacement systems (2).

The major problem to overcome in the above case, is the ability to accurately predict how GRP components will behave throughout the required design life. For metallic systems, years of experience have developed the understanding of their long term properties, simplifying design criteria. Similar levels of understanding have now to be developed in the field of reinforced plastics, before their full potential can be realised.

When GRP is used in areas where it can come into contact with an aggressive environment (e.g. hot, salt water) , knowledge is required as to how the mechanical properties of a component will be affected, particularly when under a constant stress. In applications where a constant load will be applied to the GRP, the time dependent nature of its properties will also have to be taken into account. If this is not done, problems may be encountered due to creep, whereby samples fail at sub-critical loads after a given length of time. Thus, a stress level well below the components' strength may be safely applied during short term tests, but failure may still occur during the required design life.

As a consequence of the time dependent properties of GRP, long term design predictions as to failure times at a given load level, have to be made. Several techniques are currently employed, taken mainly from the field of metallic creep testing. However, since little is known about the mechanisms of GRP creep, and how these are affected by the presence of an aggressive environment, all the models used are at best semi-empirical, or at worst pure guesswork. As a result, either serious errors occur in design predictions, or more commonly, large safety factors have to be used. This leads to dramatic over design of components, and subsequent reduction in cost benefit when changing from metallic to reinforced plastic materials.

In order to improve the current situation, attention must be focussed on the damage development within GRP bodies when under static loads, and how an aqueous environment accentuates the observed degradation. Only then can satisfactory design models for GRP components be produced. This thesis describes a programme of work established to achieve these stated aims.

1.1 Background to current work

In the past few years, since 1979, a considerable amount of research at Bath University School of Materials Science has been undertaken on the tensile creep-rupture of polyester/glass laminates in an aqueous environment. This has been funded, in the main, by the South West Regional Headquarters of the CEGB, based at Bedminster Down, Bristol, the support being provided in two ways:-

(i) A 3 year test programme, undertaken by South West Industrial Research Ltd. (SWIRL) at the university. This was designed to provide data on CEGB specified laminates exposed to a variety of loads, environments, temperatures, and matrix formulations (3, 4).

(ii) An SERC Case award studentship looking at the tensile creep-rupture behaviour of chopped strand mat/polyester laminates in a variety of environments (5).

Other work looking at the stress-rupture behaviour of woven roving/polyester laminates in water has also been recently undertaken (6).

Results obtained from the SWIRL contract (figure 1.1), showed a down turn in time to failure at low loads and elevated temperatures. This made the stated aim, of extrapolating data from a short term test programme to predict the maximum applied load for a 30 year design life,

impracticable. In order to discover the origin of this change in behaviour, the current studentship was set up to examine the mechanisms of creep in such laminates that initiated rupture. From this, environmental damage mechanisms could be identified, and the creep-rupture behaviour explained and modelled. Finally, a design prediction test routine, based on a knowledge of the creep mechanisms operating, was to be developed.

1.2 Summary of current programme

To achieve the requirements placed on this research programme initially, a whole series of tests have been undertaken. Firstly, GRP laminate sheets were produced, and the mechanical properties determined (e.g. strength, strain to failure). Having done this, the effect of immersion in water on the short term properties were investigated by such methods as residual strength tests (soaking prior to a tensile test), moisture uptake measurements, polished section microscopy (determine moisture induced damage levels), and detailed transmitted light photography (to study debonding etc).

In conjunction with this work, creep strain was measured in samples loaded to a variety of levels, in air and distilled water, to determine the mechanisms of creep, and the influence of the environment. Detailed fractography and studies of fibres exposed after resin burn-offs were also undertaken, to look for damage mechanisms that would tie in with the observed creep response.

When all these tests had been undertaken an overall picture of the environmental creep response of the GRP laminates used was obtained. From this a means of predicting long term design data for samples, loaded in air and room temperature water, has been developed.

CHAPTER 2

GLASS FIBRES

2.1 The structure of glass

Glasses are a class of inorganic materials whose physical state is intermediate between that of a solid and a liquid (7). Unlike true solids, glasses are non-crystalline (vitreous). However, they differ from super-cooled liquids in exhibiting short range atomic order producing a 'random network' structure. This is a non-equilibrium state, and after long periods of time, glasses will crystallise (devitrify).

Glasses are produced from a melt comprising 'glass former'oxides (SiO_2, B_2O_3,P_2O_5), and 'glass modifiers' (Na_2O,K_2O,CaO). Glass formers enter into a four-fold tetrahedral co-ordination with oxygen, producing strong bonds due to the high ionic potential. Glass, or network, modifiers have a relatively low ionic potential, and the most common elements used in glasses are sodium, potassium, and calcium (8). A third class of oxides, the 'intermediates', are also used in glass formation. These oxides, usually alumina and beryllia, are not capable of network formation, but they can join an existing network and alter its properties. The discussion of glasses will be restricted to the silicates, since these are the most common glasses used to produce continuous fibres.

The basic structural unit of these glasses is a small silicon cation covalently bonded to 4 large oxygen anions in a tetrahedral configuration. In the glassy state, these tetrahedra form an irregular three dimensional array by sharing corner oxygen atoms (figure 2.1(a)). Glass modifiers are held interstitially in the network by ionic type bonds. Additional oxygen atoms are introduced into the network, breaking bonds, and lowering the network strength (figure 2.1(b)). Incorporation of glass modifiers into

the network allow the mechanical properties of a fibre to be tailored to its end use requirements. Further property changes can be introduced by the addition of intermediate oxides to the network, replacing silica groups (figure 2.1(c)).

Some of the most common glasses used in fibre production are shown in table 2.1, taken from Hull (9). E-glass is the most commonly used for fibres in resin matrix composites. It is a low alkali glass possessing good strength, stiffness, drawability, electrical and weathering properties (2.6). C-glass has superior chemical resistance over E-glass, but it has lower mechanical properties and is more expensive. S-glass is again more expensive, but does have greater stiffness and temperature resistance than E-glass. These property variations stem directly from compositional changes within the broad spectrum of silicate glasses.

2.2 Manufacture of glass fibres

It is of some relevance to the current work as to how reinforcement fibres are produced. As a consequence, a brief survey of the major production route for continuous E-glass filaments will be presented in this section.

Doyle (10) outlines several production routes for glass fibre manufacture, but only the commonest method will be discussed. Firstly, high quality E-glass melts are produced, either by melting glass marble, or directly from raw materials in an integrated plant. Maximum temperatures to achieve melting are of the order of 1600°C. The process is shown schematically in figure 2.2.

From the melter, the glass passes into a forehearth heated to 1350°C. The furnace end of the forehearth conditions the glass to a working temperature around 1250°C, whilst the end section acts as a channel for glass flow into the bushings. These contain a multiplicity of platinum rimmed

nozzles, through which the molten glass falls under gravity, forming a drop. This solidifies then falls away, leaving a filament attached to each bush via a molten glass meniscus.

These fibres pass through a water spray to cool and lubricate them (11), are then size treated to provide a surface coating comprising, of a lubricant, coupling agent and barrier layer to reduce abrasion damage during subsequent processing. Drawn filaments are collected as rovings on a rotating drum, whose speed is selected to optimise the fibre drawing rate. The resultant drum of continuous fibre, called a 'cake', is then heat treated to cure the size coat and volatilise the lubricant applied, before being processed into sheets of glass reinforcement.

It will be seen later that the original fibre production route can produce variability in fibre strength, as well as altering the resistance of a laminate to environmental degradation due to inadequate coupling agent coating, water spray induced surface cracking etc.

2.3 Glass fibre reinforcement categories

Drums of fine (10μm) continuous glass filament rovings are of little use for the production of glass reinforced composites. They have to be processed into forms that can be easily handled. Over the years, techniques borrowed from the textile and paper industries have been adapted to solve this problem. Many different types of reinforcement are now produced, but they can be grouped under three main headings, as defined by Piggott (12).

(i) Chopped strand mats

(ii) Woven roving

(iii) Tapes.

2.3.1 Chopped strand mat (CSM)

The production route for these materials has been adapted from techniques used in the paper industry. Continuous rovings are chopped into short lengths (3-50mm), and allowed to settle on a continuously moving belt to form a mat, held together by a bonding emulsion. This is a highly inefficient reinforcement due to the random fibre orientation, which suppresses the maximum volume fraction of glass possible in a laminate, to around 40%. They are, however, fairly isotropic, and easy to fabricate by hand lay up, and have become widely used where high strength is not a requirement (e.g. small boat hulls).

2.3.2 Woven roving (w.r)

Continuous glass rovings can be woven to produce glass fabrics, using ordinary textile looms. Rovings can be twisted into yarn prior to weaving, but it is more usual to simply weave the rovings in their 'as supplied' state. Glass cloth is usually produced so as the fibres are in a $0/90^{\circ}$ configuration. In general, fabrics have a higher degree of anisotropy than csm, giving higher strength in the roving directions. Weave induced crimp ('waviness'), produces high elongations under load due to fibre straightening, so these laminates are of fairly low modulus. Fabrics are easy to handle, but when moulding complex shapes they are found not to 'drape' over the mould very successfully. Changing the fabric configuration can improve this property, but often at the expense of mechanical properties. Structure/property relationships in woven fabrics will be discussed later in this review (2.5).

2.3.3 Tapes

Unidirectional roving tapes are also produced for use in high strength aerospace applications. Rovings are laid on a backing paper and bonded with a partially cured resin, to produce a 'pre-preg'. These can then be

laid up in the required stacking sequence and hot pressed, to cure the resin. These materials are highly anisotropic, but high volume fractions of glass can be achieved (70%), and high strength and stiffness can be produced in the fibre directions.

In this work, only csm and woven roving reinforcements were used, so all future references to the reinforcement structure will concentrate on these two, in particular woven fabrics.

2.4 Strength of glass fibres

At room temperature, glass behaves as an ideal Hookean solid when in the pure state (i.e. silica glass). However, the addition of network modifiers can alter the detailed mechanical response, and E-glass fibres can exhibit room temperature creep and delayed failure over very long times, as described by Ernsberger (13). As was previously mentioned, the strength and modulus of an unflawed fibre depends largely on the three dimensional oxide network. As a result, the filament properties are found to be isotropic.

For commercial E-glass fibres, the tensile strength measured is a function of the processing conditions and test environment (2.6). To a very good first order approximation, strength can be regarded as a measure of the surface weakness. The classic study on the brittle fracture of glass was undertaken by Griffith, and a good summary of this work is presented by Lawn and Willshaw (14). By testing freshly drawn fibres, it was found that the observed strength approached the theoretical maximum (10GPa). On leaving fibres in the air for several hours prior to testing, strength falls from 3.5GPa to 1GPa, a level normally found when testing fibres. It was also found that by reducing the fibre diameter, strength increased. Strength was controlled by the size of the largest surface flaw present, which creates a stress concentration from which fracture initiates. These flaws grow through atmospheric moisture degradation. Reducing fibre diameter decreases the

probability of finding a severe flaw, thus increasing the strength. Oka et al (15) show that moisture induced flaw growth can only be prevented by storing fibres under vacuum.

Another source of damage in commercially produced E-glass fibres is mechanical abrasion, unavoidable during processing, particularly where glass/glass contact occurs (e.g. weaving). This surface scratching makes it impossible to ensure that the filament strength variation is minimal within a roving. A further problem in assessing surface damage is the random spread, and small size (in the region of 0.3μm), of critical flaws, making their detection in even the most advanced electron microscopes impossible. This will be further discussed in Part III.

To minimise mechanical damage, a size coat is applied to the fibre on drawing (2.2), to protect and lubricate it. To get some idea of the strength variability within rovings, figure 2.3, taken from Proctor (16), shows some typical experimental data. A comprehensive review of the sources of weakness in glass fibres has been compiled by Gurney (17).

2.5 Woven glass fabrics

While describing the properties of glass fibres, some attention should be paid to the effect of using woven, rather than straight (continuous or chopped), filament rovings. Zweben et al (18) state that fabrics have similar properties to orthogonal plied laminates, though maximum glass content in composites is lower, reducing the reinforcement efficiency. Fibre crimp (degree of bending) has also been shown to affect properties, as will be described later in this section.

Many different fabric constructions have been developed, each possessing specific properties suited to various applications. The most commonly used fabric is known as a plain weave. Since this thesis used these fabrics, the section will concentrate on these, merely mentioning some of the others available. In plain weave fabrics, each warp

(longitudinal), passes over one weft (transverse), roving, then under its neighbour, and so on (figure 2.4(a)). This can be compared to the situation in twill (figure 2.4(b)), and satin (figure 2.4(c)), weave fabrics.

The reinforcement used in this thesis was a balanced fabric, i.e. weight of warp filaments equals the weight of transverse fibres present . Plain weave reinforcements are probably the most inefficient form of fabric available. The high degree of crimp means that delamination due to fibre straightening is maximised, and the largest possible volume fraction in a resin matrix, is reduced. Finally, where complex mouldings are required, the poor drape characteristics of plain weave fabrics precludes their use. However, they are very stable (resistant to distortion), and less susceptible to fabric 'skewing' (fabre misalignment) on lay up, than other configurations. This can lead to warping and changes in stress state within fabric reinforced laminates. A good review on the effects of fabric construction on composite properties is given by Haythornwaite (19).

As a result of fibre crimp, the stress distribution along a load bearing woven filament is non uniform (cf. unidirectional fibres). Local regions of high stress are created on the outer roving surfaces of weave cross-overs. Similarily, at the mid point between cross-overs, and at the interior of such features, tensile stresses are at a minimum. Attempts to provide analytical models of the stress fields in a fabric have been presented by Ishikawa and Chou (20).

The non-uniform nature of fibre stresses in woven roving laminates is a crucial factor in the creep-rupture of the glass/polyester laminate systems tested in this thesis, and further discussion of this property will be presented in Part III. At this stage it is sufficient merely to highlight the differences in reinforcement characteristics that occur when woven rovings, as opposed to bi-directional continuous filaments, are used in composites. Some of the common terminology of fabric reinforcement,

borrowed from the textile industry, has also been outlined for future reference.

2.6 Environmental effects in glass fibres

When ordinary glass is brought into contact with moisture, Paul (21) states that alkali ions are extracted into the solution in preference to the more tightly bound silica, forming an alkali deficient surface layer, whose thickness depends on the glass composition. This forms a barrier layer to further leaching, reducing the reaction rate. Charles (22) describes this leaching in terms of three reactions:-

(i) Addition of a proton to the network

$$\equiv Si - OR + H_2O \rightleftharpoons \equiv Si - OH + R^+ + OH^- \qquad -(2.1)$$

(ii) Disruption of siloxane bonds by hydroxyl ions in solution

$$\equiv Si - O - Si \equiv + OH^- \rightleftharpoons \equiv Si - OH + \equiv Si - O^- \qquad -(2.2)$$

(iii) Non-bridging oxygen atoms interact with water, releasing a hydroxyl ion

$$\equiv Si - O^- + H_2O \rightleftharpoons \equiv Si - OH + OH^- \qquad -(2.3)$$

Proctor (23) studied the long term behaviour of glass fibres in a range of environments, identifying two distinct exposure regimes:

(i) Exposure in an unstressed state (ageing), where degradation is monitored in terms of strength loss as a function of immersion time.

(ii) Exposure at a stress level below the fibre strength until failure occurs (static fatigue). In this regime, corrosion may be accelerated, or even initiated, by the applied stress, fibre dissolution being stress dependent.

The latter regime is of most relevance to the environmental creep of GRP, but some consideration must be given to fibre ageing characteristics before static fatigue is examined (2.7)

Proctor (23) found that slight strength loss occurred after ageing E-glass fibres in water at 50°C for 30 days, though it is not clear whether coated fibres were used. The slow rate of corrosion in E-glass can be attributed to the low sodium and potassium content of these fibres. Calcium extraction is more difficult, due to its large ionic radius.

Lyons (5) presents a comprehensive review of the literature on E-glass corrosion effects, some of which are summarised below:-

(i) Fibres tested in dry nitrogen were 17% stronger than those tested in moist air.

(ii) Moist fibres when dried and tested showed an increase in strength, showing the reversible nature of humidity induced weakening.

(iii) Fibres aged in distilled water, gave a 35% strength loss after 35 weeks, that was non-reversible. This demonstrates the difference between a humid, and aqueous, environment.

(iv) Fibre strength in moist air was strain rate dependent; the higher the rate, the greater was the observed strength. At fast test rates, fibre weakening due to corrosion assisted crack growth was minimal, whereas at slow speeds, considerable environmental flaw growth could occur during the test.

(v) Fibres stored in water show surface leaching damage in the form of pits. Due to the low concentration of alkali ions in the E-glass network, there is not a uniform spread of ions throughout the network. Instead, sodium and potassium occurs in high local concentration pockets within the network. Thus, leaching causes a differential surface dissolution, in water , producing the characteristic fibre pitting often observed (24).

2.7 Static fatigue in glass fibre

Glass is subject to static fatigue, analogous in nature to metallic

stress corrosion. Withrow and Sinclair (25) define static fatigue as the growth under load of sub critical flaws in an aqueous environment, to the point where unstable crack growth can initiate, resulting in a time dependent failure. This mechanism is a function of stress, time and environment.

Some of the earliest work in this field was undertaken by Charles (22,26) who found that the previously described corrosion reactions occur at a rate determined by the applied load. The asymmetrical stress fields around a surface flaw, coupled with stress enhanced corrosion, can drive a crack through the glass network in a preferred direction. In general, stresses around a crack are at a maximum at the tip, and since dissolution rate depends on the stress level, preferential leaching acts to extend the crack front. This crack growth can continue until the critical flaw size is reached, whereupon brittle fracture of the fibre initiates. Time to failure was then considered to depend on the degree of crack extension required for fracture, as well as the ratio of crack side to tip dissolution rates. The former is a function of the stress concentration level, while the latter depends on the stress distribution around the flaw, and the composition, pressure, and temperature of the surrounding environment. Proctor (23) shows that while this model is inadequate in describing all the stress corcosion behaviour of glass fibres, the general principles outlined are fundamentally correct.

Metcalfe and Schmitz (27) studied stress corrosion in E-glass fibres. The effect of variations in pH, sodium to hydrion ratio, strain rate, temperature, availability of water, and glass composition, was examined in relation to the observed behaviour. While the process described above was still felt to operate, the chemical reactions that occur at the crack tip were altered. In this work, corrosion was found to occur through an ion exchange mechanism of the form;

$$SiONa + H^+ \rightarrow SiOH + Na^+ \qquad - (2.4)$$

rather than by network hydrolysis (22). The above reaction was shown to be controlled by the sodium ion diffusion rate at the tip. E-glass contains negligible amounts of sodium (table 2.1), but concentrations as low as 0.013% were found to be sufficient to initiate static fatigue. An incubation period for stress corrosion damage accumulation was found to precede strength degradation, whether under stress or not. This period accounted for the largest part of the time to failure during static fatigue.

Stress corrosion flaws were thought to grow in areas of undamaged surface , rather than to act in extending existing cracks. This can occur for two reasons:-

(i) The very high ratio of pristine to damaged surface, present on a fibre

(ii) Ion exchange in a flaw, such as a pit, is reduced by a build up of alkali ions within the crack, which can only diffuse away into the liquid bulk at a fairly slow rate.

This model of the chemical reactions occurring, differs from that proposed by Charles (22,26) and others. However, the broad principles of stress corrosion crack extension in a corrosive environment are unchanged.

Doremus (28) followed the ion exchange theory outlined above, presenting a mathematical model combining kinetic rate theories with classical fracture mechanics, to predict the static fatigue behaviour of brittle materials. The important feature of this model was the idea that a fatigue limit existed, i.e. a stress below which static fatigue will not occur. Experimentally, verification of the existence of this limit was not conclusive. Furthermore, results from a study of the effect that surface treatment has on the stress corrosion behaviour could not all be explained in terms of the available models. This highlights the uncertainty that still exists as to the mechanisms involved leading to static

fatigue in glass.

Dozier et al (29) produced a modified stress enhanced crack tip dissolution model based on the work of Charles (22), to account for the observed deviations of behaviour, from that predicted by theory. An expression for the crack tip displacement was found:-

$$V(c) = (1 - \nu) \frac{(K_{Ic})^2}{2E\sigma_y} \qquad -(2.5)$$

where V(c) is the crack tip displacement, K_{Ic} the critical stress intensity factor, E the elastic modulus, σ_y the yield strength, and ν is Poissons ratio. The dependence of crack speed on the stress level is shown in figure 2.5, taken from Fox (30). Three regions of behaviour are commonly found. In region 1, the crack growth is limited by the rate of the environment reaction at the crack tip, and in 2 by diffusion of the corrosive species to the crack tip. Region 3 is environment insensitive, crack speed increasing rapidly with stress until a critical flaw size is reached, resulting in failure.

From the model proposed by Dozier et al (29), a fatigue limit was again predicted. Experimentally, three types of stress/environment reactions were found, and they are shown schematically in figure 2.6(31).

(i) Flaw sharpening by stress corrosion

(ii) Simple rounding of the crack tip by corrosion

(iii) Surface advance of the crack tending to decrease curvature at the crack tip.

The first mechanism increases the rate of crack growth, while the other two retard it. The balance between these reactions depends on the stress level. Above the fatigue limit, stress concentrations at the crack tip are sufficient to ensure that dissolution is concentrated in this region, where the atomic lattice is most severely stretched. Hence, crack sharpening occurs, increasing K, which then promotes further stress corrosion crack extension.

At stresses below the fatigue limit, dissolution of the flaw faces is no longer insignificant, so that corrosion is not restricted to the crack tip. Furthermore, from figure 2.5, stress corrosion is limited by the reaction, and corrosive species diffusion, rates at low stresses. As dissolution progresses, alkali concentrations build up on the flaw, acting as a barrier to corrosive species migrating to the crack tip. Hence, K is reduced by general dissolution rounding off the crack front, preventing further crack extension. This point about changes in corrosion behaviour as a function of stress concentration will be further discussed in Part III.

To conclude, both Fox (30) and Wiederhorn (31) have produced detailed reviews of the current models of environmental stress corrosion cracking in glasses. It was confirmed (31) that static fatigue is caused by the presence of water, since fibres that had been dried and loaded under vacuum were found not to show any time dependent strength loss. From flexural tests, the static fatigue limit for glasses occurred at a stress level around 20% of the strength, though whether such a limit was found for E-glass is unclear.

For the purposes of this thesis, details of the chemical reactions leading to either crack tip or general dissolution are of secondary importance. The most important point, agreed upon within all the theories, is how an applied stress causes crack extension in a corrosive environment, by encouraging flaw sharpening through localised crack tip dissolution. Furthermore, the changes in flaw dissolution that occur at low and high stresses are very important when examining the environmental damage found during immersed creep tests.

CHAPTER 3

POLYESTER RESINS

Polyester resins were the first polymers to be considered for use as the matrix for glass reinforced plastics during the Second World War. Chemically, they can be defined as a product formed from the reaction of a polybasic acid with a polyhydric alcohol (glycol), producing a series of ester linkages (32). By varying the reactants, a whole range of polyesters, both thermosetting and thermoplastic, can be produced. One of these groups are known as unsaturated polyesters, that is they contain C = C double bonds that can further react with free radicals to produce chain cross links. All polyester resins used in composites fall within this category. They are capable of cross-linking to form a polymer chain network, and are thus thermosets. This means that, after cure, further heating does not alter their properties (below Tg), and they remain rigid. They are formed by reacting a dibasic acid with a diol, and then cross-linked in the presence of a monomer such as styrene.

The properties of these resins, that led to their use in reinforced plastics, have been summarised by Lawrence (32):-

(i) Easy to handle in liquid form

(ii) Rapid cure, particularly at elevated temperatures

(iii) Excellent dimensional stability

(iv) Good electrical properties (transparent to micro-waves)

(v) Good general physical properties.

A brief review of the structure and properties of these resins is presented in this section, as well as some discussion of the effect an aqueous environment has on these properties. This will later be related to the behaviour of glass reinforced polyesters when exposed to water during a creep test.

3.1 Polyester formation and structure

Polyesterification is typical of a condensation reaction, in which water molecules are produced at each polymerisation step. The reaction is analogous to an inorganic neutralisation reaction (i.e. acid + base = salt + water). The general reaction between a dibasic acid and a diol is given by Cowie (33) as:-

$$HO - R - OH + HOOC - R' - COOH \longrightarrow HO - R - OCO - R' - COOH + H_2O \quad -(3.1)$$

If water is removed as it forms, equilibrium is not achieved, and a bifunctional dimer is produced. This can further react by esterification to produce trimers etc., eventually producing high molecular weight, linear chain polymers. The resin used in this thesis was an isophthalic polyester, and this review will concentrate on the structure of these polymers. They are formed by the reaction of isophthalic acid (an isomer of phthalic anhydride) with a glycol, usually 1, 2 propylene glycol since this produces a polymer with a high solubility in styrene. The structure of these reactants is shown in figure 3.1.

Isophthalic resins are widely used because of their good chemical, and moisture, resistance. This will be shown in 3.3 to result from the high cross-link density possible with these polymers, resulting from the high number of unsaturated double bonds available for reaction along the chain.

Norwood (34) has presented a detailed account of the chemistry of polyester resin formation, and this is summarised in figure 3.2(a). The non-cross linked, thermoplastic, unsaturated polyester that is formed, is dissolved in a solvent containing a monomer such as styrene. This solution is the liquid resin purchased from a manufacturer. An inhibitor is also usually added to the solution, to prevent free radical cross-linking occurring during storage.

On addition of an initiator to the liquid resin, such as methyl ethyl ketone peroxide (MEKP), the styrene monomer will react with the unsaturated polyester to produce a solid, three dimensional cross linked-chain network (figure 3.2(b). Accelerators are also added to promote cure by the break-

down of any unreacted inhibitor present (3.2). Control of the cure reactions (e.g. accelerator/catalyst concentrations, cure time, cure temperature) will determine the final cross link density, which will in turn influence the final chemical, and moisture, resistance of the resin, as well as its mechanical properties.

3.2 Properties of polyester resins

Although not of direct relevance to this thesis, it was the electrical properties of polyesters that first prompted their use in glass reinforced laminates. Their high dielectric constant made them ideal for use in airborne radomes during the war, the first application recorded for GRP. This still represents an important application for these laminates.

Hull (9) has summarised the properties of thermosetting resins in general, referring specifically to polyesters. As a result of the three dimensional network of cured thermosets, properties are generally considered to be isotropic. No melting occurs on heating (cf. thermoplastics), and they maintain the form they had on curing. At the heat distortion temperature, determined by the chain structure, stiffness properties degrade rapidly, thus limiting the useable temperature range of polyesters.

The mechanical properties of a cured resin depend on the chain structure (i.e. initial reactants), and the degree of cross-linking (state of cure). Elevated temperature post-curing eliminates property changes that can occur as a result of in-service curing. Shrinkage during cure, and thermal contraction after post cure, can induce internal stresses, particularly in composites. This can further alter the mechanical response of a resin matrix in unexpected ways. It can be seen that the prediction of the mechanical properties of a resin matrix is highly complex. Some typical polyester property values have been tabulated by Hull (9) (table 3.1).

Polyester resins are normally regarded, after cure, as brittle solids. However, this is not strictly true; the degree of brittleness depends on specimen preparation and test procedures. When loaded in compression, polyesters undergo considerable plastic deformation. This is suppressed in

a tensile test by premature failure at pre-existing bulk flaws or surface cracks.

3.3 Moisture effects in polyester resins

Polyester resins, when combined with glass fibres, are widely used for applications where they are in prolonged contact with water (e.g. boat hulls). At room temperature, resin plasticisation is very limited, and the main degradation found can be characterised, broadly, as discolouration, erosion, and (in composites), fibre prominence. This can take various forms, such as crazing, debonding (in GRP), colour loss etc. (32).

The principle variables controlling resin durability in water are:-

(i) Polymer chain composition

(ii) Molecular weight

(iii) Degreee of cure

(iv) Type, and concentration, of cross-linking monomer used.

Polyester degradation occurs through hydrolysis reactions, mainly at unsaturated double bonds, so the moisture degradation resistance is improved by raising the cross link density etc., since this reduces the density of sites on the chain that can hydrolyse in the presence of water.

Norwood (34) examined the corrosion resistance of a range of resins in a variety of chemical environments. He looked at the strength degradation in resins exposed to distilled water, finding a reduction of 20% after 3 months, as well as measuring a 1% weight increase due to moisture absorption. No surface crazing, or blistering, or bulk cracking, were detected. The weight increase measured does not accurately reflect absorption levels, since low molecular weight constituents formed as a result of chain hydrolysis, as well as residual styrene, are leached out by the water, causing a balancing weight loss.

The degree of post-cure was found to affect the corrosion resistance of polyesters in strong acids and alkalis, but had little influence on the

water penetration resistance. Finally, it was stated that resin response could not be used to predict the behaviour of a polyester matrix composite when exposed to water, but this will be further discussed in Chapter 6.

To conclude this section, the work of Ashbee et al (35) should be examined. They immersed thin (3mm) polyester strips in water at elevated temperatures (60°C and 100°C) for periods up to 16 weeks. On removal, internal disc shaped cracks were observed to have formed. To explain this, they propsed a model based on the theory of osmosis. It was argued that various water soluble inclusions in the resin dissolve in the diffusant, generating a solute gradient from the inclusion to the sample face. This sets up an osmotic cell, the resin acting as a semi-permeable membrane, and a pressure build up occurs at the inclusion capable of initiating disc cracking.

An alternative explanation, rejected by the authors, is that cracking results from the internal stresses induced by resin swelling, particularly at the elevated temperatures used. In such thin sheets, these would be quite severe, and the stress concentrations generated around such soluble regions after leaching could raise the local stress levels sufficiently, to induce the crack damage found. This latter explanation would appear to be as plausible as that based on osmosis, though no definate conclusions as to the mechanisms involved have, as yet, been reached,

CHAPTER 4

THE FIBRE/MATRIX INTERFACE

The mechanical performance of a fibre composite can be shown to depend on three factors:-

(i) Strength and stiffness of the reinforcing fibres.

(ii) Strength and chemical stability of the resin matrix.

(iii) Stress transfer efficiency across the fibre/matrix interface.

A bundle of fibres would be useless as a load bearing structure, but by adding a resin matrix, shear and compressive properties are given to the body, giving it a useable mechanical response. The fibres support the load, while the resin acts as an efficient load sharing medium, as well as a barrier against filament damage. Thus, to a great extent, composite response depends on the properties of the interface region between the two components. It is thus essential to examine the chemical and physical properties of the interface before laminate behaviour can be predicted, particularly in aqueous environments.

4.1 Structure of the interface

The interface consists of a surface, common to the fibre and matrix, and the immediate region bounding this surface. It has properties different from those of the fibres and the matrix (36). Scola (37) considers the region to consist of surface and sub-surface atoms from both the matrix, and to some extent, the fibre. The number of atomic layers below the surface that influence interfacial properties is uncertain, as is the distance between the respective surfaces, though the thickness was found by Norman et al (38) to exceed 2μm. Before considering the specific nature of the glass/polyester interface, some of the general interfacial bonding theories will be discussed.

Chamis (36) classifies the bonding that occurs under 3 broad headings; chemical, electrical and mechanical. Irrespective of bond type, load transfer can be considered as a mechanical process. For bonding, constituents have to be in intimate molecular contact, i.e. adhering to each other (38). In a review paper, Erickson and Pleuddemann (39) showed that good fibre surface wetting by the liquid resin was essential to the development of strong interfacial bonds. Scola (37) also demonstrated this requirement, presenting three criteria essential for good adhesion: -

(i) The adhesive must wet the adherend surface, ensuring complete and intimate contact.

(ii) The adhesive must become viscous, or solid during bonding.

(iii) The adhesive must be able to deform during solidification to relieve internal stresses caused by thermal and cure shrinkage.

These factors place two conditions on surfaces to be bonded:-

(i) To ensure wetting, adherend surface energy must be less than that of the adhesive.

(ii) A large interfacial area of contact is desirable, regardless of the bonding present.

Various theories of interfacial adhesion have been reviewed by Wake (40), and summaries of these models are presented below. The situation is more complex in glass/polyester systems, but this will be covered in 4.2. The models of interest can be classified under five main headings:

(i) Adsorption and wetting

(ii) Interdiffusion

(iii) Electrostatic attraction

(iv) Chemical bonding

(v) Mechanical adhesion

4.1.1 Adsorption and wetting

When two surfaces are brought into intimate contact, a physical attraction occurs. Due to surface roughness and contamination, bonding is weak, so liquid resin is introduced to fill all the air gaps and promote good adhesion. To achieve this, the resin must wet the surfaces as much as possible.

Wetting is best described in terms of 2 equations. Firstly, the Dupré equation for the thermodynamic work of adhesion (Wa) is:-

$$Wa = \gamma_L + \gamma_S - \gamma_{LS} \qquad -(4.1)$$

where γ_L , γ_S , and γ_{LS} ,are the surface free energies of the liquid, solid and interface.

This can be related to the case of a liquid drop on a solid surface, using Youngs equation:-

$$\gamma_{SV} = \gamma_{SL} + \gamma_{LV} \times \cos\theta \qquad -(4.2)$$

where γ_{SV} ,γ_{SL} , and γ_{LV} , care the surface free energies of the solid/vapour solid/liquid, and liquid/vapour interfaces, and θ is the contact angle. For spontaneous wetting, $\theta = 0$. From this, Zisman introduced the concept of a critical surface tension (γc) for liquid spreading, i.e. $\gamma_{LV} < \gamma_c$. In practical terms, this means that the fibre surface energy must exceed that of the matrix for bonding to occur.

In a physical sense, these bonds result from highly localised intermolecular dispersion forces which, theoretically, can give very high glass/matrix cohesion. This does not occur in practice because of the following:-

(i) Fibre surface contamination, causing surface energy reductions.

(ii) Air and gas entrappment at the solid surface.

(iii) Large shrinkage stresses that occur on curing, leading to irrecoverable surface displacements.

Fibre wetting is a very important parameter in composites, since incomplete

surface coating by the resin can reduce stress transfer, and hence mechanical properties.

4.1.2 Interdiffusion

Bonds between two polymer surfaces can be created by the diffusion of molecules from one surface into the network of the other. Bond strength then depends on the degree of molecular chain entanglement, and the number of molecules involved. The presence of solvents and plasticisers can promote interdiffusion, the rate of which depends on molecular mobility, architecture, and constitition. When glass fibres are pre-coated with polymer prior to lay-up, good bonding is found to occur, which can partly be attributed to matrix/coating interdiffusion.

4.1.3 Electrostatic attraction

When oppositely charged surfaces are brought into contact, electrostatic bonding results, the strength of which can be related to the charge density. While this type of bonding is not relevant to the general case of fibre/resin adhesion, it could well govern the way coupling agents coat the glass surface. Thus, if ionic functional silanes are used (4.2), cationic functional groups will be attracted to an anionic surface and vice-versa. Control of pH levels can thus determine the silane molecule orientation on the glass surface, optimising coupling agent efficiency. This bonding will break down in water, so other bond types must operate during coupling agent adhesion.

4.1.4 Chemical bonding

This model best approximates the action of coupling agents on glass fibres. A chemical bond can form between compatible fibre and matrix chemical groups. Bond strength depends on the number and type of chemical

bonds present, and interfacial failure must require chemical bond breaking to occur. Bond formation and destruction processes are thought to be in a thermally activated dynamic equilibrium state.

4.1.5 Mechanical adhesion

Some bonding between fibre and matrix can occur through mechanical interlocking, where strength is achieved from the frictional forces present. When a resin completely wets a fibre, it can flow into all the surface irregularities present. Strength in tension will be low, depending on the number of re-entrant angles in the fibre surface. Shear strength, however will be high, its ultimate level depending on the fibre surface roughness. A rough surface will also increase chemical bonding potential, by raising the available surface area.

As well as mechanical interlocking, mechanical bond strength can be increased by thermally induced internal stresses, found on curing. These arise from matrix shrinkage, differential thermal contraction etc., resulting in high pull out strength as the resin shrinks onto the fibre.

4.2 Coupling agents in glass/polyester composites

When glass/polyester composites were first produced, it was found that severe strength degradation occurred on exposure to water, attributable to interfacial breakdown. Even when fibres were dried prior to encapsulation (41), the severity of moisture induced degradation was unchanged. In order to produce a water resistant bond between the inorganic fibre surface and the organic resin, an intermediate material was required. Organofunctional silanes (hybrids of silica and resin compatible organic materials), were obvious choice for this application, and have been successfully used since the 1950s. The result of using these agents, was to improve mechanical properties through an increase in bond strength, as well as

improving the interfacial resistance to moisture attack.

From surface energy considerations, glass fibres should be wetted by most liquid resins (38). However, as soon as moisture contacts glass filaments, the highly hydrophillic surface adsorbs a tightly bound layer of water, several molecules thick. Sufficient moisture pick up occurs during manufacture (2.2) to reduce the fibre surface energy from $500mJm^{-2}$ to $10\text{-}20mJm^{-2}$ (9), which is too low for polyester resins to wet the glass fibre. However, the coupling agent applied as part of the initial size coating can wet the fibre. After curing the coupling agent coat, surface energy is increased to $40mJm^{-2}$, allowing the liquid resin to wet the coated filaments. Thus, one of the ways silanes promote interfacial adhesion, is by increasing the wettability of the fibre surface.

Before considering how coupling agents increase bond strength, mention should be made of the composition of polyester compatible silanes. For optimum performance, silanes specific to the resin system chosen should be applied. Selection of coupling agents in commercial fibre manufacture is still very much an art form, shrouded in secrecy, rather than an exact science. Several years of testing go into the optimisation of coupling agent formulation. However, Pleuddemann (41), in a detailed review of silane coupling agents, looks at some polyester compatible silanes. The most common agent applied to E-glass fibres, is a cationic methacrylate-silane, the structure of which can be represented as:-

$$CH_2 = \underset{\displaystyle CH_3}{C} - COOCH_2CH_2 - \overset{\displaystyle Cl^- \quad \oplus}{N(Me_2)}CH_2CH_2CH_2Si(OCH_3)_3$$

This compound imparts good handling characteristics to the treated glass. The quaternary ammonium function in the silane acts as a promoter for the initiators used in polyester resin systems. As a result, the bonding characteristics of a coupling agent are very sensitive to the system

employed, as shown by Vaughan and Sanders (42).

When the reinforcement used is a woven fabric, the size applied in the initial manufacture is often burnt off after weaving, and a coupling agent then applied (38, 39, 41). This can cause problems, as will be demonstrated, since silane penetration to the interior of a roving cross-over may not be complete, leaving highly stressed regions of the reinforcement inadequately protected against moisture attack. Downey (43) has provided evidence that some modern fabrics are surface treated prior to weaving. Where this is the case, glass/glass contact points (e.g. cross overs), can have mechanically damaged surface coatings after weaving, again leaving these regions inadequately protected.

Adhesion promotion by silanes is still not fully understood, and none of the available theories fully predict behaviour. It is now generally accepted that silanes form a surface film, rather than discrete droplets, on the fibres. Direct observation of this film has so far proved impossible due to the low concentration of coupling agent used. Pleuddemann (41) models the system as a molecular monolayer of silane, covalently bonded to the glass surface oxides, leaving the organofunctional groups to react with the resin. This model falls within the chemical bonding theory (4.1. 4).

Yip and Shortall (44) found that bond strength predictions from the monolayer model were too high, and they modified the theory to account for observed behaviour. In this model, a dynamic equilibrium between making and breaking of hydrogen bonds between polymer segments and the glass surface, due to the presence of water molecules, is established. They concluded by stating that the interfacial bond present consisted of two mechanisms:-

(i) Chemical bonding due to the above

(ii) Mechanical bonding due to differential thermal contraction on cure.

Total bond strength is approximately 65% chemical, and 35% mechanical.

Graf et al (45) present two further models of bonding. In one, preferential adsorption of certain resin components onto the silane surface creates an incompletely cured resin layer adjacent to the fibre, imparting some desirable properties, but not explaining the moisture resistance of these coatings. In the second, an interpenetrating network region forms at the interface, through silane catalysed phase separation. They also explain how coupling agent multi-layers, found by infra-red spectroscopy, are created on the fibre surface.

In the multi-layer model, the silane interphase (region between fibre and matrix), is divided into 2 components; the chemisorbed and physisorbed. The latter can be removed by the use of organic solvents, while the former monolayer cannot. It is thought that physisorbed layers dissolve into the resin during cure, forming a complex interphase adjacent to the fibre consisting of a resin/silane oligomer mixture. This changes the local mechanical properties around fibres. The silane concentration used in a coating has been found to alter the strength of a composite, and this is explained in terms of changes in the thickness of the interphase formed. Since the reactions in this region act to break down the cross-links in the matrix, partial plasticisation occurs around the fibre. This can then act as a barrier to moisture uptake, since hydrolysis in this region is impeded by the silane linkages formed at the network sites most prone to moisture attack.

Other models exist, such as the deformable layer and restrained layer theories, all of which are reviewed in detail by Pleuddemann (41). Since infra-red spectroscopy has shown that coupling agents form multi-layers, the monolayer theory (41) can be regarded as simplistic. However, from the current thesis, it would appear that a mixture of chemical and mechanical bonding (14.5) exists at the interface in the glass/polyester laminates

examined, as found by Yip and Shortall (44). Thus, a combination of the multi-layer theory of Graf et al (45) and the model proposed by Yip and Shortall (44) would best represent the interfacial behaviour observed in Part III.

4.3 Load transfer mechanisms

The properties of a composite depend on the ability of the matrix to transmit stresses to the load bearing fibres. To model this effect, several assumptions have to be made (9):-

(i) Matrix and fibre behave elastically

(ii) Interface has zero thickness

(iii) Interfacial bonding is perfect (i.e. no strain discontinuity)

(iv) Material adjacent to fibres has the same properties as that found in the bulk

(v) Filaments are regularly arranged in a repeating array.

In real composites, (ii) - (iv) are incorrect simplifications, while (i) and (v) are not always true. Despite this, the resulting model does provide reasonable approximations of the observed behaviour.

An important factor in the discussion of load transfer is the contribution made by the filament ends, present as a result of fibre breakage, as well as when short fibre reinforcement (e .g. csm) has been used. Fibre ends disrupt the stress and strain fields in both the fibre and matrix, to a degree that increases with decreasing fibre aspect ratio. Thus, as the reinforcement length decreases, so does it load bearing efficiency.

Consider the case of a filament embedded in a lower modulus matrix with good interfacial bond characteristics (figure 4.1). When a load is applied to the composite, stress is transferred to the fibre across the interface. Around the fibre ends, strain levels fall below those in the surrounding matrix, inducing interfacial shear stresses (figure 4.1(a)).

Expressions for interfacial shear, and tensile, stresses along the fibre can be produced (9), the results from which are illustrated in figure 4.1(b).

Three important observations can be made from this analysis (36):-

(i) The shear stress at the interface increases rapidly to a peak value, then decays to zero on traversing along the fibre from its end.

(ii) The tensile stress at the fibre end is zero, but builds up along the fibre, rapidly attaining its average value, as the shear stresses from (i) decay away.

(iii) Where the matrix behaves plastically, shear stresses can be generated at the interface away from the fibre end region ($\frac{1}{2}$ lc).

The region of the fibre over which shear stresses reduce the load transfer efficiency, is known as the ineffective length. From this, it can be seen that fibres shorter than lc will not reinforce the resin matrix.

Reinforcement efficiency is dependent on interfacial bond strength, since load transfer depends on strong adhesion. The large shear forces generated within the ineffective length can result in:-

(i) Shear debonding at the interface

(ii) Cohesive failure of the matrix

(iii) Cohesive failure of the fibre

(iv) Shear yielding of the matrix.

Which of these factors determine the overall efficiency is dependent on their respective failure stresses. Fibre strength also limits efficiency, since a filament break will reduce the aspect ratio of that fibre, causing a drop in load bearing capability.

4.4 Water at the interface

The fibre/resin interface has long been regarded as a region of high moisture sensitivity, particularly in glass/polyester composites. Water can cause a dramatic loss of flexural strength, especially at elevated

temperature. Silanes can improve properties in water, but wet strength retention at elevated temperatures is still not total. For silane coated E-glass cloth in polyester, exposed to boiling water for 24 hours, a 6% drop in flexural strength has been reported (37) (c.f. 27% for untreated glass). The mechanisms of degradation must be established, from which the improvements due to the application of coupling agents can be modelled. Bascom (46) presents a good review of this field, and much of the following is taken from his work.

Firstly the locus of failure must be established. From fracture studies, the initiation and slow crack growth regions within GRP are rarely apparent. It is necessary to know where failure initiates in order to observe the effect moisture has on the whole process. Crack extension studies have therefore been undertaken using a double cantilever test specimen (46). This is a stable crack growth test, allowing initiation to be studied. Moisture induced failure was found to occur at the resin/adherend boundary. From fracture mechanics theory, failure is postulated to occur in a zone, one or two molecular layers thick. Thus, it would appear that water breaks down the interfacial bond, allowing access to moisture sensitive components, such as fibre surfaces.

To improve moisture stability, care should be taken to prevent the water reaching the interface. Filaments directly exposed to water (e.g. at edges, interfacial voids etc), are an obvious drawback. Water diffusion through resin and interfacial cracks can also cause problems. When laminates are laid up, particularly glass fabrics, wetting is never complete, and cylindrical roving voids form (5.3.1). These allow direct access to the interface for the ingressing moisture, resulting in debonding and fibre degradation.

The improvement in properties during immersion that results from using silane coatings, is as yet not fully understood. For water to reach

the interface, it must either diffuse through the matrix or along interfacial cracks (38). From the chemical bonding theory, moisture degradation is retarded by the need to break down these bonds before interfacial breakdown can occur. When debonding does initiate, at elevated temperatures, Ashbee and Wyatt (47) postulate that it proceeds by an osmotic mechanism. A pressure build up at the interface occurs, causing bond rupture, which then creates bubbles of water at the interface. In time, these coalesce, creating large regions of debonding. Other mechanisms can be the generation of thermal and shrinkage stresses at the interface as a result of matrix plasticisation (39). Vaughan and Sanders (42) predict that debonding occurs in the layer next to the interface, so that fibres are still protected by a layer of coupling agent.

All these theories are based on chemical bonding theory, which has been shown to be an oversimplification (46). It has been found that the polyester does not fully polymerise in the interphase region. This leaves a low density film around the fibres that can easily be leached, leaving moisture in direct contact with the fibre surface. Silanes are thought to either increase the interphase density by chain entanglement, or through the promotion of further polymerisation. This high density layer impedes moisture diffusion, but at elevated temperatures cannot prevent it. Once water does penetrate to the interface, siloxane bond hydrolysis occurs, weakening the fibre/coupling agent adhesion. These processes are all stress and temperature dependent. Once the bond between fibre and silane has been degraded, glass weakening through stress corrosion can initiate (46).

There are still many unanswered questions as to how a coupling agent protects the glass filaments, either by adhesion promotion, or as a moisture barrier. However, it can be seen that silanes impede, rather than prevent, moisture degradation.

CHAPTER 5

COMPOSITES

5.1 Manufacture of GRP

There are a whole range of techniques available for the production of GRP but in general they can be grouped under two main headings (48):-

(i) Open mould systems

(ii) Closed mould systems

The former techniques were the first to be developed, and are still the most widely used. However, they are very labour intensive. Closed mould forming (curing in a heated press), is easier to automate, but is only practical for relatively small components. Since the materials used in this thesis were produced by an open mould process, this review will deal exclusively with such techniques.

5.1.1 Open mould systems

All these processes rely on the fact that polyester resins will polymerise in the absence of heat and pressure. Some of the principal methods are:-

(i) Hand lay-up

(ii) Spray-up

(iii) Filament winding

Of these, the first two are by far the most common. Spray-up methods can only be used for chopped fibre laminates. Since the material used in this thesis was a mixture of csm and woven roving, laminate sheets had to be produced by hand lay-up methods, as described below.

5.1.2 Hand lay-up of GRP

After preparing a mould and coating it with a release agent, liquid resin is painted onto the mould. If a gel-coat layer is required

on the component face, this resin is allowed to gel before laying up proceeds. This layer can impart superior chemical resistance to the laminate. Having done this, a further layer of resin is applied, and the pre-shaped reinforcement layer is placed in the mould. This can be either csm or woven roving.

Fibre wetting and consolidation of the laminate is accomplished through the use of a roller or brush. To wet out the csm, the resin is 'stippled' into the mat with a nylon bristled brush. This can introduce air bubbles into the resin, creating resin voids (5.3.1), but it does ensure complete fibre wetting occurs. Consolidation is then achieved by rolling. This method is unsuitable for fabrics, since the fibre orientation would be disrupted. Instead, a split washer roller is run along both roving directions, squeezing liquid resin into the fibre bundles. Incomplete wetting may result, leaving cylindrical voids within the rovings (5.3.1.).

Further reinforcement layers are built up to attain the desired thickness, then the component is cured. In some cases, a mould is placed on top of the laminate during cure, being removed prior to post cure. This reduces thickness variations, as well as removing some entrapped air by squeezing out excess resin ('leaky mould' method). To ensure complete matrix polymerisation, cured components are often given an elevated temperature post cure. This reduces property changes that can occur in time, due to a gradual increase in cross-link density.

5.2 Mechanical properties of GRP

One of the great advantages (and disadvantages) of composites, is their large range of properties. By controlling the composition and manufacture of a laminate, specific mechanical behaviour can be built into a composite. However, properties are very sensitive to local condition changes, causing material variability (5.3). Some of the important

factors influencing behaviour include (48):-

(i) Mechanical properties of the fibre and matrix

(ii) Fibre volume fraction (V_f)

(iii) Degree of interfacial adhesion

(iv) Fibre cross section

(v) Fibre orientation

All these parameters are highly variable, particularly affecting the properties of low V_f composites. The interrelationships existing between these factors are unknown, and consequent variations in strength and stiffness have to be allowed for in design calculations. This review will present a summary of general laminate properties, followed by a section outlining the changes in behaviour that occur when fabrics are used as the reinforcement.

5.2.1 General properties

Kelly (49) has grouped the mechanical response of a laminate under two main headings:-

(i) Geometry dependent - the geometry of component phases, and their respective volume fractions influence behaviour, regardless of dimensions.

(ii) Dimension dependent - the structure or size of the components influence behaviour.

The concept of a 'rule of mixtures' was also introduced,i.e. the elastic properties of a fibre composite fall within limits defined by the strong, stiff fibres, and the weak, compliant matrix.

Harris (50) also considers the prediction of mechanical properties. By considering arrays of well bonded lamellae, possessing different moduli but identical poissons ratio, in a unidirectional lay-up, simple models for longitudinal and transverse properties can be developed (figure 5.1).

$$Ec = Em\ Vm + E_f V_f \qquad \text{(VOIGT)} \qquad -(5.1)$$

$$\frac{1}{Ec} = \frac{Vm}{E_m} + \frac{V_f}{E_f} \qquad \text{(REUSS)} \qquad -(5.2)$$

where $V_f + Vm = 1$ (i.e. zero porosity assumption). The Voigt estimate is a parallel spring model with strain continuity at the interface, while the Reuss model is a series arrangement with continuity of stress. Equation 5.1 is the mathematical definition of the rule of mixtures most commonly employed. It predicts, fairly successfully, the longitudinal modulus of a unidirectional composite. In short fibre composites, the modulus falls between the Voigt and Reuss estimate, and accurate predictions are no longer obtained. In general, the rule of mixtures does not predict the behaviour of csm or woven roving reinforced composites. Since most design criteria require response to fall within stated strain limits (51), it is essential to either model behaviour more accurately, or apply large safety factors (15-20 are common). The latter represents current practice and while some models have been developed (5.4), limited accuracy has retarded their general acceptance as design standards.

Ogorkiewicz (52) categorised glass/polyester composites under three main groupings:-

(i) Random fibre e.g. csm

(ii) Orthogonal fibre e.g. woven roving

(iii) Unidirectional fibre

In the first case, fibres are short and due to their random orientation, maximum V_f is limited to 50%. Most practical laminates have glass contents in the range 20-40%, and even fractions as low as 10% are not unknown. Chopped strand mats also exhibit a local variability of $\pm$ 10% in the glass loading across a mat width according to manufacturing tolerances (43), causing further laminate variability.

Orthogonally reinforced laminates have a more orderly array of continuous rovings, and the V_f can be pushed up to 65%, though again lower

values are found in practice. With woven fabric laminates several plies thick, the undulating lamella surface prevents close packing, and resin rich regions are formed between the reinforcement layers, depressing the maximum V_f value.

Finally, for unidirectional composites, packing density increases due to the regularity of the filament array, and glass contents in excess of 70% can be achieved. Variations in local V_f are also minimised in these fibre dominated laminates, which can be regarded more as resin bonded filament bundles than fibre reinforced resins. They have the highest specific properties (in the longitudinal direction) of any industrial material.

All 3 groupings follow the same general property trends (figure 5.2), i.e. strength and stiffness increase as a function of increasing glass content. However, important differences also arise as a result of changing the degree of property anisotropy. Random fibre composites can be regarded as isotropic, but as soon as aligned fibres are introduced, roving orientation effects induce anisotropy. With orthogonal laminates, stiffness is maximised in the fibre ($0/90^{\circ}$) directions. However, when fabrics are loaded in one fibre direction, high interfacial stresses are created in the other, producing transverse crack damage. Orthotropic laminates thus have low transverse strength. The onset of cracking has been shown by Garrett and Bailey (53) to occur at about 0.4% strain, detected as a kneee in the stress/strain curve. Since fabric laminates have failure strains of around 2.5%, it can be seen that most loaded woven roving composites will contain transverse cracks, lowering the environmental resistance.

Unidirectional composites are also orthotropic in the fibre planes, though they exhibit transverse isotropy. Within each ply, modulus can vary by up to 3 times from the transverse to longitudinal directions. These materials are only considered to be load bearing in the fibre direction.

Ogorkiewicz (52) showed that, within a small strain range, GRP behaves as a linear elastic body, particularly at high V_f . This has led to the

development of failure models based on linear elastic fracture mechanics (5.4). Other models, such as Classical Laminated Plate Theory, have been developed, and will be discussed in 5.4.

To conclude, consideration should be given to composites containing mixed reinforcement, as used in this thesis. Mixtures of csm (for its environmental resistance), and woven roving (superior load bearing properties), glass reinforcements are commonly used. The properties of such materials depend on the ply behaviour, and the proportions of each reinforcement present, as shown by Johnson (54). In general, strength and stiffness increase with increasing fabric content, though no significant increase in properties is found until the fabric represents 50% of the total glass loading (figure 5.3).

5.2.2 Woven roving composites

Glass fabric reinforced laminates have been widely used for many years, due mainly to their ease of handling when laying up. Several types of fabric are used (2.3), but this review will concentrate on the most widely used material; plain weave, since this was the reinforcement used in this thesis.

Woven glass laminates have many properties in common with orthogonal plied laminates, differing in just one vital respect; in fabrics, the reinforcing rovings are bent as a consequence of weaving. Fibre crimp is most severe in plain weave fabrics, leading to a significant reduction in reinforcement efficiency (18). The undulating fabric ply surface also prevents close packing of the reinforcement layers, producing interply resin rich regions, and reducing V_f. Furthermore, bending at roving cross-overs induces local fibre stress perturbations (20), which can have a dramatic influence on the composite performance when under load.

While plain weave fabrics are nominally balanced, slightly higher

glass loadings are normally used in the warp direction (generally, a ratio of 5/4 is stated), to achieve higher loom production levels. Crimp is also less severe in this fibre orientation and the two factors combine to give higher strength in the warp direction. White (55) found that, in a typical electrical board material(glass fabric/epoxy), the glass loading was 20% higher in the warp rovings, increasing the modulus by 28% in this direction.

The stress perturbations found in fabric laminates have been examined in some detail (20). Woven laminates are very susceptible to transverse cracking at low strains. Until cracking initiates, short term behaviour is linear elastic, and the tendency of load bearing fibres to straighten under load is constrained by the transverse rovings. Once cracking occurs, transverse rovings can move, so the restraint on fibre straightening is reduced, causing a modulus drop, observed as a knee in the load/deflection curve. The stress fields within loaded fabrics are highly complex, and not fully understood, and no attempt will be made within this thesis to provide an analytical model. It is sufficient to bear in mind that the stresses along a woven filament vary greatly, depending on the relative position within the fabric a central point in the discussion presented in Part III.

Siebert (56) looked at the problem of the in-service delamination of fabric composites, common in the chemical industry. To prevent this damage, it was considered essential to ensure total fibre wetting during manufacture. This is another problem common to woven roving composites. In a fabric, the filaments are tightly bound in rovings, making it difficult for the resin to penetrate the fibre bundles. Thus, in the central regions of rovings, and within weave cross-over points, fibre debonds, in the form of voids, are present (5.3.1.) This is particularly deleterious to flexural properties, where high interfacial shear stresses are generated.

Downey (57) shows that altering the weave density can improve the laminate properties,by allowing for higher degrees of fibre wetting and encapsulation. Problems of delamination were also attributed to fibre straightening effects, and it was found that by reducing fabric crimp, delamination could be avoided. However, it will be shown that, even when loose weave fabrics are used, complete wetting does not occur (Part III), and air voids are always trapped in the woven rovings (5.3.1).

5.3 Composite property variability

One of the major problems associated with testing composite materials, is the large variation found in supposedly identical samples, under the same loading conditions. It is impossible to eliminate this variability, due to the large number of interrelated factors that contribute to it, e.g.

(i) Filament strength
(ii) Time dependent nature of fibre strength
(iii) Fibre volume fraction
(iv) Fibre alignment
(v) Interfacial bond strength
(vi) Porosity
(vii) Matrix composition
(viii) Matrix properties
(ix) Time dependence of resin properties

Glass fibre strength is highly flaw sensitive (14), and varies according to a Weibull distribution. In general, the longer the filament the lower its strength (increased probability of a severe flaw being present). Fibre strength can be determined from the filament fracture surface (58), allowing strength distributions to be calculated. With woven fabrics, this is not practicable, since stresses vary along a fibre (20), making the critical flaw size a function of its position on the filament surface.

Other factors can induce stress concentrations within a laminate,

such as fibre misalignment, local variations in V_f, and porosity, leading to property variations. Desvaux and Greenwood (59) discuss some of the methods used to allow for data spread in the analysis of composite properties. However, the individual contribution of each factor can be isolated and studied, due to the large influence they have on mechanical response. These include porosity and strain effects, both of which are discussed below.

5.3.1. Voids in composites

It is impossible to prevent void formation in composites though, in high performance laminates, porosity is minimal. It results from a number of sources, such as air entrappment on lay-up, evolution of volatiles (e.g. styrene) on cure, inadequate filament wetting etc. Measures can be taken to reduce porosity levels, such as vacuum degassing. In low glass content laminates (around 30%), such as csm or woven roving materials, porosity levels of up to 5% are common in commercial GRP (60).

Judd and Wright (60) discuss the types of void found, how they form, techniques for determining pore content, and the effect they have on properties. Two void types have been identified:-

(i) Cylindrical intra-roving pores (within filament bundles)

(ii) Spherical resin voids (within resin rich matrix regions)

The former come about through incomplete resin penetration into the rovings as a result of filament packing, poor wettability, and resin viscosity. These voids are aligned with the fibres, creating an interfacial air gap. These are the hardest to eliminate, and the most detrimental to the composite properties. Spherical resin pores occur as a result of air entrappment, or volatile constituent evolution, on curing. They act as local stress raisers, inducing matrix cracking on loading. Careful degassing and laying-up can minimise the numbers of these defects in the matrix.

Several methods of determining pore density are outlined (60), but since they are all accurate to $\pm$ 0.5%, the simplest technique is usually

used. In this method, a polished section from a composite is prepared and examined, using a microscope equipped with a graduated eye piece. A pore count is then taken within a known surface area, and the void content calculated from:-

$$\text{VOID CONTENT } (\%) = \frac{100\ Pv}{Pt} \qquad -(5.3)$$

where Pv is the total void, and Pt the overall, cross section examined. This technique also gives information on the shape and location of voids within a composite.

Mechanical properties have been shown to be highly void sensitive, upto a level of 4% porosity (60), with a 7% decrease in interlaminar strength occurring for every 1% increase in porosity up to this maximum. Strength loss is probably due to the formation of roving voids. Above the 4% porosity level, further increases are due to resin, rather than roving, void formation which would explain the limit found. From an industrial viewpoint, rather than taking costly precautions to reduce porosity levels, it may be preferable to encourage void formation. This would improve the property reproducibility, at the expense of high strength. This is only true where an aggressive environment is absent.

Both Bascom (46) and Chamis (36) discuss the degradation that occurs in water as a result of porosity. Interfacial voids are damaging for two reasons. Firstly, in orthogonal laminates, pores lying parallel to the transverse rovings act as crack initiators, further reducing the strain level required to initiate cracking perpendicular to the applied load. This damage can then allow rapid moisture penetration by capillary flow along these transverse cracks (14.2). Secondly, they act as collection points for ingressing moisture, allowing fibre degradation to proceed, as stated by Hancox (61).

It is the environmental consequences associated with voids that are the most relevant to long term GRP properties, though their influence on

strength may be one of the factors causing the large scatter commonly found in stress-rupture data (5).

5.3.2 Strain rate effects

The time dependent nature of glass fibre strength has already been discussed (2.7), and this section will merely highlight the effect that this has on the behaviour of GRP. It should also be noted that effects due to matrix viscoelasticity will alter the time dependent properties of composites, but this will be discussed later (7.1).

Sims and Gladman (62) have shown that, for fine weave glass fabric/epoxy composites, the U.T.S. can be increased by 30% on raising the loading rate from 10^2 to 10^6 N/s (figure 5.4). They also show that rate effects only occur in glass fibre composites, concluding that at the test speeds used, rate dependence was a function of the filament properties. In discontinuous fibre composites, matrix shear load transfer occurs, and it was thought that resin rate effects may be significant. Increases in strength at high speeds have been explained in terms of fibre stress corrosion (2.7). In principle, the faster the test rate, the shorter is the time available for flaw growth, and the higher the strength.

Thomas (63,64) has studied the factors affecting glass fibre composite strength, and he has shown that at high strain rates, strength becomes independent of the matrix properties. At low rates, behaviour is highly matrix sensitive. It has been shown that the strength of a glass strand depends on the fibre length and strain rate. When encapsulated in a matrix, length effects become less significant due to load transfer between fibres. At low strain rates, fibre pull-out occurs, and the U.T.S. depends on matrix resistance to debonding. When soft waxes are used, strength falls to the level found for unloaded bundles (63). Strain rate dependence is limited in E-glass fibres (reflecting their corrosion resistant nature) at

normal test speeds, a 7% fall in U.T.S. being found on reducing the loading rate from 10-0.1mm/mm/min., when tested in a polyester matrix (cf. E-glass/beeswax system, where a 30% fall was recorded). In a subsequent paper (64), it was shown that, for E-glass/polyester systems, rate effects were insignificant when compared to the effects due to incomplete fibre wetting. It was felt that interfacial bonding was the major strength governing parameter in these materials, with strain rate having a secondary influence on properties.

In conclusion, at high strain rates, it would appear that filament properties govern the composite behaviour, while at lower speeds, resin and interfacial effects become significant (13.2)

5.4 Composite failure models

The large degree of anisotropy present in composites causes problems in the prediction of stress fields, and failure strength. Many models have been derived for isotropic materials, such as metals (65), and a similar requirement now exists for composites. Owen (66) has produced a mathematical model to predict the biaxial stresses present in many practical composites from a series of tensile tests. However, it was inadequate, in that no attempt was made to model how one failure mechanism could affect the operation of others (e.g. does delamination encourage crack growth?). It was shown by Owen and Rice (65) from tests on E-glass/polyester laminates, that interdependence between failure modes does exist. This highlighted the inadequacies of existing failure criteria, such as von Mises, derived for isotropic bodies.

The work mentioned above depends on the ability to fit test data to a mathematical model, and a need now exists to develop models that predict laminate behaviour from a knowledge of the ply properties, and stacking sequence. Two models have been taken from the realms of mathematical theory. These are Classical Laminated Plate Theory from the field of linear elastic stress analysis, and Chain-of-Bundles Theory from statistics.

These will be discussed below, along with an approach based on linear elastic fracture mechanics (LEFM).

5.4.1 Classical Laminated Plate Theory

When modelling the behaviour of common engineering materials, they are assumed to be homogeneous, and any microheterogeneity is ignored. They are also assumed to be isotropic, and simple expressions, such as Hookes law, can be used to estimate the mechanical behaviour. Fibre composites, however , are not so simple to deal with. The properties of aligned fibre composites are orthotropic. By assuming that individual plies are homogeneous (not strictly true), the properties of a composite can be calculated from a knowledge of the constituent lamella behaviour and orientation. To accomplish this, anisotropic elasticity theory is employed, requiring a large degree of matrix algebra. This section will merely summarise the derivation of laminate plate theory. A rigorous analysis and proof is given by Jones (67).

The starting point is to determine the properties of a unidirectional ply by use of the full, three dimensional Hookes Law (9):-

$$\sigma_i = \sum_{j=1}^{6} C_{ij}\,\varepsilon_j \qquad i, j = 0 \text{ t}^{o} 6 \qquad -(5.4)$$

where σ_i are the stress, and ε_j the strain, components, and Cij the stiffness matrix (figure 5.5). This equation gives 6 expressions relating stress to strain, e.g.:

$$\sigma_1 = C_{11}\,\varepsilon_{11} + C_{12}\,\varepsilon_2 + C_{13}\,\varepsilon_3 + C_{14}\,\gamma_{23} + C_{15}\,\gamma_{31} + C_{16}\,\gamma_{12} \qquad -(5.5)$$

The individual expressions are straight forward, but use of a computer is required to analyse the response of real composites.

It is more usual to relate strains to stresses, and a corresponding expression to 5.4 can be derived.

$$\varepsilon_i = \sum_{j=1}^{6} S_{ij}\,\sigma_j \qquad -(5.6)$$

where S_{ij} is the compliance matrix. By assuming each ply to be orthotropic and thin, plane stress conditions can be applied, simplifying the expression of Hookes Law (50):-

$$\begin{bmatrix} \varepsilon_{11} \\ \varepsilon_{33} \\ \varepsilon_{13} \end{bmatrix} = \begin{bmatrix} S_{11} & S_{13} & 0 \\ S_{12} & S_{33} & 0 \\ 0 & 0 & S_{66} \end{bmatrix} \begin{bmatrix} \sigma_{11} \\ \sigma_{33} \\ \sigma_{13} \end{bmatrix} \qquad -(5.7)$$

where $S_{11} = 1/E_{11}$, $S_{33} = 1/E_{33}$, $S_{66} = 1/2G_{13}$, and $S_{13} = -\nu_{31}/E_{33}$. Transformation of this tensor then gives an expression for the elastic modulus as a function of orientation.

$$\frac{1}{E_\theta} = \frac{\cos^4\theta}{E_{33}} + \frac{\sin^4\theta}{E_{11}} + \left[\frac{1}{G_{13}} - \frac{2\nu_{31}}{E_{33}} \right] \sin^2\theta \cos^2\theta \qquad -(5.8)$$

From these expressions for ply behaviour, laminate theory can be used to sum the stiffness contributions of the lamellae present in a practical composite (67).

Having developed a theory for predicting stress levels, a whole host of failure models (e.g. Tsai, Stowell and Liu) to predict composite fracture, have been developed (50). However, while these models work well for high performance composites, the materials used in this thesis do not behave in the way expected from theory. Fabric plies have highly non-homogeneous stress fields, due to stress concentrations at roving cross-overs (20), causing a breakdown in the assumptions inherent to laminate plate theory. In consequence, little use can be made of this theory in predicting the failure of woven roving composites.

5.4.2 Linear elastic fracture mechanics

Since glass/polyester laminates are composed of two brittle phases,

and behave at low strains in a linear elastic fashion, considerable interest has been shown in the application of fracture mechanics to composite strength predictions. Beaumont (68) has studied this problem, showing that failure must be controlled by the largest flaw present for a fracture mechanics approach to be applicable, i.e. composites must be flaw sensitive. This was found to be the case in high performance laminates, where V_f is high, and the interfacial bonding strong. It was possible to calculate stress intensity factors for these materials. However, in composites where bonding is not so strong, a large amount of crack blunting, as a result of debonding occurs, and strength becomes flaw insensitive. In these circumstances, LEFM cannot be used to predict strength.

Several other workers (69-72) have used fracture mechanics to predict the strength of laminates containing macroscopic stress concentrators (i.e. holes and cracks). Nuismer and Whitney (69) and Waddoups et al (70) have produced models that successfully predict the strength of high performance carbon/epoxy composites containing notches, though these are largely curve fit excercises. Konish et al(71) found that failure mechanisms were edge crack dominated, though again this was in high performance composites. Kanninen et al (72) show that LEFM can only be used in materials where microstructural effects are negligible, allowing the composite to be regarded as homogeneous.

When woven roving composites are considered, microstructural effects clearly dominate, and it has been demonstrated (55) that the behaviour of glass fabric/epoxy laminates do not fall within the scope of LEFM. Glass/polyester bonding is not strong (4.2), allowing considerable crack deviation and blunting to occur. Secondly, it has been shown (53) that fabric laminates are only linear elastic up to 0.4% strain . Thus, the whole basis of LEFM breaks down at low strain levels. As a final point, it will be shown that GRP is, in fact, viscoelastic (7.1). Thus, once again, this failure model is not applicable to the materials tested in this thesis,

only working with high performance (carbon/epoxy) composites.

5.4.3 Bundle strength theories

A totally different approach to failure is to consider how microstructural elements behave under load. One of the ways to do this, is to regard a composite as a bundle of fibres which possess variable strengths. These models are based on theoretical studies of the strength of flawed fibre bundles, rather than determined from a macroscopic study of composite behaviour. Coleman (73) presents a good review of the models available . When classical fibres are considered, i.e. not embedded in a matrix, the following assumptions have to be made:-

(i) Fibre strength is time independent

(ii) A fibre breaks at its weakest point

(iii) Fibre strength does not fall to zero, regardless of length.

Assuming a Weibull distribution in fibre strength, it was found that the ratio of the tensile strength of a bundle to the mean tensile strength of the constituent filaments, decreases monotonically with increasing fibre strength dispersion.

Two probability distribution functions have been described by Harlow and Phoenix (74,75) to account for the behaviour of a simple fibre bundle:-

(i) Strength distribution amongst fibres

(ii) Fibre length distribution within the bundle

The first factor is the most important, and is usually represented by a Weibull distribution function. The second factor allows for the case where some fibres are loaded before others. When a load is applied, a fibre will break, transferring load to all the other fibres, increasing the probability of subsequent failures. The distribution of breaks is determined by the defect population in each fibre, and so the location

of each break is independent of its predecessor. Once a fibre breaks, it ceases to be load bearing . Eventually, sufficient breaks accumulate to initiate bundle failure, break position along the gauge being a random function of each fibre.

Bunsell (76) applied the general principles of bundle theory to the case of fibre reinforced resin composites. In this case, fibre/matrix adhesion, and the shear stresses around a break, allow load transfer to be limited to neighbouring filament regions. Thus, the zone of influence of a fibre break is restricted to a segment of the fibre length, increasing local stresses, rather than the overall bundle stress level. Even after failure, filaments can thus still remain load bearing (figure 5.6). In this case, behaviour is modelled as a chain of fibre bundles, where breaks in one segment do not influence the properties of filament lengths in its neighbours. An increase in strength is found, since the chances of finding a severe flaw in a segment, sufficient to cause failure in a fibre neighbouring a break zone, is much less than in the case where the whole bundle is overloaded.

Composite strength models can be derived from chain-of-bundles theory, and Harlow and Phoenix (74,75) detail the analytical techniques involved. Practical solutions are almost impossible to compute, numerical convergence methods being required even for the case of a 4 fibre bundle,. They also present an expression for the stress concentration around filament breaks within a chain segment. The load concentration factor (Kr) for an unbroken fibre adjacent to r filament breaks is given by:-

$$Kr = 1 + r/2 \qquad -(5.9)$$

This equation will be further discussed in Part III.

While simple mathematical solutions for composite strength based on this theory have not yet been developed, the principles outlined represent the best available model of the mechanical response of GRP. This is particularly true for woven fabrics, since this model can allow for the heterogeneous nature of the reinforcement plies.

CHAPTER 6

MOISTURE EFFECTS IN COMPOSITES

The behaviour of GRP in an aqueous environment, particularly at elevated temperatures, and /or under static load, has been shown to differ from the properties already detailed (9). Since the major application for GRP has been the replacement of steels in corrosive environments, it is important to determine how the environment alters the mechanical response.

When estimating the changes in properties that occur during immersion, several interrelated factors have to be considered:-

(i) Moisture diffusion rates

(ii) Diffusion mechanisms

(iii) Moisture diffusion within a laminate

(iv) Effect of moisture on constituent properties

(v) Temperature and applied load.

6.1 Moisture uptake

When a laminate is exposed to an aqueous environment, analytical and experiemental techniques to predict property changes under fluctuating temperature and moisture content, have to be developed. Springer (77) outlines the parameters that have to be determined as the temperature (T), and moisture content (C), vary with time (t):-

(i) Temperature distribution within the laminate as a function of position and time.

(ii) Moisture concentration as a function of position and time

(iii) Mass of water present as a function of time

(iv) Changes in laminate behaviour as a function of time

When certain conditions are satisfied, (i) - (iii) can be determined analytically, while testing is required to quantify performance changes (6.3). These conditions are (77):-

(i) Heat transfer through the laminate is by conduction only, and is described by Fourier's law.

(ii) Moisture diffusion can be described by use of Ficks 2nd law of Diffusion.

(iii) Temperature equilibrium is reached much more rapidly than the maximum moisture content, decoupling Fourier's and Fick's laws.

(iv) Thermal conductivity and mass diffusivity depend solely on the temperature, and are independent of moisture content and stress level within the body.

When the above assumptions are valid, moisture uptake is said to be 'Fickian', i.e. obeys Fick's law, which can be written in the form (7):-

$$\frac{dm}{dt} = - DA \frac{\partial c}{\partial x} \qquad -(6.1)$$

where m is the mass of diffusant passing through a cross section, A. C is the mass concentration, and D the diffusion coefficient, which can vary with temperature and pressure.

Shen and Springer (78) looked at unidirectional carbon/epoxy composites, and found that uptake approximates to Fickian behaviour. They developed an analytical model to determine the overall diffusion properties of such laminates from short term tests. Experimentally, samples were immersed and moisture content, measured as a weight change, plotted against $\sqrt{t}$ (figure 6.1). The initial straight slope has a gradient proportional to the composite diffusivity, D, given by:-

$$D = \pi \left(\frac{H}{4M_m} \right)^2 \left(\frac{M_2 - M_1}{\sqrt{t_2} - \sqrt{t_1}} \right) \qquad -(6.2)$$

where h is the sample thickness. From this simple test routine, the moisture uptake characteristics of a laminate under a whole range of test conditions can be predicted, giving the assumption of Fickian behaviour.

Having demonstrated the usefulness of Ficks Law in predicting moisture uptake, some thought should be given to the case where this theory does not apply. In composites, the following factors can all cause deviations from the above theory.

(i) Cracks or delaminations occur in the composite, altering its structure.

(ii) Moisture propogates along the fibre/matrix interface

(iii) Voids occur in the laminate

(iv) Matrix diffusion is non-Fickian

Composites, in particular low glass content polyester materials, exhibit at least one of the above, and often a combination of several factors, so that Ficks law can at best be regarded as an approximation to diffusion. Since it represents the only analytical model available for predicting moisture content in a composite, many workers (79-89) have attempted to apply it, with varying degrees of success.

When high performance carbon/epoxy composites are examined, Ficks Law is generally found to give good approximations to moisture absorption rates. Collings and Copley (79) use Ficks Law to calculate moisture gradients from a finite element analysis, from which they derive an accelerated moisture ageing technique for aerospace composites. Similar work on CFRP was also undertaken by Edge (80), while Weitsman (81), and Leung and Kaelble (82), all demonstrate that water uptake in these systems is Fickian.

Fickian behaviour has, however, also been reported in less advanced (low V_f) composites. Loos and Springer (83) studied diffusion in glass/polyester sheet moulding compounds. Weight change as a function of $\sqrt{t}$ was monitored, from which Fickian diffusion was found to occur. However, moulding compounds contain a significant amount of calcium carbonate filler, which can be leached out of the matrix during immersion. This will affect the moisture uptake, measured as a function of sample weight increase, since the calculated level will include a weight loss element due to leaching. Since deviations from theory normally occur through higher than predicted uptake (as a result of cracks etc.), this weight loss

mechanism may cause anomolous diffusion to appear Fickian. Ellis and Found (84) also show Fickian diffusion occurs in csm/polyester composites, but again weight loss mechanisms would lead to inaccuracies in the measurement of the moisture uptake reported.

When examining the literature on glass fibre reinforced resins, particularly polyesters, the concensus of opinion is that anomolous diffusion, rather than Fickian, occurs. Menges and Gitschner(85) show that only 'ideal' composites will obey classical diffusion models. In real glass/resin systems, matrix swelling occurs, inducing internal stresses that alter the diffusion characteristics. The lower the glass content used, the greater is the influence of swelling stresses on water uptake. Dewimille et al (86) came to similar conclusions, and they list some of the mechanisms that occur in real laminates:-

(i) Diffusion into the matrix without visible degradation

(ii) Initiation of microdamage,increasing the diffusion rate

(iii) Weight loss due to leaching

The combination of these factors leads to anomolous diffusion.

Farrar and Ashbee (87) consider that diffusion in glass/epoxy composites is anomolous. They demonstrate how the matrix region adjacent to a fibre induced sufficient swelling stresses to increase the local diffusion rate, as well as initiate interfacial debonding and cracking. Both of these factors increase the moisture uptake to a greater extent than that predicted from theory. Bonniau and Bunsell (88) show how the degree of matrix cure affects water absorption in glass/epoxy laminates. Resin cure affects the magnitude of matrix swelling that occurs during immersion, once again showing how internal stress build ups can alter the diffusion behaviour of these low fibre fraction composites. Polyesters are more susceptible to swelling than epoxies (3.3), so anomolous diffusion would be more likely to occur in glass reinforced polyesters, a point confirmed by the literature.

Marshall et al (89) studied diffusion in csm/epoxy composites by using tritiated water as the diffusant. In this way, uptake could be followed by sectioning the samples, and measuring the emitted radioactivity. Non-Fickian diffusion was thus attributed to the clustering of moisture in the resin, either at polar groups along the polymer chain, or in micro-voids. This method is very useful, as any weight loss during immersion does not affect the measurements, and diffusion coefficients can be calculated, despite the anomolous diffusion found. However, the higher ionic potential of tritium, compared to water, may cause greater clustering around polar groups on the polymer chain than would normally be expected.

Another factor influencing the diffusion behaviour of a composite is the relative humidity. Jones (90) shows that deviations from Ficks Law occur both in CFRP, and GRP at high relative humidity. Wright (91) shows how moisture uptake rate, and maximum moisture content, increases with relative humidity (figure 6.2). As a general rule, immersion in water leads to anomolous diffusion, while at lower relative humidities, Fickian behaviour can be obtained (86).

Anomolous diffusion can be attributed to two factors, resin swelling and defect formation. High performance composites contain low levels of resin, and void contents are minimal. Hence, they approach the 'ideal' state to which Ficks Law applied (85). Glass/polyester composites, on the other hand, contain much higher percentages of both resin and porosity (5.3), which can influence absorption, as shown by Kaelble (92). As a consequence, Ficks Law is no longer applicable, and anomolous diffusion results, making theoretical predictions of moisture content impossible .

6.2 Effect of load and temperature on moisture uptake

Having shown that diffusion in glass/polyester composites does not normally follow the available absorption models, some thought should be given to the effect of temperature and applied load on the moisture uptake

of these materials. Springer (77) has shown that the diffusion coefficient of a composite varies with changes in applied stress and temperature. Temperature fluctuations cause an exponential change in D, and in most practical cases, this is the dominant effect, and changes with stress can be ignored. Shen and Springer (78) further found that maximum moisture content is independent of temperature, being solely a function of the relative humidity. This is contrary to the generally expected case, where increases in maximum moisture content occur as the temperature is raised (91). Since temperature increases diffusion rate, it would appear unlikely that Mm would not also be raised. From results found in this thesis, maximum absorption levels were found to depend on the test temperature (11.1). Thus, it is concluded that for GRP, maximum uptake levels will depend on temperature.

Increasing the test temperature can increase diffusion rates, as well as Mm, through an increase in composite free volume. This can occur in two ways. Firstly, at the microstructural level, temperature rises increase the polymer chain mobility in the matrix. This raises the level of chain disorder, reducing the cross link density by thermally activated bond breaking, and leads to an expansion of the polymer network. This increase in free volume allows easier access to the network for the diffusing moisture, accelerating uptake rate and level. Secondly, at the macrostructural level, differential thermal expansion in a laminate has been shown by Jones et al (93,94) to induce thermal strains in the composite. This can cause micro-cracking, providing paths of easy diffusion for the ingressing moisture. These cracks also create air gaps in the composite, which can become filled with water, increasing the maximum moisture content attainable. Thus, the temperature dependence of diffusion in GRP, can be attributed to the changes in internal free volume that occur on heating.

When a load is applied to a composite immersed in water, the resulting build up of damage, particularly in orthogonal laminates, where transverse cracking occurs at low loads (20), would be expected to increase absorption

rates, as has been found (89). Stress concentrations in the test pieces were found to further increase local diffusion rates by up to a factor of 7. This observation is particularly relevant to woven fabric composites, where regions of high stress exist at the roving cross-over points. Thus, not only is the critical filament flaw size minimised in these areas, but also the water uptake to this zone is increased, leading to enhanced fibre surface corrosion. While rapid moisture diffusion ('wicking') along interfaces was not found to occur in this work, it was suggested that this may occur in laminate systems where interfacial bonding is not as strong as in epoxies, such as glass/polyester composites.

Rotem and Elizov (95) found that applied loads increase water uptake in S-glass/epoxy laminates, attributing this observation to rapid diffusion along interfaces. By applying a load, interfaces can be stretched apart, allowing water to penetrate and rupture any remaining bonds by hydrolysis reactions.

The link betwen moisture uptake and stress has been well established. Dorey (96) found that, above certain threshold levels of moisture content and stress (1% and 45% respectively for CFRP), stress significantly affects the diffusion rate. This was attributed to damage initiation at the threshold stress, producing paths for moisture ingress by capillary flow mechanisms. These thresholds depend on the material system, and will be much lower for woven glass fabric composites (6.4). The onset of damage will be accelerated by moisture induced swelling stresses, and the moisture content threshold can be regarded as the level of water uptake needed to initiate hydrolytic swelling (87).

Swelling stresses, when superimposed on to an applied load, can induce a variety of damage states, such as debonding, resin cracking, and ply delamination. All of these mechanisms, coupled with the increase in free volume associated with resin swelling, can increase water uptake in GRP.

While the general concensus of opinion is that moisture uptake increases with applied load, Wyatt (24) found the opposite to be true. Thin film (200μm) polyester/glass laminates were examined, and it was found that water absorption was inhibited by an externally applied stress. Moisture uptake was considered to occur by an osmotic process (4.4). Pressure build ups within voids, and at interfaces, can cause debond, and matrix crack,damage in the composite, leading to increased water uptake. When an external load is applied, sufficient micro-damage can be created to relieve these pressure build ups, allowing soluble constituents to escape from the laminate, causing a drop in osmotic driving force that reduces the diffusion rate. Large scale damage through pressure build ups is also reduced, reducing the availability of easy diffusion paths into the sample. It should be noted that this effect is only seen in thin film laminates, and the anomolous results described may result from the relaxation of swelling stresses that occur under constant displacement loading, as used in these tests.

6.3 Influence of defects on moisture uptake

It has been made clear that anomolous diffusion in GRP results from the imperfect nature of its structure. The influence of voids on composite strength has already been examined (5.3.1), but mention should be made as to their influence on the moisture degradation of composite properties. This can occur in several ways. When at the interface, they can act both as moisture reservoirs for glass hydrolysis, and as debond initiation sites (46). Boudreau (97) looked at the effect of woven fabric coupling agent composition on interfacial breakdown, showing the degradation was inversely proportional to the bond strength. When a good bond is achieved, intra-roving porosity is minimised i.e. interfacial environmental stability is a function of the fibre/matrix bond.

Resin voids can also accelerate environmental degradation in GRP. Moisture migrates preferentially to these high stress matrix sites (89), creating water pockets dispersed throughout the resin. This causes differential swelling between void sites and the bulk matrix, inducing internal stresses sufficient to initiate cracking from these pores, further increasing water uptake. Osmotic pressure cracking (24) may also occur in these regions.

When a stress is applied to a laminate, stress concentrations around a void (particularly those lying parallel to the transverse rovings), can initiate damage at low loads. This will, in itself, increase diffusion. All the other mechanisms mentioned will be accelerated by an applied stress.

Grayson (98) used a profiling technique to examine moisture distributions in CFRP. While macroscopic behaviour was Fickian (as measured by sample weight gain), moisture pockets were found to form at the microstructural level, possibly due to segregation at the interface (97), or in voids, or at sites of local heterogeneity within the matrix. In all cases, differential swelling can occur, leading to damage in the ways already mentioned. Apicella et al (99) found that the exothermic cure reactions found in unsaturated polyesters, can raise laminate temperatures by differing degrees throughout the sample volume. This can lead to variations in matrix cure, with some incompletely cured regions remaining. These regions are more susceptible to hydrolysis, thus they absorb more water, and can create damage in the manner above. Post-cure treatments can eliminate this problem, by ensuring that all the matrix is fully cured.

6.4 Property degradation of GRP in water

Having established how moisture is absorbed by a laminate, and its distribution within a sample, the effect this has on the mechanical

properties of GRP must be examined. Dorey (96) shows that resin hydrolysis, responsible for swelling (6.1), acts to reduce the overall cross link density in polyesters, leading to matrix plasticisation. This reduces the mechanical properties of the resin, and makes it more susceptible to creep. Tg is also reduced, degrading the elevated temperature response of the matrix.

Pritchard and Taneja (100) show that hot water induces resin plasticisation in csm/polyester composites, as described above. Furthermore, even when unloaded, surface gel-coat cracking was observed, resulting from the swelling stresses generated in this surface layer. Once the gel-coat cracks, stress concentrations are established, and enhanced diffusion can occur. A cracked gel-coat is more detrimental to the properties of immersed GRP than no gel-coat at all.

Hot water can also include interfacial breakdown and, ultimately, fibre surface hydrolysis (100). Debonding occurs whether under stress or not, but when unstressed, degradation is confined to the surface plies. When loaded to strains in excess of 0.4% , debonding spreads rapidly throughout the sample, probably as a result of crack initiation. As an example of the degradation found in hot water, a 50 day exposure to boiling water (no load applied) reduced flexural strength by 59%, and modulus by 28%.

Hogg and Hull (101), in a comprehensive review of environmental degradation in GRP, show that water absorption affects the behaviour of each composite constituent. Resin plasticisation occurs, which may be reversible, reducing matrix properties. The leaching of low molecular weight material from the resin further reduces its properties irreversibly.

At elevated temperatures, serious degradation in the form of swelling and leaching occurs. This produces resin cracks that both weaken the laminate, and increase water penetration rates. This was found (101) to reduce the stress-rupture life of GRP, and it was suggested that the use of more flexible resins could prevent cracking, and improve the moisture

resistance. Since the current work has found that resin cracking accelerates stress-rupture (Part III), this approach would appear to have considerable benefits.

Interfacial breakdown can also occur in water, reducing transverse strength etc. This also allows moisture to come into contact with the glass fibres, causing stress corrosion weakening to occur (3.5). With E-glass fibres bound in a resin matrix, simple immersion in room temperature water is unlikely to cause significant strength loss. When under stress, or at elevated temperatures, the situation changes, and significant strength loss, due to accelerated fibre corrosion rates, is found with time.

Due to a mismatch in the thermal expansion coefficients of glass and polyesters, temperature changes can induce large thermal interfacial strains in a composite. This can create damage, and weaken the laminate. Jones and Mulheron (102) found that much higher thermal strains were induced in wet laminates during a temperature cycle. Thus, absorption of water also leads to an increase in the temperature sensitivity of a composite exposed to fluctuating temperatures.

A common phenomenon in glass/polyester laminates that contain a gel-coat, is moisture induced blistering. This ruptures the protective gel-coat, creating a stress concentration, and allowing rapid transport of water into the composite. Adams (103) shows blistering to be a function of the gel-coat permeability and void content. In essence, leaching produces a solute gradient through the gel-coat to moisture filled pores, creating an osmotic cell (4.4). Pressure build ups in the void then deform the gel-coat layer above, eventually bursting it. It was in order to prevent complications, due to blistering, in the interpretation of results, that the samples tested in this thesis had no gel-coat applied to them (Part III).

The most important consideration in this thesis, is the relationship between laminate strength and various combinations of water, stress and temperature. Roberts (104) found that a limiting strain level existed for applied loads to accelerate environmental degradation in GRP at room temperature. This was attributed in the case of fabric laminates, to the onset of transverse fibre debond cracking that occurs on loading. Strain was used to define the crack initiation point, as this was found to remain constant, whereas the load level varied between samples. The idea of a limiting strain to define the onset of moisture degradation was also used by Downey (57), and its importance as a design criteria will be emphasised in Part III.

Roberts (104) also demonstrates the existence of the synergism between water and stress. GRP exposed to boiling water for 5 hours underwent a 26% strength loss, while a load of 25% UTS alone produced no property degradation. When combined, failure occurred after 5 minutes.

Pritchard and Taneja (105,106) outline the type of damage found in csm/polyester laminates exposed to water at elevated temperatures (105):-

(i) Gel coat cracks

(ii) Internal disc cracks

(iii) Debonding of fibre rovings

(iv) Resin cracks associated with debonding

(v) Water accumulation around debonded filaments.

In a subsequent report (106), it was shown that a strain of 0.4% had to be induced before moisture degradation was accelerated, again being attributed to the onset of cracking. It was reported that, for temperatures below $80^{o}C$, no significant strength loss occurred after 500 hours.

Ishai (107,108) studied the effect of temperature on moisture degradation after long term exposures. It was found that, as previously mentioned, diffusion rate increased with temperature, causing a correspond-

ing increase in moisture degradation (107). It was also concluded that as before, a strain limit to load intensified degradation exists. In a later study (108), the effect of moisture uptake on GRP was presented as a 3-stage process:-

(i) Moisture uptake into the relatively large spaces in the matrix, such as pores and cracks.

(ii) Water penetration to the fibre/matrix interface

(iii) Irrecoverable weight loss due to leaching.

Stage (i) induces resin swelling, and represents the major damage mechanism during cold water immersion, while stage (ii) has no permanent degrading effect. In hot water however, coupling agent hydrolysis and fibre corrosion can occur during stage (ii), causing permanent strength loss. Stage (iii) only occurs in hot water. An applied load would accelerate all these mechanisms, allowing fibre degradation and residual strength losses, even at room temperature. Several workers, such as Proctor (16), and Lyons (5), also report that no strength loss occurs in GRP immersed in water at temperatures below 50°C.

Finally, Short et al (113) looked at woven glass/polyester composites exposed to the marine environment. It was found that, when unstressed, diffusion was primarily due to transport through the resin surfaces. Subsequent flexural tests showed that failure occurred through weave cross-over delamination, indicating that preferential moisture attack at these high stress points initiates debonding.

CHAPTER 7

CREEP IN COMPOSITES

7.1 Viscoelastic properties of composites

It has long been known that polymers exhibit time dependent mechanical properties, attributed to molecular chain sliding under an applied load. In thermosetting resins, cross-linking reduces the chain mobility, and the viscoelastic response of these materials becomes a function of the cross-link density present. Under constant load conditions, resins give a creep response identical in form to that found in metals (figure 7.1) (7). In the primary creep zone, response is a combination of elastic and chain orientation mechanisms, and is recoverable. Secondary creep occurs by a viscous flow mechanism, and can be classified as a steady state region. Deformation is irrecoverable, as is tertiary creep strain, where necking and final failure account for the rapid increases in strain rate.

Viscoelastic materials can be categorised into linear, and non-linear, bodies (114). For a linear viscoelastic body, both the elastic and viscous strains are proportional to the applied stress, allowing a Hookes law type analysis to be undertaken. This has been done for both polymers, and resin matrix composites (115).

A useful property of these materials is that there is a time-temperature equivalence in properties i.e. by testing at high temperature, response after long times can be predicted. For this to be possible, it has to be assumed that a single, thermally activated damage mechanism occurs in a viscoelastic body. Property predictions are made using the Boltzmann Superposition Principle, based on the time-temperature equivalence found in polymers (114). The principle behind data shifting is shown in figure 7.2, where a unified stress relaxation master curve is produced by shifting data from a series of elevated temperature , short time,tests. Shift factors are determined experimentally, using a WLF type

equation defined by Crowson and Arridge (116) as:-

$$\log a_T = \frac{a\,(T - Tg)}{b + T - Tg} \qquad -(7.1)$$

where Tg, the glass transition temperature, is a reference point, and a and b are constants.

Many non-linear viscoelastic bodies require the use of vertical shift factors as well. In this case, they are said to thermorheologically complex materials (T.C.M.), whereas linear viscoelastic materials are thermorheologically simple (T.S.M.). Thermosetting resins, due to their cross-linked structure are non linear, and hence T.C.M.'s. The application of time-temperature superposition to the prediction of composite creep response will be further discussed in 8.3.1.

Many workers have used viscoelasticity theory to explain the time dependence of GRP properties. Yoshida (117) studied the dynamic viscoelastic response of woven roving composites. It was found that the complex modulus of elasticity depended on glass content (figure 7.3). Since most of the composite viscoelastic response is a function of the matrix properties, as the level of glass present increases, the creep response will fall as shown. With fabric laminates, crimp straightening under load can occur, either through debonding, or as a result of matrix viscous flow, causing further complications (13.2).

Composites are generally regarded as non-linear viscoelastic materials. Nicolais et al (118) attributes this to the presence of a high cross-link density region of matrix at the interface, that disrupts the network flow characteristics. Ashton (119), Schapery (120), and Lou and Schapery (121), on the other hand, attribute non-linearity to the presence of stress concentrations within the laminate, which can locally accelerate viscous flow. Matrix softening, due to changes in cross-link density in moist environments, for example, also changes the fibre/matrix interactions that occur, causing non-linearity. Woven fabrics create large stress variations

within a laminate, making behaviour highly non-linear, and a viscoelastic analysis in this case is highly complex and inaccurate.

Other detailed theoretical analyses of fibre reinforced composite response have been presented by Babich and Lipatov (122), and Pobedrya (115). To summarise, time dependence in composites is largely a property of the viscoelastic matrix used, creep rates varying with such factors as glass content, temperature, and cross-link density. For linear systems, simple models exist for the prediction of properties. Non-linearity in composites is due to the presence of stress concentrations, causing local perturbations in the bulk matrix response. This complicates analysis, and may prevent the use of time-temperature superposition for the prediction of long term creep response (8.3.1.)

7.2 Creep mechanisms in GRP

In many practical applications, the creep properties of GRP represent the limiting factor in long term design calculations. A component loaded to, say, 50% of its strength, may undergo creep-rupture in time, particularly at elevated temperatures, causing a potential hazard. To predict creep response, a detailed knowledge of time dependent properties must be obtained.

Some of the early work on GRP was undertaken by Bott and Barker (124). It was found that cs m/polyester laminates were more susceptible to creep than woven fabrics, due to the resin dominated properties of short fibre composites. Glass fibres were shown not to creep, the only deformation observed coming from roving crimp straightening as the resin flows. In the tertiary stage, elongation was largely due to fibre slippage and pull-out during fracture. Of great relevance to this thesis was the observation that secondary creep strain increased in discrete steps, rather than continuously, in woven roving composites (Part III), as shown in figure 7.4.

This was attributed to a 'slip-stick' mechanism of interfacial adhesion, coupled with progressive fibre rupture.

Diggwa and Norman (125) have outlined 5 factors contributing to creep in GRP:-

(i) Creep of the glass

(ii) Creep of the resin

(iii) Rupture of the glass

(iv) Resin fracture

(v) Rupture or slippage at the interface.

Fibre creep is an insignificant factor in the final behaviour. It was found in this work that strain steps occur infrequently, usually as a result of large resin crack formation, and they attributed the damage in figure 7.4 to 'slip-stick' in the test equipment. However, this work was undertaken on filament wound GRP, whereas step-wise strain growth is found in fabric laminates. (Part III).

Jansson (126) also studied the types of damage found during flexural creep in woven roving laminates (figure 7.5):-

(i) Transverse weft fractures - these include resin cracks running parallel to the weft fibres.

(ii) Longitudinal weft fractures - these appear in regions of high shear stress

(iii) Intrastrand fractures - these occur in resin rich regions at roving cross overs

(iv) Minor resin fractures - these occur in resin rich regions as a result of matrix flow.

Acoustic emission monitoring was also undertaken during creep, and the results show that very little activity occurs in the secondary creep phase (figure 7.6). This was attributed to resin creep, in the absence of cracking. Rapid increases in the tertiary zone activity correspond to fracture initiation.

Bhatnagar et al (127) found that creep response depends on fibre

orientation, with maximum creep strain occurring in $\pm 45^{\circ}$ laminates, demonstrating the resin dominant nature of GRP creep. It was also found that tertiary creep was rarely observed, suggesting that final fracture in creep is very rapid. Sturgeon (128) also attributes the time dependent properties of GRP to the resin matrix, but in a rather different way. When a load is applied, matrix creep is constrained by the elastic glass fibres present. As a result, stress relaxation occurs within the resin, transferring further load to the fibres, extending them elastically. Thus, the time dependent elongation observed is a relaxation effect, and the phenomenon is thus known as 'relaxation creep'. This model explains creep in unidirectional GRP.

Holmes and Rahman (129) studied flexural creep in woven fabric laminates, outlining the various stages of GRP creep:-

(i) Gradual straightening of woven rovings under load, assisted by matrix creep.

(ii) Resin creep in high stress regions, such as fibre breaks and weave cross-overs.

(iii) Progressive debonding with subsequent filament slip relative to the resin and other fibres.

(iv) In the latter stages of creep, fibres become overloaded due to (i) - (iii), causing random periodic, filament rupture, the rate of which accelerates to fracture.

Creep strain also increases with load, due to accelerated resin flow and higher primary creep damage levels.

Lilholt (130) shows that the presence of glass fibres in GRP act to reduce the resin creep rate, in agreement with previous findings (128). A model of creep based on metallic creep laws (8.1) is outlined, and shown to work well with metal matrix composites, as was a similar model propounded by Street (131). These models give no real insight into the operational mechanisms of GRP creep, without which the applicability

of such models is highly suspect (8.2).

Several other workers have studied various aspects of GRP. Cherry and Harrison (132) shows that, under a static flexural load, the strength of GRP reduces by up to 50% after 1 year, attributible to time dependent crack growth. Weidemann and Ogorkiewicz (133), and Koeneman and Kicher (134), both demonstrate that creep is a matrix dominated property, creep rate being found to vary with fibre orientation in unidirectional composites.

In conclusion, creep in GRP is a function of the matrix viscoelastic response, constrained to some extent by the glass fibres. Stress build ups can occur as a result, causing resin and filament damage growth, fibre elongation due to matrix relaxation (128), crimp straightening in fabrics etc., as a function of time. Rupture occurs by the accumulation of damage, leading to composite strength loss (132). Creep response is a function of glass content, fibre orientation and configuration (straight or woven), resin formulation, internal stress levels, applied load, and temperature.

7.3 Creep-rupture of GRP

The usual method to determine the long term properties of GRP is the creep, or stress, rupture test, where samples are loaded to various fractions of their strength, and the time to failure (ttf) recorded. Plots of load against log (ttf) are then used to extrapolate short term data (upto 2 years), to predicted load levels for failure after, say 30 years. This method has been shown to work well with isotropic materials (8.1), where creep is governed by a single activated mechanism. Composite response is complicated by its anisotropic nature, and several interrelated mechanisms have to be considered. Creep-rupture plot linearity cannot, therefore, always be assumed (4) (figure 1.1).

The degree of linearity present has been shown to depend on the degree of resin dominance in the creep response (135,136). Steel (135) shows that, raising the test temperature for woven roving creep tests,

improved the creep rupture plot linearity, by raising the matrix creep response, allowing for crimp straightening. Resin flow is an activated process, and hence standard creep laws apply. This was also shown by Chiao et al (136), where creep was shown to have no effect on the fibres until rupture initiates.

The reliability of GRP components in service is largely a result of overdesign, safety factors of 15-20 being not uncommon. This is uneconomical, and long term design data is required to improve this situation. Desvaux and Smith (137) outline the requirements for such test programmes.

(i) Replicate tests should be undertaken at a variety of loads

(ii) Experimental data should extend to $\frac{1}{3}$ of the design life, reducing extrapolation errors.

(iii) Cost efficiency must be maximised.

Safety factors are still envisaged to account for environmental effects. This routine appears simple, but GRP suffers greatly from variability in its mechanical response (5.3), which can cause a large degree of spread in ttf (figure 7.7). At the same load level, log (ttf) can vary by 4 orders of magnitude. This is mainly due to the varying strength of GRP samples. Replicate tests, at the same load level, do not give identical % strength values within each test piece, thus ttf at an assumed load of, say, 50% UTS, will vary, since some samples may be at 60% UTS, while others are only loaded to 40% UTS. This is a problem inherent to creep-rupture testing, and will only be overcome when a means of determining the test-piece strength prior to a creep-rupture programme, has been developed. This point is illustrated by Aveston and Sillwood (138), where unidirectional composites (low strength variance), show low levels of creep-rupture time variability.

To enable extrapolation, the statistical variance in GRP properties must be allowed for, in one of two ways (137):-

(i) Test sufficient samples to reveal the extent of the scatter bands, determine the glass content of each test piece, and normalise the applied stress accordingly.

(ii) Determine glass content non-destructively, then pre-select samples to obtain scatter band values.

The former approach is time consuming, since well over 100 replicate tests would be required at each load level (139,140) (Appendix 1). The latter method has been used with some success (137), using density , x-ray, and radiographic,techniques to measure the glass content.

The effect of fibre content can be allowed for,using standards laid down in BS 4994 (141). In this case, thickness effects are eliminated by defining strength in terms of the Ultimate Tensile Unit Load (UTUL):-

$$\text{UTUL} = \frac{\text{BREAKING LOAD}}{\text{SAMPLE WIDTH X GLASS CONTENT}} \qquad -(7.2)$$

An average value of V_f is used in this expression, so the observed scatter is not greatly reduced. It does have the advantage of simplicity, and was thus used in this thesis (Part II). Lyons and Phillips (142) used a similar approach, defining an Ultimate Reinforcement Stress (URS) as:-

$$\sigma_R = \frac{\sigma_{ULT}}{V_f} \qquad -(7.3)$$

More complex analyses, using Weibull statistics, have been presented by workers such as Lifshitz (143), Robinson and Chiao (144), Chiao et al (145), and Hahn and Chiao (146). They all assume that results scatter is a function of the strength variation found in the roving filaments.

Phillips (147) outlines 5 assumptions that are inherent to the conventional creep-rupture test:-

(i) Below the failure stress (σ_o), a functional relationship exists between applied load (σ_t), and ttf.

(ii) σ_t/σ_o is a parameter that measures the tendency for delayed failure.

(iii) σ_o is a reproducible material property

(iv) σ_o can be measured in a short term test

(v) The functional relationship between stress and ttf, is of the form:-

$$\frac{\sigma_t}{\sigma_o} = A - B \log t \qquad A, B \text{ are constants} \qquad -(7.3)$$

With the exception of (iii), which is allowed for in the above models, all the normalisation techniques discussed rely on these assumptions. In general, these factors do not apply in composites, and a more complex relationship between stress and ttf exists. Thus, the stress-rupture test can be seen to be inadequate for the accurate prediction of long term GRP properties.

7.4 Environmental effects

It has been demonstrated (6.4) that moisture degrades the mechanical properties of glas/polyester composites. Under creep conditions, the interrelationships between stress, temperature, moisture and ttf would be expected to change the observed behaviour (7.2). Creep strains are greatly magnified in water; increases of upto 200% have been reported for GRP (124). Allan (148) found that this increase is a function of fibre orientation, i .e. much larger increases found in 90° laminates when exposed to water, than were observed in the 0° direction (resin dominance). Wang and Wang (149) attribute this increase to resin plasticisation during immersion. Hydrolysis reactions reduce the cross-link density of the polyester matrix, allowing greater chain mobility, and hence viscous flow (creep).

Hoa (150, 151) found for SMC, that larger creep strains occurred in water, and that immersion extended the tertiary creep region. SMC is a low glass content composite, and again matrix creep in water was used to explain the observed changes. Data scatter also reduced in water (150), probably as a result of a decrease in notch sensitivity due to matrix plasticisation. A suprising result (151), was the observation

that creep life was greater in water than air, contrary to general opinion. Much of this increase, however, was due to the extended nature of the tertiary region, as a direct result of resin plasticisation. This is not found in fibre dominated composites, though evidence of increases in tertiary creep for fabric laminates, has been found in this thesis (12.4)

Wu and Ruhman (152,153) found that ttf is reduced in an active environment (benzene). Matrix swelling stress generation was found to be insufficient to explain this reduction. Instead, it was considered that sorption reduces the energy required to create new surfaces in a sample, initiating debonding, crack formation etc., leading to premature rupture through damage accumulation. Moisture is considered to behave in a similar fashion.

The reduction in ttf commonly found on immersion, has been attributed to stress-corrosion of the E-glass reinforcement (5). This mechanism is well known to cause failure in acid or alkali environments (104), by reactions already discussed (2.5).

Hull and Hogg (154) found that transverse crack damage, formed during loading, accelerates the strain corrosion of GRP. For an acid environment, 4 stages of nucleation and growth were identified (figure 7.8):-

(i) Viscoelastic response on loading (environment insensitive)

(ii) Load relaxation due to slow deformation and micro-fracture. Crack nucleation, and s low growth occurs in this region.

(iii) Sharp fall in load due to the growth of large strain corrosion cracks and delaminations.

(iv) Rapid, unstable, crack propogation, leading to fracture.

Price and Hull (155) show that stress-corrosion is a brittle crack propogation process, creating a smooth fracture surface. In essence, a crack that would not propogate under the applied load, can do so in a corrosive environment, by crack tip dissolution (2.7.). Stress

concentrations at the crack tip enhance corrosion, preventing crack blunting through general dissolution. Jones et al (156), and Hogg (157), show that corrosion rate is a function of the diffusion rate of active species to the crack tip, and matrix fracture toughness. In a brittle matrix, stress corrosion failure of a fibre can cause the propogation of a resin crack to the neighbouring filament, causing rapid fracture. A tough matrix retards crack propogation through blunting, requiring the diffusion of further corrodent to the crack tip to initiate fracture in a neighbouring filament (figure 7.9). These conclusions have been confirmed by workers such as Birch-Kiss anyi et al (158), and Hogg et al (159).

Lyons (5) extended the above arguements to the case of csm/polyester laminate creep-rupture in water. Water, present in ionic form, hydrolyses glass fibre surfaces, by hydrogen ion substitution when under stress, initiating stress corrosion failure. However, Wyatt (24) demonstrates that E-glass fibres corrode in water, whether under load or not. Furthermore, resin hydrolysis during immersion causes an increase in matrix toughness, which retards stress-corrosion crack propogation (155-159). It is felt that, when immersed, fibre corrosion is accelerated, not initiated, as would be the case in stress-corrosion. Thus, it would be more accurate to describe the fibre degradation mechanism in water as stress-enhanced-corrosion, rather than stress-corrosion, since the latter is a conjoint action, whereas corrosion has been found to occur in the absence of load.

In conclusion, water can affect the creep response of GRP in two main ways. Firstly, resin hydrolysis leads to an increase in creep strain, and extension of the tertiary creep region. Surface energy requirements for flaw growth are also reduced, weakening the laminate. Secondly, fibre strength loss as a result of aqueous corrosion reduces the ttf of a sample at any given load.

CHAPTER 8

ACCELERATED CHARACTERISATION OF GRP

8. 1 Metallic creep laws

Since most current GRP design predictions are made using techniques developed for metals, some mention of these methods should be included in this review. Metallic creep response is a classic, three stage process (figure 7.1). In the primary region, creep is due to plastic deformation, that is resisted by strain hardening. This is a function of log (time), and is known as 'logarithmic creep' (160).

Secondary creep is a steady state process, caused by dislocation climb, which overcomes the original strain hardening. This is an activated process, dependent on dislocation diffusion rate, and is known as 'power law' creep in consequence. It is this region that is the most important in engineering design, and most extrapolation techniques are based on the response in this zone. Finally, tertiary creep, resulting from cavitation, crack formation etc., leads to necking down and fracture. This again is an activated process.

Detailed analysis of the damage mechanisms operating in the various creep regions, as shown by Ashby and Jones (161), is time consuming, and much simpler approaches, such as stress-rupture testing, are normally used in practice.Models have been developed, based on power law creep response, that can fairly accurately predict long term behaviour from short term tests. In the secondary region, it has been established that an Arrhenius relationship exists between strain rate and stress (7, 160, 161,162,163). Harris (164) presents a summary of some of the most commonly used models.

8.1.1 Dorn model

This assumes that strain rate ($\dot{\varepsilon}$) varies according to:-

$$\dot{\varepsilon} = Af(\sigma)\, e^{-Q/kT} \qquad -(8.1)$$

where $f(\sigma)$ can be any required function. Plots of $\dot{\varepsilon}$ VS 1/T give the activation energy, Q, from which a $\log (\dot{\varepsilon} + Q/kT)$ VS $\log\sigma$ master plot can be obtained. This approach does not require the use of extrapolation, but does require creep, rather than the simpler stress-rupture, tests to be undertaken. No knowledge of the operational stress function is required.

8.1.2 Larson-Miller model

This is the most widely applied model, based on the stress-rupture test, where it is assumed that :-

$$\dot{\varepsilon} = \frac{1}{t.t.f.} \qquad -(8.2)$$

From this,

$$-\log (ttf) = \text{Log } A - \frac{Q}{kT} \qquad -(8.3)$$

A master curve can be obtained from this by plotting the Larson-Miller parameter, P(where P = T (log A + log ttf)),against $\log\sigma$. This is a simple extrapolation, but inaccuracies can be introduced by its empirical nature.

A similar approach to this is the Manson-Hafferd model, where a modified form of P is used, though again the empirical nature of this technique leads to problems in extrapolation.

All the models mentioned are curve-fit exercises, and the results obtained from them are not consistent. Inaccuracies in all the models tend to over-predict design lives, with potentially dangerous consequences. Despite this, with safety factors, they are all fairly successfully used in design calculations. Since composite creep response is of the same basic form as that found in metals, it was decided to use the widely accepted stress-rupture techniques already in existence, to predict the long term properties of GRP, with limited success (8.2).

8.2 Current GRP design criteria

When designing a load bearing component from GRP, it must be ensured that the design stresses are insufficient to cause fracture, throughout its predicted service life. This means that design predictions must account for creep, and creep-rupture, mechanisms that operate, making the standard engineering practice of dividing the UTS by a safety factor unsatisfactory. This approach, enshrined in the current standards leads either to chronic overdesign, or premature failure.

Roberts (104) has reviewed all the current design methods, including that above. Some attempts are made to quantify stress-rupture effects, by undertaking short term tests (up to 3 years), then extrapolating data using modified metallic creep models (e.g. Larson-Miller). To reduce the data scatter problems already discussed (7.3), a whole host of statistical normalisation techniques have been developed, to endeavour to ensure that the creep-rupture curve gradient is accurately determined (147), with little success.

All current design models suffer from a lack of physical significance. A linear relationship between stress and log (ttf) has been shown not to exist (figure 1.1), resulting in dangerous over-estimates of sample life, particularly in hostile environments (147). As a result, large safety factors still have to be applied, leading to uneconomic overdesign.

It can be seen that the methods currently used to determine the long term behaviour of GRP over several decades, are totally empirical. To improve this situation, damage mechanisms must be identified, and models developed, that are soundly based on the observed creep response. This is a complex problem due to the non-homogeneous, anisotropic properties of GRP, but must be overcome, before the full potential of GRP composites can be developed.

8.3. Creep prediction models

In recent years, a whole host of models based on the observed creep response have been developed, with varying success. Menges and Roskothen (165) regarded the laminate as a linear viscoelastic body. Complex stress-strain relationships were then developed, and substituted into Laminated Plate Theory (5.4). This model, apart from being unrealistically complex as a design criterion, suffers from other drawbacks. Firstly, most composites show non-linear viscoelastic response, and secondly, Laminated Plate Theory only applies to high performance, plied laminates, whereas most GRP is used in chopped,or woven,formulations.

The two most popular approaches to this problem are:-

(i) Time-temperature superposition

(ii) Chain-of-bundles theory

In the former, creep is regarded as a resin dominated effect, while in the latter, time dependent failure is considered to be fibre dominated.

8.3.1 Time-Temperature Superposition

The principles behind time-temperature superposition in polymers have already been summarised (7.1), and demonstrated schematically (figure 7.2). The assumption inherent to this model, is that temperature changes alter the rate of a deformation mechanism, not the mechanism itself. Many workers have extended the use of this theory to the area of resin dominated composite creep, such as Brinson and co-workers (166-170), Crossman and Flagg (171), Menges and Brintrup (172), and Daugste (173). All the theories are basically very similar, and this section will concentrate on one approach only (166).

An outline of the test procedure envisaged is given in figure 8.2. Firstly, time-temperature superposition is employed to obtain a creep compliance master curve for a unidirectional ply. Then, laminate theory is used

to predict the stresses in a laminate comprised of such plies, and finally, a failure model is used to predict fracture under given load conditions.

When compiling the ply creep compliance curve, vertical as well as horizontal, shifting has to be undertaken, because composites are thermo-rheologically complex (7.1). Data shifting is either undertaken graphically, or by means of specially developed statistical models. In either case, it represents a curve-fit exercise, the stages of which are shown schematically in figure 8.3.

The stress analysis required after the construction of ply creep master curves assume that linear viscoelastic behaviour occurs in the lamella. Finally, the long term stress-rupture life of a composite is predicted by using a suitable failure criterion, in conjunction with an incremental laminate stress analysis, to extrapolate short term, elevated temperature, test data to long design lives (around 30 years).

The basic T.T.S. model was found to be inadequate, particularly in wet environments, so further shift factors have had to be developed. Models, such as Time-Temperature-Stress (T.T.S.S.), and Time-Temperature-Stress-Moisture (T.T.S.M.S.), superposition have been developed (166). The introduction of each new shift factor pushes the model further from a physical, to an empirical status, since shifts are determined from test data, not theory. Despite these refinements, deviations from predicted response can still be seen to occur after 200 hours (figure 8.4).

The inadequacies of laminate theory and linear viscoelasticity have already been discussed (5.4.1, 7.1), the only source of error left to discuss is the assumption that one damage mechanism occurs throughout composite creep. It has been shown througout this review that a whole variety of damage is generated in GRP, dependent on stress, temperature and environment. Thus, the assumption that creep mechanisms at high test temperatures are identical to those that occur after long times, is highly

suspect, particularly when figure 1.1 is examined. The whole basis for the use of T.T.S. can be seen to break down in the vast majority of engineering composites, making design extrapolation from this complex approach highly inaccurate.

8.3.2 Chain-of-Bundles Theory

It has been shown (5.4.3) that a fibre composite can be modelled as a bundle of variable strength filaments embedded in a resin matrix, load transfer medium. This restricts load transfer from a broken filament to neighbours within a segment, d (figure 5.6) (75). Lifshitz and Rotem (174) outline chain of bundles theory for composites, producing an expression for probable failure strength (σ^*):-

$$\sigma^* = V_f \ (adBe)^{1/B} \qquad a, B \text{ are constants} \qquad -(8.4)$$

Load transfer occurs through matrix shear, so that when viscoelastic behaviour is exhibited by the resin, load transfer length, d, becomes an increasing function of time under stress, dependent on matrix creep properties. A schematic representation of this time dependent failure model (174) is given in figure 8.5.

As d increases, composite strength decreases, due to the increasing probability of encountering a severe fibre flaw, in high stress regions around a filament break. This is particularly serious where stress concentrated regions around breaks overlap, due to increases in d, since sufficient local loading may be induced to initiate an 'avalanche' of further filament breaks. In theory, d could become infinite, whereupon bundle strength falls to the level found in non-bonded rovings. While the detailed analytical model developed did not accurately predict failure (174), the basic approach outlined has potential for future development.

Other workers, such as Rotem and Elizov (95), Kelly and McCartney (175), and Aveston et al (176), have developed bundle theory a stage further, by superimposing moisture effects onto the above model. It was found that d increases in water due to debonding (174), which must be accounted for

in calculations,by determining interfacial bond strength as a function of time. Fibre degradation through stress-corrosion has also been included in the analysis (175, 176).

From Weibull statistics, the number of fibres (N) in a population (No), having flaws smaller than a length, a, is given by:-

$$N = No \exp -\left(\frac{ao}{a}\right)^{m/2} \qquad -(8.5)$$

where $$ao^{\frac{1}{2}} = \frac{K_{Ic}}{Y\sigma_o} \qquad -(8.5a)$$

K_{Ic} is the critical stress intensity factor, Y and σ_o are material constants During a stress-rupture test, these flaws grow to a critical length, initiating progressive filament failure. Expressions for the number of breaks occurring with time has been developed (175):-

$$\left[\left(\frac{F}{No\sigma oA}\right)^{n-2}\left(\frac{N(t)}{No}\right) - \frac{1}{m}\left(\frac{N(t)}{No}\right)^{n-1}\left(\ln\left(\frac{No}{N(t)}\right)^{\frac{n-2}{m}-1}\right]\frac{1}{No}\frac{dN}{dt}\right.$$

$$= \tfrac{1}{2}.a.K_{Ic}^{n-2}.Y.\sigma_o^{2}\left(\frac{F}{No\sigma oa}\right)^{n} \qquad -(8.6)$$

where F is the applied foce, A the cross sectional area, and n is a constant. From this, predictions of ttf through stress corrosion flaw growth can be made. Failure occurs as dN/dt becomes very large.

This model represents the best way forward in the development of prediction techniques. Problems due to stress concentrations, fibre orientation, and the effect of crimp in woven fabrics, still have to be overcome. To account for stress variations due to the use of fabric reinforcement, approaches similar to those described in 5.2.2 (20), may be incorporated into the bundle failure theory outlined. In time, such approaches will supplant the unsatisfactory standard techniques currently used.

PART TWO

EXPERIMENTAL WORK AND RESULTS

CHAPTER 9

MATERIAL CHARACTERISATION

9.1 Manufacture of test-pieces

Three laminate constructions were used throughout this thesis, the details of which are presented in table 9.1. Each of them were used for different test programmes:-

(a) Woven roving (w.r.)/'Cellobond' polyester. This was used for some of the porosity measurements undertaken (10.1), as well as early test work on the creep monitoring system.

(b) Single ply w.r./'Crystic' polyester. This was used for the determination of the fibre break density induced as a function of tensile pre-load (9.4).

(c) Mixed w.r./c.s.m./'Crystic' polyester. These samples were used in all the other tests described. They were laid up according to the C.E.G.B. specification previously used (3.4), except that no gel-coat was applied. This enabled direct comparisons to be made between test-pieces from the two programmes.

All the above samples were produced in the same manner, differences only coming in composition and post-cure schedule (table 9.1). The single ply sheets were laid up four to a mould, each layer separated by a sheet of Melinex release paper. In all other respects, manufacture of these plates followed the procedure used for mixed reinforcement laminates.

To begin with, the resin was outgassed under vacuum after it had been mixed with the accelerator and catalyst. This was done in an attempt to reduce the final porosity levels. It was found to have a negligible effect on the 100% w.r. sheets. With the mixed reinforcement samples, the resin "stippling" essential to wet out the c.s.m., induced sufficient air bubbles to counter balance any benefit from de-gassing. As a consequence, the practice was dropped when laying up the mixed reinforcement samples.

Sample sheets were made up from 350mm^2 reinforcement plies, which were impregnated with resin by means of a roller and brush, then pressed between glass sheets. Woven plies were laid up in a 0/90^o configuration, the warp direction being placed alternately at 0^o and 90^o, to counteract the unbalanced nature of most glass fabrics (2.3). To ensure constant thickness, the glass sheets were separated by 4mm^2 steel spacers, then clamped in a wooden frame to prevent warpage during cure. In each case, plates were left in the mould for 24 hours to cure, then demoulded and post-cured. Due to their unbalanced construction, single ply sheets were left in the mould during post-cure, again to prevent warpage.

From the above plates, samples of dimensions, 250 x 35mm, were cut, parallel to a roving direction. They were profiled to a "dog-bone" shape using a high speed router, giving an effective gauge length of 70mm (figure 9.1). Holes were drilled in the sample ends in order to attach the creep rig load train. The majority of test-pieces used were of this form, the exceptions being those used for residual strength, and fibre break density, measurements. Here, the requirement was for large numbers of samples (up to 24) to be cut from each plate. Thus, straight sided coupons, 150 x 25mm, were produced. For the residual strength tests, aluminium end tabs were glued onto the sample, using Araldite 2004 adhesive. This prevented acoustic noise generation from the loading grips influencing the recorded sample activity. (11.4).

9.2 Tensile properties

Prior to the determination of tensile strength, it was necessary to calculate the average glass volume fraction for the GRP used. This was used to calculate strength in terms of the Ultimate Tensile Unit Load (U.T.U.L.), according to equation 7.2. This measure has been found to reduce the variability associated with creep-rupture data (7.3).

Rectangular sections, 35 x 25mm, were cut from 3 mixed reinforcement sample plates, ground to ensure that the sides were parallel, accurately weighed,

and measured. From this, composite density was determined. The resin matrix was then burnt off at 450°C, and the remaining glass reweighed. Knowing the density of glass to be $2.56 \times 10^3 kgm^{-3}$ (9), the glass volume fraction was calculated from:-

$$V_f = \frac{Vg}{Vc} = \frac{Mg}{\rho g Vc} \qquad - (9.1)$$

where Vg and Vc are the volume of fibre and composite respectively, Mg, the mass, and ρg, the density, of glass. The average V_f determined was 0.27 ± 0.06, a value subsequently used when ever a measure of glass content was required.

The glass content of 100% w.r. samples was not determined in this study, since a measure of UTUL was not required. However, by examining polished sections, and referring to related test programmes (6), it was found that the V_f of these materials was virtually the same as above.

Tensile tests were performed on an Instron 1195 Universal Testing Machine, at a cross-head speed of 0.5mm/min. This rate was selected as being representative of that found during creep loading (12.3). Four samples from the w.r./c.s.m. material were tested, each cut from a different plate, to determine the variability in strength between GRP laminate sheets. Three 100% w.r. samples were also tested; in this case all test-pieces came from a single sheet. This was done to see how strength varied on changing the reinforcement patterm.

It can be seen from figure 9.2 that a 'knee' occurred in the load/deflection curve at approximately 20% of the breaking load. This behaviour is characteristic of woven fabric laminates (20). The results from this section are presented in table 9.2. Mixed reinforcement strength has been quoted in terms of its U.T.U.L., and ultimate tensile strength (U.T.S.), the latter being used as a comparison for the 100% w.r. GRP strength data.

From these results, it can be seen that the strength variability was little affected by reinforcement pattern; variability in both cases was approximately 7%. The same variability was found between plates of the same lay-up, i.e.

general variations in GRP strength outweighed any differences between sheets due to manufacture. It was also found that, on going from a 4 ply w.r., to a 2 ply w.r./4 ply c.s.m. lay-up, the strength was reduced by 25%, despite almost identical glass contents in the two materials.

9.3 Load rate tests

It has already been shown that GRP strength is dependent on the rate of load application (5.3). To confirm this, tensile tests were undertaken at 5 cross-head speeds, 4 samples being tested at each rate. The load rates used were 0.5, 1.0, 5.0, 10.0, and 50.0mm/min. Low rate tests were concentrated on, since this was the regime most pertinent to creep studies. Strain was monitored using a 25mm gauge length extensometer, attached to the sample by knife edges. From these tests, GRP strength and failure strain were obtained as a function of displacement rate.

Figures 9.3 and 9.4 show the results from this programme, where the error bars shown represent $\pm$ 1 S.D. from the mean value. It can be seen that, at displacement rates below 10mm/min, strength was independent of strain rate (figure 9.3). Above this value, increasing displacement speed led to an increase in sample strength, as predicted from the literature (62-64). Deviations from expected behaviour at low strain rates will be discussed in 13.2.

Failure strain against cross-head speed (figure 9.4), showed a 2-stage response. A minimum value of strain was recorded at 5.0mm/min. Below this level, the failure strain increased rapidly with falling test speed, rather than decreased as the literature would suggest. At high strain rates, behaviour again conformed to the predicted pattern, i.e. gradual increase in failure strain with increasing cross-head speed.

9.4 Fibre break density determination

In order to obtain an estimate of the level of fibre breaking that occurred as a sample was stressed in tension, a series of single plies 0/90% w.r. test-pie

were loaded to various fractions of the average UTUL, then examined. Load levels used ranged from 0-100% UTUL, a total of 11 samples being thus treated, one at each stress. A cross-head speed of 0.5mm/min was used during loading.

Having subjected each sample to the required pre-load, a 50mm long section was cut from the gauge length. The resin was burnt off from this section at 450°C, and the remaining glass mat carefully separated out into 0° and 90° rovings. From the 0° fibre bundles, about 200 filaments were carefully removed and placed in a petri-dish containing tetrahydrofuran (T.H.F.). This acted as a solvent for any remaining glass binder, helping to disperse the filaments. Great care was taken to ensure that the fibres were merely displaced latterally, while retaining their longitudinal position relative to each other. In this way, the position of fibre breaks in each roving could be determined, as well as their frequency.

After dispersing the roving bundle, the fibres were examined using a transmitted light microscope, at a magnification of 100X. The number of fibres present was determined, followed by the number of observed breaks, for each load level. Since fibres were nominally 50mm in length, fibre break density was calculated as the number of breaks per mm of fibre. Five filament bundles were examined from each sample, from which the average fibre break density could be determined as a function of applied load.

The results are shown in figure 9.5. A three stage curve was produced, with changes in behaviour occurring at 20, and 50% UTUL. It was also found, by studying the location of breaks, that a change in the observed damage occurred at 50% UTUL. Below this load level, fibre fractures were dispersed randomly throughout the sample, separated sufficiently to have no influence on each other. Above 50% UTUL, neighbouring filaments were observed to break side by side, creating roving transverse microcracks. This damage, termed multi-filament fracture (M.F.F.), consisted of between 2 and 8 neighbouring breaks. There was a general trend toward increasing numbers, and size of M.F.F. damage, as the level of pre-load applied increased above the threshold level.

CHAPTER 10

MICROSCOPY

A large proportion of the microscopy undertaken for this thesis concentrated on the study of samples tested in the course of previous creep-rupture programmes (3,4). By doing this, observations could be made on samples that had failed after long times (up to 3 years) under load in sea water, at a variety of immersion temperatures. The study of damage in immersed creep-rupture tests was undertaken mainly, using samples from the above programme. Test pieces taken from the dry creep tests performed for this thesis were also examined, to determine the damage accumulation that causes creep-rupture in air.

10.1 Pore density determination

The major problem encountered during creep-rupture testing of GRP, is the large spread found in values of time to failure (t.t.f.), obtained at a given load level. This leads to uncertainty in the prediction of the long term properties of these materials, which can only be alleviated by careful control of the contributing variables (5.3). The major cause of this variability is the variation found in GRP strength, since load levels applied during creep are calculated as a fraction of the average strength.

A major factor that affects the strength of a composite, is the level of porosity present (5. 3). Voids have been shown to act as stress concentrations, which reduce the applied load required to propogate failure. The level of porosity present was also one of the few variables that could be measured, so it was decided to investigate the effect of sample void content on its t.t.f. in a creep-rupture test.

The investigation was undertaken using two, related, approaches:-

(a) 5 samples that had all failed at the same load level, in an immersed creep-rupture test, were examined, and pore contents estimated. These results were then compared to the values of ttf found for each sample, to see if any correlation between porosity and life could be established.

(b) 2 groups, 4 samples in each, of 100% w.r. GRP samples were produced, one where resin outgassing had been undertaken (9.1), and one where resin agitation had been used,to deliberately increase porosity levels. Both sets of samples were loaded to 70% UTUL in water, and the ttf recorded, to see if any correlation existed between failure time and manufacturing process.

Sample void content was estimated in the same way for both sets of experiments. Sections through the test-piece were cut and mounted for examination, from a variety of locations along the gauge length. These sections were ground and polished using standard metallographic techniques, then examined at a magnification of 40X, using a projection microscope.

A graduated eye-piece was used to measure out a $10mm^2$ area of the sample. All voids falling within this region were then measured and, assuming a spherical cross section for resin pores, and a rectangular one for intra-roving voids (46), the area of each section filled by porosity was determined. Void content was then calculated according to equation 5.3. This was done for 3 section orientations,longitudinal, transverse, and planar, at 5 separate regions of the sample gauge length, giving 15 porosity readings per test-piece, from which the average void content was calculated.

The results from these studies are presented in table 10.1. Looking firstly at (a), an initial trend seemed to exist linking low void content with long ttf. Figure 10.1 shows the porosity found in a sample with a failure time of about 10 days, while figure 10.2 is of that found in a test-piece that failed after 1 day at the same load. When pore counts were undertaken, however, no correlation between void content and ttf was found.

When samples from (b) were examined, no correlation was found to exist between ttf and manufacturing process, i.e. outgassing had no effect on the sample

creep-rupture properties. Furthermore, no significant difference in the level of porosity present could be found between outgassed, and untreated, samples; all results fell in the range 2-4%. Degassing reduced the resin void content by approximately 50%, but the level of intra-roving porosity was, if anything, higher. This was due to a decrease in fibre wetting that accompanied attempts to reduce resin void content. Because of this, it was decided to discontinue the practice of resin vacuum outgassing.

10.2 Fractography

The fracture surfaces from approximately 50 creep-rupture samples have been examined, 30 after failure in water at a variety of stresses and temperatures, and 20 after testing in air. In all cases, the procedure used to study them was the same as that described below.

The fracture surface was removed with a hacksaw, mounted on an aluminium planchette, then gold sputter coated, to make the sample conducting. Because of the large area of surface to be coated, 2 separate treatments were undertaken to ensure an adequate covering of gold was applied. The sample was then examined using a JEOL 35D scanning electron microscope (S.E.M.), fitted with an EDAX facility (10.4). Movement of pull out fibres in the electron beam proved to be a problem at high magnifications, but despite this many useful observations were made of the damage created during creep-rupture.

It would be expected that, if failure in water occurred through stress-corrosion (c.f. acidic environments), the fibre pull-out lengths at the fracture surface should decrease as a function of time immersed (7.4). Figures 10.3 and 10.4 show that this did not happen. The only change in length observed occurred when comparing immersed, with dry, creep-rupture behaviour. In the latter case, pull-outs were so extensive that fibres had to be trimmed, in order to fit into the microscope.

Lyons (5) showed that creep-rupture in csm/polyester laminates initiated through stress-corrosion. It was found that the failure path could be traced back to a region of slow crack growth, identified as a zone of short fibre

pull-out. In the samples examined for this thesis, fibre overlay made examination of the resin bed difficult, but no evidence of the above behaviour was observed . The only regions of short fibre pull-out observed occurred around stress concentrating defects, such as resin rich regions (figure 10.5). Examination of the resin bed also revealed the existence of intra-roving voids, aligned parallel to the transverse woven rovings (figure 10.6).

No obvious differences were found between the fracture surfaces of dry and immersed creep samples, except for the longer pull-outs found in air. Therefore, it was decided that the differences known to exist between ttf in the two environments, was due to aqueous attack of the fibre/matrix interface, and the E-glass reinforcement itself. So, a more detailed examination of these regions was undertaken.

10.3 Fibre surface studies

The examinations undertaken in this section again used the S.E.M., the work being split into 2 sections:-

(a) Fracture surface pull-out fibre condition

(b) General fibre condition, away from the failure region.

The latter studies were undertaken by cutting a section from the sample gauge length, and burning the resin off at 450°C. The remaining glass plies were separated,and mounted on aluminium planchettes for examination. To prevent filament movement, an aluminium foil collar was used to secure the fibre ends. This left a section, 10 x 15mm, of the ply surface visible for study. Finally, a 2-stage gold sputter coating was applied, prior to insertion in the SEM.

In order to be able to examine the condition of fibres at the interior surfaces of woven fabric fibre cross-overs, glass mats were also separated into warp and weft rovings. These were then mounted individually, cross-over interior regions uppermost, in the manner described above . 10 test-pieces were examined in this way, 4 from samples that failed in air after up to 1 month, and 6 from samples that had been loaded for similar times prior to failure, in water at 60°C.

10.3.1. Pull-out studies

One of the first observations made was that, rather than individual filaments breaking at a random position along their length and pulling out, it was sometimes found that M.F.F. pull out occurred. The number of neighbouring breaks observed varied from 5 (figure 10.7 (a)) up to a significant fraction of the total roving population (figure 10.7 (b)). These features were found to occur in the longitudinal woven rovings, at the peaks of the transverse roving cross-over regions (figure 10.8), i.e. regions of high local fibre stress. All the examples shown are from samples tested in air, but the same damage was also found after immersed creep-rupture testing.

When individual filaments were examined at high magnification, considerable differences between dry and immersed sample condition became apparent. Figure 10.9 (a), taken from a sample that had failed after 1 day at 60% UTUL, in water at 60°C, shows that fibre /matrix bonding had been severely degraded by the water, with no residual resin debris present on the fibre after pull out. Comparing this with a fibre from the fracture surface of a sample loaded to 70% UTUL in air for a similar time (figure 10.9 (b)), showed that in this case, interfacial bonding remained coherent up to failure. This resulted in the formation of a firmly bonded resin sleeve on the load bearing fibres after fracture.

Samples that had been immersed in water at 60°C, at a load level of 25% UTUL, for $2\frac{1}{2}$ months, showed direct evidence of fibre degradation on the surface of the pull-outs. Figure 10.10 shows the condition of such filaments, both in the region of fibre fracture (figure 10.10 (a)) and areas remote from this zone (figure 10.10 (b)). Damage, in the form of surface leaching, was fairly severe around the fibre break, decreasing in severity away from this region. This would be expected, since fibre failure occurs at the weakest point along a filament, which in this case would be the point most severely degraded by the moisture.

In order to confirm that the observed damage was induced by moisture,

dry creep test sample pull-out fibres were also examined. Where it was possible to study fibre surface condition, such as regions where intra-roving porosity had created local areas of interfacial breakdown, none of the above damage was found. It was also shown that this damage was absent from fibres studied prior to resin encapsulation (figure 10.11), i.e. it was not a manufacturing defect.

10.3.2. Resin burn-offs

Having established the existence of fibre corrosion pit damage in immersed creep test-pieces, it was necessary to establish the location of this damage in the composite as a whole. When reinforcement plies from such samples were examined, no corrosion damage was found on the outer ply surfaces (figure 10.12). However, when individual rovings were examined, corrosion pits were found in longitudinal fibres. This damage occurred on the interior surfaces of weave cross-overs (figure 10.13). The occurrence of this pitting was highly random, and attempts to quantify the growth of damage as a function of time immersed under load, were unsuccessful.

When the reinforcement from dry creep test-pieces was examined, no evidence of moisture induced fibre weakening was found, even in the interior regions of weave cross-overs. To ensure the damage observed was not an artefact caused by charging in the electron beam, samples were re-coated several times, being examined between each treatment. No change in the damage shown was found to occur, confirming the damage to be a real effect.

10.4 EDAX analysis of resins

If the damage described above (10.3) was due to the leaching of network modifier ions from the glass surface (2.5), it would be expected that an increase in the concentration of these ions (Na^+, K^+, and Ca^{2+}) would occur in the resin matrix, during immersed creep-rupture testing. To study this, the composition of the matrix from the GRP tested was analysed, using the EDAX facility present

on the SEM used for this work.

Three resin conditions were analysed:-

(a) 'As-cast ' resin,i.e. no glass present

(b) Matrix composition after creep testing in air

(c) Matrix composition after creep testing in distilled water at 60°C.

The resin composition from 3 samples was analysed in (b) and (c), while only 1 'as cast' sample was examined. Gold coating had to be undertaken to prevent sample charging, but the coating deposited was thin enough to allow the beam to penetrate to the resin substrate. The beam was focussed on resin rich regions between fibres, to prevent errors due to the presence of glass. In all cases, a 100 second scan was undertaken,at a magnification of 20,000X. All other parameters, such as horizontal and vertical display scaling on the EDAX unit, were also kept constant, to allow direction comparisions to be made between treatments.

Three representative EDAX spectra are shown in figure 10.14. It can be seen that, for the 'as cast' resin (figure 10.14 (a)), the only peaks visible were due to the gold coating. EDAX is unable to detect low atomic number species, e.g. C, H, and O, and so the pure resin composition cannot be determined by this method. The analysis of resin from dry creep test-pieces (figure 10.14 (b)), showed the existence of small amounts of calcium, probably from sub-surface fibres. The silicon content of such fibres was masked by the large gold peak present. Lastly, when the resin from immersed creep-rupture samples was analysed, considerably higher levels of calcium were detected (figure 10.14 (c)). This increase was attributed to the dissolution of calcium from fibre surfaces. No increases in sodium and potassium levels in the matrix were found.

10.5 Optical microscopy

Sections taken from well over 100 samples, covering the whole range of tests performed for this thesis, were mounted and polished as before (10.1), then examined using a projection microscope. Useful information on GRP

performance under load has been obtained, some of which will be outlined in this section, while the remainder will be covered later (11.3).

Two types of void have been identified, as previously mentioned (10.1). Figure 10.15 shows how resin voids, created by gas entrappment during cure, often form at matrix/roving interfaces. These voids act as stress raisers, initiating matrix cracking under load (figure 10.16), a serious problem when this occurs at the interface. The second, and in general more damaging (5.3.1) type of void,was found to occur within rovings (figure 10.17). They were elongated parallel to the woven fibres, producing regions of debonding. Since intra-roving porosity resulted from incomplete resin penetration into the tightly bound woven rovings, there was a tendency for these defects to form at the most inaccessible regions of the fabric, i.e. weave cross-over interfaces (figure 10.18). These voids were also seen to act as crack intiation sites (figure 10.19).

Cracking was found to occur in "as received" samples, particularly in the region of weave cross-over points (figure 10.20). This was attributed to differential thermal contraction of the matrix and reinforcement after post-cure. This region of the material was also shown to act as a damage initiation site when under load (figure 10.21), further demonstrating the stress raising nature of cross-overs.

When under load, various other forms of damage have been identified. Transverse cracking, created at low loads prior to the onset of creep (9.2.), was found to occur in both immersed and dry creep-rupture samples. This was accompanied by severe roving cracking and debonding. (figure 10.22).

CHAPTER 11

MOISTURE EFFECTS

11.1 Water uptake measurements

In order to characterise moisture absorption in glass/polyester laminates, a series of water uptake tests were performed on samples, subjected to a variety of temperatures and stresses. Since the samples used were not pre-dried, it was first necessary to determine the moisture content of 'as received' material. This was done by weighing a sample, then drying it at 60°C. Weight loss was monitored until 2 consecutive readings were the same. Since this loss was due to the desorption of water from the sample, moisture content was expressed as:-

$$\% \text{ Moisture Content} = \frac{Mi - Mf}{Mi} \times 100 \qquad - (11.1)$$

where Mi was the initial, and Mf the final, recorded sample weights.

To determine the effect of both temperature and stress, the following test conditions were used. Immersion in distilled water at:-

(a) Room temperature (23°C)
- (i) 0% UTUL
- (ii) 40% UTUL
- (iii) 60% UTUL

(b) 60°C
- (i) 0% UTUL
- (ii) 30% UTUL
- (iii) 60% UTUL

In each case, around 18 samples were used. Rectangular test coupons were used for the zero load tests, while standard 'dog-bone' creep specimens were used for the remainder of the work. The load levels chosen were selected to give estimated failure times of 2 and 40 days, according to figure 1.1.

For the zero load measurements, all the prepared test coupons were immersed at the relevant temperature level, then individually removed from the environment at regular time intervals up to 44 days. On removal, a section was cut from the sample for future examination, and the remainder immersed in water at room temperature for 30 minutes, to compensate for any weight loss during cutting. After this time interval, the coupon was retrieved, surface moisture removed, and then accurately weighed. It was then dried at 60°C until constant weight was achieved, then moisture content calculated according to equation 11.1. Drying took about 2 weeks. In this way, curves of moisture uptake against time immersed were built up.

For the measurement of uptake when under stress, each group of samples was loaded in the creep rig (12.1) to the required level, then individual test-pieces removed for examination at regular time intervals, chosen to cover the estimated ttf range. On removal, a rectangular section was cut from the sample gauge length, then immersed for 30 minutes in room temperature water. Moisture content was then determined using the method outlined above. The remainder of each sample was retained for future studies. (11.2 - 11.3).

11.1.1. Water uptake at room temperature

Figure 11.1 shows the results obtained for all the tests undertaken in distilled water at 23°C. The 'as received' moisture content used was 0.26%. The scatter in results found was fairly large, as is usually found in measurements of this kind. It was found that the applied load increased both the uptake rate, and overall moisture content, in the manner expected (6.2). Initial uptake rate increased by 30% under load, from 0.7%/day at 0% UTUL, to 1.0%/day at 60% UTUL.

11.1.2 Water uptake at 60°C

Figure 11.2 shows uptake at elevated temperatures. Applied load

affected uptake in an identical fashion to that at 23°C. The change in temperature was found to increase both uptake rate, and overall moisture content, at each load level. For example, after 40 days, moisture content at 60°C was twice that at 23°C for the same stress conditions, while the initial uptake rate was increased by 38% under load, going from 1.1%/day at 0% UTUL, to 1.8%/day at 60% UTUL.

11.1.3 Moisture content after long term immersion

Two samples that had been loaded in water for long times were dried at 60°C, and the weight loss recorded against drying time, to determine the effect of stress and temperature on the maximum moisture content of GRP. The 2 samples had been subjected to the following conditions:-

(a) 18 months at 20% UTUL in water at 40°C

(b) 3 years at 35% UTUL in water at 23°C.

The results from this work are shown in figure 11.3. It can be seen that sample (a) absorbed 3.5% moisture, 1% more than (b), showing the dominant effect temperature had on water absorption.

11.1.4 Ficks Law moisture uptake

In order to calculate diffusion coefficients for each of the above treatments, figures 11.1-11.3 were replotted as uptake vs. $\sqrt{t}$ (6.1). It was found that diffusion in all the tests was anomolous, whether results determined from repeated measurements on a single sample (figure 11.4), or from separate samples tested for different times (figure 11.5), were considered. In the light of other work (see below), the additional effort required to estimate diffusion coefficients from this data, using models that account for variability in sample composition, did not seem to be justified.

11.2 Debonding studies

Having removed a section for water uptake measurements, samples from

the above programme were examined to determine the growth of moisture induced debonding, particularly in the load bearing w.r. plies, as a function of time under the various test conditions described (11.1). Samples were studied using transmitted light, debonding being revealed as regions of shadow in the otherwise translucent material. Having found the observed debond damage to be irreversible on water desorption, samples from the zero load water uptake test were examined after drying (11. 1). In all cases, a record of the damage found in a sample after immersion, was recorded using a camera fitted with a 105mm close up lens.

To determine the moisture transport route into loaded samples, 2 test-pieces, with edges sealed using silicone rubber, were loaded to 60% UTUL in water, at 60°C. The level of debonding found on failure, after 2 days, was then compared to a sample that had failed after 1 day, under the same conditions, with exposed edges.

Finally, the build up of weave debonding with time was quantified, for samples tested at 60°C. To do this, photographs taken of samples were over-laid with tracing paper, and the test-piece outline, and regions of debonding, sketched out. These tracings were then placed upon standard metric graph paper, and an estimate of the total area of each test-piece covered by weave debond patches was obtained through square counting. This was done for 5 samples, at each load level, immersed for varying lengths of time, from which curves of % weave debonding against time immersed could be drawn.

11.2.1. Debonding of immersed samples under zero load

(a) 23°C - At room temperature, no significant levels of debonding were detected after 47 days in water, even in the outer c.s.m. plies.

(b) 60°C - At elevated temperatures, the rate of debonding was accelerated, outer c.s.m. debonding being first observed after 1 day by the increased prominence of the fibres (figure 11.6 (a)). This continued to expand, being virtually complete after 11 days (figure 11.6 (b)). Weave cross-over debonding, initiating from sample edges, was first detected after 15 days (figure 11. 6 (c)).

From these 2 tests, the influence of temperature on the speed of interfacial breakdown in these materials was demonstrated.

11.2.2. Debonding of samples loaded to 30% UTUL in water, at 60°C

It was found that outer c.s.m. debonding occurred under load at the same rate as above (11.2.1. (b)). However, interfacial degradation occurred much faster in the w.r. plies. This damage was concentrated at the weave cross-over regions, producing a characteristic 'chequer-board' pattern of shadow under transmitted light. Weave debonding was first observed after just 1 day (figure 11.7 (a)), at the sample edge, and it had spread throughout the sample by day 7 (figure 11.7 (b)). No transverse cracking was observed in these samples when unloaded, despite the fact that such damage was found to occur at 20% UTUL when loaded in a tensile strength test (11.4), i.e. cracking at 30% UTUL was reversible on unloading.

11.2.3. Debonding of samples loaded to 40% UTUL in water, at 23°C

This was the same, in principle, as found at zero load, i.e. debonding rate was reduced in comparision to samples loaded at elevated temperatures, but the general trends in damage formation were the same. No significant levels of outer c.s.m. debonding were found after 47 days (c.f. 11.2.1. (a)). Weave cross-over debonding was first detected at the sample edges after 7 days, but damage propogation at this temperature was so slow, that no 'chequer-board' pattern of shadow was established by day 47 (c.f. 11.2.2.) Samples loaded to this level were found to contain permanent transverse crack damage.

11.2.4. Debonding of samples loaded to 60% UTUL in water

(a) 23°C - The effect of increasing the applied load at room temperature, was to accelerate the rate of weave debonding (c.f. 11.2.3.). In this case, woven roving debonding was first observed after 2 days, and by the time failure

occurred (day 4), a faint pattern of 'chequer-board' shading had been established throughout the sample. Again, no outer c.s.m. debonding was observed at this load level.

(b) 60°C - At this temperature, weave debonding was very rapid, being first observed at the sample edges after just 1 hour (figure 11.8 (a). After 7 hours, woven ply interfacial breakdown was virtually complete (figure 11.8(b)). Outer c.s.m. debonding was not found at this load level because sample failure occurred in 1 day, whereas c.s.m. breakdown was shown to require longer immersion times than this (11.2.1).

In both of the above cases, severe transverse crack damage was created. By sealing the sample edges, preventing water flow through these cracks, it was found that the level of weave cross-over debonding damage was greatly reduced. Figure 11.9 shows the condition of an edge sealed sample after 2 days in water at 60% UTUL, and 60°C.

11.2.5. Summary of debonding observations

(a) When immersed under zero load, diffusion of water into the sample occurred mainly through the sample faces, with the outer c.s.m. debonding first.

(b) Face dominated diffusion rate was temperature dependent, but insensitive to load.

(c) On loading, transverse cracks were created, allowing rapid moisture ingress to occur via samples edges, through capillary flow up these channels.

(d) Edge diffusion rate was both temperature, and load, sensitive.

(e) Under load, weave debonding occurred at the highly stressed roving cross-over regions, producing a 'chequer-board' pattern of interfacial degradation.

(f) Increasing the test temperature accelerated, rather than altered, the mechanisms of diffusion and debonding.

11.2.6 Analysis of debonding at 60°C

Figure 11.10 shows the results from the quantitative analysis of weave debonding as a function of immersion time, at the 3 stress levels used. It can be seen that increasing the applied load led to an increase in the rate of weave cross-over debonding, and a reduction in the time required to initiate this degradation. At 30% UTUL, a maximum debond level of 65% was attained after 30 days, after which no further degradation was observed. Despite the rapid nature of debonding at 60% UTUL, this level of debonding was not attained, due to the low ttf at this load, i.e. failure occurred before debonding was complete.

A plateau at 8% in the amount of debonding, was reached by day 20 for samples immersed under zero load. However, after 44 days, a further increase in debonding was becoming apparent. This trend was confirmed by looking at samples immersed under zero load for 6 months at 60°C (11.4), where weave debonding had reached the 65% level.

Finally, some thought was given to the prediction of moisture content as a function of time, using diffusion laws. This was required as a measure of the moisture induced property degradation to be expected in GRP. Figure 11.11 shows the relationship between moisture content, and the level of debond damage at 3 load levels. This was found by cross-plotting data from figures 11.2 and 11.10. For example, to produce a level of 10% weave debonding would require a moisture content of 2.8% at zero load, but only 0.9% at 60% UTUL. Thus, it can be seen that the relevant parameter for assessing moisture degradation in GRP, containing woven fabric plies, is the location of moisture concentrations, rather than the overall level of uptake. Thus, it was felt unnecessary to calculate diffusion coefficients for the material studied.

11.3 Moisture induced matrix cracking studies

To assess the contributions made by temperature, moisture, and stress, to the growth of damage during creep loading, sections cut from samples from the

above programmes (11.1-11.2), were mounted and examined using an optical microscope. The test conditions studied were as before, i.e. immersion in distilled water at:-

(a) 23°C
- (i) 0% UTUL
- (ii) 40% UTUL
- (iii) 60% UTUL

(b) 60°C
- (i) 0% UTUL
- (ii) 30% UTUL
- (iii) 60% UTUL

A section cut from each of the samples tested under the given conditions was examined, to establish the manner of damage accumulation with time at each test condition.

11.3.1. Damage development during immersion at zero load

The general pattern of matrix crack growth found was the same at 60°C as that found at room temperature, and the following description applied to both test temperatures. No cracking was found in 'as received' samples (figure 11.12 (a)), and this remained the case until test- pieces had been immersed for 6 days. At this time, moisture induced crack damage was observed to initiate from internal defects, such as resin voids (figure 11.12(b)). This cracking then became more pronounced as immersion time increased.

11.3.2 Damage development during immersion in water at 30% UTUL and 60°C

At this stress level, no transverse crack damage was found to occur on loading (figure 11.13). There was no observed change in the pattern of damage growth from that outlined above, i.e. applied load had no effect on the level of internal matrix cracking found during immersion in water.

11.3.3 Damage development during immersion in water at 40% UTUL,and 23°C

Transverse crack damage, initiated on loading, was observed to occur at this load level (figure 11.14). After this, further matrix cracking initiated after 6 days (figure 11.15) in the same manner as described in 11.3.1.

11.3.4 Damage development during immersion in water at 60% UTUL

In this case, after initial loading induced transverse crack creation, no further growth in damage was observed, either at 23°C or 60°C. Since moisture induced cracking initiated after 6 days, while samples at this load had a ttf of upto 4 days, this would be expected.

11.3.5 Summary of observations

The growth of matrix cracking within immersed samples of GRP was found to depend solely on the presence of moisture, and was independent of both applied load and temperature. Thus, any differences in laminate response found under the various test conditions described, must have been due to the growth of debonding in the fabric reinforcement (11.2),and aqueous corrosion of the fibres themselves (10.3).

11.4 Residual strength tests

A series of tensile tests were performed to determine the effect that immersion at zero load for long times (6 months) had on the strength of the GRP used. Two immersion temperatures were used:-

(a) Room temperature (23°C).

(b) 60°C

For each set of tests, 24 test coupons were cut from a single GRP sheet, as stated in 9.1. Twelve of these samples were then immersed at the required temperature in distilled water, for 6 months. The remainder were tested dry, to provide a reference strength.

Tests were performed on an Instron 1195, at a cross-head speed of 0.5mm/min, to allow acoustic monitoring of the test. Eight samples, from each of the 4 groups, were monitored to failure,using an AETC A.E. System, linked to a microcomputer for data collection and analysis. Using software developed at Bath University, plots of total acoustic events, and load, against deflection, were produced. The remaining 4 samples from each group were monitored photographically, 2 using ordinary, and 2 cross-polarised, transmitted light. The latter was used to reveal stress fields created on loading. Test-pieces were back-lit, and photographed at 10 second intervals, from zero load to failure, using a camera equipped with a 105mm close up lens. In this way, a record of damage accumulation during loading was obtained,for each of the pre-conditioning treatments used.

The results from this work, are presented in table 11.1. Strength loss was measured as the difference between the average dry,and pre-soaked, U.T.S. for each test plate. A slight drop in strength of 15% was recorded after soaking at 23°C, but at 60°C, degradation was much more severe, and a strength loss of 30% was recorded. Sample condition before and after pre-soaking at 60°C is shown in figure 11.16. Condition after immersion at 23°C was unchanged from that observed in dry test-pieces.

11.4.1. Acoustic behaviour of dry samples

A very high level of acoustic activity was recorded throughout sample loading, first damage occurring at about 20% of the fracture load, where the load/deflection curve 'knee' point was located (figure 11.17 (a)). It was found that samples pre-soaked at 23°C produced identical results to these outlined for tensile testing of dry material.

11.4.2 Acoustic behaviour after pre-soaking at 60°C

Considerable changes in behaviour were found after this pre-condition treatment. The load/deflection 'knee' point became less pronounced, and

occurred at around 9% of ultimate load. Acoustic activity was greatly reduced (figure 11.17(b)), and the point of onset less distinct.

11.4.3 Photographic monitoring of dry tensile test

Transverse cracking was first detected at a load of approximatley 20% UTUL (figure 11.18). When studied under cross-polarised light, it was found that outer ply loading commenced at this stress (figure 11.19), i.e. c.s.m. became load bearing above the load/deflection 'knee' point.

Damage initiation, from the sample edges, commenced in the c.s.m. plies at 50% UTUL (figure 11.20 (a)), while a load level of 70% UTUL was required to induce weave cross-over stress whitening (figure 11.20 (b)). Cracks began to form in the longitudinal woven rovings at 80% UTUL, initially at the sample edges (figure 11.20 (c)). On further loading, these cracks continued to grow, eventually coalescing to produce fracture (figure 11.20 (d)). Samples pre-soaked at 23°C behaved in exactly the same manner as described above.

11.4.4. Photographic monitoring of tensile behaviour after pre-soaking at 60°C

Considerable debond whitening had occurred during preconditioning, and this led to a change in behaviour from that found in dry tests. Figures 11.21 and 11.22 give a comparison of the sample condition under load of dry (figure 11.21), and pre-soaked (figure 11.22), test-pieces when studied using cross polarisers. In the latter case, no damage build up was observed during loading prior to fracture, and there was a complete absence of stress pattern colouration throughout the test.

CHAPTER 12

CREEP STUDIES

12.1 Development of monitoring system

The creep rigs used for this thesis comprised 8 lever arm loading points, attached to a steel frame. Samples were attached to the load arms using bolted end plates (figure 12.1). A stainless steel tank was placed between the load arms, allowing sample loading to be achieved during immersion in distilled water (figure 12.2). Weights were applied to the far end of the load arm. Due to the lever arm ratio used, the sample stress was magnified by a factor of 20. Initial loading of a sample was achieved by supporting the arm with a scissor-jack while the weights were attached, then lowering at an approximately constant rate until the sample supported the load.

Much of the monitoring of creep in GRP previously undertaken, particularly in water, has used transducers attached to the loading arms to monitor deflection (124). This leads to uncertainty, since the results obtained could be due to a load rig artefact, rather than true material deflection. Thus, it was decided to monitor creep deflections directly from the test-piece gauge length, to determine whether secondary creep was continuous, or occurred in discrete steps. Strain gauges were selected for these measurements.

Several problems accrued from this decision:-

(a) Anisotropic strain fields - on loading, the strain levels within a composite are highly variable, and great care was needed to ensure that readings were realistic.

(b) Small secondary creep strains - the readings of deflection obtained during secondary creep can be swamped,by thermal expansion in the sample, or i^2R losses in the gauge circuitry.

(c) Zero drift in water-strain gauges exposed to water fail to operate properly after a short time.

(d) Gauge failure on loading - it was found that, when gauges were attached to the sample faces using the recommended polyester adhesive, transverse cracks, formed during loading, passed through the gauge, making them inoperative.

To overcome these problems, the following procedures were used:-

(a) Strain gauges of 30mm length were used, to produce a representative "average" output.

(b) Dummy gauges were used, in a half-bridge measuring circuit, to balance out any deflections due to thermal expansion. To reduce i^2R losses, gauge leads were all cut to the same length, which was kept below 1m.

(c) Araldite epoxy adhesive was used as a moisture barrier, both by coating the exposed gauge face and connections, and attaching the gauge to the sample. The latter prevented moisture attack from behind.

(d) Gauge cracking was alleviated by attaching it to the sample edge, rather than the face.

Having developed a means of converting sample deflection into an electronic signal, a system for processing and recording this data was required. It was decided to use a Commodore PET 4032 micro-computer to collect data, so an analogue/digital converter had to be built, that was capable of monitoring 8 strain channels from the creep rig, for times of up to 1 year. Because of the requirement for long term accuracy, it was essential that the A/D had low drift characteristics, producing errors below the required strain resolution (0.01% strain).

The monitor was developed, and built, 'in house'. Microprocessors were chosen for their low drift, rather than high speed, characteristics, giving a channel scan rate of 4 seconds. To improve detection sensitivity, a variable gain amplifer was used. This gave an amplification of 5 to 50dB, the former level being used throughout these tests. Channels were read in sequence, the reading being fed, via a multiplex unit, to the computer's memory.

The software used to monitor creep was adapted from a programme kindly supplied by workers at Liverpool University. A machine code sub-routine was written to run the strain monitor, and it was called up every 35 seconds by the main programme, to scan the gauge output. Increases in strain were then

stored on floppy disc, along with the elapsed time. From these data files, strain readings were printed out, and creep curves manually drawn, on completion of a test. The monitoring equipment used, including a PAC 3004 AE Analyser (12.3-12.5), is shown in figure 12.3.

12.2 Interrupted creep tests.

A series of 16 samples were loaded to 72% UTUL in air, and then removed for examination individually, at regular intervals upto 32 days. Sample condition after unloading was recorded using transmitted light photography, after which, sections were cut and polished, for examination using an optical microscope. In this way damage accumulation, both cracking, and stress whitening around fibre rovings, during a dry creep test could be monitored.

On loading the samples, transverse cracking was found to occur. There was no increase in matrix damage found during the time under load, and stress whitening due to debonding in the load bearing w.r. plies, was not observed until immediately prior to failure. This confirmed that the debonding found earlier (11.2) resulted from the action of the aqueous environment, rather than the applied load.

While the polished sections showed no increase in cracking with time, macroscopic transverse cracks, up to a roving width in length, were found to occur at irregular time intervals (figure 12.4). This periodic damage was also found to occur in immersed creep tests, where debond shading revealed this cracking to occur at the roving cross-overs. It was observed that final fracture tended to occur through coalescence of these roving transverse cracks, normally at the neck of the 'dog-bone' profile.

12.3 Creep tests in air

Using the apparatus described in 12.1, a programme of creep testing in air was undertaken. Six load levels, in the range 57-85% UTUL, were investigated. Between 4 and 8 samples were loaded at each stress. Creep strain as a function of elapsed time was recorded for all samples. In addition,

acoustic activity was monitored in at least 50% of the samples tested at each load level.

Acoustic activity was monitored using a PAC 3004, Four Channel Real Time A.E. Analyser unit, data being stored on floppy disc for future analysis. The system was run in 2-channel mode, allowing 2 samples to be monitored simultaneously, to conserve disc space. Due to limitations on the time register, tests could only be monitored for 18 hours, so for long ttf samples, only the initial acoustic activity was recorded. From the stored data, print-outs of total events, and event amplitude, against elapsed time, were produced. To ensure result comparability, all data was collected at a gain of 60dB, with a 0.2V threshold level.

12.3.1. Creep monitoring

Traditional creep-rupture data for this material was generated by this programme, the results of which are presented in table 12.1, and figure 12.5. In the latter case, the error bars represent the difference between the lowest, and highest, recorded time to failure (ttf). It can be seen that at high loads, in excess of 80% UTUL, there was an increase in creep-rupture, plot gradient.

Figure 12.6 presents a series of creep curves drawn for samples tested at a variety of load levels. Below 80% UTUL, classical 3-stage creep behaviour occurred, though in most cases, failure was so rapid that the tertiary creep region was not detected. Secondary creep was found to increase in discrete steps, these occurring at irregular time intervals. Above 80% UTUL, the secondary creep region became vanishingly small, with failure initiating immediately after primary creep. This transition coincided with the gradient change in figure 12.5.

12.3.2 Acoustic emission monitoring

The acoustic event vs. time curves found for the above samples, were of a 3-stage form, similar to the creep curves described above. This similarity can be seen in figure 12.7(i), where the acoustic data collected at a variety of load levels is presented. Total events recorded were found to decrease with reductions in applied load.

When event amplitude vs. time charts were studied (figure 12.7 (ii)), periodic high amplitude peaks were found to occur during secondary creep, in samples loaded to levels up to 80% UTUL. These peaks were of a similar intensity to amplitude levels recorded during loading, where transverse cracking was observed to occur. Above 80% UTUL, signal amplitude remained at a constant, high, level throughout the test.

Comparing event amplitude data with the corresponding sample creep curve, showed that several of these high amplitude peaks occurred at the same time as the secondary creep strain jumps (figure 12.8). The remaining signal peaks were attributed to damage growth outside the measuring range of the strain gauge.

12.3.3 Analysis of creep data

From the creep curves produced, various other parameters were plotted against applied load, as defined in figure 12.9. ε_i, the maximum primary strain induced at a given % UTUL, was proportional to the actual applied stress in the sample. ε_s, the maximum secondary creep strain, was used to denote the creep failure strain, since on passing into the tertiary creep region, fracture is considered to initiate (126). $\varepsilon(t)$, the total creep strain, was simply defined as the difference between ε_s and ε_i.

When these parameters were plotted (figure 12.10), some interesting observations were made:-

(a) A linear relationship existed between both ε_s, and ε_i, and applied

load, the latter extrapolating to zero at 0% UTUL in the manner expected.

(b) Total creep strain decreased with increasing applied load, extrapolating to zero at 100% UTUL, again, an expected result .

(c) The level of creep failure strain (ε_s) was always in excess of the previously determined minimum tensile failure strain for this material. (9.3). By extrapolating ε_s back to this strain level (shown as the line AB), a creep-rupture limit was defined to exist at the corresponding load (15.5.1.). This limit was found to occur at 50% UTUL.

It was further found that a plot of ε_i vs. ttf (cf. creep-rupture curve, where ε_i was proportional to the applied stress), tended to a limit, at a level of ε_i produced by applying a stress of 50% UTUL (figure 12.11). Thus, both sets of data produced identical creep-rupture limits.

12.4 Immersed creep studies

A series of creep tests were performed on samples immersed in distilled water at room temperature, in the above manner. In this case, 4 replicate tests were undertaken,at each of 8 load levels, in the range 39-85% UTUL. Two samples at each load level were monitored using the A.E. analyser, as well as the strain monitor. To accomplish this , a small region at the top of the sample was left unimmersed, and the A.E. transducer attached at this point. Strain gauges were coated,to prevent moisture degradation (12.1).

The results obtained during acoustic emission monitoring were identical to those found during creep in air (figure 12.7).

12.4.1 Creep monitoring

From the creep-rupture data collected during these tests (table 12.2) it can be seen that the presence of an aqueous environment reduced GRP failure times, at load levels below 80% UTUL (figure 12.12). Above this

level, behaviour became environment insensitive.

Some typical creep curves obtained in this section are shown in figure 12.13. It can be seen that the basic form of creep response was identical to that found in air. The major differences found were matters of detail. Firstly, the overall level of creep in water was increased over that found in air, and secondly, tertiary creep was more often observed to occur, i.e. immersion in water extended the tertiary region. Finally, creep-rupture occurred at load levels previously stated not to cause time dependent failure in air (12.3.3.)

12.4.2 Analysis of creep data

An identical procedure to that outlined in 12.3.3. was followed using the creep data produced during immersion (figure 12.14), from which the following observations were made:-

(a) ε_i vs. applied load in water was identical to the results found in air, i.e. maximum primary creep strain level was environment insensitive.

(b) Higher levels of creep strain were found in water, though again, $\varepsilon(t)$ extrapolated to zero at 100% UTUL.

(c) The gradient of the creep failure strain (ε_s) line was reduced by testing in water In this case, extrapolating back to AB, gave a creep-rupture limit at a load level of around 30% UTUL (15.5.2.)

Once again, by plotting ε_i vs. ttf (figure 12.15), a rupture limit was observed to occur at a level of ε_i produced on loading to 30% UTUL. From previous results (11.4), it was around this load level that transverse cracking was first observed to occur.

12.5 Initial load rate tests

Tests were performed to determine the effect of initial load application rate on the failure time of GRP loaded in air, in an attempt to improve data reproducibility. A single load arm rig was used, in conjunction with a constant

cross-head displacement rate tensile test machine. The lever arm was raised using the cross-head, and a sample mounted. Weights were attached, sufficient to produce a load level of 79% UTUL, and the lever arm lowered at a constant cross-head speed until the sample supported the entire load. After this, the cross-head was de-coupled from the lever arm, and the sample ttf recorded as a function of loading rate.

Three cross-head speeds were used, 0.1, 1.0, and 10.0mm/min, 4 samples being tested at each rate. Damage growth during creep loading was also monitored, by use of the PAC A.E. analyser.

Figure 12.16 shows that no relationship linking ttf with initial loading rate was evident. Since GRP is viscoelastic, increases in loading rate would increase the level of brittle crack damage in the sample. Thus, it must have been the case that any changes in damage levels induced by rapid initial loading, were masked by the general variability found in GRP.

From the A.E. work, it was found that a relationship did exist between initial damage (number of events recorded in the first 600 seconds of a test) and ttf (figure 12.17). The major determining factor in the creation of this damage was the applied stress level, with initial load rate producing only a secondary effect (15.2).

PART THREE

D I S C U S S I O N

CHAPTER 13

MECHANICAL PROPERTIES OF G.R.P.

13.1 Tensile properties of mixed reinforcement G.R.P.

It can be seen from figure 9.2 that these laminates, containing a high proportion of w.r. reinforcement, were only elastic at low loads. At approximately 20% of ultimate, the load/deflection curve changed gradient, creating a "knee". When monitored photographically, it was found that this change in tensile behaviour corresponded to the onset of cracking along the transverse woven fibre/matrix interfaces (figure 11.18). This was also the point at which stress gradients were first observed in the c.s.m. plies under examination between cross-polarisers (figure 11.19).

The formation of a 'knee' in the load/deflection curve of fabric laminates, tested in tension, has been widely reported (20). If a fabric is stressed parallel to either of the roving directions, deflections are produced as the longitudinal rovings straighten under load. Initially, the transverse rovings present do not constrain this movement to any great extent, but rather accomodate it through an increase in fibre crimp. As loading progresses, this accomodation becomes more difficult, and the level of constraint on fibre straightening in the load bearing rovings increases to a point where further deflections are not possible through this mechanism.

Glass fabrics can deflect to a much larger extent than straight fibres, through the dual action of longitudinal straightening (non-linear), and elastic fibre extension. When held in a brittle matrix, however, straightening in the longitudinal rovings is prevented by the resin phase. At low loads, therefore, total response is due to the elastic extension of fibre and matrix constituents.

It has been shown (50) that GRP is very weak when loaded transverse to the fibre direction, failure occurring through fibre/matrix debonding. In fabric laminates, containing 50% of the reinforcement in the transverse direction, this weakness leads to the formation of transverse cracks at low loads,

initiated through transverse fibre/matrix bond breakdown. Once this damage has initiated, transverse rovings are capable of limited movement, which then allows fibre straightening to occur in the longitudinal direction. This increase in sample deflection then causes a drop in modulus, resulting in the observed load/deflection behaviour.

Straightening of the longitudinal woven rovings can induce debonding in the load bearing direction, particularly, at weave cross-overs, though evidence of this is normally only found close to failure. However, this change in modulus, after transverse crack initiation, does change the load bearing characteristics of mixed reinforcement laminates. At low stresses, all the load is supported by the continuous (i.e.w.r.), reinforcement, with negligible levels of stress transfer to the more compliant c.s.m. plies. After transverse crack formation, overall laminate compliance increases, and load transfer to the c.s.m. plies becomes significant (figure 11.21.).

At load levels close to failure (figure 11.21), delaminations have been found to occur at woven roving cross-over points, as a result of longitudinal fibre straightening. This damage initiated at the sample edges, where stress concentrations were high due to the discontinuity present, and spread into the sample on further loading. Fibres in these cross-over regions were highly stressed, due both to the bending present in woven rovings, and the drop in load transfer efficiency. The latter occurred as a result of localised delamination. Fracture of the sample eventually resulted from an accumulation of filament breaks in these high stress regions, creating cracks that coalesced to produce the final failure path.

13.2 Load rate effects

With these low V_f composites (around 30%), the viscoelastic nature of the matrix can have a significant influence on the tensile properties. In particular, standard mechanical properties will be a function of the load rate used on testing (7.1). However, it has also been found that glass fibres have a time dependent strength due to stress corrosion (62), despite their

elastic response up to the point of failure. In many instances, the fibre and matrix time dependent properties are in direct competition, and the final response becomes a combination of the two.

When the strength of mixed reinforcement GRP as a function of load rate was determined (figure 9.3), it was found that an increase in strength occurred at high rates. Up to displacement speeds of 10mm/min, strength was independent of rate effects. The failure strain, as a function of load rate, was found to show a two-stage response (figure 9.4), passing through a minimum at 5mm/min.

At low test speeds (below 5mm/min), behaviour was dominated by the viscoelastic nature of the matrix. The resin was capable of viscous flow in this load rate regime, reducing the matrix constraint on the longitudinal woven rovings, and so reducing resistance to crimp straightening. The slower the rate of loading used, the higher would have been the level of matrix viscous behaviour, and correspondingly, the lower the constraint on longitudinal fibre straightening. Thus, failure strain would be expected to increase with decreasing test speed, since for a given applied stress, higher deflections would occur through increased levels of crimp straightening. At these low load rate levels, fibre strength remained constant, because stress corrosion weakening effects at slow test speeds became rate independent.

At high load rates (above 5mm/min), matrix response became predominantly elastic, and a change from viscoelastic resin, to elastic fibre, dominated behaviour occurred. The time dependent strength of a glass fibre is controlled by moisture induced surface flaw growth. In essence, the slower the rate of loading used, the longer is the time available for flaw growth through stress corrosion mechanisms (5.3), causing a loss in fibre strength. Since fibres are elastic to failure, breaking strain also increases with increasing test rate. Thus, in the high load rate regime, strength and failure strain of the GRP tested, would be expected to increase with increasing test speed, as was observed.

Within the load rate regime most pertinent to the current work (i.e. below 1mm/min), viscoelastic response dominated the behaviour of GRP. This was of particular importance when analysing the time dependent properties of the laminates tested for this thesis, and the results from this section will be further discussed in conjunction with the creep data obtained (15.5).

13.3 Fibre break density

As will be shown later (15.5), the number of fibre breaks created during loading (figure 9.5), and their location, was a critical parameter in determining the delayed failure characteristics of mixed reinforcement G.R.P. laminates. It was found that a 3-stage curve was created for fibre break density as a function of applied load.

Up to 20% UTUL, the rate of growth in the number of breaks, increased from zero load. A decrease in the rate was then found between 20 and 50% UTUL, after which the number of breaks observed again increased rapidly, up to the breaking load. Above 50% UTUL, it was observed that some fibre breaks occurred in the form of multi-filament fractures (9.3), whereas samples loaded below this level merely contained random distributions of breaks.

Where this random distribution of breaks was created, little overall strength loss was found. Stress concentrations around a break are very small, as can be seen from equation 5.9. Hence, for a single break, the level of stress concentration produced in neighbouring fibres is only 1.5 , which is unlikely to precipitate further fibre fractures.

At loads where M.F.F. damage was created (above 50% UTUL), the situation altered. The stress concentrations around these features were now of a level sufficient to promote further damage, e.g. for a 3 strand break, Kr = 2.5, resulting in the increased rate of fibre break creation found.

The reasons for the change in damage growth rate found at 20% UTUL were less clear. This load level, however, was significant, coinciding with the change in load/deflection behaviour found when transverse cracking initiated (13.1). Due to fibre bending, woven rovings at cross-over points

are subjected to stress concentrations which could produce filament fractures, even at very low loads. Thus, while longitudinal roving straightening was constrained by the matrix, these stress concentrations accelerated the growth of filament fracture damage. Around 20% UTUL, transverse cracking initiated, allowing longitudinal rovings to straighten, causing a fall off in the level of stress in the cross-over regions. This drop in stress levels then led to the observed fall in the rate of filament break damage growth.

13.3.1. Multi-filament fracture damage creation

It was stated above that weave cross-over points are regions of high stress, because of the fibre deformation created locally. Fibres on the outer surface of a woven roving ply have to withstand severe flexural, as well as tensile loads at the apex of a cross-over, and become overstressed in these regions. It was explained above how, at loads below 50% UTUL, longitudinal woven roving straightening reduced the level of these stress concentrations.

However, fibre straightening in the load bearing fibres leads to an increase in transverse roving curvature (12.1), and a build up in the level of constraint on straightening occurs as the bending of transverse fibres becomes more difficult. Thus, a situation could be envisaged where a load level is reached, where further load bearing roving straightening is prevented by the resistance created in the transverse fibres, after which stress concentrations would again build up.

This represented the key to establishing how MFF damage was created in these tests at 50% UTUL. Assuming that the load required to prevent further roving straightening occurred around 50% UTUL, stress concentrations at weave cross-overs were sufficiently high to promote filament fracture. Once one fibre broke in this high stress region, further rises in stress level were produced, inducing fracture in neighbouring fibres, creating multi-filament fractures of between 2 and 8 strands.

The creation of MFF damage during initial loading in a creep test, was considered to be an essential requirement for the initiation of creep-rupture in mixed reinforcement GRP loaded in air (15.5)

CHAPTER 14

MOISTURE EFFECTS

14.1 Water uptake in mixed reinforcement GRP laminates at zero load

As was shown in Part II (figure 11.5), anomolous diffusion was found to occur when samples were immersed in water, regardless of the stress and temperature conditions used. In the absence of load, it was found that debond whitening first occurred in the outer c.s.m. plies of a test-piece. This increase in surface fibre prominence as a function of time immersed, occurred most noticeably at elevated temperature (14.3), within the time scale of the experiment (figure 11.6). At 60°C, the onset of w.r. ply debonding was found to occur much later than c.s.m. interfacial breakdown, while at room temperature, it was not found at all, even after 6 months.

The debonding observed in these experiments must have been due to the effects of moisture uptake, since samples were immersed at zero load. Thus, by following the manner of debond development, the path taken by the moisture into the sample bulk could be determined. Since the outer c.s.m. plies were the first regions affected by the moisture, diffusion was considered to be face dominated. This would be expected, since the total area of face exposed to moisture was far in excess of the area at the sample edges. Furthermore, in the absence of easy diffusion paths (e.g. cracks), water uptake occurs primarily through resin hydrolysis reactions. Samples faces had a surface concentration of polyester matrix in direct contact with the water that would promote hydrolysis, whereas the edge did not.

The non-Fickian nature of diffusion in the materials tested was attributed to the relatively high porosity levels present. As water penetrates a resin matrix, hydrolysis reactions break down the network cross-link density, causing the resin to swell. This is constrained by the presence of glass fibres, inducing internal stresses in the sample, mainly concentrated in the matrix, and resin/fibre interface, regions. The porosity within the immersed laminate, particularly resin voids, act as local stress

raisers, and when swelling occurs, crack initiation from these defects can result. Such damage was found to occur when samples were immersed in distilled water (figure 11.15). These cracks can then act as paths of easy diffusion, accelerating moisture uptake, causing apparent diffusivity to change with time.

Even if the above cracking did not occur during water uptake, voids upset the classical models of diffusion,by allowing moisture pockets to build up in a sample. In this way, increased moisture absorption occurs, simply through the creation of a higher internal free volume for water to occupy, than would be the case in a perfect composite.

Other mechanisms that would account for the anomolous diffusion observed include resin leaching. In this case, chain hydrolysis reactions produce low molecular weight components, which are then dissolved out of the matrix. Again, this would lead to an increase in internal free volume within a GRP test-piece, allowing for accelerated moisture uptake to occur.

In conclusion, it was found that, for the above reasons, water diffusion into mixed reinforcement GRP occurred through the sample faces, at a rate that could not be predicted from classical models of diffusion, such as Ficks Laws.

14.2 Water uptake during immersion under stress

It was found that, regardless of temperature, both the rate of moisture absorption, and the overall moisture content, of samples, were increased in the presence of an applied load (figures 11.1 and 11.2). The influence of temperature on water uptake will be examined later (14.3), while this section will look at the differences in behaviour due to the level of stress applied to a sample,regardless of test temperature.

14.2.1 Water uptake at 30% UTUL

It was found that outer c.s.m fibre debonding occurred at the same rate as that found in samples immersed under zero load (11.2). From this,it was concluded that moisture uptake through the sample faces occurred at a rate

independent of the applied load level. However, the rate at which the w.r. cross-over regions debonded was accelerated at 30% UTUL. This fact, coupled with the increase in moisture uptake found in samples immersed under load, suggested that a new moisture transport path into the GRP had been activated.

Examination of ordinary tensile test-pieces (11.4.3.) showed that transverse cracking initiated in these materials at around 20% UTUL. However, from a study of polished sections taken from samples stressed in tension and subsequently unloaded, it was found that this damage was reversible at 30% UTUL, indicating that the crack paths created were small. Transverse cracking was observed to occur at the fibre/matrix interfaces present in the transverse woven rovings.

The cracks formed under load penetrated to the sample edges, and when immersed in water, provided paths of easy moisture access into the sample. Thus, when immersed under load, the overall rate of moisture uptake into the GRP was accelerated, by the additional contribution made by capillary flow of water through these cracks, from the sample edges. Therefore, at this load level, moisture uptake was attributed to a combination of face (large surface area), and edge (paths of easy access), diffusion mechanisms.

The increase found in the level of overall moisture content was attributed to an increase in the internal free volume of the sample available for the moisture to occupy. This was due to the increased level of damage created under load. These transverse cracks open up paths for moisture penetration to intra-roving voids in the fabric plies (figure 10.6), which can then lead to further degradation, both at the fibre/matrix interface, and in regions of fibre surface contacting these moisture pockets. When under zero load, moisture penetration to these defects would be restricted, as a result of preferential water transport to the resin voids present.

14.2.2. Water uptake at 40% UTUL

At this load level, transverse crack damage formed on loading was irreversible, resulting in the creation of wider paths of easy moisture trans-

port into the sample. In consequence, the balance between face, and edge, dominated diffusion mechanisms was further shifted towards the latter.

14.2.3. Water uptake at 60% UTUL

Due to the creation of high levels of damage at this load level, the amount of moisture diffusion through the sample edges was so large as to make the behaviour totally edge dominated. Indeed, sample failure occurred prior to any significant levels of face diffusion becoming apparent. Thus, matrix damage created by resin hydrolysis and swelling was reduced at this load level, since these phenomena were essentially a result of face dominated water absorption.

In conclusion, applied stress was found to increase water absorption by changing diffusion from a sample face, to an edge, dominated process, due to the creation of damage. The degree of damage (i.e. load level), determined the contribution to overall water uptake made by capillary flow along cracks from the sample edges.

14.3 Effect of test temperature on water uptake

It was found in 11.1 that, regardless of the applied stress, increasing the test temperature from 23-60°C, led to a rise in water uptake. This section will discuss some of the most likely mechanisms that would operate in these materials, both for the case where face,and edge, dominated diffusion mechanisms operated, i.e. behaviour at zero load, and under stress, respectively.

14.3.1. Temperature effects during immersion at zero load

With a thermosetting resin, temperature changes,below T_g, do not significantly alter the observed mechanical properties (cf. thermoplastics). However, raising the temperature can increase chain mobility, which in turn can initiate cross-link scission. Thus, the polymer network becomes more disordered at elevated temperature, thermal expansion results, and internal free volume is increased.

When glass/polyester laminates are exposed to water at elevated temperatures,

the more open nature of the matrix network allows water transport to occur at an accelerated rate. The increased internal free volume created also allows for an increase in the amount of water absorbed by the matrix.

During sample face dominated water uptake, moisture was abosrbed through resin hydrolysis. This is a chemical reaction, so that increasing temperature levels increased the reaction rate, in an Arrhenius fashion. Thus, the levels of resin plasticisation and swelling would have been increased, raising the internal stress present in the sample, which then further accelerated moisture uptake through resin cracking, etc. (6.2). A by-product of resin hydrolysis is matrix damage due to leaching (14.1), so that temperature increases will also have led to an increase in the loss of low molecular weight constituents from the polyester matrix.

14.3.2. Temperature effects during immersion under load

The level of test temperature used would also have influenced the rate of edge diffusion found in loaded samples, for a variety of physical reasons. Firstly, thermal expansion of the GRP at 60°C would have produced an increase in the dimensions of the easy diffusion paths created through cracking. Secondly, differential thermal expansion between fibre and matrix is known to generate interfacial stresses in composites. Thus, transverse crack initiation would have occurred at a lower applied load, and the general damage levels been increased, at elevated temperatures. Both of these factors would lead to increased water uptake as the test temperature was raised from 23°C - 60°C.

Finally, the rate of capillary flow up the cracks presentwas also temperature dependent, higher flow rates occurring at elevated temperatures.

14.4 Relevance of moisture uptake to the degradation of GRP in water

In high performance composites, e.g. carbon/epoxy systems, a functional

relationship is often found to exist between mechanical property degradation, and moisture content (6.1). Thus, it is important to determine diffusion coefficients for these material, to predict the moisture induced degradation levels expected in service. In most high performance composites, diffusion is found to approximate to that predicted by Ficks Law. As a result, many analytical models of degradation in humid environments have been developed (77-80).

In lower V_f composites, as used in this work, diffusion is normally found to be non-Fickian (anomolous), making the calculation of diffusion coefficients highly problematical. However, the question that next arises is, "is this a problem?". Since water will collect in voids and cracks within the GRP, it would be much more use to look at the effect of local moisture concentrations, rather than overall uptake levels. This is particularly relevant, since voids act as stress concentrators. Water collection in these defects can produce increased levels of resin hydrolysis locally, leading to an increase in stress sufficient to induce matrix cracking through differential swelling of the matrix. In the case of intra-roving voids, debonding, or even fracture, of the glass fibre reinforcement can occur through this mechanism.

Similarily, in GRP containing w.r. plies, weave cross-overs have been seen to debond preferentially in water (11.2). Since they are known to be regions of high stress, moisture attack at cross-overs will be more degrading to the overall performance of a sample, than if c.s.m. fibres were subjected to aqueous corrosion (14.6). Both of these localised forms of moisture induced degradation occur at very low overall moisture contents.

In conclusion, it was found in this work that overall moisture content of the GRP tested gave no indication of the degradation that occurred, when samples were immersed in water. The important factor was seen to be the rate at which water penetrated to points of weakness in the laminate, such as woven roving cross-over points. In consequence, no attempt was made to calculate diffusion coefficients; instead, the location of moisture pockets within a sample were monitored, mainly through the debonding created at weave cross-overs (below).

14.5 Fibre debonding during immersion of GRP

The rate at which interfacial breakdown occurs within a laminate, is a crucial factor in determining sample degradation due to moisture uptake. It was shown in Part I that debonding will reduce the interfacial load transfer efficiency of GRP, and hence its strength and stiffness (6.4). This arises from an increase in fibre ineffective length, causing a reduction in strength towards the level found in unbonded fibre bundles (5.4.3). In water, fibre strength can also be decreased by the corrosive effect moisture has on E-glass filament surfaces (2.5), so the faster debonding occurs, the sooner surface attack can initiate in the reinforcement.

14.5.1 Fibre debonding of GRP immersed at zero load

In the absence of load, the only debonding found after immersion for 44 days occurred in the outer c.s.m. plies, at a rate dependent on the temperature (figure 11.6), as discussed in 14.3. However, after 6 months at 60°C, considerable levels of weave, as well as c.s.m., debonding were found (figure 11.16). This was attributed to the growth of thermally activated damage at long times, i.e. leaching and resin cracking, allowing rapid moisture uptake into the woven roving plies (14.6). Long term immersion at room temperature had no such effect, showing the thermally activated nature of debonding.

The laminate structure used for this work was selected to optimise mechanical properties, and moisture degradation resistance. For this reason, w.r. plies were selected for their load bearing characteristics, and ease of handling, and c.s.m. plies for moisture resistance. Basically, when water penetrates the sample, the idea is that the outer c.s.m. plies trap the moisture at the surface through sacrificial debonding, protecting the load bearing woven rovings.

The laminates tested would only work in the above fashion in situations where diffusion of water occurred through the sample faces. This was found

to be the case at zero load (14.1), and the outer c.s.m. plies did act to prevent moisture transport in to the load bearing fabric layers, particularly during short term immersion.

14.5.2. Fibre debonding of GRP immersed under load

When samples immersed under load were examined, it was found that the load bearing woven rovings debonded much faster than above (14.5.1), at a rate determined by temperature and stress (11.2). It was also found that the outer c.s.m. debond rate was unaffected by the applied load. Changes in diffusion mechanism, from face,to edge, dominated behaviour occurred, as a result of transverse crack formation.

Once diffusion of moisture began to occur through capillary flow up these transverse cracks, the role of the outer plies was diminished. Rapid uptake via the samples edges bypassed the c.s.m. moisture barrier, passing straight into the load bearing woven reinforcement instead.

It was seen that weave debonding was concentrated in the roving cross-over regions (figure 11.8 (b)). These regions of high stress created areas of enhanced water diffusivity locally (6.2), causing a build up of debonding. This can cause severe problems for a number of reasons. Firstly, debonding extends the ineffective length of fibres in these high stress regions, reducing strength locally towards that of a fibre bundle. This drop in load transfer efficiency, coupled with the stress concentration present, can induce fibre failure in these regions, which would further increase stress levels. Secondly, the critical fibre flaw size at cross-overs, particularly on the outer face of a roving, is at a minimum due to the presence of tensile bending stresses. Since it was these fibres that came into direct contact with the moisture pockets formed, stress-enhanced fibre corrosion would have led to severe degradation in the cross-over regions.

14.6 Degradation of GRP immersed in water

The build up of damage found during immersion of mixed reinforcement GRP samples could be attributed to a variety of mechanisms. Strength loss due to interfacial breakdown has already been discussed (14.5), so this section will deal with the damage found to occur in the fibre and matrix phases.

14.6.1. Moisture induced matrix cracking of GRP

It was found that moisture induced cracking (figure 11.15) occurred at a rate independent of temperature and stress (11.3), largely initiating from defect sites, such as resin voids. Other high stress regions, such as weave cross-overs, were also found to promote this crack growth.

As moisture was absorbed by the polyester matrix, hydrolysis of the polymer chain network occurred, causing a breakdown in the cross-link density. This would have produced resin swelling, but the presence of the glass fibres constrained this expansion, and so internal stresses within the matrix, and fibre/matrix interfaces, built up. The defect population in the samples, acting as stress concentrators, then magnified these stresses locally to an extent where matrix cracking was created. (figure 11.12).

While changes in temperature would have been expected to affect the swelling characteristics of the matrix, leading to increased stress levels and higher crack density at 60°C, this was not found to occur. Increased levels of resin hydrolysis did occur at elevated temperatures, producing an increase in moisture uptake, etc. (11.1). However, this had a dual effect on matrix properties. As well as increasing resin swelling, it also produced a higher level of matrix plasticity, since network cross-linking was degraded (3.3). Thus, while internal swelling stresses were increased at 60°C, so was the level of matrix stress relaxation, and the latter would have caused relief of stress concentrations around voids and weave cross-overs. This balance of temperature effects then created the lack of sensitivity, matrix crack damage during immersion, exhibited.

When under stress, it was shown that the extra moisture uptake into a sample occurred through capillary flow, along crack paths created in the material (14.2). The level of face diffusion into the matrix remained constant. Since only the latter would have contributed to resin swelling, it would be expected that applied load had no effect on the moisture induced cracking observed in the matrix, as was found.

14.6.2. Glass fibre degradation during immersion in water

It was shown in Part I, that fibre pitting, often found in glass exposed to water, can be attributed to surface hydrolysis reactions (2.5). Network modifier ions (e.g. Na^+, K^+ and Ca^{2+}), present in the glass surface as local concentrations, can be removed by aqueous leaching. This causes a local breakdown in the network, which can promote further corrosion. Pitting was found to occur in the fibres taken, from woven roving plies of immersed creep-rupture test-pieces. (15.5). This confirmed that moisture penetration to the w.r. reinforcement when under load, did cause fibre degradation, as well as strength loss through debonding (14.5.2.).

From the resin analysis undertaken using EDAX (figure 10.14), an increase in the matrix calcium content was found, after samples had been immersed under load at elevated temperatures in a creep-rupture test. Since polyester resins do not contain a significant calcium content, and distilled water was used as the immersion medium, these calcium concentrations must have leached from the E-glass fibre surfaces present. Since, in E-glass, CaO is the major network modifier present, with Na_2O, and K_2O, present only in trace quantities, the latter would not be expected to show up. However, from theory, glass fibre corrosion initiates through the removal of Na^+ by hydrolysis, with the flaw created then rounded into a pit by Ca^{2+} leaching (2.5).

Na^+, and K^+, have small ionic radii in comparision to Ca^{2+}. This, coupled with their low concentration in E-glass, would allow the former ions to diffuse out of the GRP easily, whereas Ca^{2+} became trapped in the matrix. This would explain why only calcium was detected during resin analysis.

14.6.3 Residual strength of GRP after immersion at zero load

A measure of the severity of moisture degradation, on the properties of GRP immersed in water for long times, was obtained by performing tensile tests on dry, and pre-soaked, samples. Two pre-soak temperatures were used:-

(a) Room temperature ($23^{o}C$)

(b) $60^{o}C$

(a) $23^{o}C$

- it was shown in Part I that, when GRP is immersed in water at room temperature for a time prior to tensile testing, negligible levels of strength loss occur (5, 96, 107). A similar result was found in this work. Some debond damage had occurred in the outer c.s.m. plies prior to testing, and a reduction of 15% was found in the recorded strength (11.4). This was probably due to matrix crack damage created through moisture uptake (14.6.1). In all other respects, tensile test behaviour after pre-soak, was no different from that found in dry tests, the outer c.s.m. having successfully protected the w.r. reinforcement from moisture degradation.

(b) $60^{o}C$

- at elevated temperatures, pre-soaking caused a much more severe strength loss of 30%, and also produced a change in the overall load/deflection behaviour. The knee point in the load/deflection curve (figure 11.17) became less distinct, and the load it occurred at fell to 9% of ultimate. Since it has been demonstrated that this feature was attributable to the onset of transverse cracking (13.1), moisture uptake must have altered this damage mechanism.

Since after 6 months at $60^{o}C$, the w.r. reinforcement present had largely debonded, the constraint on longitudinal w.r. straightening during loading, was reduced. This resulted in the load/deflection knee point (i.e. load required to initiate straightening), being reduced by around 35% after pre-soak.

The level of debonding and plasticisation of the matrix, created after pre-soaking at $60^{o}C$ also explains the lack of damage found during a tensile test (figure 11.22). Stress colouration, when examined using cross polarisers, shows that load transfer via the matrix is occurring. Once the

fibre/matrix interface was broken down by moisture, this could no longer happen, and all the stress applied had to be supported by the longitudinal woven rovings, behaving as simple fibre bundles. Resin plasticisation reduced matrix cracking,through stress relaxation under load.

In a dry tensile test, the main damage observed was transverse cracking, followed by stress whitening, then matrix cracks running from fibre break regions, until final fracture occurs (figure 11.21). After pre-soak at elevated temperature,transverse rovings had already debonded, along with the weave cross-overs, so the first 2 damage mechanisms would be absent. Similarily, debonding would prevent matrix cracks initiating from fibre roving breaks, since the 2 constituents were de-coupled. Thus, the only damage observed on loading a pre-soaked sample was final fracture, and the level of acoustic activity was reduced accordingly.

CHAPTER 15

CREEP IN GLASS/POLYESTER LAMINATES

15.1 The creep-rupture test

The most usual way of predicting the design life of a GRP component, is by means of a creep-rupture test. Briefly, data from a series of short term tests, is plotted as applied load vs. log (ttf) (7.2). By assuming the existence of a linear relationship, simple extrapolations can then be undertaken, to determine the load level at which a component can be loaded without failing during the required design life. Even in homogeneous materials, such as metals, this is fraught with difficulties (164), and when composites are used, material variability makes the whole approach highly suspect.

Attempts have been made in this work to identify the causes of GRP variability as a first step in the improvement of design life prediction. During creep-rupture in air, the variation in ttf found for samples subjected to the same load, was up to 3 orders of magnitude. In water, while still extensive, the scatter in ttf data was found to be reduced (figure 12.12). Failure time scatter was attributed to the variation in strength that occurs in GRP materials (5.3.).

In air, the creep-rupture plot gradient was fairly shallow, a change in applied load of 6% UTUL producing a one order of magnitude shift in ttf. In water, the gradient was steeper, at around 11% UTUL per order of magnitude.

Since the tensile strength of the mixed reinforcement GRP tested varied by $\pm$ 9%, problems immediately become apparent. In a creep-rupture test, the applied load is calculated as a fraction of the average breaking load. Individual sample strengths would have varied from this value, so that for a supposedly identical applied load, replicate creep-rupture test-pieces were at very different stress levels. By comparing creep-rupture plot gradients with the measured GRP strength variability, scatter in ttf data corresponded to a variation of $\pm$ 9% UTUL in applied load, both in air and water. Hence, to reduce failure time variability, either sample strength must be known prior to creep-rupture testing (clearly impossible), or strength variability in GRP must be controlled.

Some of the factors causing variability, such as porosity, strain rate, and glass content, were studied, and their relative contributions assessed. It was found that so many other variables existed, that attempts made to reduce scatter in ttf results, such as the use of U.T.U.L. to allow for the effect glass content has on sample strength, were of limited value. Until it is possible to determine how the various factors producing GRP strength variability (5.3) interact on loading, it will be impossible to control GRP behaviour sufficiently to reduce scatter in creep-rupture ttf data.

While large scatter bands in ttf data still exist, the creep-rupture test, as applied to GRP, will remain an unsatisfactory design criterion. Even assuming a linear relationship exists, the slope of such a line can be varied to such an extent within the scatter bands, that failure time predictions for a given load level could vary between, say, 2 and 2000 years.

Statistical extrapolation methods, such as linear regression, are only appropriate where sufficient replicate tests have been undertaken to accurately determine the extent of scatter. For GRP, this has been found to require over 100 tests at each load level (appendix I), whereas normal practice is to test between 4 and 10 samples. An inevitable loss of accuracy results during extrapolation.

Finally, considerable doubt exists as to whether a linear relationship between applied load and log (ttf) exists, for GRP. Results obtained, both in previous studies (figure 1.1), and during the current work (figure 12.12), show that deviations from linearity occur, both at high loads, and long failure times. With this in mind, linear extrapolation of creep-rupture data for these materials would clearly lead to inaccuracies.

15.2 Creep loading rate effects in GRP

Although the rate at which initial sample loading occurred was not found to affect the ttf of the GRP tested (12.5), some important results were found from this study. One of the first things to mention in this section, was that

deflections due to initial loading of samples represented only about 20% of the total primary creep strain recorded.

As GRP is a viscoelastic material (7.1), the amount of damage created during loading should increase with increasing strain rate, since stress relief due to matrix flow would be reduced. This would be particularly true in w.r. reinforced laminates, since the higher the strain rate used, the lower the fibre straightening potential under load becomes. Stress levels at weave cross-overs would be greater at high strain rates, initiating higher levels of M.F.F. damage above 50% UTUL. Thus, the level of damage created in the primary creep region should be determined by the overall strain rate.

It will be shown (15.5) that, in order to initiate creep-rupture in these materials when loaded in air, M.F.F. damage zones must be created during primary creep. Thus, since the severity of such damage is a function of the overall primary creep strain rate, and GRP ttf is determined by the density of M.F.F. zones present in a sample, life during creep should vary according to the primary creep rate.

To a certain extent, the above model of behaviour was confirmed by experiment. It was found that initial damage levels in a sample, measured as the number of acoustic events produced during the first 600 seconds of a test, did influence the failure time of samples loaded to 79% UTUL (figure 12.17), i.e. increasing primary creep damage levels reduced sample ttf. However, no effect, due to altering the rate of initial load application from 0.1 - 10.0 mm/min. was found, on the level of initial damage, or sample ttf.

As was stated above, only 20% of the primary creep region was taken up by initial loading, leaving a large part of the primary deflection during creep, uncontrollable. Behaviour between the end of initial loading and the onset of secondary creep, was largely determined by the sample strength. Thus, primary strain rate, and hence overall initial damage levels, was governed predominantly by sample strength, and variations due to initial load application rate produced only a minor, secondary effect.

15.3 Creep of GRP in air

In order to overcome the problems associated with creep-rupture testing of GRP, the time dependent properties of the materials used were characterised by the measurement of creep strain. In conjunction with this, observation of the damage development during creep of mixed reinforcement laminates was undertaken. From these two approaches, the mechanisms of creep, and ultimately creep-rupture, were determined.

15.3.1. Creep in samples loaded to in excess of 80% UTUL

At high loads, the secondary creep region became vanishingly small (figure 12.6). Very high levels of acoustic activity, both in terms of count rate, and amplitude, were recorded throughout the sample life (figure 12.7), showing the rapid nature of damage accumulation at this applied load level.

When loaded above 50% UTUL, it was observed that fibre break growth rate increased rapidly with applied load. (figure 9.5). Thus, at loads above 80% UTUL, fibre break creation during primary creep was very severe, with high levels of critical M.F.F. damage produced. On top of this, it was seen in 15.2 that primary strain rate, which governs the level of initial damage created, was largely a function of the applied load. Therefore, further increases in fibre break density produced on loading would be created, due to this load rate effect.

The effect of primary creep strain rate on behaviour would become critical at high loads, since it would push the level of initial damage further towards that required to initiate sample fracture, through an accumulation of breaks in the load bearing fibres. Thus, after the maximum primary creep strain was reached at these loads, the initial damage created was so severe that failure of the sample initiated immediately, so that no secondary creep region was produced, and tertiary behaviour then governed the recorded ttf.

15.3.2 Creep in samples loaded below 80% UTUL

At lower load levels, classic creep behaviour was observed (figure 12.6). In most cases, tertiary creep was not observed, because the final fracture occurred at a rate too rapid to be recorded by the monitor (12.1). There was a decrease in acoustic activity as the applied load was reduced and at these load levels, both the event count rate, and amplitude, curves obtained had a 3-stage form, analogous to the creep curves obtained (figure 12.7). In the primary, and where monitored, tertiary, creep regions, acoustic count rates and amplitudes were high, reducing considerably during secondary creep. In the latter region, periodic high amplitude signals were recorded.

During secondary creep, strain was found to increase in discrete steps at random time intervals, rather than continuously, as found in metals and polymers (7.2). Thus, creep response of GRP was found to be more than a simple function of the matrix viscoelastic behaviour. It was found that a correlation existed between the time at which secondary strain jumps occurred, and the detection of high amplitude acoustic signals mentioned above (figure 12.8). Initially, it was thought that these periodic strain jumps were due to individual filament fractures, formed as a result of matrix creep induced overloading of fibres (76, 174). However, the magnitude of the deflections produced, up to 0.1% strain, appeared too large to be explained in this manner.

The amplitude level of acoustic events recorded at the time of secondary creep strain step-growth, were comparable to A.E. count amplitudes detected during initial loading. In the latter case, cracking along transverse woven roving/matrix interfaces was observed. It has been shown by Dickson et al (177), that high amplitude acoustic events in bi-directional laminates are caused by transverse crack growth, as was the case in this work. Thus, it was decided that the strain jumps observed during secondary creep were caused by the formation of transverse cracks in the samples. The random creation of small transverse cracks, observed while under load at weave cross-over points, would support this idea (figure 12.4). These cracks were attributed to the

time dependent failure of fibre bundles, up to a roving in size.

It was felt that, as a result of matrix creep, fibres became progressively overloaded, increasing the fibre break density present as secondary creep progressed. In high stress regions, such as in the vicinity of weave cross-overs, matrix creep rate was accelerated, and changes in local stress level required to produce filament fracture reduced. Hence, filament break formation tended to become focussed in these regions, when MFF damage was present after loading the sample.

When sufficient fibres have failed locally, the stress concentration created would lead to the propogation of a transverse crack through the longitudinal roving bundle (figure 15.1). Progressive blunting of such cracks, by the action of fibre/matrix interfaces, and a reduction in driving force as the crack tip moved away from the region of maximum stress concentration (weave cross-over apex), prevent sample fracture. Instead, small transverse cracks were formed in the longitudinal woven rovings, as observed, initiating from M.F.F. damage sites in the glass fibre.

15.3.3. Analysis of creep data from samples loaded in air

The plots of ε_i, ε_s, and $\varepsilon(t)$, vs. applied load (figure 12.10) produced, made possible some highly significant observations. The creep failure strain, ε_s (12.3), was always found to be in excess of the previously determined minimum tensile failure strain (13.2).

Failure strain in GRP containing high levels of w.r. reinforcement, has been shown to depend on the strain rate used during testing. The slower the rate, the more time is allowed for resin viscous flow to occur under load, the effect of which is to reduce the level of matrix constraint on longitudinal woven fibre straightening. Thus, higher deflections to failure occur, through fibre straightening induced stress relief, etc. (13.2). The creep strain rate of GRP, dependent as it is on the applied load level, is low in comparison to that used in a tensile test. Hence, it would be expected that the creep failure strain recorded would always be in excess of the minimum tensile breaking strain, because in the latter case, matrix constraint

on fibre straightening is at a minimum. This was indeed found.

By extrapolating the creep failure strain line back to the minimum tensile failure strain level (A-B in figure 12.10), a point corresponding to an applied load level of 50% UTUL was reached. It was predicted by Lifshitz and Rotem (174), that a creep-rupture limit exists for GRP at this load level, i.e. applied stresses of less than 50% UTUL should not lead to time dependent failure. Since, from the above, creep failure strain was shown to always be in excess of the instantaneous (high strain rate) failure strain, it would appear reasonable to assume that where ε_s fell beneath the line A-B, insufficient creep strain was produced to initiate rupture. This would agree with other workers (174).

By plotting the predicted creep-rupture limit onto the curve of ε_i vs. log (ttf) (figure 12.11), it was found that data, analogous to a creep-rupture plot, tended to the same limit. Thus, from the two approaches, the existence of a creep-rupture limit at 50% UTUL for GRP tested in air (174), was supported. Reasons for the existence of such limit will be discussed in 15.5.

15.4 Creep of GRP in water

The basic creep response found when samples were immersed in room temperature water was the same as that described above, i.e. at loads above 80% UTUL, secondary creep was not observed and behaviour was environment independent, while below this level secondary creep occurred in discrete steps. The major changes found when loaded to less than 80% UTUL were that:-

(a) Failure time at a given load was reduced by immersion in water.

(b) Higher levels of creep strain were recorded while in water, for for same applied load .

(c) Secondary creep strain jumps built up over several minutes, rather than instantaneously, as in air.

(d) Tertiary creep region was extended in water.

The last three effects were all attributable to the resin plasticisation that occurred as a result of water uptake. The reduction in ttf found, was due mainly to moisture induced degradation of the glass rovings, and fibre/matrix interface regions.

15.4.1 Effect of water uptake on the creep of GRP

It was described previously how matrix constraint on woven fibre straightening was reduced, through resin plasticisation, and fibre/matrix debonding, during aqueous immersion (14.6.3.). At 23°C, the latter effect is minimised, so that increases in the level of creep strain found were due mainly to an increase in matrix creep behaviour as the polymer chain network was broken down, by hydrolysis. This allowed for greater longitudinal roving straightening under load, causing an increase in sample deflection.

Due to matrix plasticisation in water, crack propogation rates through the resin phase would have been decreased, through an increase in crack blunting potential. Thus, both the growth of secondary creep, transverse fibre roving cracks, and the ultimate fracture path, would have been retarded by the higher energy requirements of driving a crack through a plastic, rather than brittle, matrix (figure 7.9). This would explain the changes found in (c) and (d) in the presence of an aqueous environment.

15.4.2. Reductions in ttf due to the presence of an aqueous environment

When immersed under load, it was found that the weave cross-over regions debonded preferentially, through moisture collection at these regions of stress concentration (11.2). The matrix/roving interfacial breakdown caused a local drop in load transfer efficiency, further increasing fibre stress in these regions. This can be sufficient to create M.F.F. damage zones, or extend those already formed, from which creep-rupture could have initiated (15.5.2.).

A further consequence of the formation of moisture pockets at weave cross-over stress concentrations, would have been an increase in the level of stress enhanced fibre corrosion, both through an increase in stress levels, and because the rovings were in direct contact with water. Corrosion damage, in the form of surface pits was found to occur in the longitudinal rovings, at the interior regions of weave cross-overs (figure 10.13). Originally, it was thought that fibre corrosion occurred solely in this region, either as a result of incomplete fibre coupling agent coating, or else frictional damage of the coating during weaving. Intra-roving voids in weave cross-over interior regions would have further accelerated local damage, by creating moisture pockets. The major drawbacks to this theory were:-

(a) Pits were not observed to occur at fibre fracture surfaces.

(b) Fibre surfaces at weave cross-over interior faces contain high surface compressive stresses, which would decrease the potential for critical flaw growth.

(c) Moisture accumulation occurred predominantly at the outer surfaces of the w.r. cross-over regions.

Thus, rather than fibre flaw extension occurring through corrosion in these regions, general dissolution of surface defects occurred, producing the observed pitting.

On the outer surfaces of a cross-over, the situation was different. High surface tensile stresses were produced through roving bending, and since these regions were in direct contact with water, stress-enhanced corrosion surface flaw extension, leading to failure of longitudinal filaments, occurred. This damage was not detected at the fibre fracture surface, since the critical flaw size required for failure was of the order of a few hundred angstroms, which was not resolvable in the SEM. Thus, the observed pitting damage, while showing that fibre corrosion occurred, was not responsible for the observed reduction in sample failure time when immersed.

The observed reduction in ttf when samples were loaded in water, was found to result from:-

(a) Reductions in reinforcement efficiency through debonding.

(b) Increase in stress concentrations, and M.F.F. damage, at weave cross-overs, again as a result of debonding.

(c) Fibre degradation, due to stress-enhanced corrosion surface flaw growth.

Since fibre failure through aqueous corrosion was concentrated in regions of high stress (i.e. cross-over points), M.F.F. damage was considered to be created during immersed creep at loads below 50% UTUL (15.5.3.).

15.4.3. Analysis of creep data from immersion tests

Using an identical approach to that of 15.3.3., a creep-rupture limit was predicted to exist for GRP creep while in water at room temperature (figures 12.14 and 12.15). However, in this case, the creep failure strain vs. applied load gradient was much shallower, pushing the predicted limit back to a load level of around 25-30% UTUL.

This load level was found to roughly coincide with the transverse cracking initiation stress in a tensile test (figure 11.18). Thus, it was concluded that enhanced moisture diffusion through the sample edges was required, before the environment could affect the creep response of these GRP laminates when immersed at room temperature. This would agree with the arguments of previous workers (56, 104). A design criterion based on the strain required to initiate cracking, rather than a fraction of UTS, was proposed for GRP when subjected to a load in a corrosive environment.

15.5 Postulated creep mechanisms for mixed reinforcement GRP laminates.

15.5.5. Creep in air

The relationship between matrix creep response and GRP time dependent behaviour has already been demonstrated (7.3). The degree of creep prior to

failure depends on both the volume fraction, and configuration, of the glass rovings present, i.e. discontinuous reinforcement (c.s.m.) leads to a large creep response under load, whereas high V_f, unidirectional laminates, show little time dependence. With woven reinforcement, large deflections during creep occur by longitudinal fibre straightening, as the matrix resin deforms. Thus, the high creep strains found in this work were a function of the w.r. ply crimp, and the matrix viscoelasticity.

As the matrix deformed under load, there was a time dependent increase in fibre ineffective length (174), causing a rise in the levels of stress present in the load bearing glass rovings. This would produce a progressive increase in the fibre break density, particularly around stress concentrations, such as roving cross-overs. Thus, damage accumulation during creep was concentrated in these regions of the reinforcement.

At load levels below 50% UTUL, the damage created during primary creep consisted of randomly distributed fibre breaks that have a negligible stress raising effect (equation 5.9). Furthermore, stress relief at cross-overs occurred at low loads, since the longitudinal rovings present were able to straighten under load (13.3). In consequence, M.F.F. damage was not created on initial sample loading, and the stress concentrations present were insufficient to promote longitudinal roving cracking at weave cross-overs. Since this damage growth was considered to initiate GRP creep-rupture, it was considered that at loads where M.F.F. zones were not created, time dependent failure would not occur.

Above 50% UTUL, M.F.F. damage was created at cross-overs during loading. The resulting increase in stress levels around these points of the weave, then concentrated further fibre break accumulations into these areas of the sample. This initiated roving transverse crack formation during secondary creep, which in turn build up in time to produce creep-rupture. Sample failure time depended on the rate of critical damage accumulation. This was a

function of the applied load level, which in turn was found to govern the primary creep strain rate. The latter parameter was considered to control the initial levels of damage created on loading (15.2).

From the above, while sample ttf can be seen to depend, to a certain extent, on the applied load, other subsidary effects do cause deviations from linearity, in a standard creep-rupture plot. At high loads (above 80% UTUL), primary creep damage levels were shown to be sufficient to initiate tertiary behaviour prior to the onset of secondary creep. Since the relationship between applied load and log (ttf) refers to secondary creep behaviour (8.1), deviations at high loads would be expected. Similarily, at loads below 50% UTUL, creep-rupture was predicted not to occur, so again deviations from linear creep-rupture behaviour would occur.

15.5.2. Creep in water at room temperature

Rather than activating new creep mechanisms, the presence of an aqueous environment merely led to alterations in the above behaviour. Above 80% UTUL, ttf was so short that the water present had no time to affect the GRP response, i.e. the laminates tested were environment insensitive at high loads. This would suggest that environmental effects were concentrated in the secondary creep region. The observed environmental effects fell into three main categories.

Firstly, moisture induced matrix plasticisation led to an increase in resin, and thus laminate, creep rate. Since the constrainton longitudinal woven fibre straightening was reduced in water (15.4), the levels of creep strain produced prior to failure were also increased. Plasticisation also led to a reduction in crack propogation rate through the matrix, causing an extension in the tertiary creep regions, and an increase in transverse crack formation time (15.4).

Secondly, fibre/matrix debonding due to moisture increased the rate of fibre ineffective length elongation,over that found in air (15.5.1.). As a result, the time dependent loss of reinforcement efficiency found during creep, was accelerated when water was present. This is turn would have increased the rate of damage accumulation, causing a drop in sample t.t.f. Interfacial breakdown also allowed the moisture direct access to the glass reinforcement.

Finally, moisture penetration to the load bearing fibre rovings led to a drop in filament strength,through stress-enhanced fibre surface corrosion. The rate of flaw growth due to corrosion,was a function of both the stress and temperature present. Temperature changes affected the rate of glass network leaching. Stress level affected behaviour in two ways. Firstly, the rate of crack tip extension during corrosion depends on the stresses present at the crack tip (2.5), and secondly, the size of flaw required to cause filament fracture decreases with increasing stress.

At load levels between 80 and 50% UTUL, the above factors all lead to a reduction in ttf at a given load, as compared to behaviour in air. Below 50% UTUL, a combination of fibre corrosion and debonding were thought to lead to the creation of M.F.F. damage at loads where it was not produced in the primary region. Since both moisture uptake, and fibre degradation, increased with increasing stress level, moisture induced fibre failure during creep was concentrated at cross-over points, where elevated local stresses existed. Thus, as water penetrated to these regions, debonding of the rovings occurred. This caused further increases in fibre stress locally, due to a drop in matrix load transfer efficiency. Then, the water attacked these highly stressed fibres, causing a localised build up of M.F.F. damage, from which subsequent initiation of creep-rupture could occur.

15.6 Creep-rupture of GRP immersed in water at elevated temperatures

From the results obtained for this thesis, it is now possible to explain the creep-rupture behaviour of mixed reinforcement GRP previously found (4), shown in figure 1.1. At elevated temperatures, a knee was found to exist in the creep-rupture plot at 50% UTUL. Since the transition from environment insensitive, to sensitive, behaviour was found to occur at 80% UTUL (figure 15.3), the change in mechanism found was not due to an incubation period for corrosion damage to cause fibre weakening.

Instead, the change in behaviour was due to the alteration in fibre break pattern,created at 50% UTUL in woven fabric reinforced laminates (13.3). It has been stated above that moisture induced degradation, leading to a reduction in ttf, is a function of stress and temperature. Above 50% UTUL, stress concentrations around weave cross-overs were high, due to the creation of M.F.F. damage (15.5). Thus, degradation rate was predominantly a function of the applied load. Below 50% UTUL, stress concentrations were reduced due to the absence of M.F.F. damage, and the influence of temperature on the behaviour would become significant. So, the observed creep-rupture plot knee was due to a change in environmental degradation, from stress, to a combination of stress and temperature, dominated behaviour (figure 15.3) Since the creep-rupture behaviour was split into three distinct regions, dependent on environment, stress, and temperature, any linear relationship determined for these GRP laminates would be highly suspect.

CHAPTER 16

ACCELERATED CHARACTERISATION OF GRP

16.1 Draw backs of current models

Although most of the currently available methods for determining the long term behaviour of composites have been discussed (7.2, 7.3), a comparison between each would be constructive, prior to discussion of the design criteria developed from this thesis.

Firstly, the most widely used approach, the creep-rupture test, has been shown to be unsatisfactory for use with GRP. Since a large number of variables can be seen to produce the observed creep response of GRP, the assumption of linearity between load and log (ttf) leads to inaccuracy (cf. metallic creep). This was particularly true where an aqueous environment was also present during creep. Because of the variability found in ttf data, safety factors have to be so large (around 20), as to make the whole process of creep-rupture testing unnecessary. Empirical design criteria, such as dividing composite strength by a safety factor of the same magnitude, would be as accurate, and less time consuming, as the creep-rupture test.

Models based on observed composite response represent the future in terms of design prediction. However, one such approach, time-temperature-superposition, suffers from as many drawbacks as creep-rupture testing. Firstly, it must be assumed that only one damage mechanism exists over the whole temperature/time range of a creep test. This was clearly not the case for the GRP samples tested. In order to produce expressions that describe observed creep response, so many experimentally determined factors have to be used, as to make the whole method an empirical curve-fit excercise. Thus, this method as applied to low fibre content GRP laminates, is no more accurate than the creep-rupture test, and considerably more complex in nature.

The approach most suited to the GRP laminates considered in this work, is the time dependent bundle strength model (174-176). At present, solutions based on this model are too complex for general application, but the basic approach would be worth developing. One complication to overcome for mixed reinforcement GRP is the inhomogenuous nature of fibre stresses present, both

in the c.s.m., and w.r. plies, when under load. While development of such models was outside the scope of this thesis, this approach represents the best analytical model for the creep behaviour of GRP.

16.2 Proposed design criterion for mixed reinforcement GRP

Approaches to the prediction of ttf based on applied load are inaccurate, since the actual sample stress level has to be assumed from the average UTUL, rather than measured (15.1). By basing predictions on sample strain instead, measurements could be made directly of deflection, overcoming the above uncertainty. This was the basis for the work performed for this thesis.

By undertaking a series of short term creep tests, up to 1 year in length, two compatible methods for design strain prediction have been found. Both predicted the existence of creep-rupture limits, so that design based on deflections not exceeding these levels, would ensure the absence of time dependent service failures. The limits found from each approach were consistent, and could be explained in terms of observed damage mechanisms (15.5).

16.2. 1. Maximum creep failure strain model

This was based on the assumption that, for a viscoelastic body, the instantaneous tensile failure strain (εt) represents the lowest level of deflection that can cause sample failure (15.3.3). Thus, in a creep test, maximum secondary creep strain, used as the failure strain for these materials, must exceed εt at rupture.

By measuring creep failure strain against applied load, results can be extrapolated back to the level of εt. This point represents the minimum load that can be applied to cause time dependent failure. Once εs falls below εt, insufficient damage accumulates during creep to initiate creep-rupture . When this was done using the results from the current work, a creep-rupture limit was found to exist at 50% UTUL in air (figure 12.10), and 25% UTUL in water at 23°C (figure 12.14). Further testing at elevated temperature would reveal how the εs gradient varied with temperature, from which the existence

of other limits could be predicted.

By performing short term creep tests under the service conditions required, simple extrapolation would reveal the creep-rupture limit for use in design calculations. Then, much smaller safety factors, perhaps in the range 2-5, could be used, reducing the level of over-design currently necessary for GRP components.

16.2.2. Maximum primary creep strain model

The level of maximum primary strain induced on loading GRP represents a measure of the initial damage created on loading, and has been seen to determine the sample ttf. It is largely a function of the applied stress, and by plotting ε_i vs. log (ttf), a curve analagous to a creep-rupture plot is obtained. When this was done for the current data, it was found that the results tended to a limit corresponding to a load of 50% UTUL in air (figure 12.11), and 25% UTUL in water at 23°C (figure 12.15), as before.

This method of design has one overriding advantage. Having produced an ε_i vs. log (ttf) plot, the results can be used in a diagnostic, as well as predictive fashion. By monitoring component deflection during initial loading, if the strain produced exceeds the creep-rupture limit, i.e. time dependent failure will occur, component life can be read directly from the curve.

A combination of the 2 methods discussed above would produce predictions of the load levels that can safely be applied to GRP, without causing creep rupture under the required service conditions.

CHAPTER 17

CONCLUSIONS

1. For all the immersion conditions examined, moisture diffusion was shown to be non-Fickian, due to the presence of defects in the sample.
2. Moisture uptake was found to increase with applied load, due to the formation of easy diffusion paths, after transverse crack initiation. Enhanced uptake changed diffusion from a face, to an edge, dominated mechanism.
3. Increases in temperature also led to an increase in GRP diffusion rate.
4. The rate at which weave debonding occurred during immersion was dependent on stress and temperature, while c.s.m. debond rate remained constant.
5. Woven roving debonding was concentrated at weave cross-over points in the laminate.
6. General matrix damage growth was found to occur during immersion in water, at a rate independent of stress and temperature, after about 6 days. Cracking resulted from a build up of swelling stresses, particularly at resin pore sites, and cross-over interface regions.
7. Immersion at 60°C for 6 months, reduced the tensile strength of the GRP by 30%. Similar soaking treatments at 23°C produced a 15% strength loss.
8. Tensile failure strain was shown to be rate dependent, due to a combination of stress corrosion, and viscoelastic, mechanisms.
9. It was found that above 50% UTUL, multi-filament-fractures (M.F.F.) occurred in longitudinal woven rovings, in the region of cross-overs.
10. In air, it was postulated that M.F.F. regions represented a critical damage state to initiate creep-rupture.
11. In water, fibre corrosion could produce M.F.F. damage during creep loading, allowing creep-rupture at stresses where it should not occur in air.

12. Sample variability made the prediction of ttf from creep-rupture data highly unsatisfactory.
13. Secondary creep strain was found to increase in discrete steps, caused by the creation of transverse cracks in the longitudinal fibre rovings at cross-overs. This was found in both air, and water.
14. When immersed in water, the tertiary creep region was extended as a result of resin plasticisation.
15. Creep was found to be a matrix dominated property, with resin flow under load contributing to longitudinal woven roving straightening, both in air and water.
16. Above 80% UTUL, creep-rupture was environment insensitive.
17. Reductions in ttf during immersion were found to be due to stress-enhanced fibre corrosion weakening of the reinforcement. Between 80, and 50% UTUL, weakening was stress dependent, while at lower loads, temperature effects became significant.
18. Moisture degradation was found to reduce ttf, by concentrating damage at weave cross-overs. At room temperature, it was found that enhanced edge diffusion of water was required to initiate moisture degradation in the reinforcement.
19. Below 25% UTUL, creep-rupture became environment insensitive, due to the absence of transverse cracking.
20. No simple relationship existed between applied load and log (ttf) during creep-rupture of mixed reinforcement GRP.
21. Two self consistent design criteria, based on observed damage growth, have been developed, to predict the existence of a creep-rupture limit under the test conditions used, from a series of short term creep tests.

REFERENCES

1. PARKYN, B - "Historical background". Glass Reinforced Plastics in Construction. p. 1.

2. BRYAN-BROWN, M.H.; WALKER, D.M.; WYATT, R.C. -"Advances in the use of GRP for the power industry" - CEGB South West Region, S.S.D. Report, October 1980.

3. HEPPEL, N; PHILLIPS, M.G. - "The tensile stress-rupture behaviour of GRP in aqueous environments". SWIRL Report, No. 1921, November 1980.

4. HEPPEL, N.W.; PHILLIPS, M.G. - "The tensile stress-rupture behaviour of GRP in aqueous environments". SWIRL Report, No. 2451, 1983.

5. LYONS, K. - "Environmental degradation of GRP". Ph. D. thesis, University of Bath, November 1983.

6. PHILLIPS, M.G. - "Long term strength of glass reinforced plastics in wet environments". University of Bath, School of Materials Science Report, 1983.

7. WYATT, O.H.;DEW-HUGHES,D. - Metals, Ceramics, and Polymers. Published by Cambridge University Press, 1974.

8. BORAX CONSOLIDATED LTD - Glasses. Published by Borax Consolidated Ltd., 1965.

9. HULL, D - Introduction to Composite Materials. Published by Cambridge University Press, 1981.

10. DOYLE, P.J. - Glass - Making Today. Published by Portcullis Press, 1979.

11. MOHR, J.G.; ROWE, W.P. - Fiber Glass. Published by Van Nostrand Reinhold, 1978.

12. PIGGOTT, M.R. - Load Bearing Fibre Composites. Published by Pergamon Press, 1980.

13. ERNSBERGER, F.M. - "Elastic properties of glasses". Glass Science and Technology. Volume 5. Published by Academic Press, 1980, p.1.

14. LAWN, B.R.; WILSHAW, T.R. - Fracture of Brittle Solids. Published by Cambridge University Press, 1975.

15. OKA, Y.; WAHL, J. ;TOMOZAWA, M. - "Swelling and mechanical strength of glass". Journal of Non-Crystalline Solids, 38 and 39, 1980. p.397.

16. PROCTOR, B.A. - "Fibre reinforced composite materials" Faraday Special Discussions of the Chemical Society, No.2, 1972. p.63.

17. GURNEY, C. -"Sources of weakness in glass" - Pro . Royal Society, London. A. (282), 1964. p.24

18. ZWEBEN,C;SMITH,W.S.; WARDLE,H.W. -"Test methods for fibre tensile strength, composite flexural modulus and properties of fabric reinforced laminates". Composite Materials: Testing and Design, 5th Conference, New Orleans, 1978. p. 228.

19. HAYTHORNWAITE, E. - "The effect of fabric construction and properties on the physical properties of glass fabric-resin laminates". British Plastics Federation Reinforced Plastics Technical Conference, 1958.

20. ISHIKAWA, T.; CHOU, T.W. -"Stiffness and strength behaviour of woven fabric composites". Journal of Materials Science, volume 17 (11), November 1982. p. 3211

21. PAUL, A. - "Chemical durability of glass". Chemistry of Glasses. p. 100.

22. CHARLES, R.J. - "Static fatigue of glass I" - Journal of Applied Physics, volume 29 (11), November 1958, p. 1549.

23. PROCTOR, B.A. - "The long term behaviour of glass fibre reinforced composites". NATO Advanced Study Institute "Glass Current Issues", April 1984.

24. WYATT, R.C. - "Weakening mechanisms in fibre reinforced polyester resins exposed to water". Ph.D. thesis, University of Bristol, 1968.

25. WITHROW, S.P. ; SINCLAIR, G.M. -"Environmentally assisted crack growth in glass". Corrosion Fatigue: Chemistry, Mechanics and Microstructure Conference Proceedings, University of Connecticut, June 1971, p. 749.

26. CHARLES, R.J. - "Static fatigue of glass II" Journal of Applied Physics, volume 29 (11), November 1958. p. 1554.

27. METCALFE, A.G.; SCHMITZ, G.K. -"Mechanism of stress corrosion in E-glass filaments". Glass Technology, volume 13 (1), February 1972. p. 5.

28. DOREMUS, R.H. - "Models of static fatigue in brittle materials". Corrosion Fatigue: Chemistry, Mechanics, and Microstructure Conference Proceedings, University of Connecticut, June 1971, p. 743.

29. DOZIER,S.A. ;KINSER, D.L. ;PACKMAN, P.F. -"A Study of crack morphology in static fatigue of glasses". Corrosion Fatigue: Chemistry, Mechanics and Microstructure Conference Proceedings, University of Connecticut, June 1971, p. 754.

30. FOX, P.G. -"Mechanisms of environment sensitive cracking in glasses".

31. WIEDERHORN, S.M. - "Environmental stress corrosion cracking of glass". Corrosion Fatigue: Chemistry, Mechanics and Microstructure Conference Proceedings, University of Connecticut, June 1971, p.731.

32. LAWRENCE, J.R. - Polyester Resins: Published by Reinhold Publishing Corporation. 1960.

33. COWIE, J.M.G. - Polymers: Chemistry and Physics of Modern Materials. Published by Intertext Books, 1973, p. 25.

34. NORWOOD, L.S. - "Polyester resins in corrosive environments". Pipecon. Proceedings of International Conference, London, June 1980.

35. ASHBEE, K.H.G.; FRANK, F.C.; WYATT, R.C. - "Water damage in polyester resins". Proc. Royal Society, London, A (300), 1967, p.415.

36. CHAMIS, C.C. - "Mechanics of load transfer at the interface". Composite Materials, Volume 6, Interfaces in Polymer Matrix Composites. Published by Academic Press, 1974, p.31.

37. SCOLA, D.A. - "High modulus fibres and the fibre-resin interface in resin composites, II". Composite Materials, Volume 6, Interfaces in Polymer Matrix Composites. Published by Academic Press, 1974, p.246.

38. NORMAN, R.H.; STONE, M.H.; WAKE, W.C. - "Resin-glass interface".

39. ERICKSON, P.W.; PLUEDDEMANN, E.P. - "Historical background of the interface - studies and theories". Composite Materials, Volume 6, Interfaces in Polymer Matrix Composites. Published by Academic Press, 1974. p.1.

40. WAKE, W.C. - "Theories of adhesion and uses of adhesives: a review". Polymer, volume 19, 1978. p.291.

41. PLUEDDEMANN, E.P. - Silane Coupling Agents. Published by Plenum Press, 1982.

42. VAUGHAN, D.J.; SANDERS,J.W. -"Premium composite performance from new glass finishes". 29th Annual Technical Conference, RP/C Institute, SPI, 1974.

43. DOWNEY, R.A. - Private Communication.

44. YIP, H.W.C.; SHORTALL, J.B.; - "The interfacial bond strength in glass fibre/polyester resin composite systems, part 2. The effect of surface treatment". Journal of adhesion, volume 8, 1976. p.155.

45. GRAF, R.T.;KOENIG, J.L.; ISHIDA, H. - "The influence of interfacial structure on the flexural strength of E-glass reinforced polyester". Journal of Adhesion, volume 16.p. 97.

46. BASCOM, W.D. - "Water at the interface". Journal of Adhesion, volume 2, 1970, p. 161.

47. ASHBEE, K.H.G.; WYATT, R.C. - "Water damage in glass fibre/resin composites". Proc. Royal Society, London, A (312), 1969, p.553.

48. PARKYN, B. - "Methods of manufacture of GRP". Glass Reinforced Plastics in Construction. p.36.

49. KELLY, A - "Composite principles". Fatigue and Creep of Composite Materials. Proceedings of the 3rd RISO Symposium on Metallurgy and Materials Science, 1982. p.51.

50. HARRIS, B. - "The mechanical behaviour and testing of composite materials". University of Bath, School of Materials Science Report, April 1982.

51. PARKYN, B -"Mechanism of fibre reinforcement and material design". Glass Reinforced Plastics in Construction, p.9.

52. ORGORKIEWICZ, R.M. - "Mechanical behaviour of fibre composites"

53. GARRETT, K.W.; BAILEY, J.E. - "The effect of resin failure strain on the tensile properties of glass fibre reinforced polyester cross-ply laminates". Journal of Materials Science, volume 12, 1977, p. 2189.

54. JOHNSON, A.F. - "Engineering design properties of GRP". British Plastics Federation. Publication No. 215, 1978.

55. WHITE, R.J. - "The effect of holes and cracks on the strength of glass fabric reinforced epoxide laminates". University of Bath, School of Materials Science Industrial Training Report, 1981.

56. SIEBERT, O.W. - "The case against woven roving ". 37th Annual Conference, RP/C Institute, SP1, January 1982.

57. DOWNEY, R.A. - "Engineering textiles - a route to better mechanical properties in composites". Fibre Reinforced Composites. Proceedings of P.R.I. Conference, Liverpool, April 1984.

58. JARAS, A.C.; NORMAN, B.J.; SIMMENS, S.C. - "The measurement of glass fibre strength in composites from studies of their fracture surfaces." Journal of Materials Science, volume 18, 1983, p. 2459.

59. DESVAUX, M.P.E.; GREENWOOD, J.H. -"The problem of material variability in the testing of GRP laminates". Fatigue and Creep of Composite Materials. Proceedings of the 3rd RISO International Symposium of Metallurgy and Materials Science, 1982, p. 199.

60. JUDD, N.C.W.; WRIGHT, W.W. -"Voids, and their effects on the mechanical properties of composites - an appraisal". SAMPE Journal, January/ February 1978, p.10.

61. HANCOX, N. - Private Communication.

62. SIMS, G.D.; GLADMAN, D.G. - "Effect of test conditions on the fatigue strength of a glass fabric laminate: Part A - frequency". Plastics and Rubber:Materials and Applications, May 1978, p. 41.

63. THOMAS, W.F. - "An investigation of the factors affecting the strength of glass fibre strand. Part 2". Glass Technology, volume 13 (1), 1972, p.17.

64. THOMAS, W.F. - "An investigation of the factors affecting the strength of glass fibre strand. Part 3. The strength in Polyester resin". Glass Technology, volume 13(4), 1972 p.122.

65. OWEN, M.J.; RICE, D.J. - "Biaxial strength behaviour of glass fabric reinforced polyester resins". Composites, January 1981, p.13.

66. OWEN, M.J. -"Biaxial fatigue of composites with short and long fibres". Fatigue and Creep of Composite Materials. Proceedings of the 3rd RISO International Symposium on Metallurgy and Materials Science, 1982, p. 101.

67. JONES, R.M. - "Mechanics of Composite Materials. Published by McGraw-Hill, 1975.

68. BEAUMONT, P.W.R. - "Fracture mechanics approach to failure in fibrous composites". Journal of Adhesion, volume 6 (1), 1974, p. 107.

69. NUISMER, R.J.; WHITNEY, J.M. - "Uniaxial failure of composite laminates containing stress cencentrations". Fracture Mechanics of Composites, ASTM STP 593, 1975, p. 117.

70. WADDOUPS, M.E.; EISENMANN, J.R.; KAMINSKI, B.E. - "Macroscopic fracture mechanics of advanced composite materials". Journal of Composite Materials, volume 5, October 1971, p. 446.

71. KONISH, J.R.; SWEDLOW, J.L.; CRUSE, T.A. - "Experimental investigation of fracture in an advanced fibre composite". Journal of Composite Materials, volume 6, 1972, p. 114.

72. KANNINEN, M.F.; RYBICKI, E.F.; BRINSON, H.F. - "A critical look at current applications of fracture mechanics to the failure of fibre-reinforced composites". Composites, January 1977, p. 17.

73. COLEMAN, B.D. - "On the strength of classical fibres and fibre bundles". Journal of the Mechanics and Physics of Solids, volume 7, 1958, p. 60.

74. HARLOW, D.G.; PHOENIX, S.L. - "The Chain-of-Bundles Probability Model for the strength of fibrous materials I: Analysis and conjectures". Journal of Composite Materials, volume 12, April 1978, p. 195.

75. HARLOW, D.G.; PHOENIX, S.L. - "The Chain-of-Bundles Probability Model for the strength of fibrous materials II:A numerical study of convergence". Journal of Composite Materials, volume 12, May 1978, p.314

76. BUNSELL, A.R. - "The role of the matrix" AGARD Lecture Series No 124. 1974.

77. SPRINGER, G.S. - "Introduction of environmental effects on composite materials". Environmental Effects on Composite Materials. Published by Technomic Publishing Co., 1981, p.1

78. SHEN, C.H.;SPRINGER, G.S. - "Moisture absorption and desorption of composite materials". Environmental Effects on Composite Materials. Published by Technomic Publishing Co., 1981, p.15.

79. COLLINGS, T.A.; COPLEY, S.M. - "On the accelerated ageing of CFRP". Composites, volume 14 (3), 1983, p. 180.

80. EDGE, E.C. - "Analysis of moisture gradients in service and in the laboratory". Composites, volume 14(3), 1983, p.189.

81. WEITSMAN, Y. - "Diffusion with time varying diffusivity, with application to moisture sorption in composites". Journal of Composite Materials, volume 10, July 1976, p. 193.

82. LEUNG, C.L.; KAELBLE, D.H. - "Moisture diffusion and microdamage in composites". Resins for Aerospace Symposium, Honolulu, April 1979, p. 419.

83. LOOS,A.C.; SPRINGER, G.S.; SANDERS, B.A.; TUNG, R.W. -"Moisture absorption of polyester/E-glass composites". Enviromental Effects on Composite Materials. Published by Technomic Publishing Co. 1981, p.51.

84. ELLIS, B.; FOUND, M.S. -"The effects of water absorption on a polyester/chopped strand mat laminate". Composites, volume 14(3), 1983. p. 237.

85. MENGES, G.; GITSCHNER, H.W. - "Sorption behaviour of glass-fibre reinforced composites and the influence of diffusing media on deformation and failure behaviour". Advances in Composite Materials.3rd International Conference on Composite Materials, Paris, 1980 .p.25.

86. DEWIMILLE, B.; THORIS, J.; MAILFERT, R.; BUNSELL, A.R. - "Hydrothermal ageing of a unidirectional glass-fibre epoxy composite during water immersion". Advances in Composite Materials. Proceedings of ICCM 3, Paris, August 1980. p.597.

87. FARRAR, N.R.; ASHBEE, K.H.G. - "Self-Stress-enhanced water migration in composites". Resins for Aerospace Symposium, Honolulu, April, 1979. p.435.

88. BONNIAU, P.; BUNSELL, A.R.; - "Water absorption by glass fibre reinforced epoxy resin". Composite Structures: Proceedings of the 1st International Conference on Composite Structures, Paisley, September 1981. p.92.

89. MARSHALL, J.M.; MARSHALL, G.P.; PINZELLI, R.F. - "The diffusion of liquids into resins and composites". 37th Annual Conference, RP/C Institute, January 1982.

90. JONES, F.R. - "Model composite beams for environmental testing". TEQC 83. Proceedings of the International Conference on Testing, Evaluation, and Quality Control of Composites, Guildford, September, 1983. p.193.

91. WRIGHT, W.W. -"The effect of diffusion of water into epoxy resins and their carbon fibre reinforced composites." Composites, July 1981, p.201.

92. KAELBLE, D.H. -"Experimental analysis of hydrothermal ageing in fibre reinforced composites". Resins for Aerospace Symposium, Honolulu, April 1979. p. 395.

93. JONES, F.R.; MULHERON, M.; BAILEY, J.E. - "Generation of thermal strains in GRP, Part I. Effect of water on the expansion behaviour of unidirectional glass-fibre reinforced laminates." Journal of Materials Science, volume 18, 1983. p. 1522.

94. JONES,F.R.; MULHERON, M.; BAILEY, J.E.; - "Generation of thermal strains in GRP, Part II. The origin of thermal strains in polyester cross-ply laminates". Journal of Materials Science, volume 18, 1983 p. 1533.

95. ROTEM, A.; ELIZOV, S. - "Effect of temperature and marine environment on the rupture strength of fibrous composite materials". Fatigue and Creep of Composite Materials. Proceedings of the 3rd RISO International Symposium on Metallurgy and Materials Science. 1982, p. 305.

96. DOREY, G. -"Environmental degradation of composites". Practical Considerations of Design, Fabrication, and Tests for Composite Materials. AGARD Lecture Series No. 124, October 1982.

97. BOUDREAU, R.J. - "Glass fabric finishes. Effects on the kinetics of water absorption and laminate physical and electrical properties." 37th Annual Conference, RP/C Institute, SPI, January 1982.

98. GRAYSON, M.A. - "Measurement of the distribution of water in a graphite/epoxy by precision abrasion mass spectrometry". Resins for Aerospace Symposium, Honolulu, April 1979. p.449.

99. APICELLA, A.; MIGLIARESI, C.; NICOLAIS. L.; IACCARINO, L.;ROCCOTELLI, S.; - "Influence of processing on the water ageing of unsaturated polyester based composites." TEQC 83. Proceedings of the International Conference on Testing, Evaluation and Quality Control of Composites, Guildford September, 1983, p. 171

100. PRITCHARD, G.;TANEJA, N. - "Nature and extent of water damage in glass laminates". 29th Annual Technical Conference, RP/C Institute, SPI, 1974.

101. HOGG, P.J.;HULL, D. -"Corrosion and environmental deterioration of GRP". Developments in GRP Technology - (1) - Published by Interscience, 1983, p. 37.

102. JONES, F.R.; MULHERON, M.; -"The effect of moisture on the expansion behaviour and thermal strains in GRP". Composites, volume 14(3), 1983, p.281.

103. ADAMS, R.C. -"Variables influencing the blister resistance of marine laminates". 37th Annual Conference, RP/C Institute, SPI, January 1982.

104. ROBERTS, R. C. - "Design, strain and failure mechanism of GRP in a chemical environment." Reinforced Plastics Congress, Brighton, November 1978. p.145.

105. PRITCHARD,G.;TANEJA,N. -"Water damage in polyester/glass laminates. Part I. An apparatus for the study of water damage in uniaxially stressed materials". Composites, volume 4, July/September 1973. p.181

106. PRITCHARD,G.;TANEJA,N. - "Water damage in polyester/glass laminates. Part 2. Microscopic evidence". Composites, volume 4, July/September 1973. p.199.

107. ISHAI, O - "Environmental effects on deformation, strength and degradation of unidirectional glass fibre reinforced plastics. 1. Survey". Polymer Engineering and Science, volume 15(7), 1975. p.486.

108. ISHAI, O. - "Environmental effects on deformation, strength and degradation of unidirectional glass fibre reinforced plasts. 2. Experimental study." Polymer Engineering and Science, volume 15(7), 1975. p.491.

109. HOJO, H.; TSUDA. K. - "Effects of chemical environments and stress on corrosion behaviours of glass fibre reinforced plastics and vinyl ester resin". 34th Annual Conference, RP/C Institute, SPI 1979.

110. REGE,S.K.;LAKKAD, S.C. - "Effect of salt water on mechanical properties of fibre reinforced plastics". Fibre Science and Technology, volume 19, 1983. p. 317.

111. CAMERON, J.B. - "The temperature limitations of reinforced plastics in aggressive environments." Trans. Journal Plastics Institute. October 1967. p.681.

112. SCRIMSHAW,G. -"The effect of environment on the properties of GRP". Pipecon. Proceedings of International Conference , London, June 1980.

113. SHORT, D.; STANKUS, A.W.;SUMMERSCALES, J. - "Woven glass-fibre reinforced polyester-resin composites exposed to the marine environment". TEQC 83 Proceedings of the International Conference on Testing, Evaluation and Quality Control of Composites, Guildford, September 1983, p.212.

114. COWIE, J.M.G. - Polymers:Chemistry and Physics of Modern Materials. Published by Intertext, 1973. p.236.

115. POBEDRYA, B.E. - "Application of the theory of viscoelasticity to composite materials, Mechanics of Composite Materials. Volume 15(3) 1979.p.271

116. CROWSON, R.J.;ARRIDGE, R.G.C. - "Linear viscoelastic properties of epoxy resin polymers in dilation and shear in the glass transition region. 1. Time-temperature superposition of creep data". Polymer, volume 20(6), 1979, p.737.

117. YOSHIDA, H. - "Viscoelastic properties of fibre reinforced plastics". Resins for Aerospace Symposium, Honolulu, April 1979 p.247.

118. NICOLAIS, L.; GUERRA, G.; MIGLIARESI, C.; NICODEMO. L.; BENEDETTO, A.T.; "Viscoelastic behaviour of glass reinforced epoxy resin". Polyer Composites, volume 20, July 1981, p.116.

119. ASHTON, J.E. - "Non-Linear viscoelastic characterisation of non-linear response of fibrous composites". Journal of Composite Materials, volume 2, 1968. p. 116.

120. SCHAPERY, R.A. - "Deformation and failure analysis of viscoelastic composite materials". A.S.M.E. AMD, Volume 13, 1975, p.127.

121. LOU, Y.C.; SCHAPERY, R.A. ; "Viscoelastic characterisation of a non-linear fibre reinforced plastic". Journal of Composite Materials, volume 5, 1971, p. 208.

122. BABICH, V.F.; LIPATOV, Y .S. - "On shift and resolubility of relaxation maxima with change in properties of the boundary polymer layer in composite materials." Journal of Applied Polymer Science, volume 27(1), 1982, p.53.

123. SCHAPERY, R.A. - "Viscoelastic behaviour and analysis of composite materials". Composite Materials, volume 2, 1974, p.85.

124. BARKER, A.J.; BOTT, T.R. - "Creep in glass fibre reinforced plastics". Industrial and Engineering Chemistry, volume 59, July 1967, p.46.

125. DIGGWA, A.D.S.; NORMAN, R.H. - "Mechanism of creep of GRP" Plastics and Polymers, October 1972 p. 263.

126. JANSSON, J.F. - "Creep and fracture initiation in fibre reinforced plastics". Kem Kem, volume 8(5), 1981, p.292.

127. BHATNAGAR, A.; LAKKAD, S.C.;RAMESH, C.K. - "Creep in high glass content unidirectional and bidirectional GRP laminates". Fibre Science and Technology, volume 15(1), 1981, p.13.

128. STURGEON, J.B. - "Creep of fibre reinforced thermosetting resins". Creep of Engineering Materials, p. 175.

129. HOLMES, M.;RAHMAN, T.A. - "Creep behaviour of glass reinforced plastic box beams". Composites, volume 11, April 1980. p.79.

130. LILHOLT, H. - "Relations between matrix and composite creep behaviour". Fatigue and Creep of Composite Materials. Proceedings of the 3rd. RISO International Symposium on Metallurgy and Material Science,1982. p.63.

131. STREET, K.N. -"Steady state creep of fibre reinforced materials". The Properties of Fibre Composites. Proceedings, National Physical Laboratory, November 1971. p.36.

132. CHERRY, B.W. - "Strength and fracture toughness of glass fibre reinforced plastics." Applied Polymer Symposium, No 17. 1971. p.73.

133. WEIDEMANN, G.W. ; OGORKIEWICZ, R.M. - "Tensile creep of a unidirectional glass-fibre epoxy laminate". Composites, volume 5, May 1974. p. 117.

134. KOENEMAN, J.B.; KICHER, T.P. - "Creep behaviour of elastic fibre/epoxy matrix composite materials". Composite Materials: Testing and Design ASTM STP 497, 1972. p.503.

135. STEEL, D.J. - "The creep and stress-rupture of reinforced plastics". Trans. Journal Plastics Institute, October 1965. p.161.

136. CHIAO,C.C.;SHERRY,R.J.;CHIAO,T.T. -"Strength retention and life of fibre composite materials". Composites, volume 7(2), 1976, p.107.

137. DESVAUX, M.P.E.; SMITH, G - "Long Term reliability of GRP". Fibre Science and Technology, volume 18, 1983. p.53.

138. AVESTON,J.; SILLWOOD, J.M. - "Time dependent strength of unidirectional glass reinforced plastics in air, water and dilute sulphuric acid". Fatigue and Creep of Composite Materials. Proceedings of the 3rd RISO International Symposium on Metallurgy and Materials Science, 1982. p.161.

139. COCHRAN,W.G.;COX,G.M. - Experimental Designs. Published by John Wiley and Sons, 2nd Edition, 1957.

140. CHATFIELD, C. - Statistics for Technology . Published by Chapman and Hall, 1983.

141. WYATT, R.C.;NORWOOD, L.S.;PHILLIPS, M.G. - "The stress-rupture behaviour of GRP laminates in aqueous environments". Composite Structures. Proceedings of the 1st International Conference, Paisley, September 1981. p.79.

142. LYONS, K.B.;PHILLIPS, M.G. - "Creep-rupture and damage mechanisms in glass reinforced plastics". Composites, volume 12, October 1981. p.265.

143. LIFSHITZ, J.M. - "Time dependent fracture of fibrous composites". Fracture and Fatigue. Published by Academic Press, 1974.

144. ROBINSON, E.Y.;CHIAO, T.T. - "Analysis of stress-rupture data from S-glass composites". 27th Annual Conference, RP/C Institute, SPI, February 1972.

145. CHIAO,T.T.;LEPPER,J.K.;HETHERINGTON,N.W.;MOORE,R.L. - "Stress-rupture of S-glass/epoxy composites". Journal of Composite Materials, volume 6, July 1972. p.358.

146. HAHN,H.T.;CHIAO,T.T - "Long term behaviour of composite materials". Advances in Composite Materials. Proceedings of the 3rd International Conference on Composite Materials, Paris, August 1980. p.584.

147. PHILLIPS, M.G. - "Prediction of long-term stress-rupture life for glass fibre reinforced polyester composites in air and in aqueous environments" Composites, volume 14(3) 1983, p.270.

148. ALLEN, R.C. - "Effect of moisture on flexural creep of resins". 37th Annual Conference, RP/C Institute, SPI, January 1982.

149. WANG,C.S.; WANG,A.S.D.- "Creep behaviour of glass/epoxy composite laminates under hygrothermal conditions". Advances in Composite Materials: Proceedings of the 3rd. International Conference on Composite Materials, Paris, August 1980. p.569.

150. HOA, S.V. - "Effects of liquids on the stress-rupture lives of fibre glass reinforced plastics." Test Methods and Design Allowables for Fibrous Composites, Philadelphia, October 1979. p.411.

151. HOA,S.V. - "Creep of fibre glass reinforced plastics in liquid environments". Advances in Materials Technology in the Am-1980, San Fransisco, August 1980, p.63.

152. WU, E.M.;RUHMAN, D.C. - "Stress-rupture of glass-epoxy composites-environ - mental and stress effects". Composite Reliability: Proceedings of the Symposium, Las Vegas, 1974, p.263.

153. RUHMAN,D.C;WU, E.M. - "The effects of solvents and stress on the stress-rupture life of glass epoxy composites". Plast. Chem.Pap., Volume 31(1) 1971, p.501.

154. HULL,D.; HOGG,P.J.; - "Nucleation and propogation of cracks during strain corrosion of GRP". Advances in Composite Materials, 3rd International Conference on Composite Materials, Paris, August, 1980, p.543.

155. PRICE, J.N.;HULL, D. - "Propogation of stress corrosion cracks in aligned glass fibre composite materials". Journal of Materials Science volume 18, 1983, p.2798.

156. JONES,F.R.;ROCK,J.W.;WHEATLEY,A.R. -"Stress corrosion cracking and its implications for the long term durability of E-glass fibre composites". Composites, volume 14(3), 1983. p.262.

157. HOGG, P.J. - "Factors affecting the stress corrosion of GRP in acid environments". Composites, volume 14 (3), 1983. p.254.

158. KISBENYI,M.B.; HARRISON, D.; PINZELLI,R.; EYRE,D.M.; MARSHALL, G.P. "The effect of post-cure on environmental stress corrosion of vinyl ester laminates and gel coat layers".

159. HOGG,P.J.;PRICE,J.N.;HULL,D. -"Stress corrosion of GRP". Fibre Reinforced Composites 84. Proceedings of PRI Conference, Liverpool, April, 1984.

160. ILLSTON, J.M.;DINWOODIE,J.M.;SMITH,A.A. - Concrete, Timber, and Metals. Published by Van Nostrand Reinhold, 1979.

161. ASHBY,M.F.;JONES,O.R.H. - Engineering Properties. An Introduction to their Properties and Applications. Published by Pergamon Press, 1980.

162. HARRIS, B.;BUNSELL,A.R. - Structure and Properties of Engineering Materials. Published by Longman, 1977.

163. REED-HILL,R.E. - Physical Metallurgy Principles. 2nd Edition. Published by Van Nostrand, 1973.

164. HARRIS, B. - Final Year Lecture Course, University of Bath, School of Materials Science. 1982.

165. MENGES,G.;ROSKOTHEN,H.J. -"Prediction of the creep behaviour of reinforced plastics". Polymer Engineering and Science, volume 15, July 1975. p.544.

166. BRINSON, H.F. - "Experimental mechanics applied to the accelerated characterisation of polymer based composite materials". New Physical Trends in Experimental Mechanics, April 1981, p.3.

167. DILLARD, D.A.;BRINSON,H.F. - "A numerical procedure for predicting creep and delayed failures in laminated composites". Long Term Behaviour of Composites, ASTM STP 813, 1983, p.23.

168. GRIFFITH, W.I.;MORRIS,D.H.;BRINSON,H.F. - "Accelerated characterisation of graphite/epoxy composites". Advances in Composite Materials, 3rd International Conference on Composite Materials, Paris, August, 1980. p.461.

169. BRINSON,H.F.;MORRIS,D.H.;YEOW,T.T. - "A new experimental method for the accelerated characterisation of composite materials". VDI - Berichte, Nr.313, 1978.

170. BRINSON,H.F.;MORRIS,D.H.;GRIFFITH,W.I. - "Creep-rupture of polymer-matrix composites". Experimental Mechanics, volume 21, September 1981, p.329.

171. CROSSMAN,F.W.;FLAGS, D.L. - "Dimensional stability of composite laminates during environmental exposure." 24th National SAMPE Symposium, San Fransisco, May 1979, p.990.

172. MENGES,G.;BRINTRUP, H. - "Long term behaviour of RP/C laminates at temperature changes and simultaneous mechanical load-glass fibre reinforced plastcs". The Wide World of Reinforced Plastics. Proceedings of the 29th Conference, Washington, February 1974.

173. DAUGSTE, C.L. - "Joint application of time-temperature and time-stress analogies to constructing unified curves". Polymer Mechanics, volume 10(3), 1974. p.359.

174. LIFSHITZ,J.M.;ROTEM,A. - "Time dependent longitudinal strength of unidirectional fibrous composites". Fibre Science and Technology, volume 3, 1970, p.1.

175. KELLY, A.;MC.CARTNEY, L.N. - "Failure by stress corrosion of bundles of fibres". Proc. Royal Society, London A. volume 374, 1981. p.475.

176. AVESTON, J.;KELLY,A.;SILLWOOD,J.M. - "Long term strength of glass reinforced plastics in wet environments". National Physical Laboratory Report, DMA(A), 18, October 1980.

177. DICKSON,R.F.;JONES,C.J.;HARRIS,B.;REITER,H.;ADAM,T. - "Effects of moisture on high performance laminates." 1st International Symposium on Acoustic Emission from Reinforced Composite, SPI, July, 1983.

APPENDIX ONE

The estimation of the number of replicate tests required to obtain statistically meaningful time to failure (ttf) error bands in the creep-rupture test, was undertaken using methods outlined by Cochran and Cox (139). The details of the method used are presented below.

When using statistical significance tests on the creep-rupture data generated, such as the student 't' test, the minimum acceptable standard error would be 5%. If using an analysis requiring an accurate measure of the limits of error occurring in a test, to predict the form of relationship that existed between applied load and ttf, a level of standard error has to be set. Thus, the first step was to decide on a standard error of 5% for these calculations, giving confidence limits of 90%.

Having decided upon the standard error required for the experiments, an estimate of the residual standard deviation of sets of samples tested at consecutive load levels had to be made. Several techniques exist for this purpose, but since data from similar experiments was already available (4), this was used, by means of a method known as the "within sample variation " technique.

For this method, the mean and standard deviation of the failure time was calculated at each load level, the latter being known as the "within-unit standard deviation". Then, the standard deviation of the mean values was determined, this value being known as the "between-unit standard deviation". for n observations per load level, the residual standard deviation is given by:-

$$(\text{between-unit S.D.})^2 + \frac{(\text{within-unit S.D.})^2}{n} = \text{r.s.d.} \qquad - (A.1)$$

Having obtained an estimate of r.s.d. from previous results (using equation A.1), and set the standard error (s.e.) to the required value, the number of replicate tests (r) required, to produce this spread was calculated from:

$$r = 2 \times \left(\frac{\text{r.s.d.}}{\text{s.e.}}\right)^2 \qquad - (A.2)$$

	E-GLASS	C-GLASS	S-GLASS
SiO_2	52·4	64·4	64·4
Al_2O_3 , Fe_2O_3	14·4	4·1	25·0
CaO	17·2	13·4	———
MgO	4·6	3·3	10·3
Na_2O , K_2O	0·8	9·6	0·3
Ba_2O_3	10·6	4·7	———
BaO	———	0·9	———

(all values in wt.%)

Table 2.1

Typical glass fibre compositions (9).

PROPERTY	UNITS	VALUE
DENSITY	Mgm^{-3}	1·2 - 1·5
ELASTIC MODULUS	GNm^{-2}	2 - 4·5
POISSON'S RATIO		0·37 - 0·39
TENSILE STRENGTH	MNm^{-2}	40 - 90
FAILURE STRAIN	%	2
HEAT DISTORTION TEMPERATURE	°C	50 - 110
CURE SHRINKAGE	%	4 - 8
WATER UPTAKE 24 HRS. AT 20°C	%	0·1 - 0·3

Table 3.1

Typical properties of polyester resins (9).

	MIXED REINFORCEMENT	100% W.R
RESIN	Scott Bader Crystic 625TV	B.P. Cellobond
ACCELERATOR CATALYST (MEKP)	2wt.%	2wt.% 1·5wt.%
REINFORCEMENT	1×300 g/m² c.s.m 1×830 g/m² w.r (warp) 2×300 g/m² c.s.m 1×830 g/m² w.r (weft) 1×300 g/m² c.s.m	4×830 g/m² w.r
CURE	24hrs. at 20°C 5hrs. at 60°C	24hrs. at 20°C 72hrs. at 40°C

Table 9.1

Structure of GRP laminates used.

	MIXED REINFORCEMENT	100% W.R
STRENGTH (MPa)	154·3 ± 11·1	212·0 ± 15·9
UTUL (MNm^{-1})	2·19 ± 0·10	———
ε (%)	1·75 ± 0·22	———
E (GPa)	89·3 ± 8·9	———

Table 9.2

Tensile strength data for laminates tested.

	POROSITY (%)	TIME TO FAILURE (HRS.)
100% W.R		
NOT OUTGASSED	3·2 ±1·2	19 - 45
OUTGASSED	1·9± 0·51	24-121
MIXED LAY-UP		
	1·4	253
	1·9	141
	2·1	292
	3·7	29
	3·4	52

Table 10.1

Results from porosity measurements undertaken.

	AS RECEIVED STRENGTH (MPa)	PRE-SOAKED STRENGTH (MPa)
23°C	179·0 ± 6·9	152·6 ± 7·0
60°C	165·0 ± 11·6	109·2 ± 5·5

Table 11.1

Residual strength data.

LOAD (%UTUL)	TIME TO FAILURE (SECS)			
85	90	226	241	587
	700			
80	240	253	260	720
79	1200	4080	4932	10 800
	18 000	176 400	252 000	777 600
72	15 600	204 550	531000	3369 600
68	972	1476	57 600	144 000
	4579 200			
60	3801 600	20736 000+	20736 000+	20736 000+
57	9700 000	10392 005	34819 200+	34819 200+

+ Sample not failed

Table 12.1

Creep-rupture data from samples tested in air.

LOAD (% UTUL)	TIME TO FAILURE (SECS.)			
85	66	138	156	178
79	127	297	431	522
72	240	300	720	2880
66	1440	4500	7200	15 240
59	3988	4176	61 200	79 200
53	97 200	277 917	1814 400	3196 800
46	5443 200	6652 800+	6652 800+	6652 800+
39	1440 000	6048 000	8035 200+	8035 200+

+ Sample not failed

Table 12.2

Creep-rupture data from samples tested in water, at room temperature

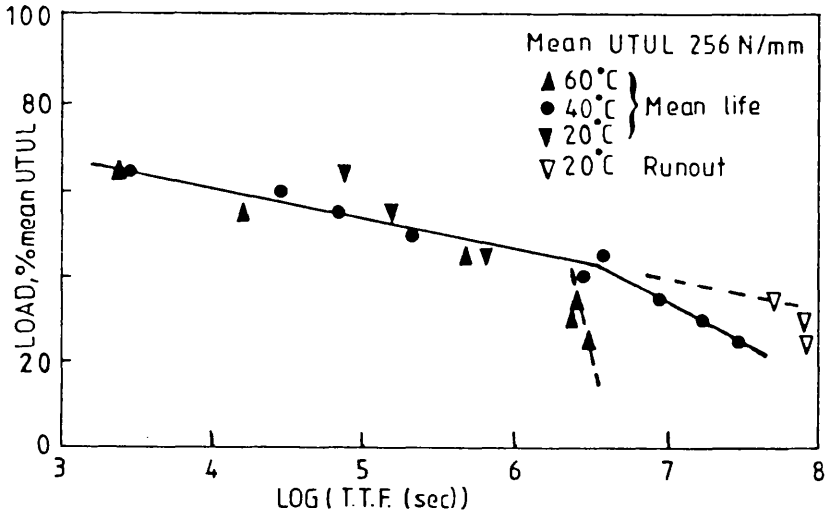

Figure 1.1

Mean lifetime as a function of tensile load, for polyester glass laminates tested in sea water at three temperatures. Full lines, best fit for tests at 40°C (4).

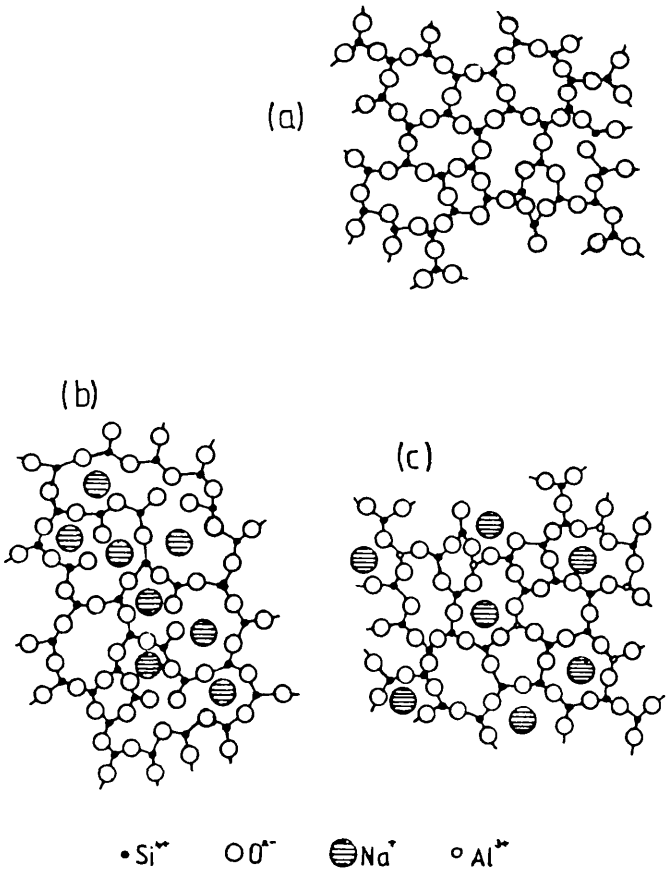

Figure 2.1

Structure of glasses: (a) Silica network (b) Network modified glass e.g. soda-silica (c) Intermediate glass e.g. alumina-silica (7).

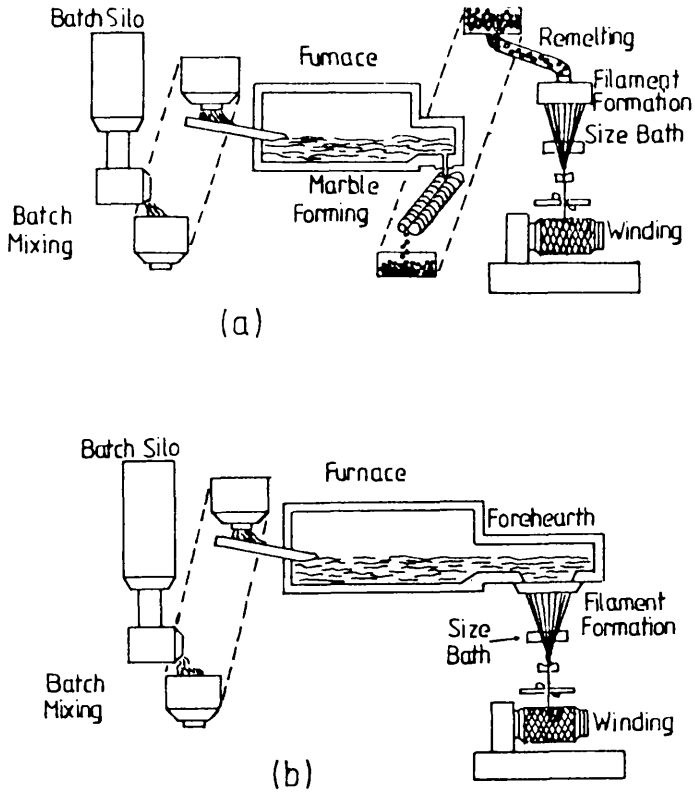

Figure 2.2

Schematic representation of continuous filament fibre glass production processes: (a) Marble melt (b) Direct melt (11).

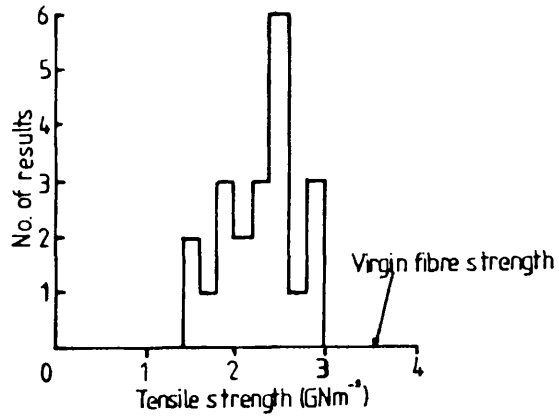

Figure 2.3

Tensile strengths of single E-glass fibres, 2cm test length, extracted from a strand and compared with the strength of virgin fibres (9).

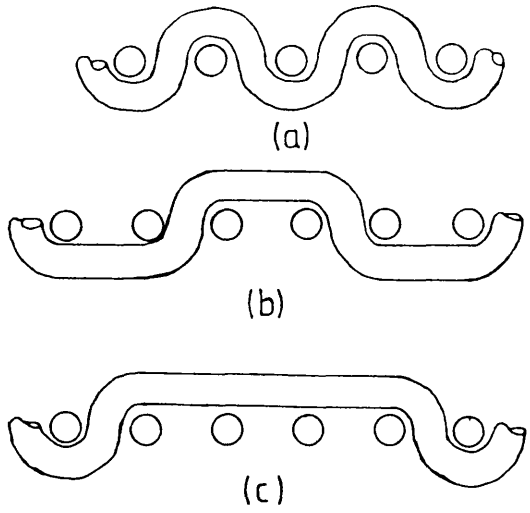

Figure 2.4

Schematic representation of standard fabric patterns: (a) Plain weave (b) Twill weave (c) Satin weave (18).

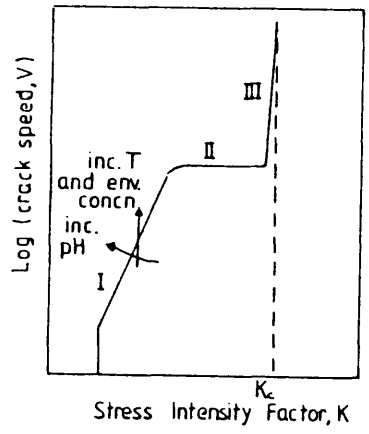

Figure 2.5

Typical crack speed dependence on stress for a material susceptible to environment sensitive fracture. The effects of temperature, environment concentration and pH on region I are indicated by the arrows (30).

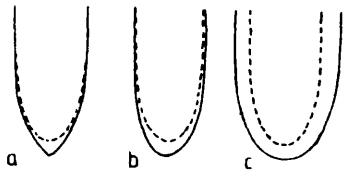

Figure 2.6

Hypothetical changes in flaw geometry due to corrosion or dissolution: (a) Flaw sharpening as a result of stress corrosion (b) Flaw growth such that the rounding of the tip by stress corrosion balances the lengthening of the flaw (c) Rounding by corrosion or dissolution (31).

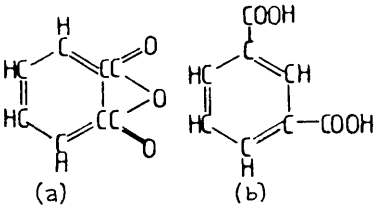

Figure 3.1

Phthalic anhydride (a), and its isomer Isophthalic acid (b), used in the production of polyester resins (32).

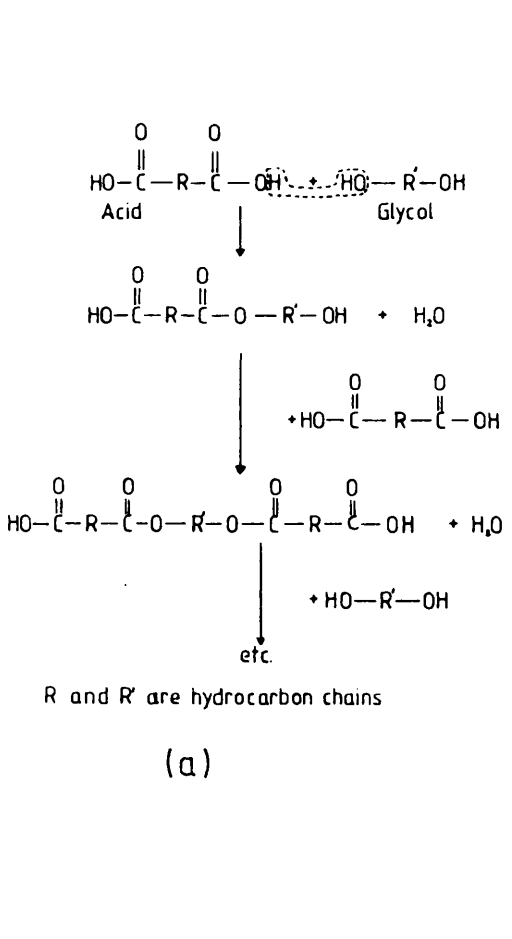

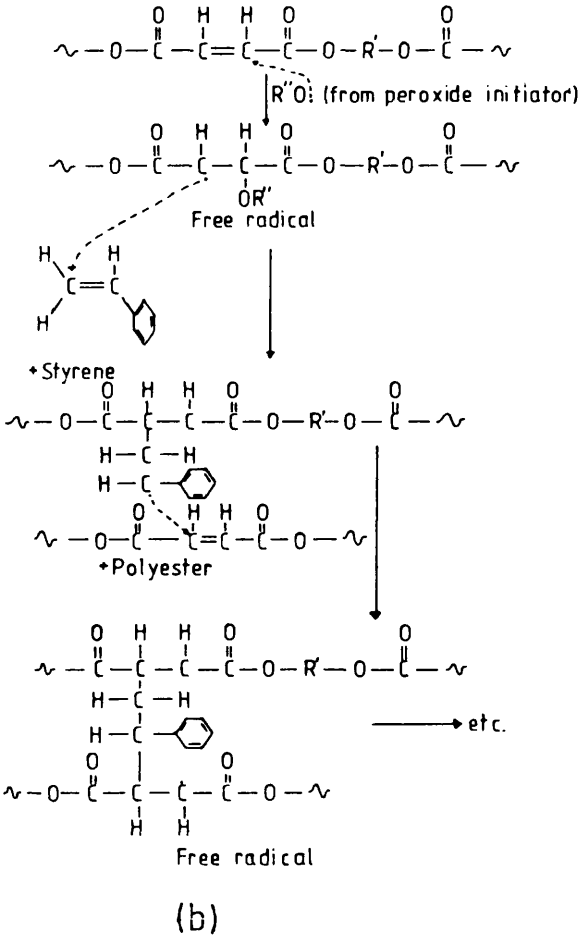

Figure 3.2

Representation of the reactions involved in the production of unsaturated polyester resins (a) Acid-glycol condensation reactions (b) Cross linking in unsaturated resins (34).

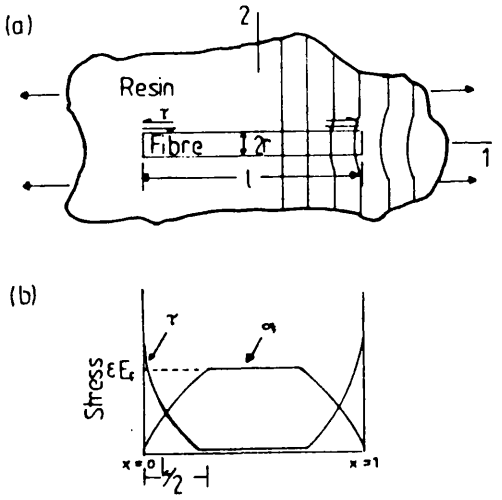

Figure 4.1

(a) Diagrammatic representation of deformation around a discontinuous fibre embedded in a matrix subjected to a tensile load parallel to the fibre. (b) Variation along the fibre of tensile stress in the fibre and shear stress at the interface. Matrix and fibre remain elastic and the interface bond is perfect (9).

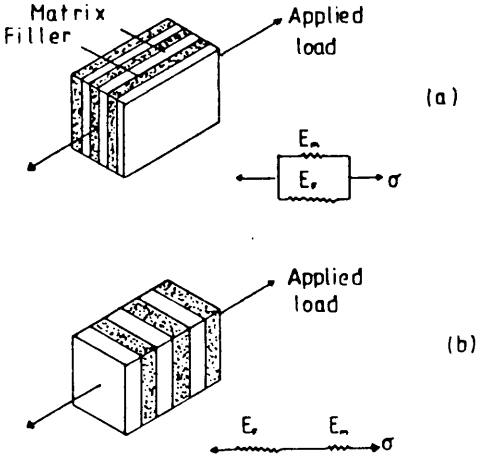

Figure 5.1

Parallel and series arrangements of matrix and filler in a model composite. In each case $E_f > Em$ and $V_f = Vm$. (a) Parallel model ($V_f = 0.5$) (b) Series model ($V_f = 0.5$) (50) .

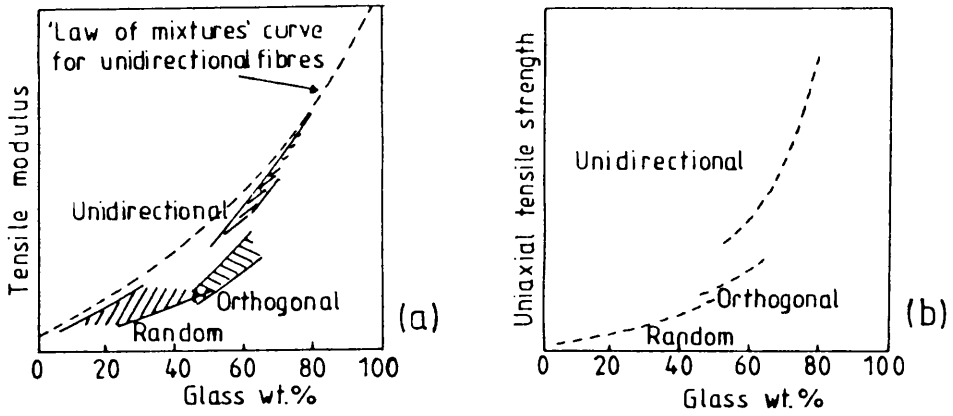

Figure 5.2

(a) Tensile modulus vs. glass content by weight, for the three principal categories of glass fibre/plastic composites. (b) Tensile strength vs. glass content by weight (52).

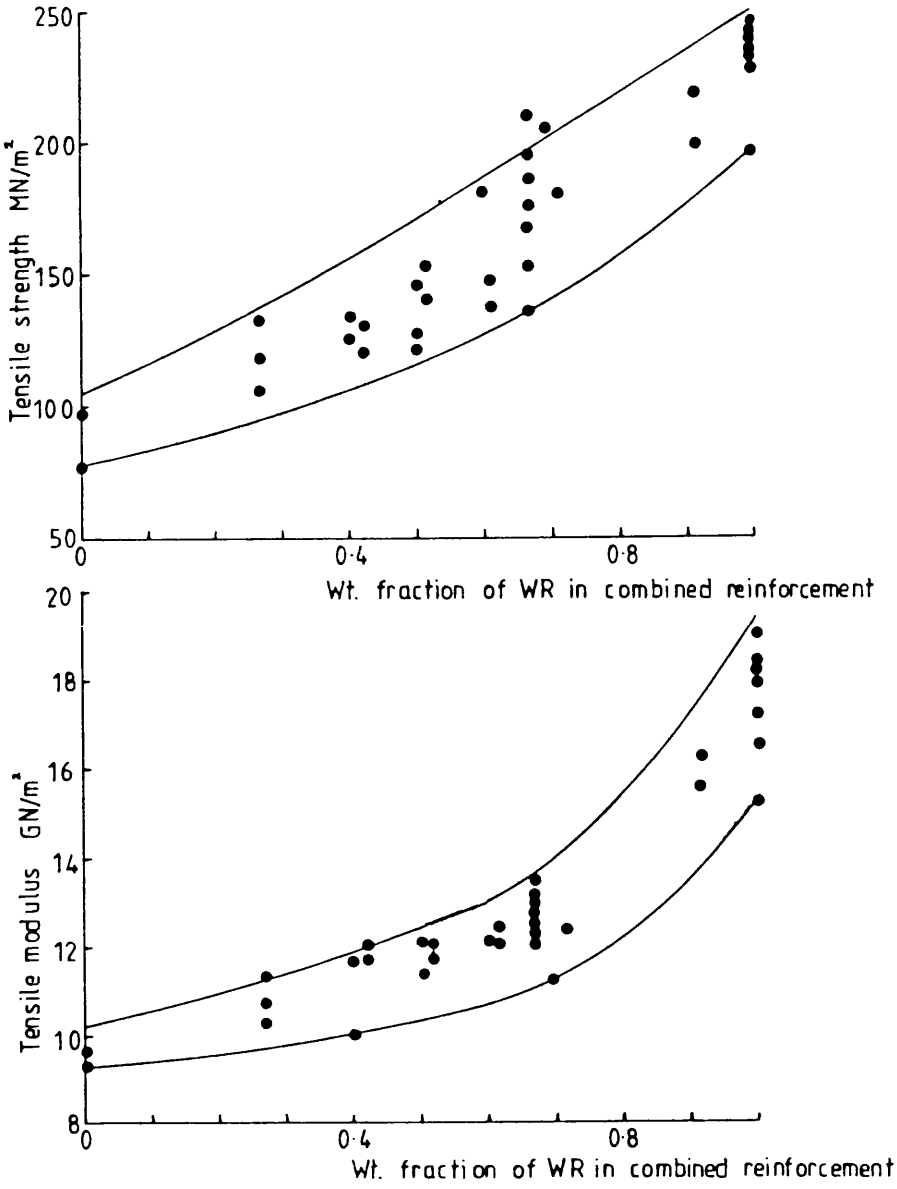

Figure 5.3

Tensile strength and modulus data for combined WR/csm/polyester resin laminates. Data obtained from UK materials suppliers, and it refers to several glass/resin systems (54).

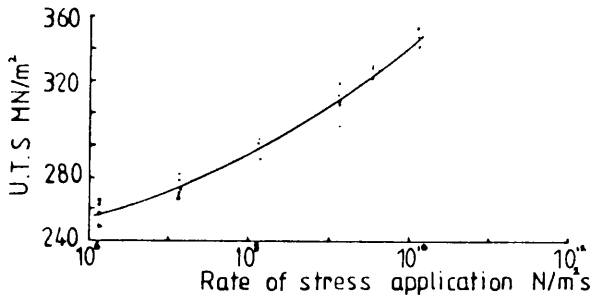

Figure 5.4

Ultimate tensile stress as a function of loading rate (62).

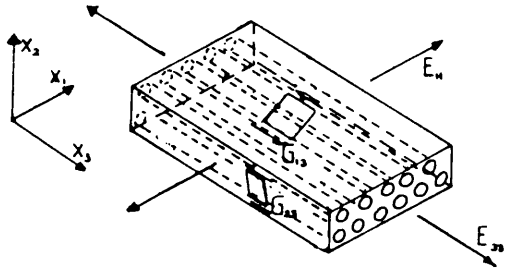

Figure 5.5

Elastic properties of a composite material referred to Cartesian co-ordinates. In a unidirectional composite of this type the shear moduli, G_{13} and G_{23}, are approximately equal and less than G_{12}, and $E_{22} \approx E_{11}$ (50).

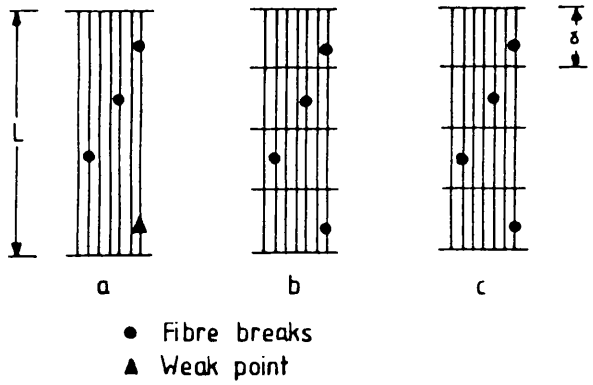

Figure 5.6

(a) Breaks of fibres in a fibre bundle lead to them playing no further role in load sharing over their whole length. As they are completely unloaded a second failure at the next weakest point is not normally possible. The remaining intact fibres are required to support the load previously taken by the broken fibres in an applied load test. (b) A composite can be considered as a chain of interlinked fibre bundles. Each break is isolated in its link and the stress increase in the remaining intact fibres in the link is that due to supporting the load carried in only one instead of all the fibres. As breaks are isolated, a fibre can fail more than once (76).

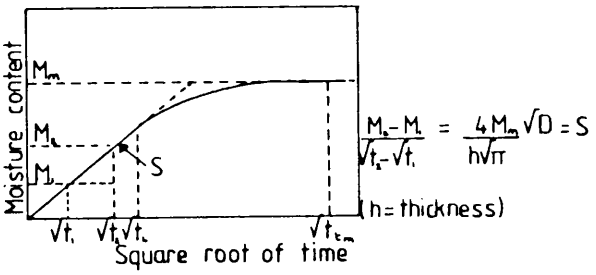

Figure 6.1

Illustration of the change of moisture content with the square root of time for Fickian diffusion (78).

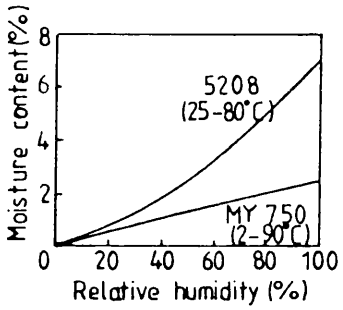

Figure 6.2

Relationship between equilibrium moisture content, relative humidity and temperature for MY 750 and 5208 epoxy resins (91).

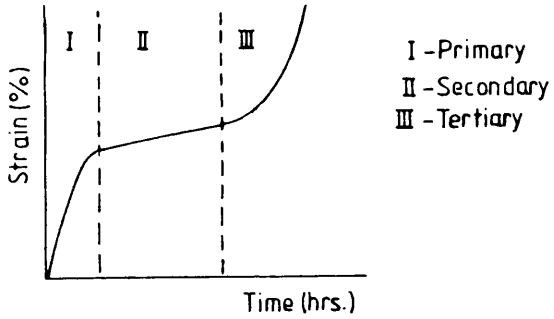

Figure 7.1

Schematic representation of the classical, three stage creep curve.

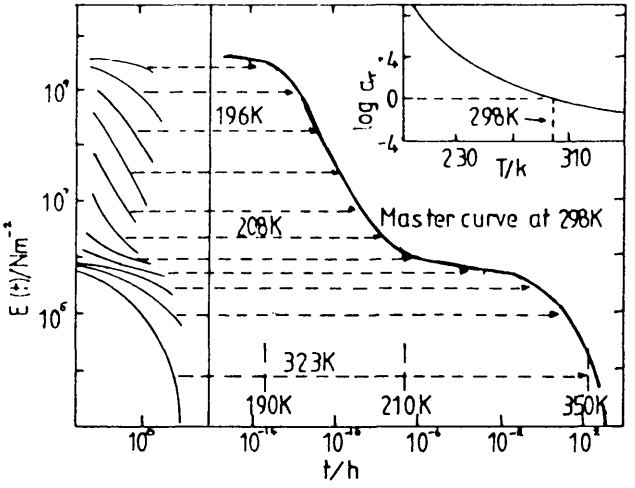

Figure 7.2

Illustration of the time-temperature superposition principle using stress-relaxation data for polyisobutylene. Curves are shifted along the axis by an amount, a_T (inset). The reference temperature in this instance is 298 K (114).

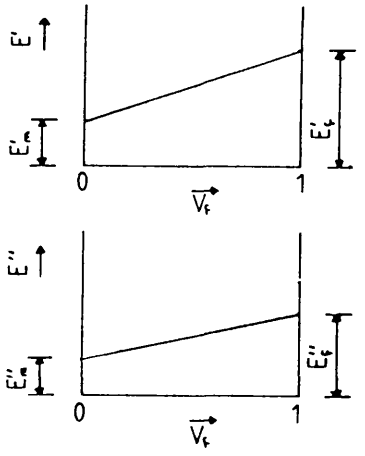

Figure 7.3

Theoretical relationship between the modulus of elasticity and the reinforcement content (117).

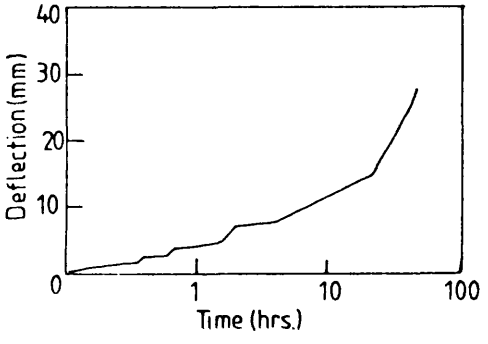

Figure 7.4

Incremental growth in creep strain found for woven glass cloth polyester composites (124).

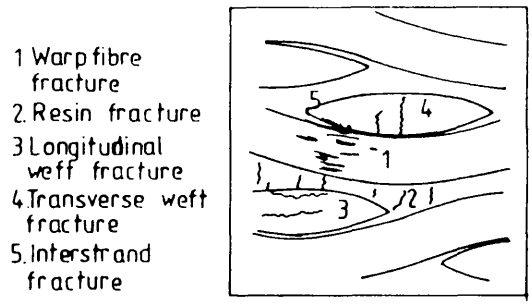

Figure 7.5

Fracture modes during creep in woven roving laminates (126).

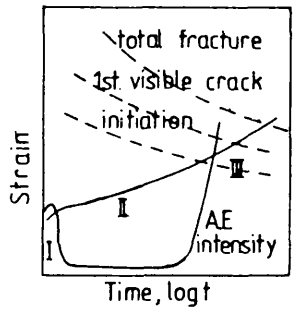

Figure 7.6

Fracture phenomena during creep (126).

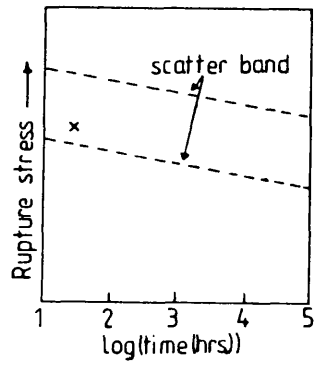

Figure 7.7

Schematic representation of the scatterband of stress-rupture properties for SMC (137).

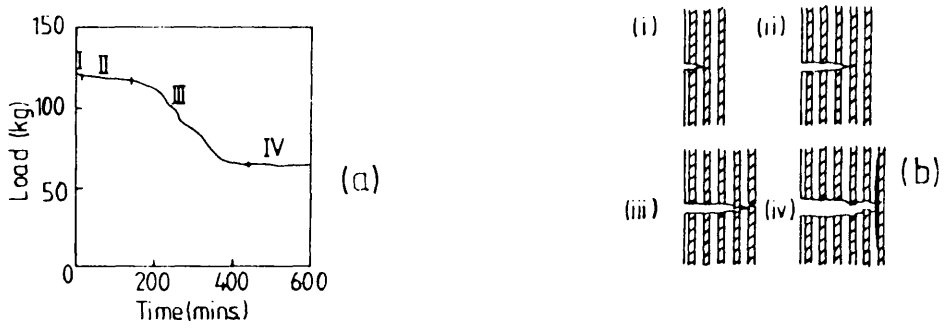

Figure 7.8

(a) Typical load relaxation curve for a strain corrosion test. (b) Model of fracture processes in aligned GRP test pieces tested in a corrosive environment: (i) nucleation of first crack by acid attack on fibre, (ii) growth of flat crack by fibre fracture at the tip of the resin crack, (iii) development of small amount of pull-out due to out of plane fibre fracture. (iv) delamination cracks at tip of flat crack (154).

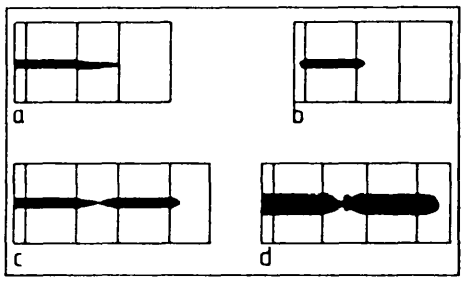

Figure 7.9

Schematic representation of stress corrosion crack growth illustrating the role of the matrix. (a) If the matrix is brittle, fibre fracture may result in simultaneous resin fracture, up to the next fibre. (b) For a tough matrix, only limited crack growth can occur, and further acid diffusion is required to fracture the next fibre. (c) Subsequent fracture of the second fibre causes back-cracking in the matrix, resulting in fracture surface coalescence (d) In highly ductile matrices, plastic flow and cavitation, rather than coalescence, occurs. (157)

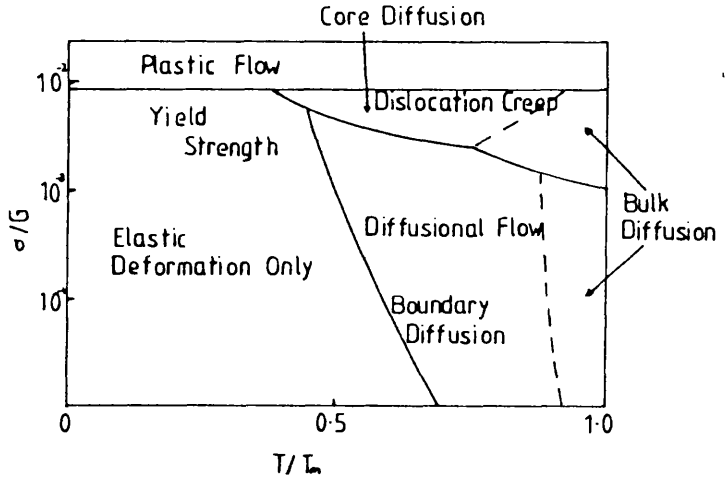

Figure 8.1

Deformation mechanisms at different stresses and temperature during metallic creep (161).

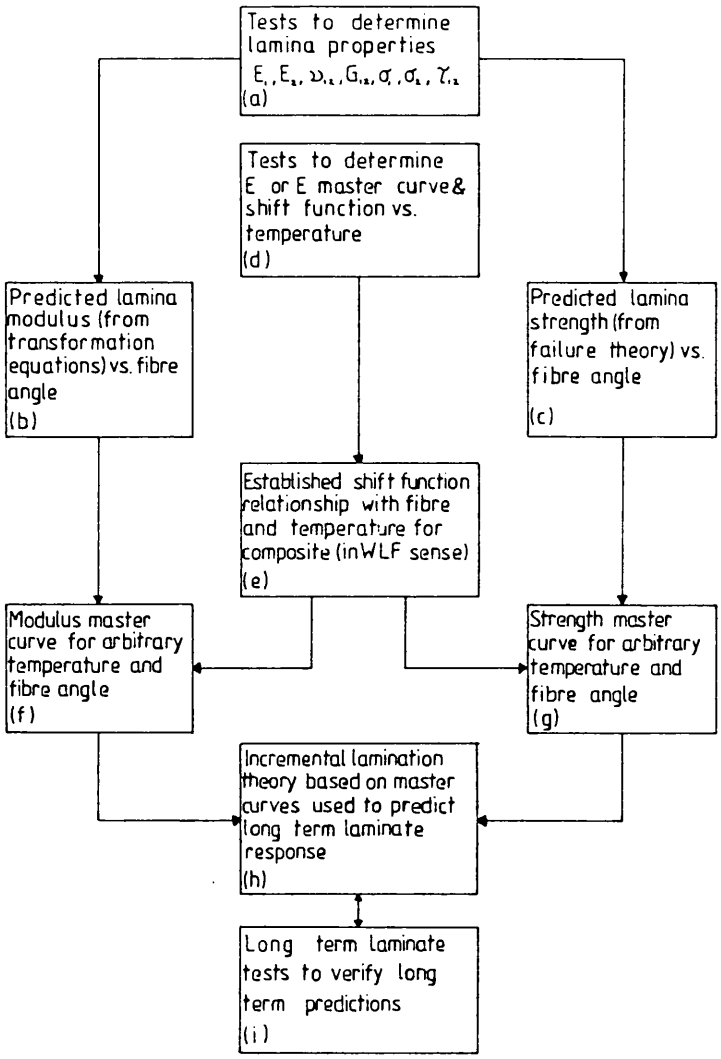

Figure 8.2

Flow chart for proposed laminate accelerated characterisation and failure prediction procedures (166).

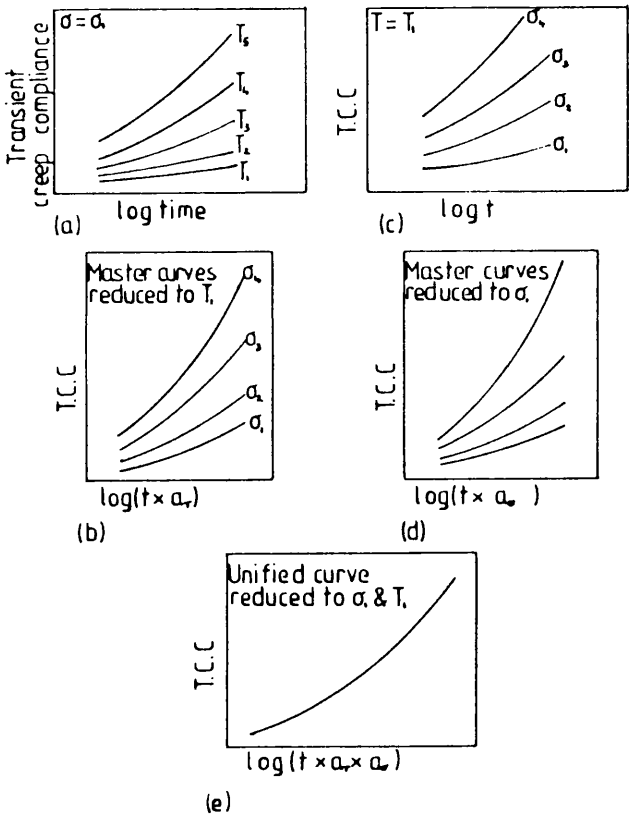

Figure 8.3

Schematic diagram to illustrate the time-stress-temperature superposition principle (166).

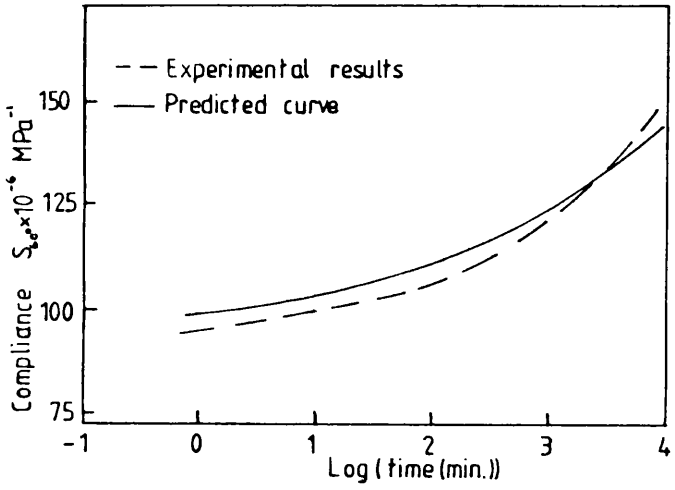

Figure 8.4

Comparison of predicted and experimental results for CFRP creep compliance (166).

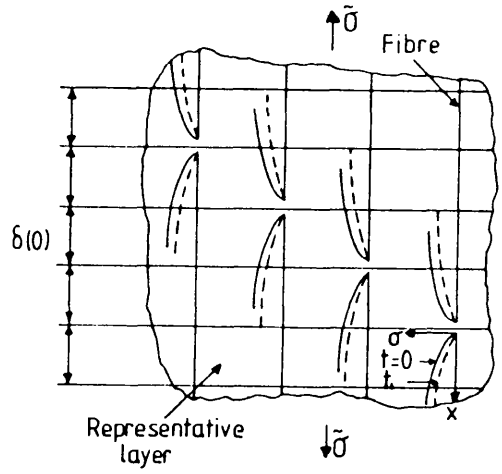

Figure 8.5

Time-dependent chain-of-bundles tensile failure model (174).

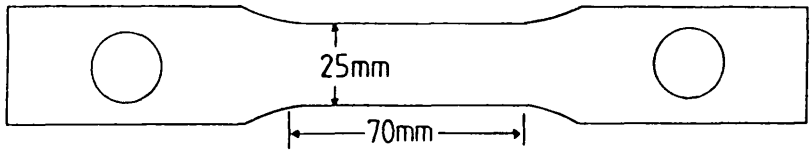

Figure 9.1

Representation of test-piece, showing the size and shape used.

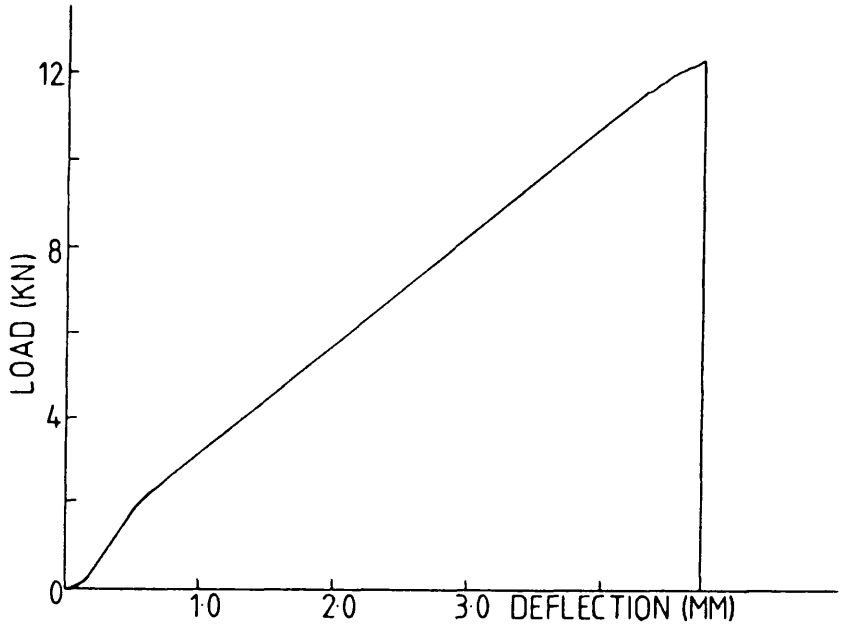

Figure 9.2

Typical load/deflection curve for tensile tests at a cross head displacement rate of 0.5mm/min.

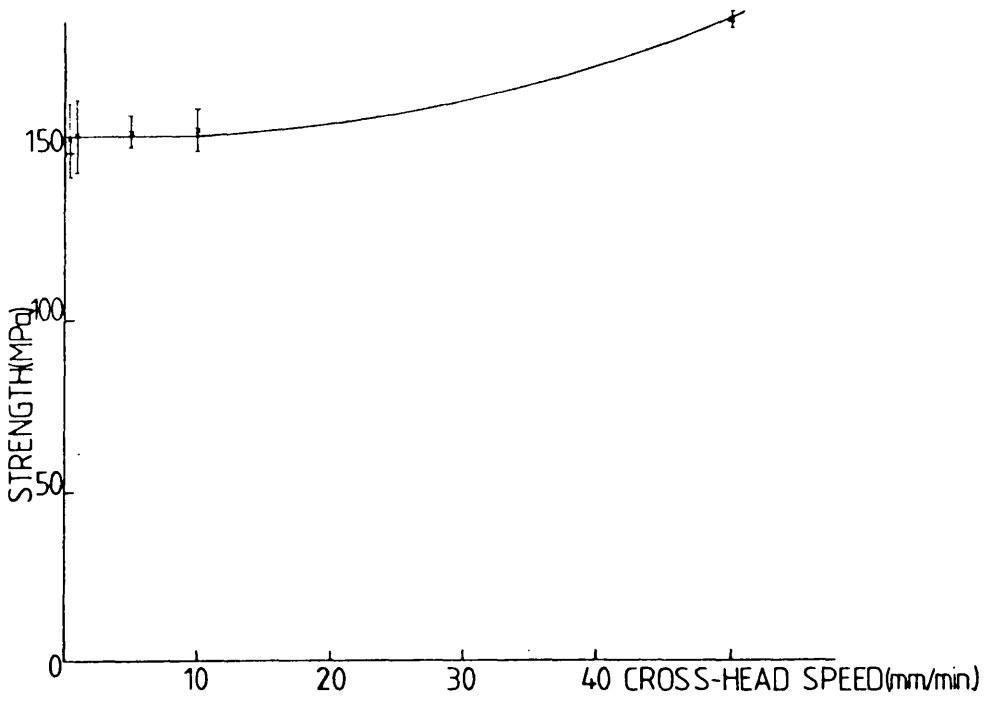

Figure 9.3

GRP strength as a function of strain rate, in a tensile test.

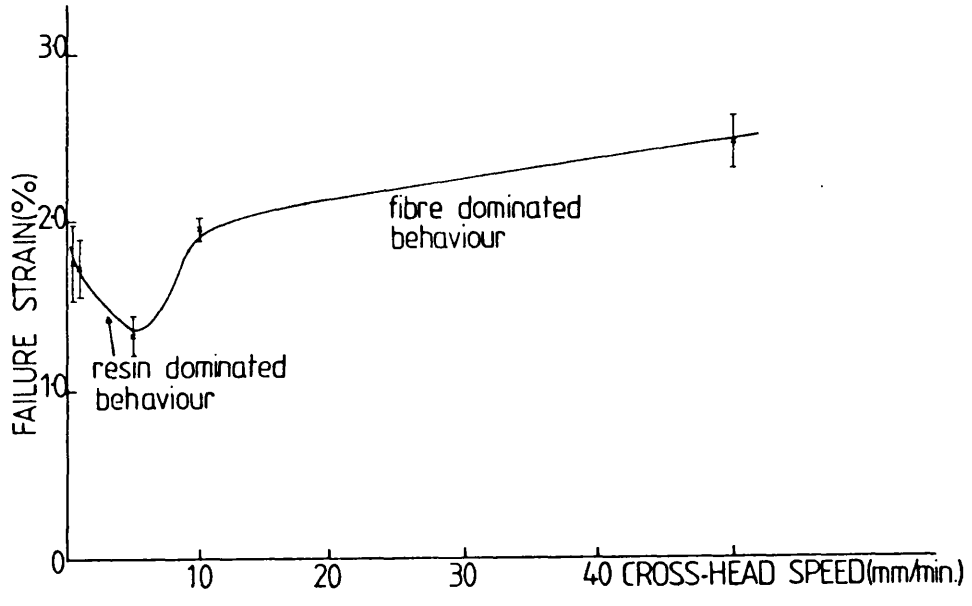

Figure 9.4

GRP failure strain as a function of strain rate, in a tensile test.

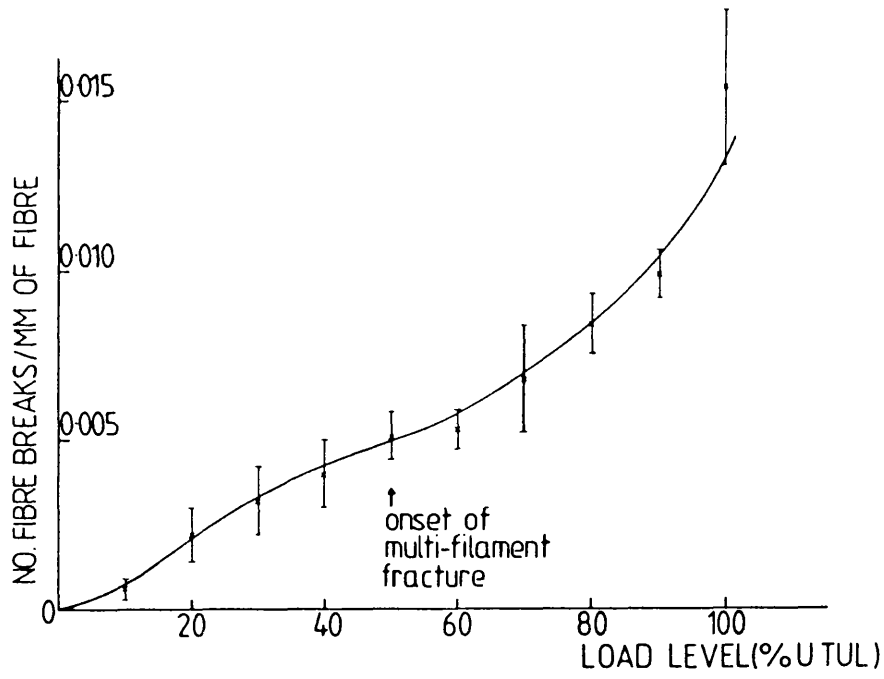

Figure 9.5

Density of fibre breaks in the longitudinal rovings of single ply fabric laminates as a function of applied load.

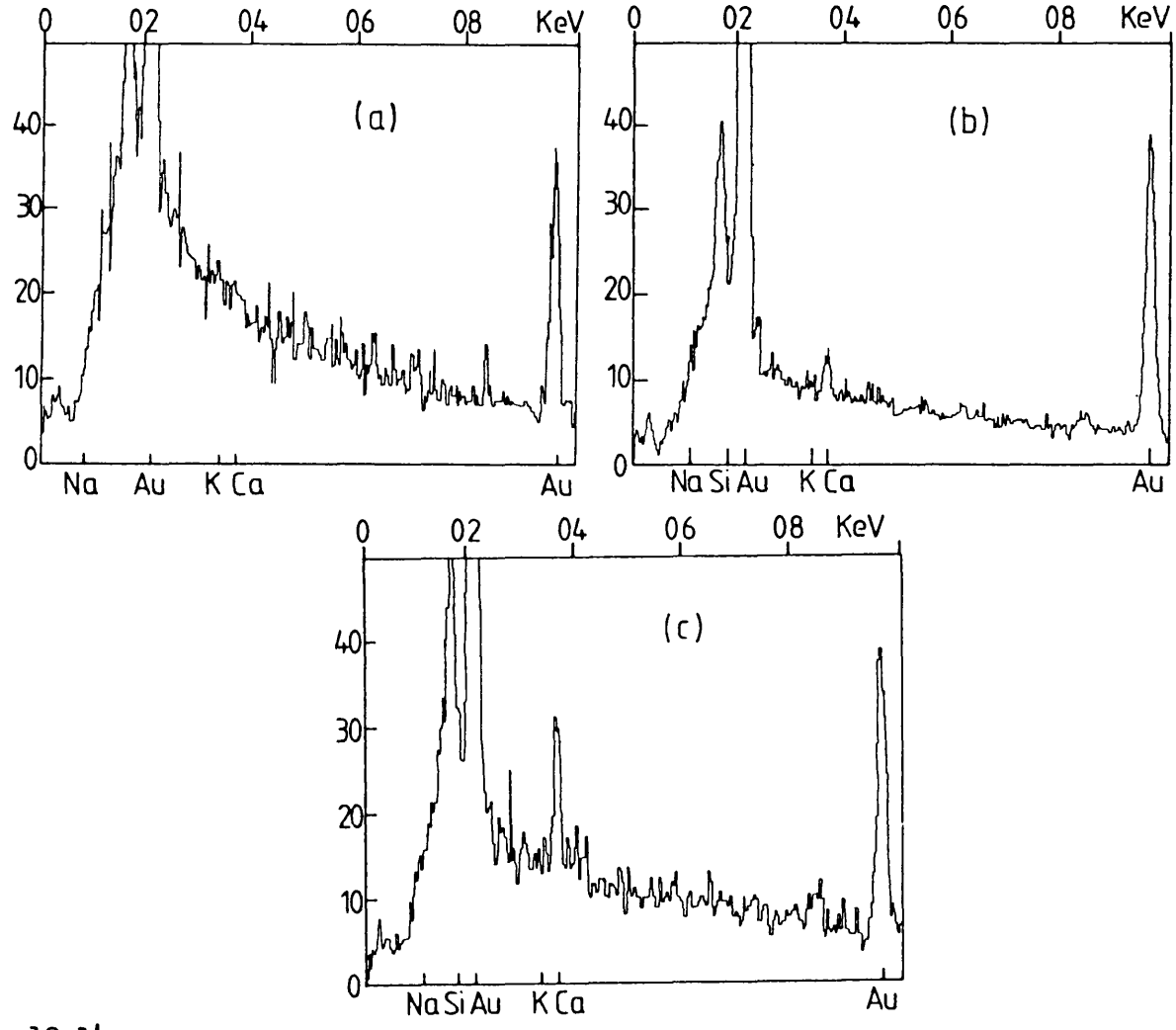

Figure 10.14

EDAX plots showing the composition of: (a) pure polyester resin, (b) resin from dry creep-rupture fracture surface, and (c) resin from immersed creep-rupture surface. Gold peaks produced from the coating applied to prevent

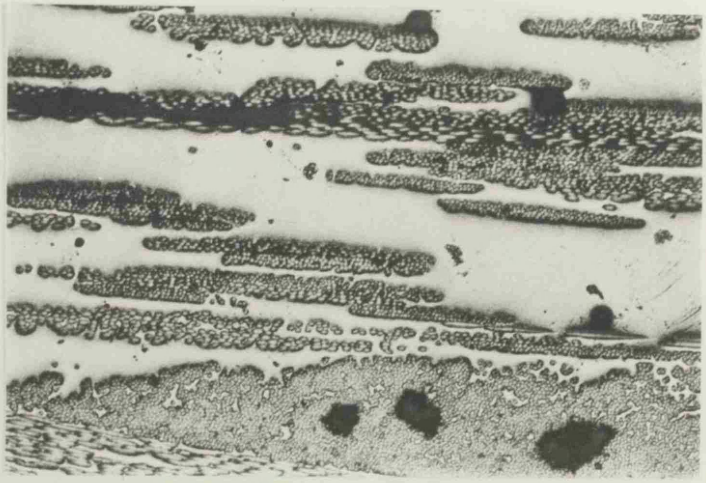

Figure 10.1

Optical micrograph of a GRP polished section, showing typical porosity found in a low void content specimen (x 38).

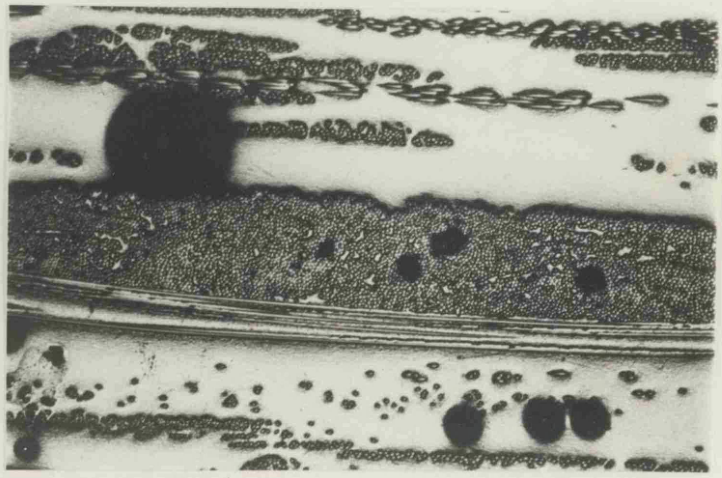

Figure 10.2

Optical micrograph of a GRP polished section, showing typical porosity found in a high void content specimen (x 38)

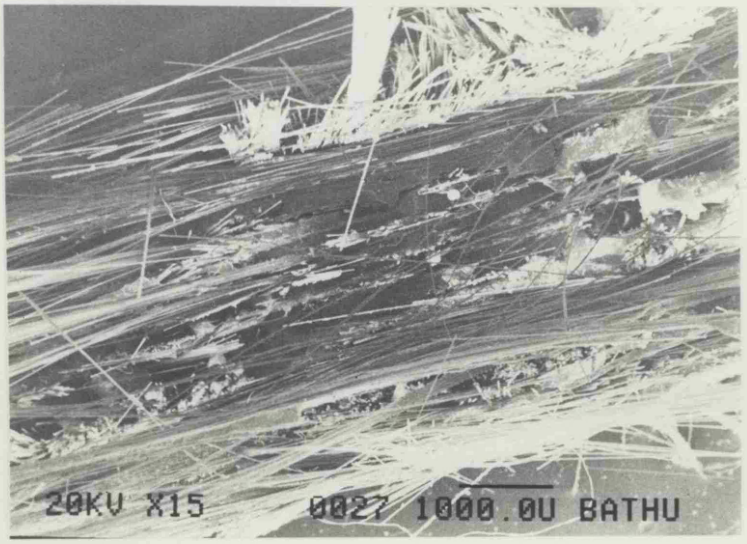

Figure 10.3

Scanning electron micrograph of the fracture surface from a creep-rupture test-piece that failed after 1 day in water at 60°C.

Figure 10.4

Scanning electron micrograph of the fracture surface from a creep-rupture test-piece that failed after 1 month in water at 60°C.

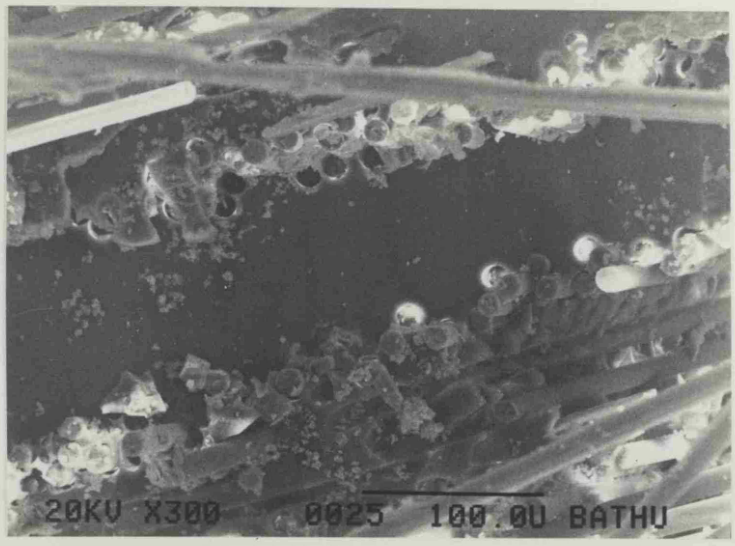

Figure 10.5

Scanning electron micrograph of the fracture surface from an immersed creep-rupture test-piece, showing resin rich regions bordered by short fibre pull-outs.

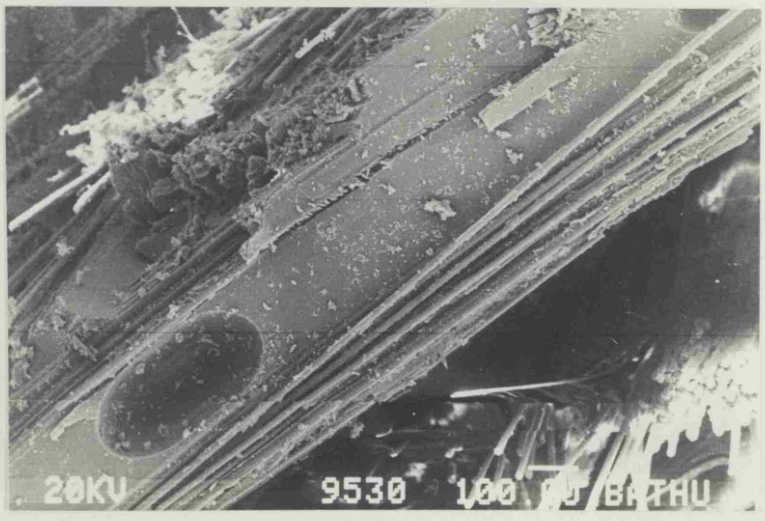

Figure 10.6

Scanning electron micrograph of an immersed creep-rupture test-piece, showing the existence of intra roving voids in the transverse weave rovings at the fracture surface.

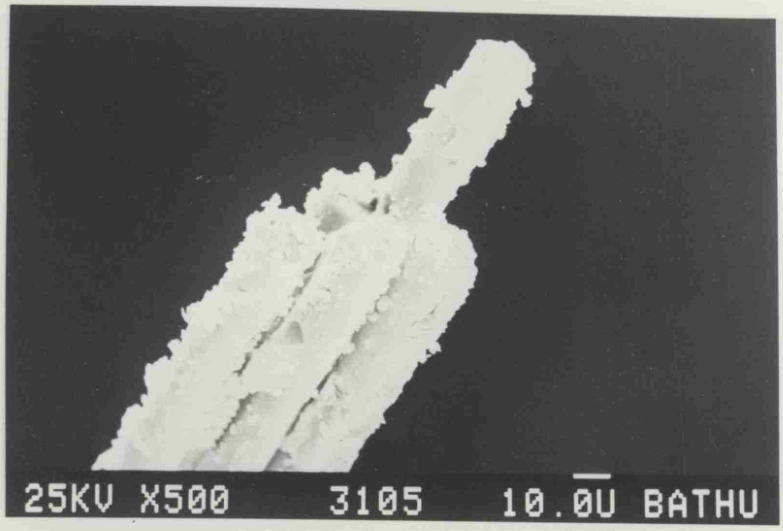

(a)

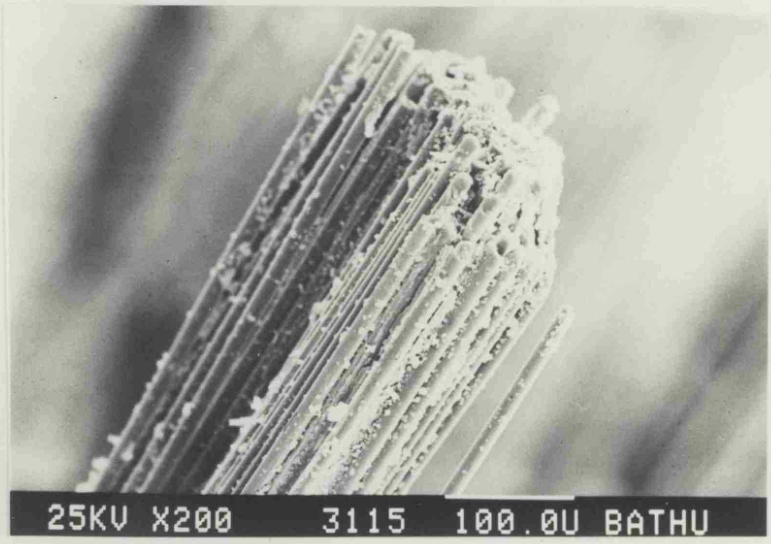

(b)

Figure 10.7

Scanning electron micrographs, showing the existence of multi-filament fibre fractures in the longitudinal weave rovings at the fracture surface of a dry creep-rupture sample.

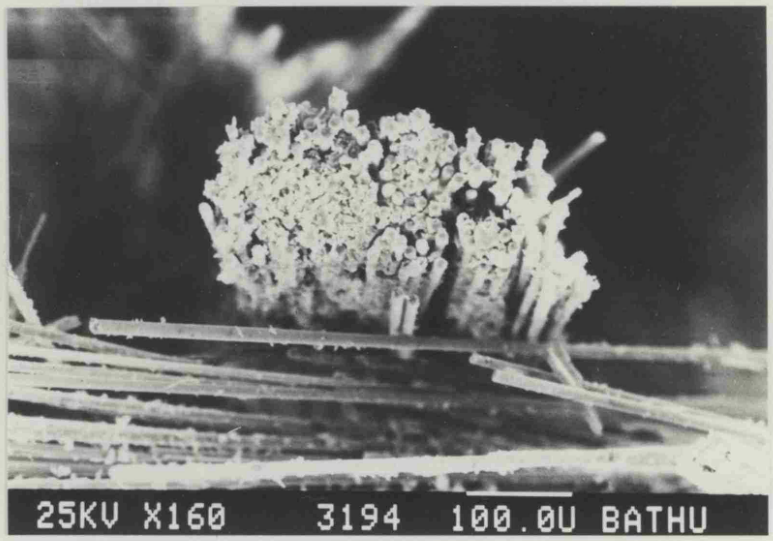

Figure 10.8

Scanning electron micrograph of the fracture surface from a dry creep-rupture test-piece, showing that multi-filament fractures occurred at weave cross-overs.

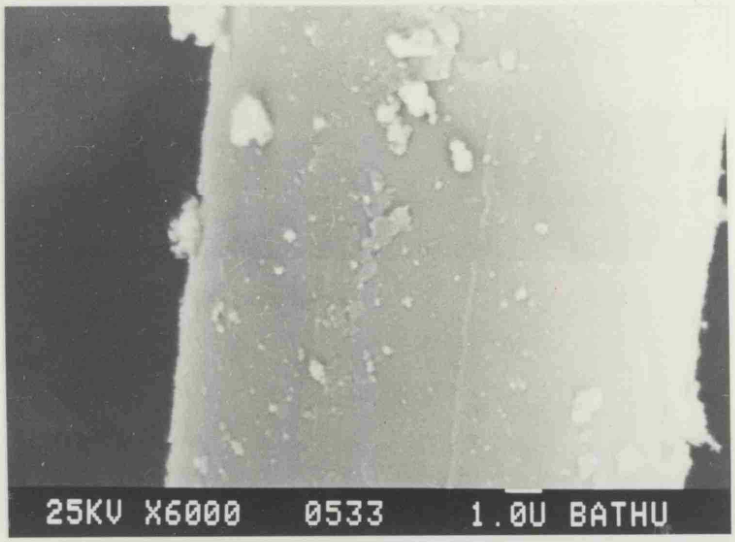

(a)

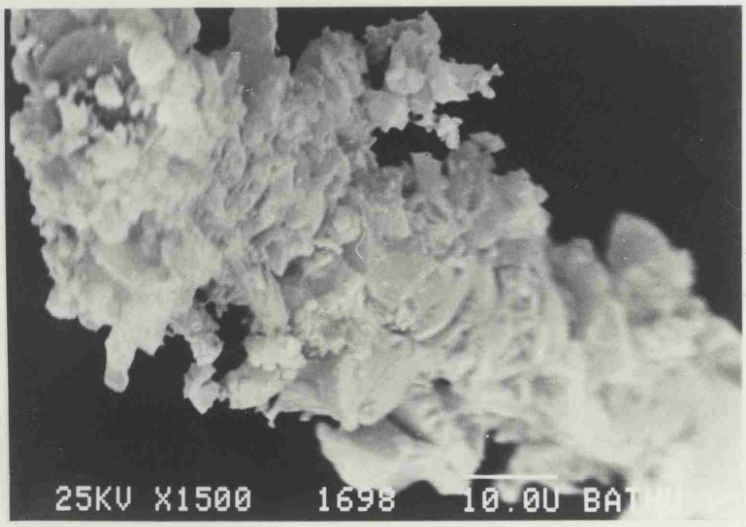

(b)

Figure 10.9

Scanning electron micrographs showing the typical condition of pull-out fibre surfaces at the fracture surface of; (a) a creep-rupture test-piece that failed after immersion in water, and (b) a creep-rupture sample tested in air.

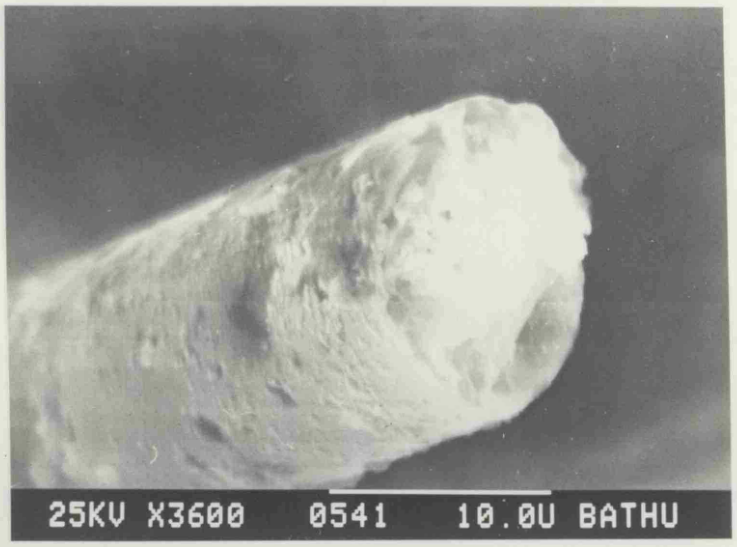

(a)

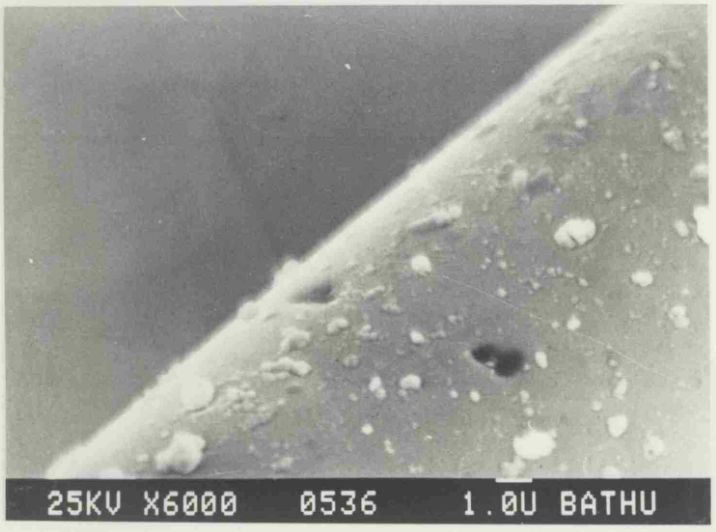

(b)

Figure 10.10

Scanning electron micrographs showing the fibre corrosion damage observed on pull-out fibres from creep-rupture surfaces after immersion in water at 60°C for $2\frac{1}{2}$ months; (a) in the filament fracture region and (b), fibre surfaces away from this zone.

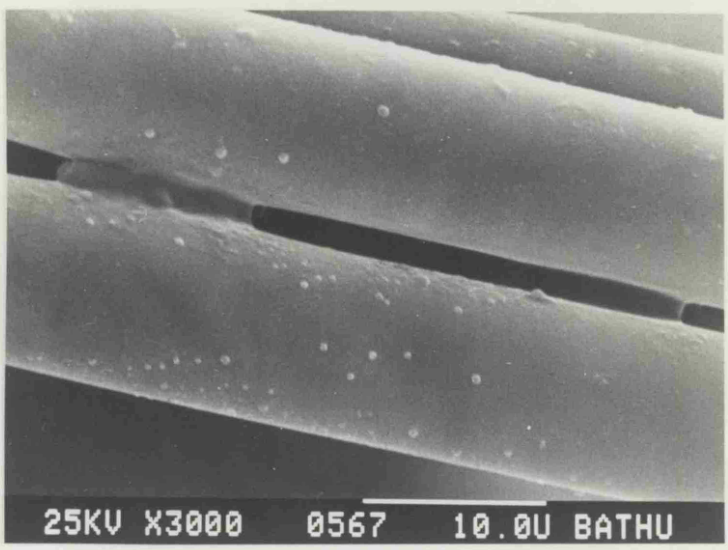

Figure 10.11

Scanning electron micrograph of the surface condition of filaments from 'virgin' glass rovings, prior to encapsulation in a resin matrix.

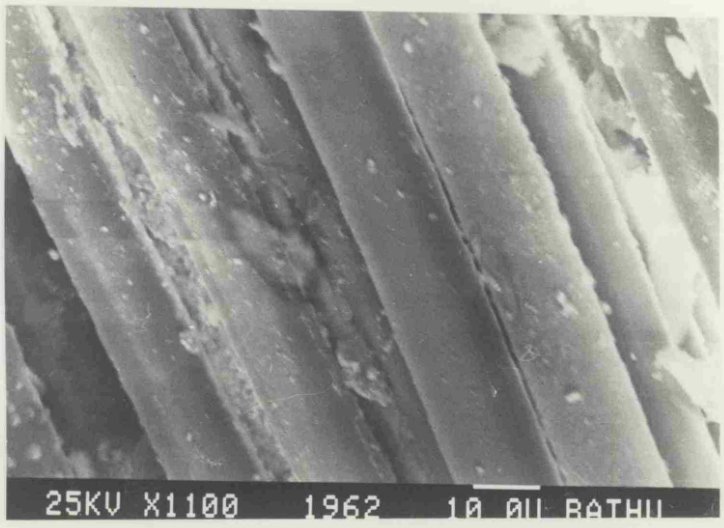

(a)

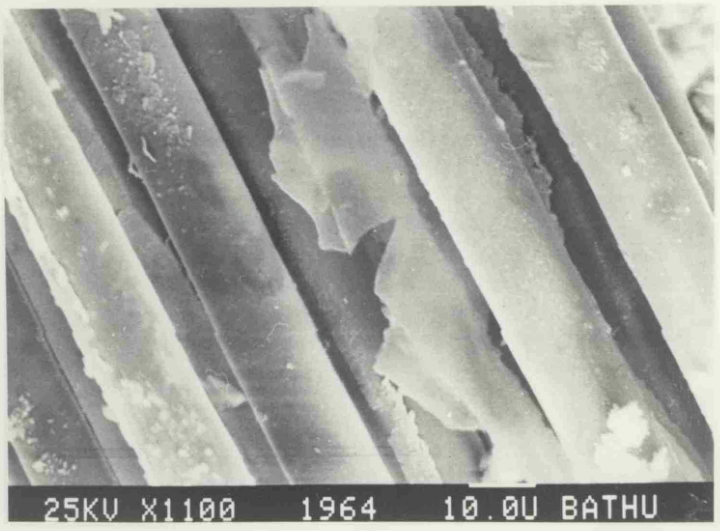

(b)

Figure 10.12

Scanning electron micrographs of the condition of reinforcement plies, revealed by resin burn-offs, from creep-rupture test-pieces immersed in water at 40°C for 18 months. (a) Fibre condition on the outer surface of fabric plies. (b) Fibre condition in the outer c.s.m. plies.

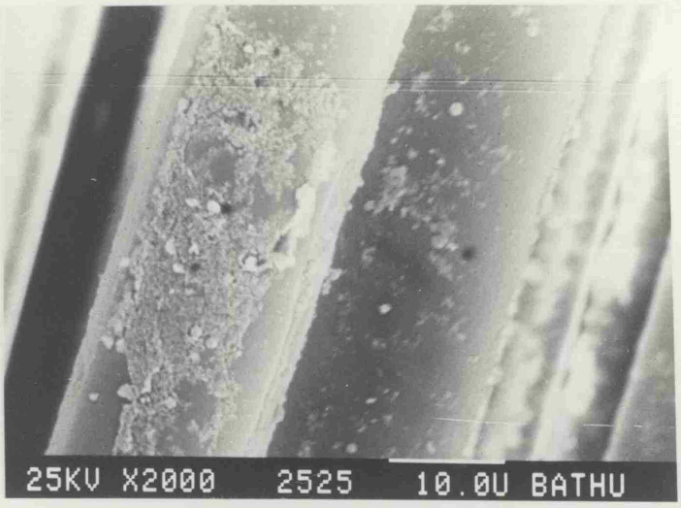

(a)

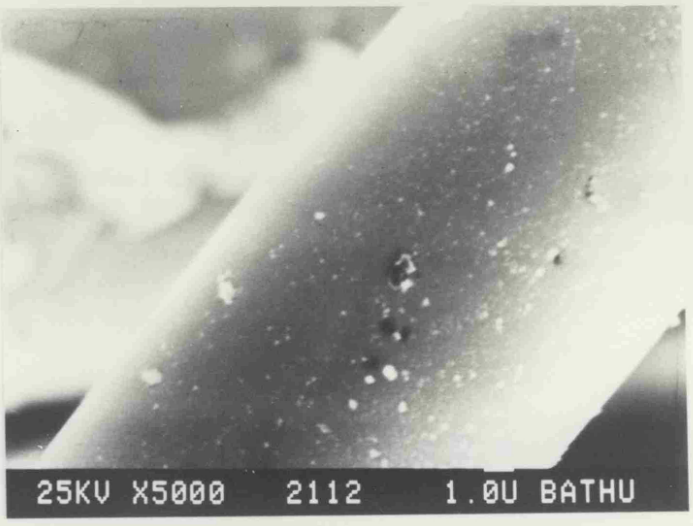

(b)

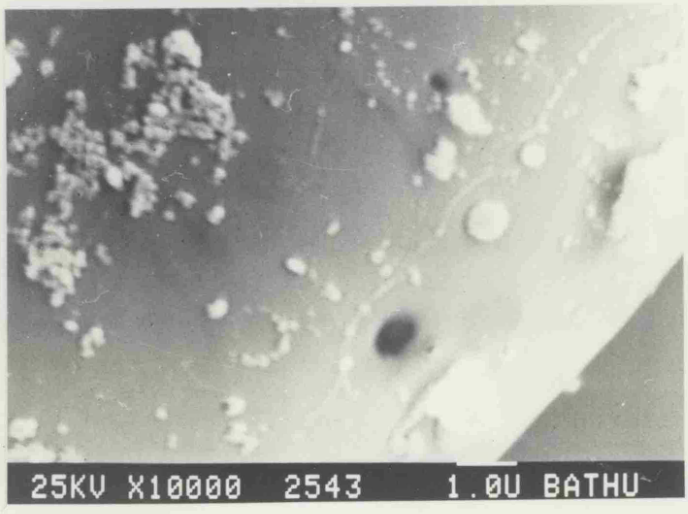

(c)

Figure 10.13

Scanning electron micrographs showing fibre pitting damage at the inner surfaces of weave cross-overs from immersed creep-rupture test-pieces. In all cases, damaged fibres were from the longitudinal rovings in the woven reinforcement.

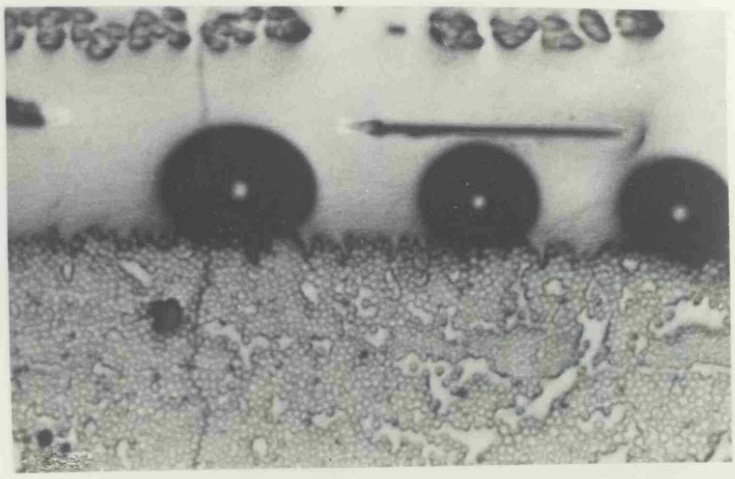

Figure 10.15

Optical micrograph of a polished section taken from a tensile test-piece, showing the formation of resin voids at the matrix/roving interface. (x 77).

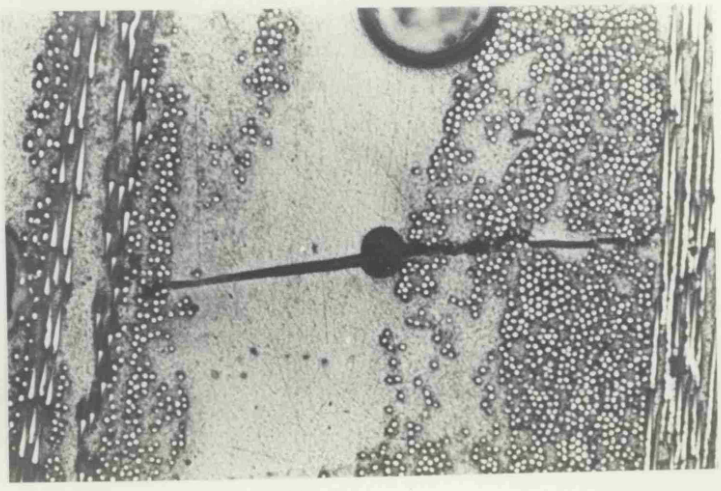

Figure 10.16

Optical micrograph of a longitudinal polished section from an immersed creep-rupture sample, showing crack initiation from a spherical resin void (x 77)

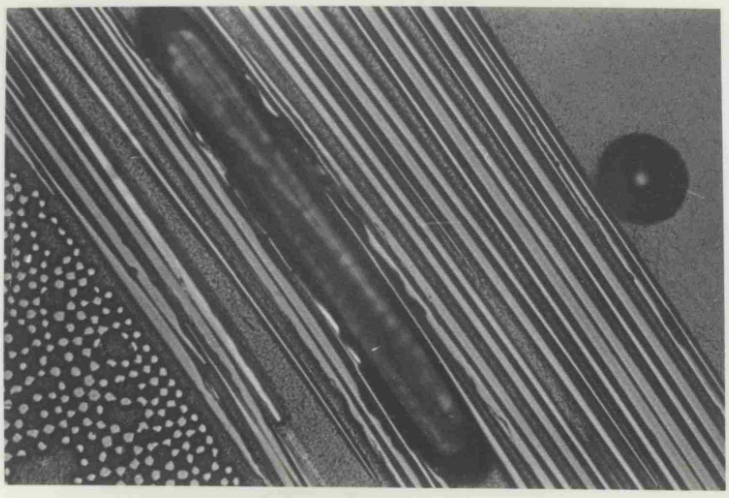

Figure 10.17

Optical micrograph of a polished section taken from a laminate sheet, showing cylindrical intra-roving void formation (x 154).

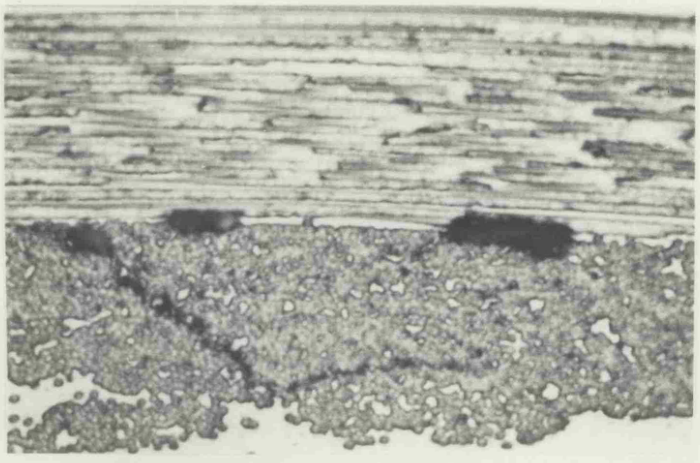

Figure 10.18

Optical micrograph of a polished section from a laminate sheet, showing concentrations of intra-roving voids at weave cross over regions. (x 77)

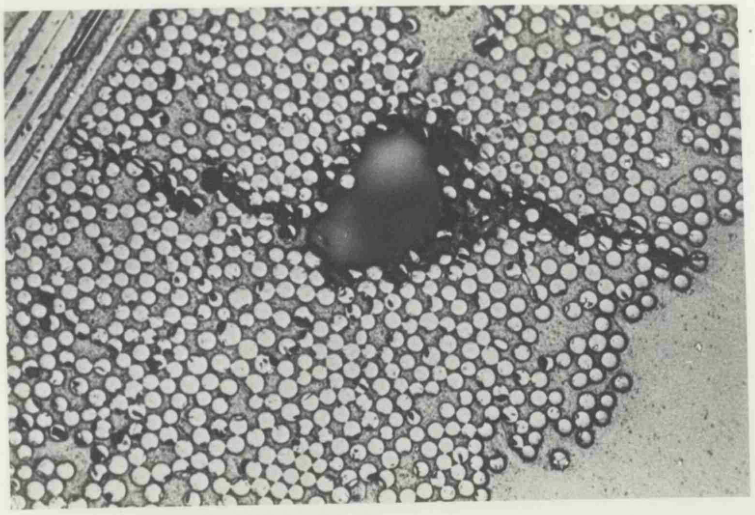

Figure 10.19

Longitudinal polished section through an immersed creep-rupture sample, showing evidence of crack initiation from intra-roving voids. (x 154)

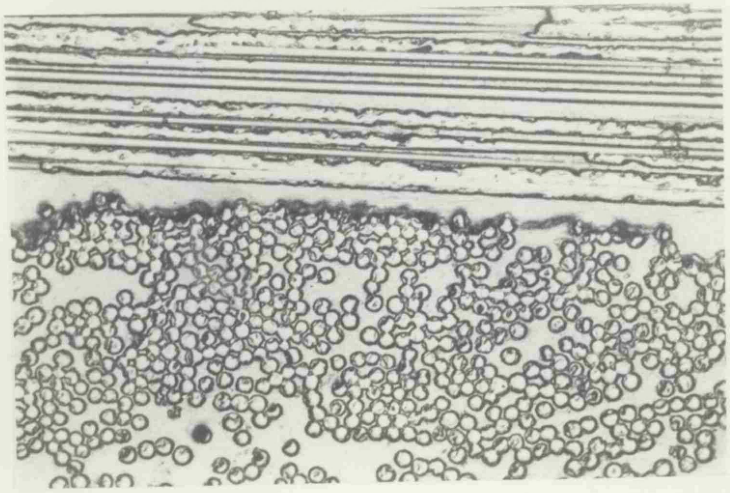

Figure 10.20

Section through an untested laminate sheet, showing evidence of interfacial, post-cure, thermal, cracking (x 154).

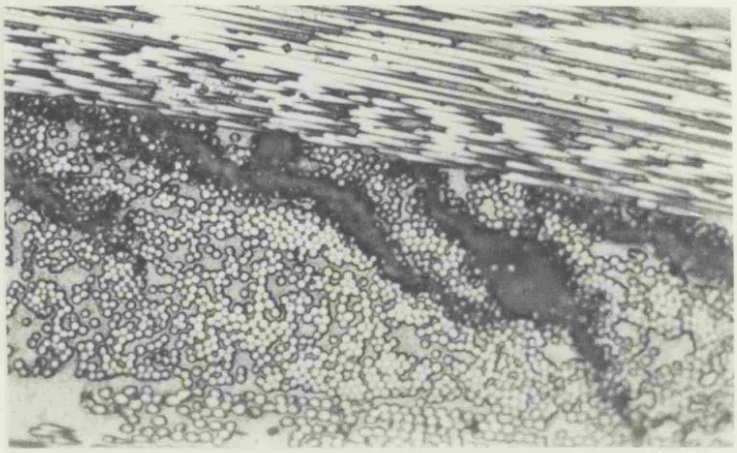

(a)

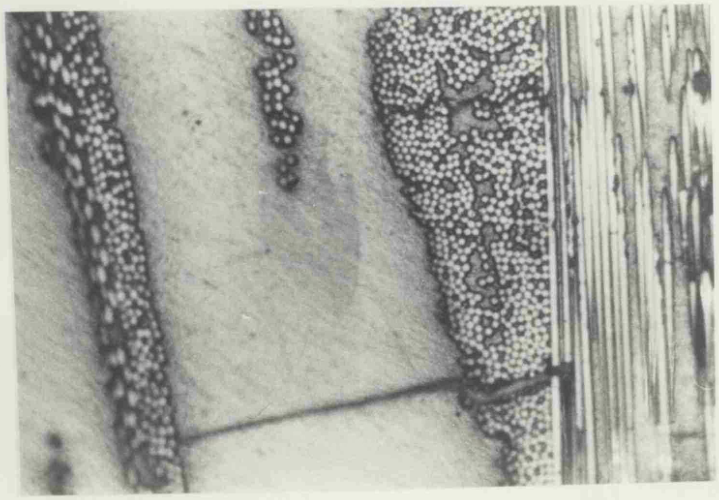

(b)

Figure 10.21

Longitudinal sections from immersed creep-rupture test-pieces, showing crack propogation from the weave cross-over interfaces (x 77).

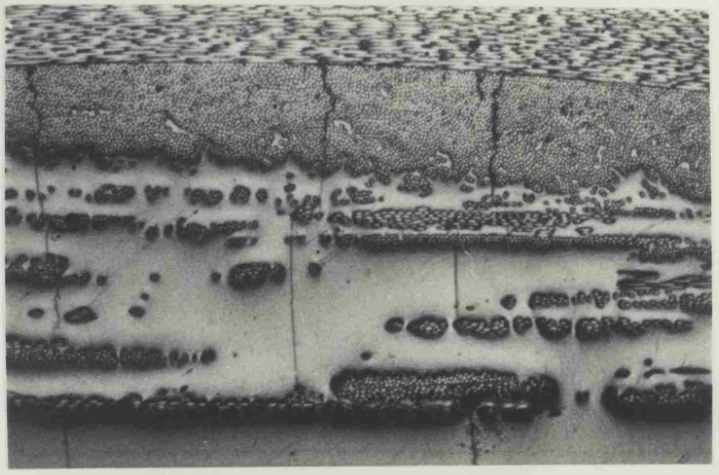

(a)

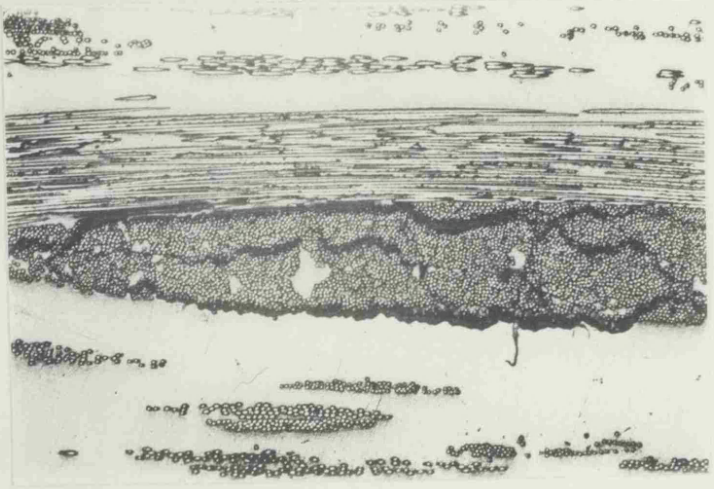

(b)

Figure 10.22

Transverse sections from immersed creep-rupture samples, showing the observed crack damage (x38).

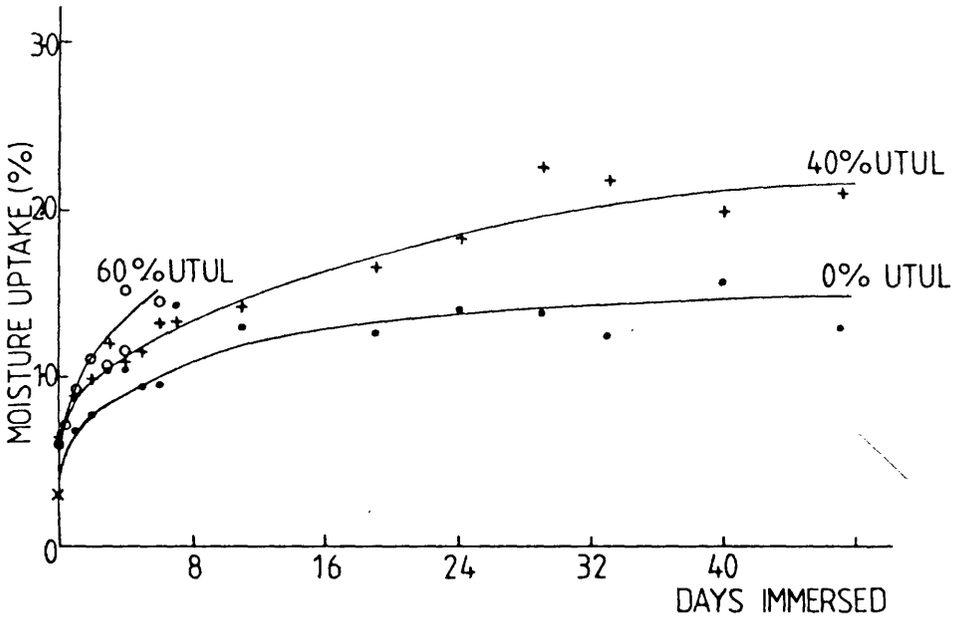

Figure 11.1

Water uptake vs. time for samples immersed in water at 23°C. Moisture contents determined by drying samples to constant weight.

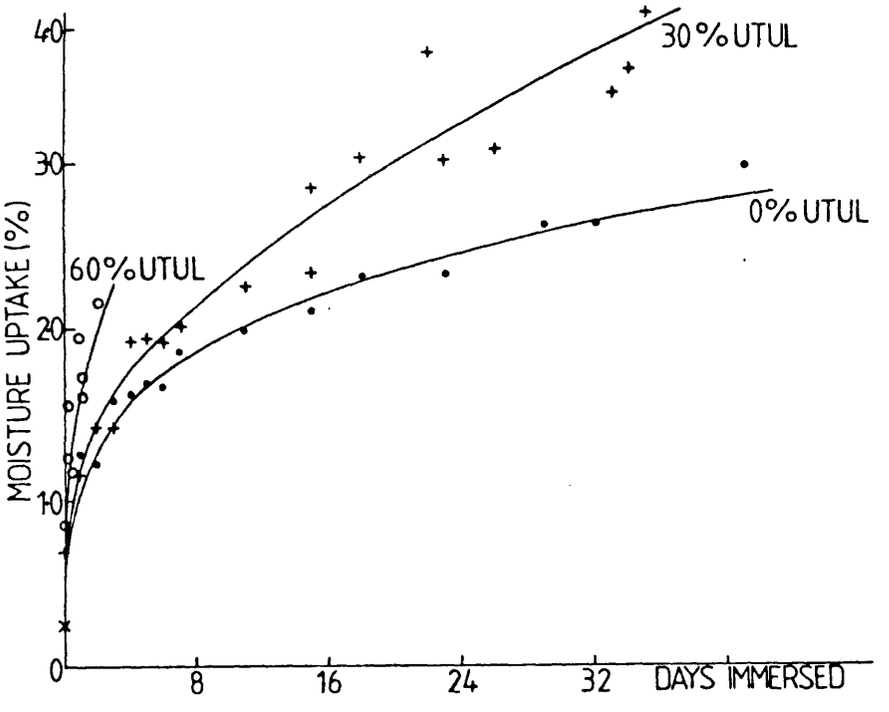

Figure 11.2

Water uptake vs. time for samples immersed in water at 60°C. Moisture contents determined by drying samples to constant weight.

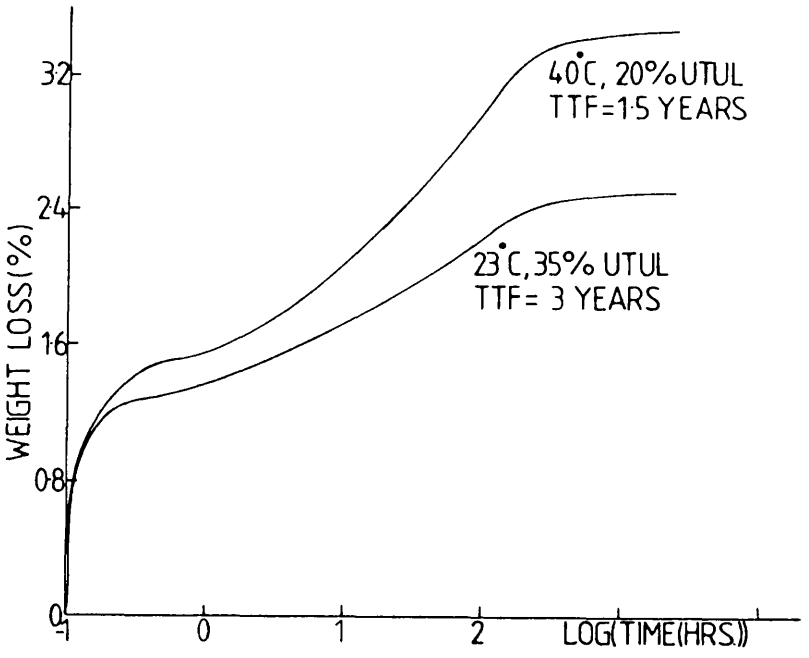

Figure 11.3

Weight loss vs. time for samples, previously immersed under stress, during drying at 60°C.

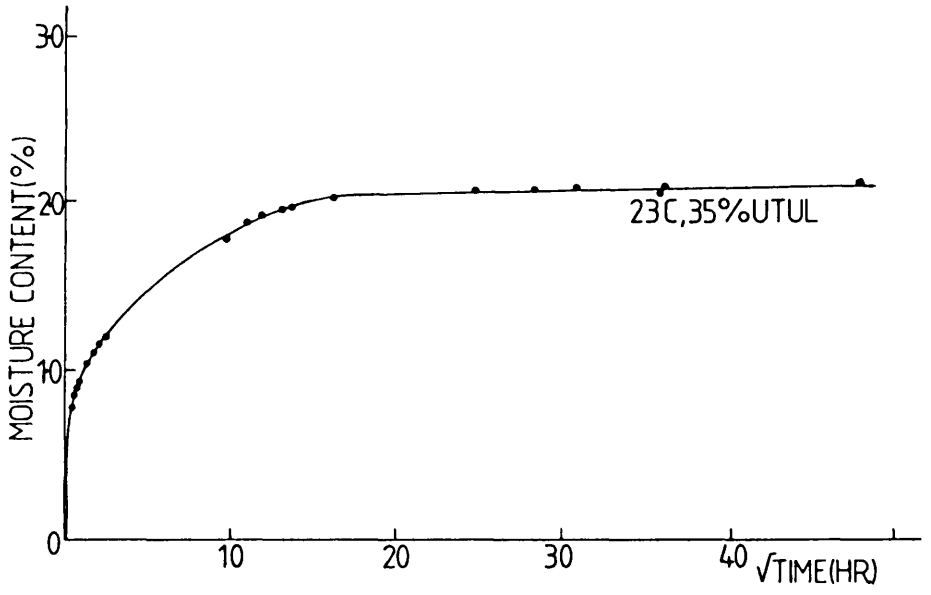

Figure 11.4

Weight loss against $\sqrt{t}$ for sample drying at 60°C, after a prior immersion of 18 months at 40°C, under a stress of 25% UTUL.

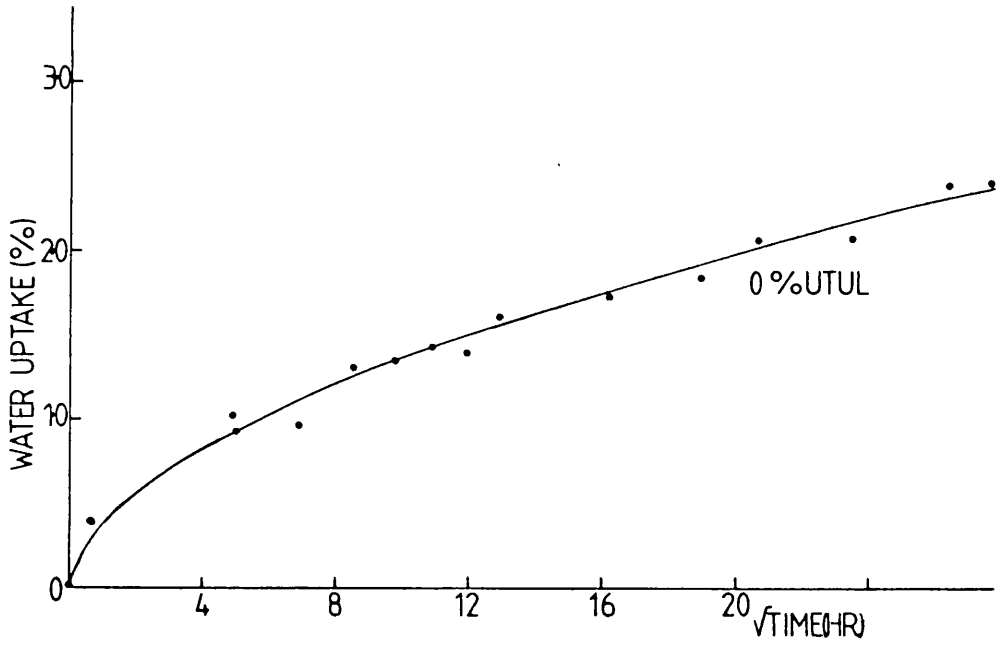

Figure 11.5

Moisture content as a function of the square root of time for samples soaked at 60°C.

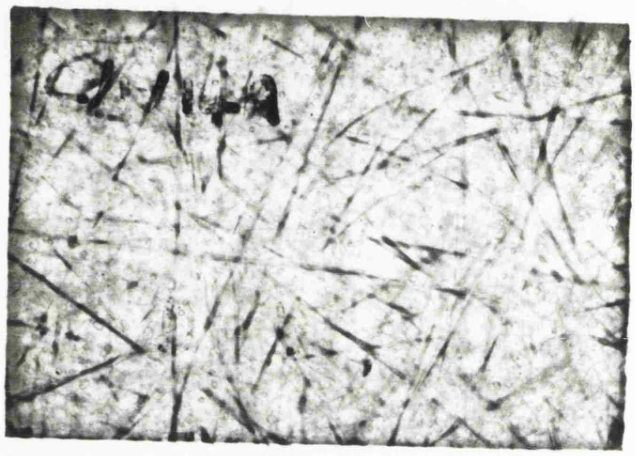

(a)

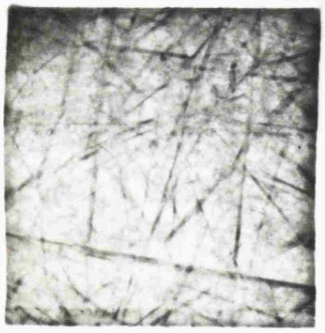

(b)

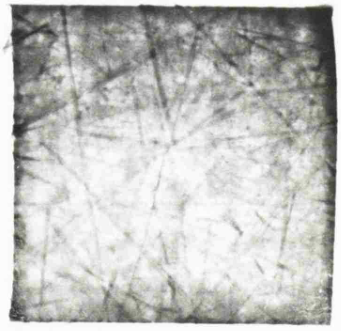

(c)

Figure 11.6

Transmitted light photographs of samples immersed at 60°C, revealing the extent of debonding after; (a) 1 day, (b) 11 days, (c) 15 days

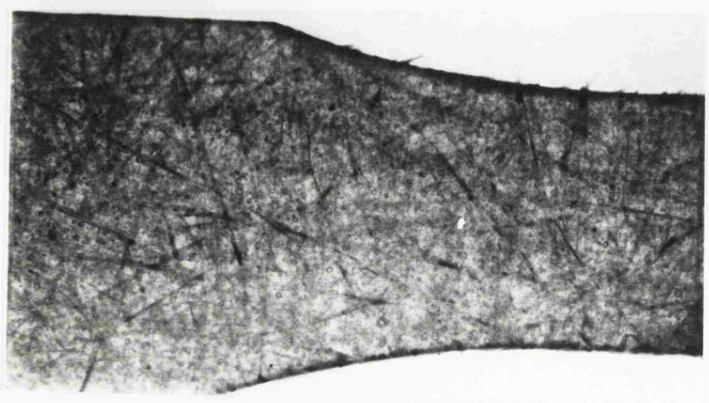

(a)

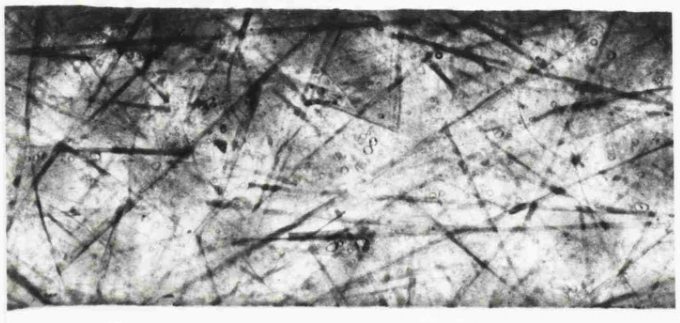

(b)

Figure 11.7

Transmitted light photographs of samples immersed at 60°C, under an applied stress of 30% UTUL, revealing the extent of debonding after: (a) 1 day, (b) 7 days.

(a)

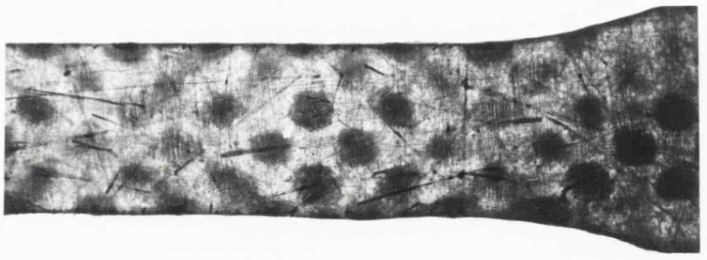

(b)

Figure 11.8

Transmitted light photographs of samples immersed at 60°C, under an applied stress of 60% UTUL, revealing the extent of debonding after; (a) 1 hour, and (b) 7 hours.

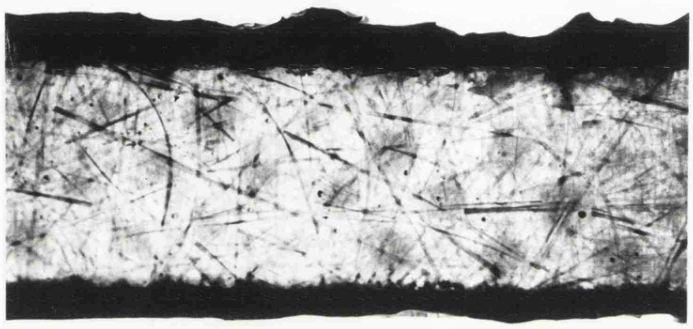

Figure 11.9

Transmitted light photograph of a sample immersed at 60°C, under an applied load of 60% UTUL, with edges sealed with silicone rubber, showing the extent of debonding after 2 days.

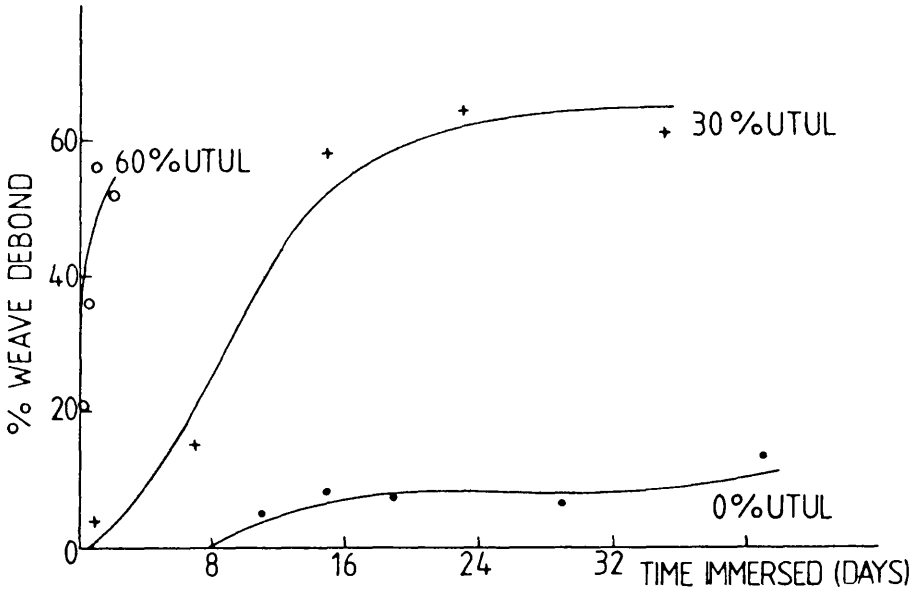

Figure 11.10

Extent of weave debonding as a function of time immersed at 60°C.

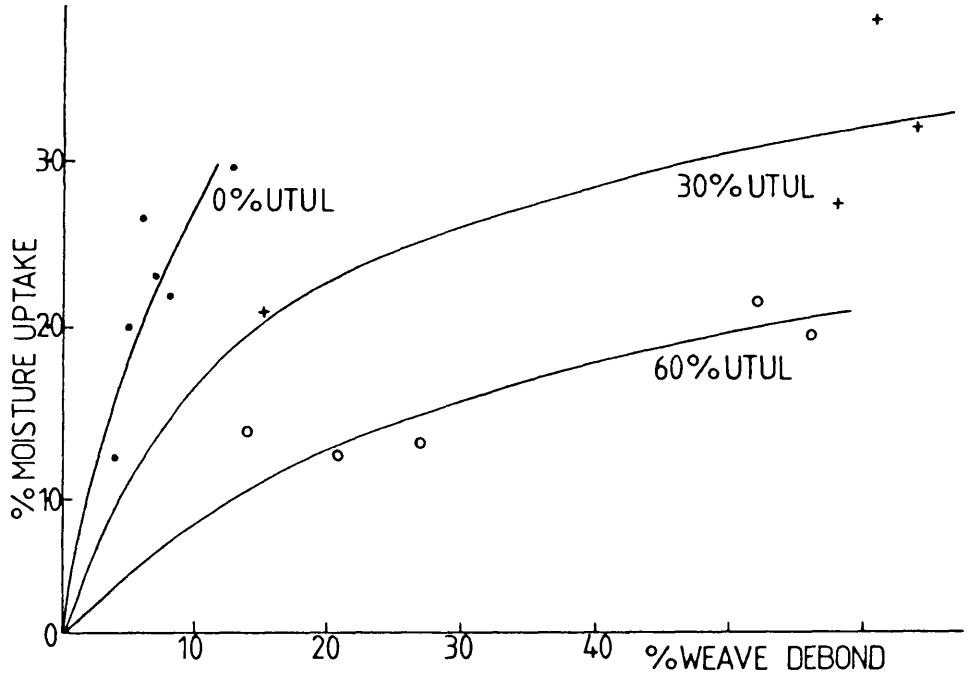

Figure 11.11

Moisture uptake against extent of debonding, for samples immersed at 60°C.

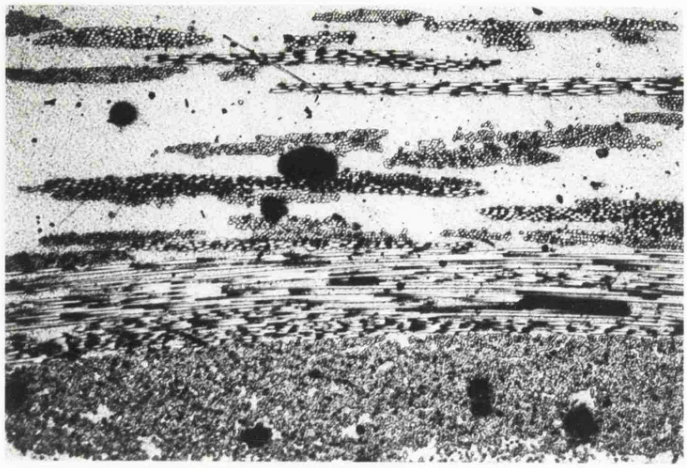

(a)

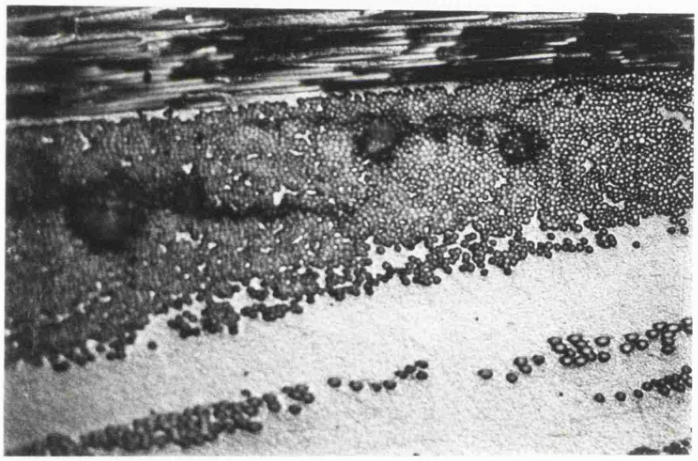

(b)

Figure 11.12

Optical micrographs of polished sections from samples of GRP, showing the extent of cracking; (a) In the 'as received' state (x 38) and (b) after a 6 day immersion in water at 60°C (x 77).

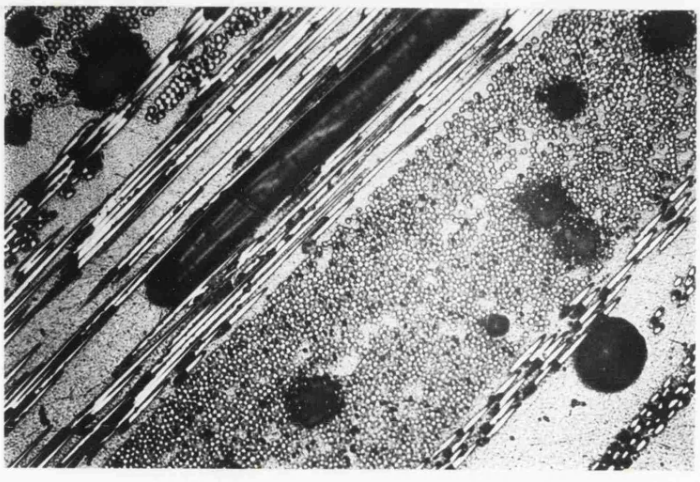

Figure 11.13

Longitudinal section from a sample, loaded to 30% UTUL in water at 60°C, then removed, showing the lack of initial load induced transverse cracking (x 77).

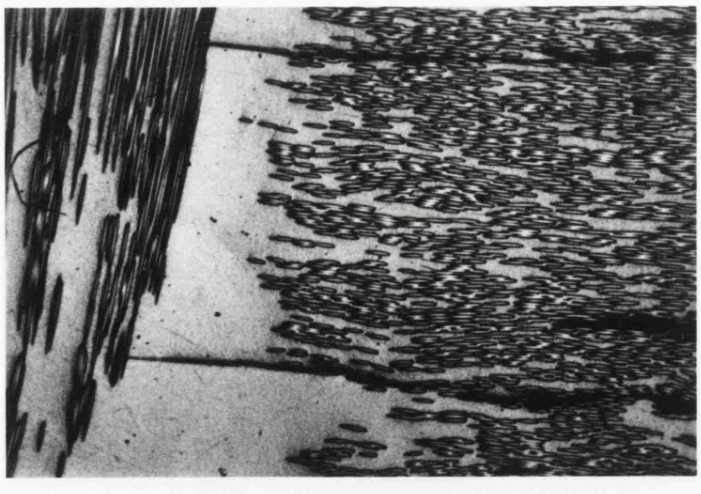

Figure 11.14

Surface section from a sample, loaded to 40% UTUL in water at 23°C showing the transverse crack damage formed during initial loading (x 77).

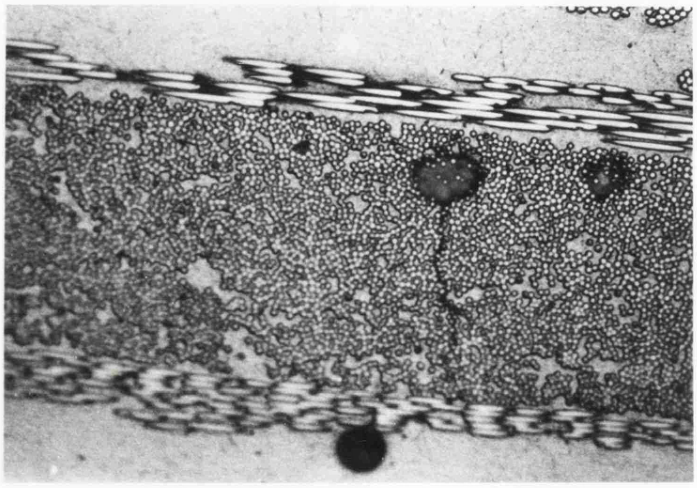

Figure 11.15

Polished section from a sample immersed in water at 23°C for 6 days, showing the onset of moisture induced cracking from internal defects (x 77)

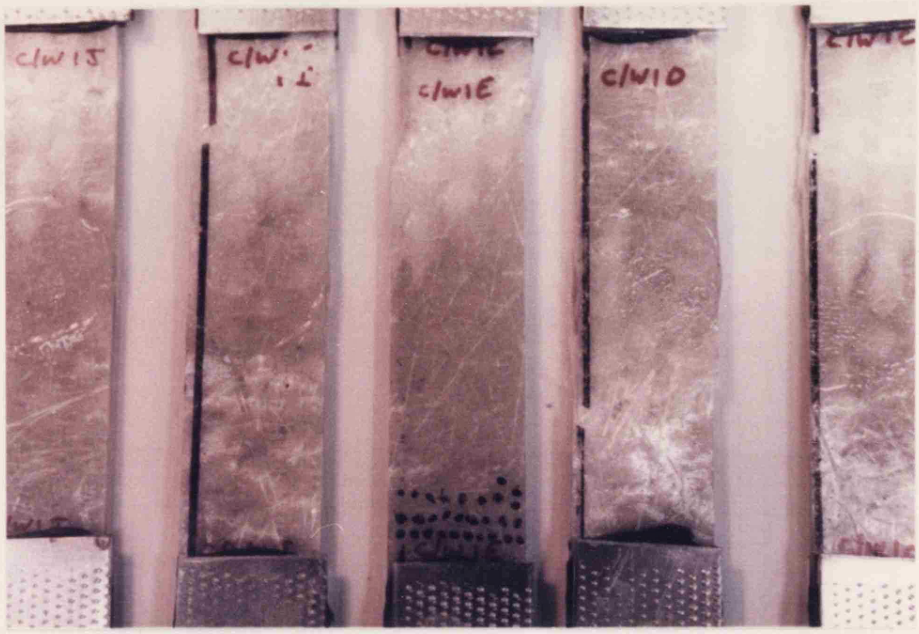

(a)

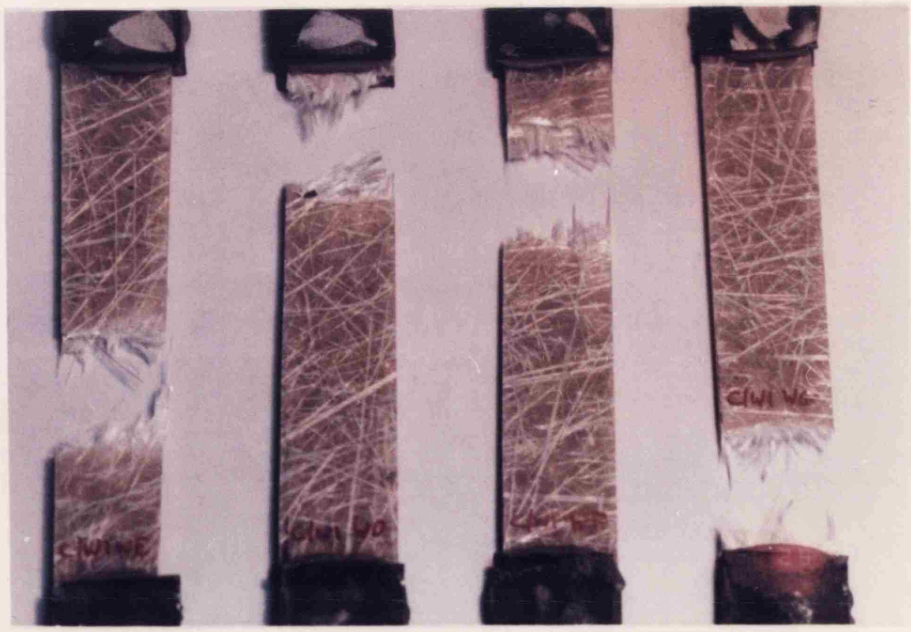

(b)

Figure 11.16

Condition of tensile test coupons from residual strength programmes (a) 'As received' samples (b) Condition of samples after a presoak of 6 months at 60°C.

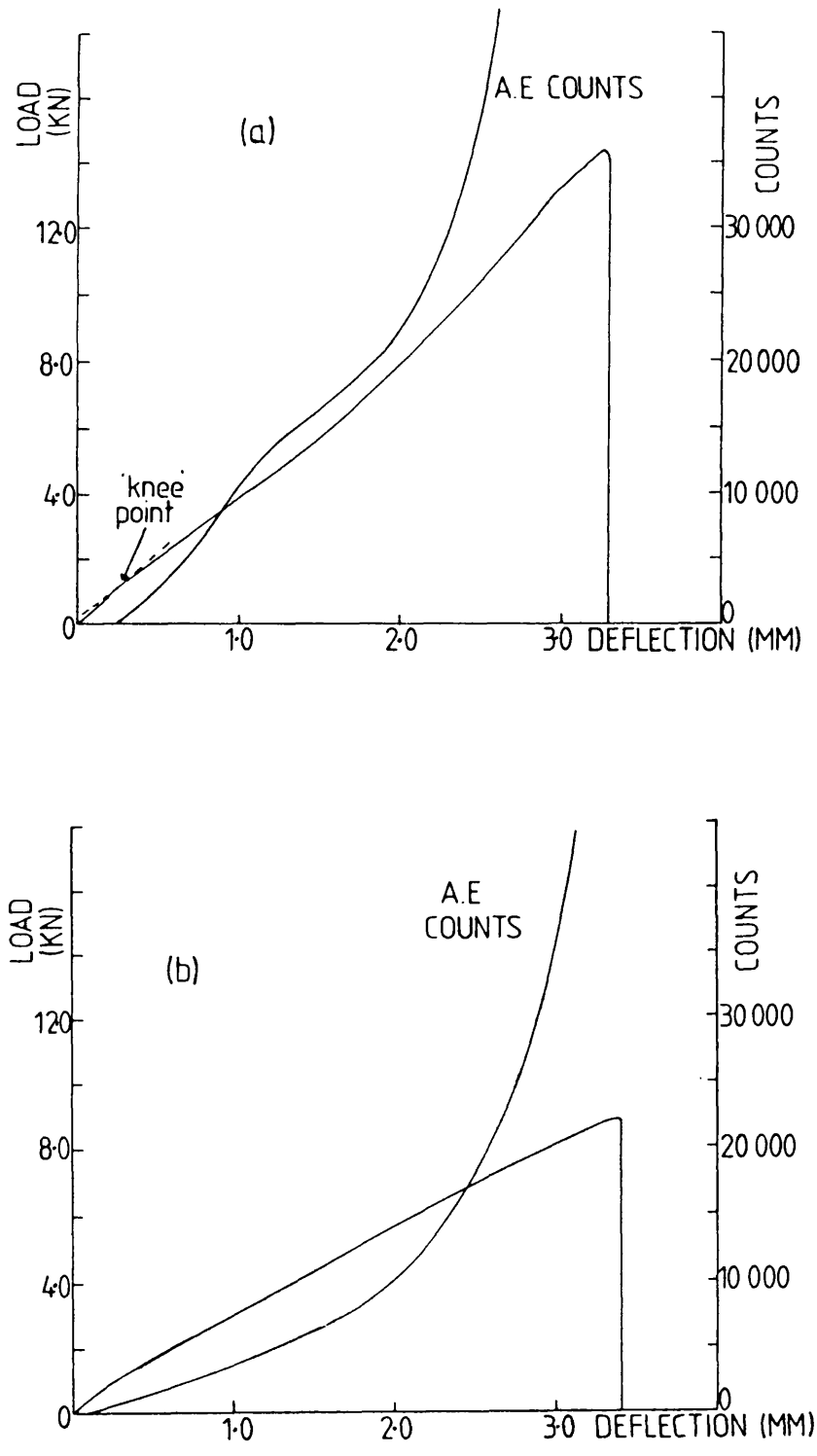

Figure 11.17

Acoustic emission, and load, as a function of sample deflection during residual strength tests (a) 'as received'. (b) Pre-soak at 60°C.

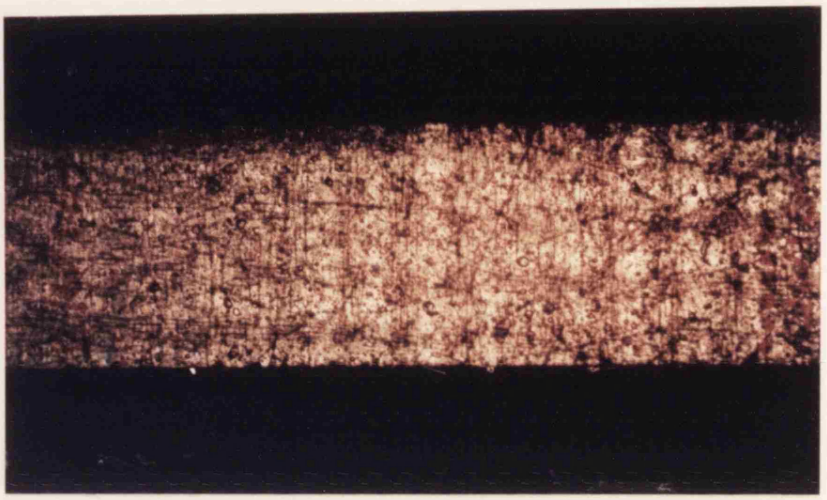

Figure 11.18

Transmitted light photograph of a dry tensile test-piece, loaded to 20% ultimate load, showing the onset of transverse cracking.

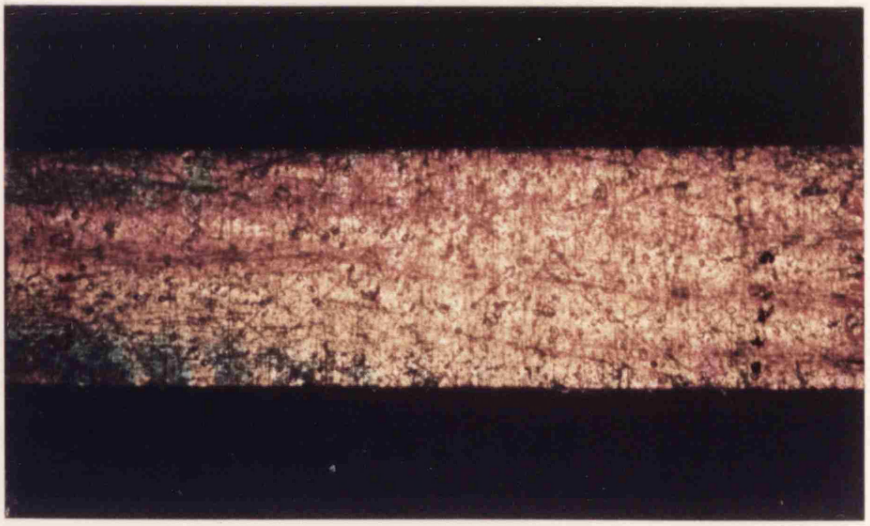

Figure 11.19

Transmitted, cross polarised, light photograph of a dry tensile test coupon loaded to 22%, ultimate load, showing the onset of stress transfer to the outer csm plies.

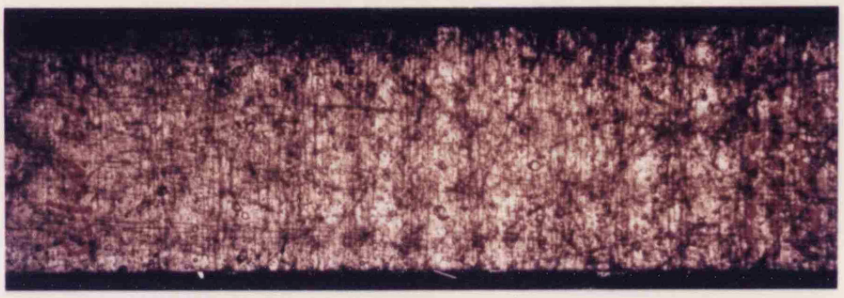

(a)

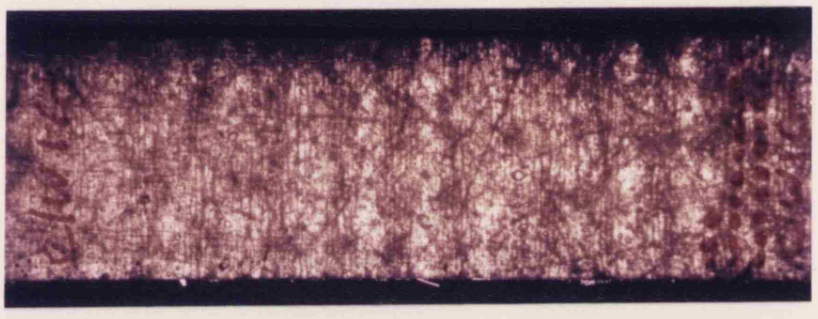

(b)

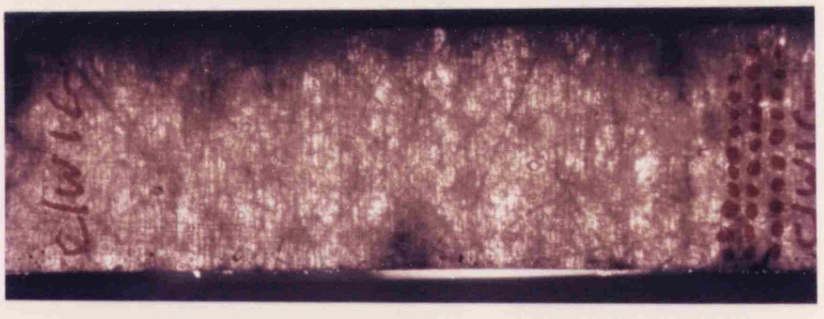

(c)

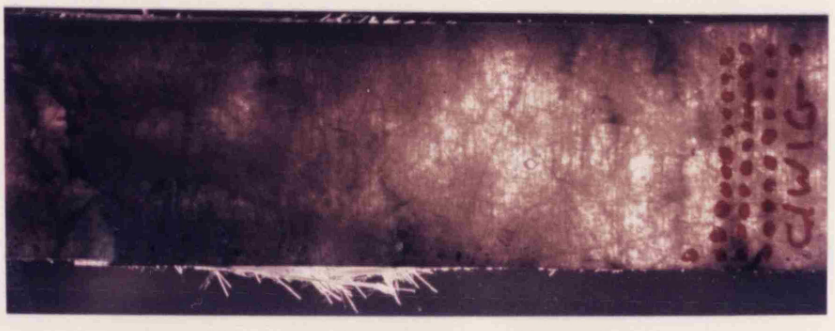

(d)

Figure 11.20

Transmitted light photographs showing the build up of damage in a dry tensile test-piece during loading (a) Load = 50% (b) Load = 70% (c) Load = 90% ultimate (d) Fracture.

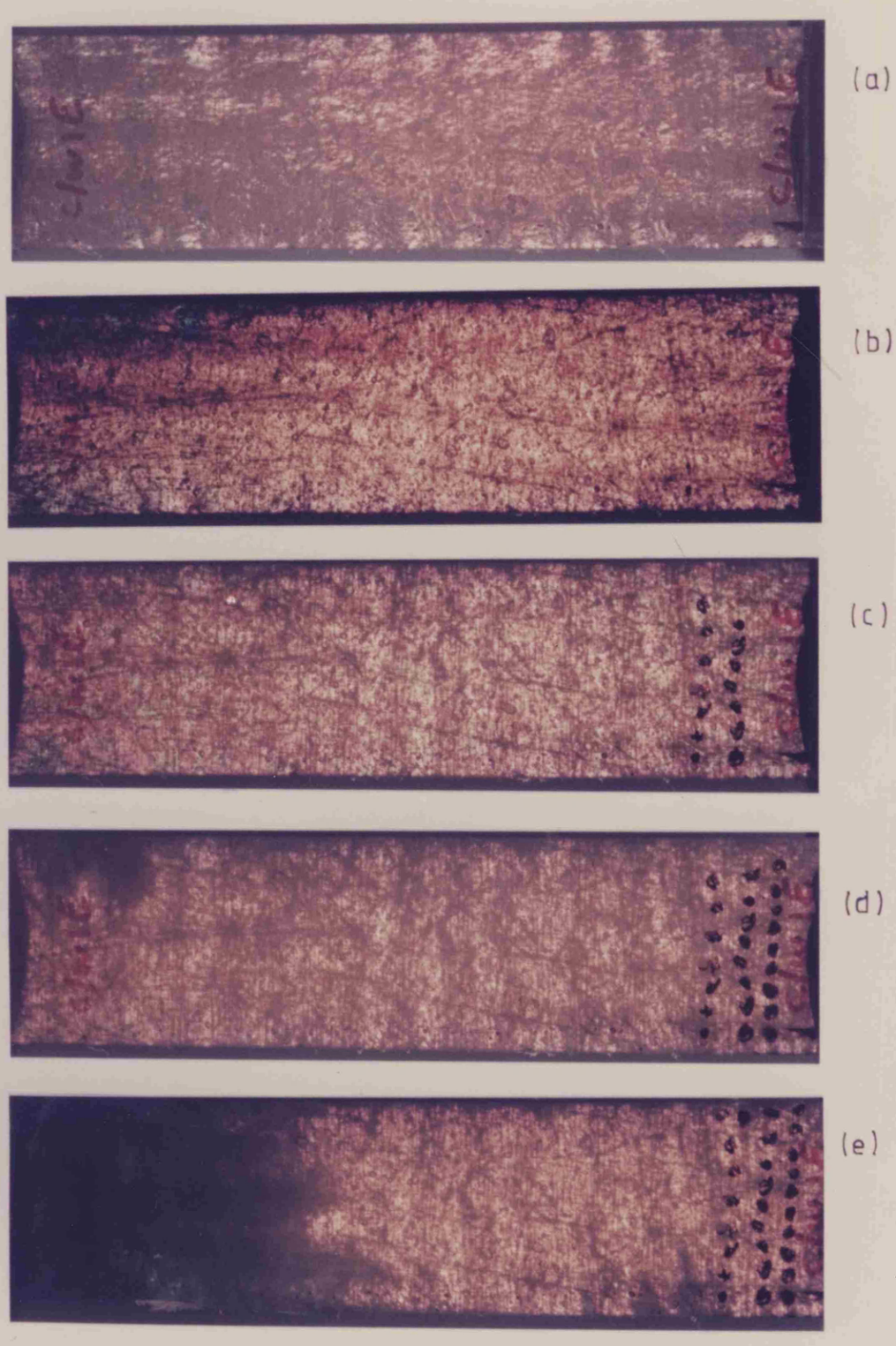

Figure 11.21

Transmitted, cross polarised, light photographs showing damage build up during loading of a dry tensile test coupon. (a) Unloaded (b) Load = 10% (c) Load = 50% (d) Load = 80% ultimate. (e) Fracture.

(a)

(b)

(c)

Figure 11.22

Transmitted, cross polarised, light photographs showing damage build up during loading of a sample presoaked for 6 months at 60°C. (a) Unloaded (b) Load = 95% ultimate (c) Fracture.

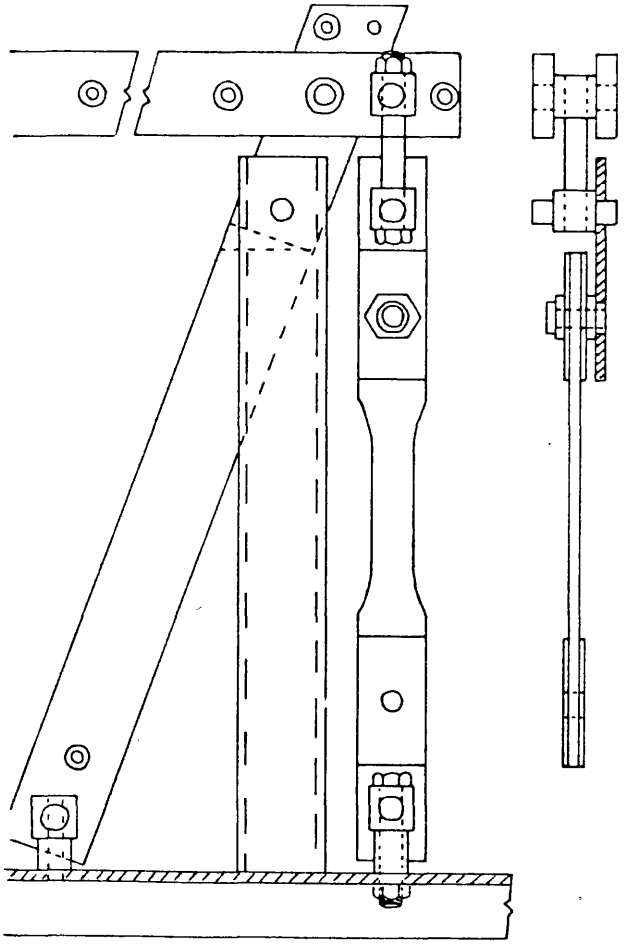

Figure 12.1

View of sample creep loading rig attachments (half size)

Figure 12.2

General view of creep loading rigs

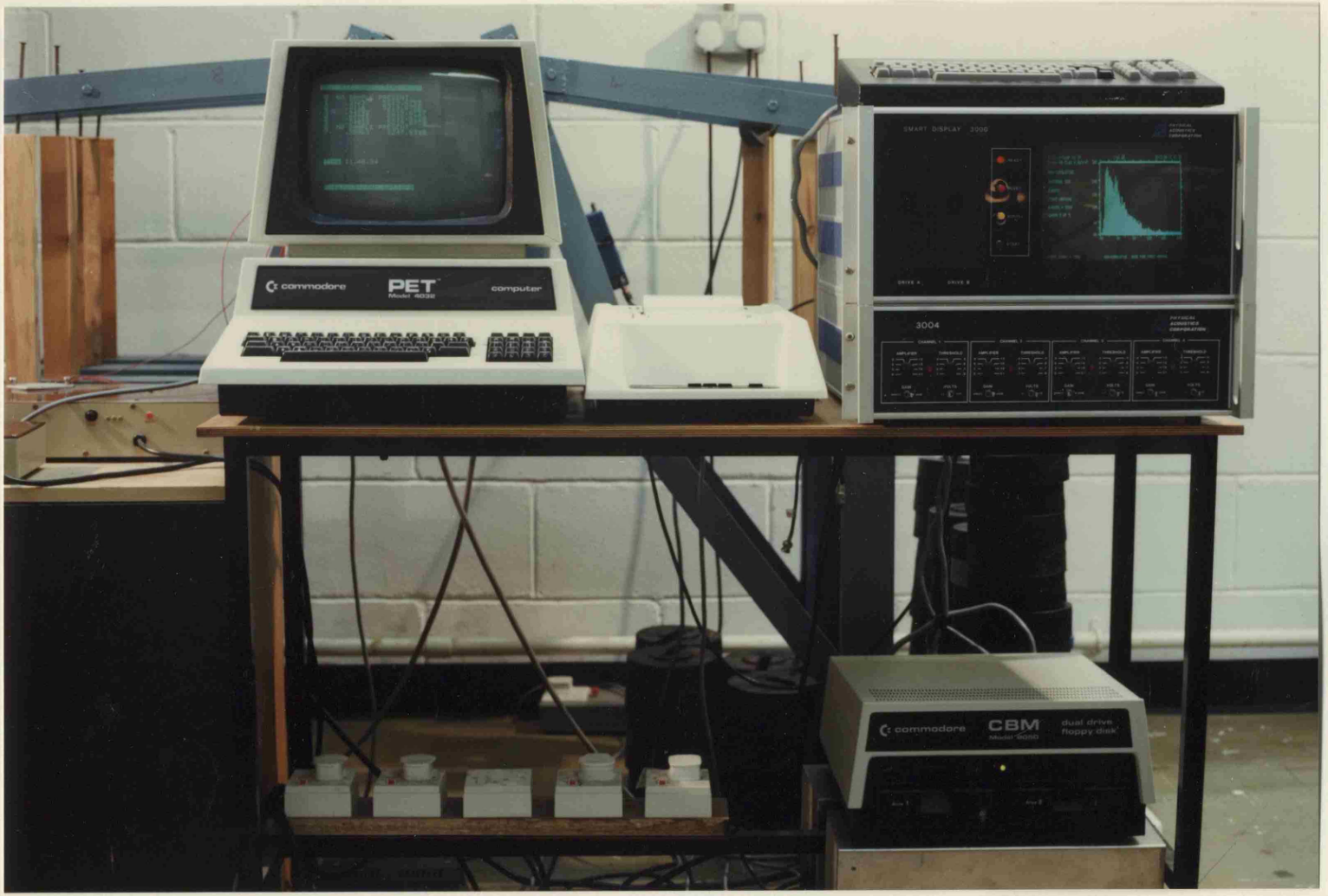

Figure 12.3

Monitoring equipment used during creep tests.

Figure 12.4

Transmitted light photograph of a dry creep specimen, showing transverse crack formation in longitudinal rovings at weave cross-over points.

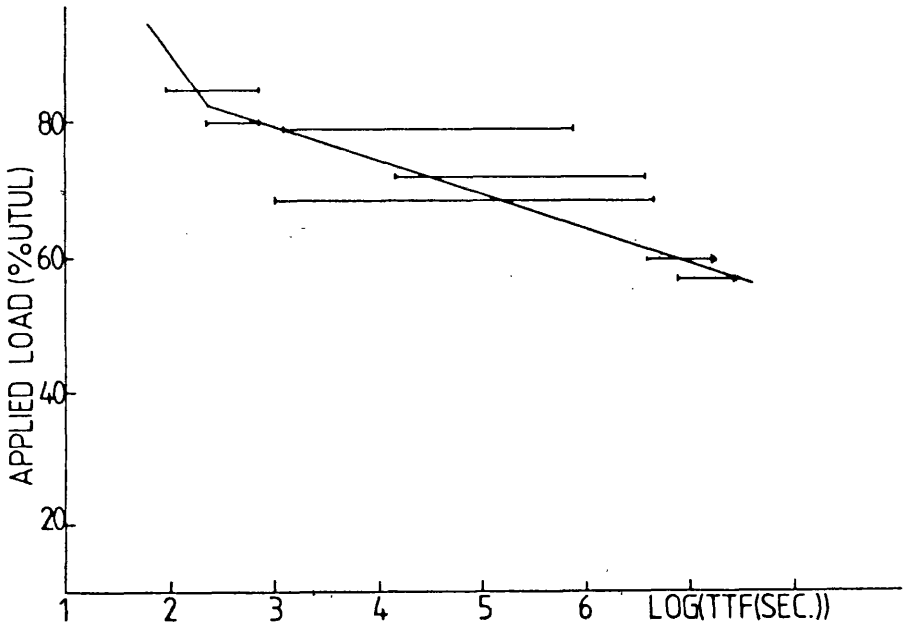

Figure 12.5

Creep-rupture plot for GRP loaded in air. Error bars represent the difference between minimum and maximum values of ttf recorded at each load level.

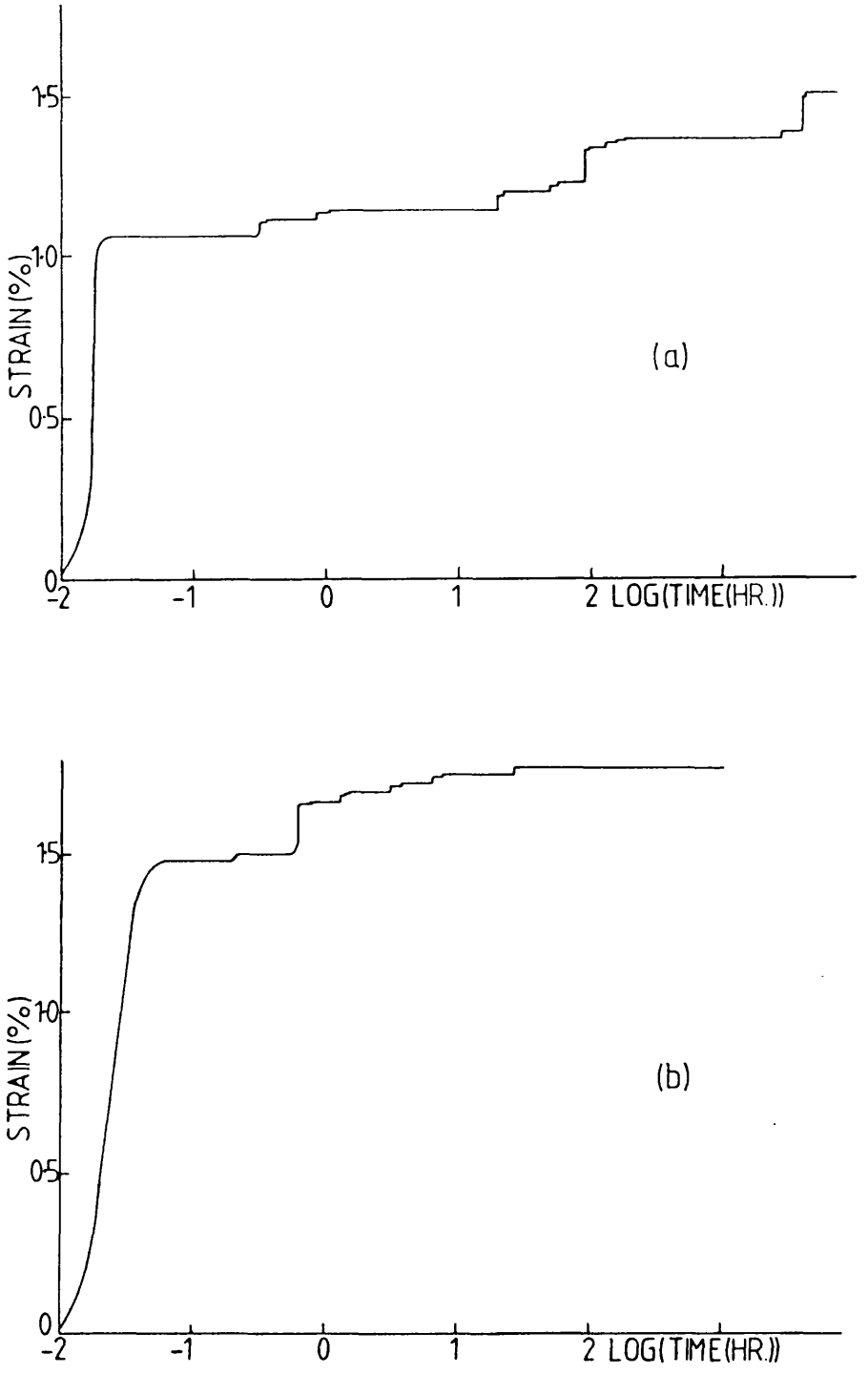

Figure 12.6

Typical creep curves for samples loaded in air at a variety of stress levels: (a) 57% UTUL, (b) 72% UTUL, (c) 79% UTUL (d) 85% UTUL.

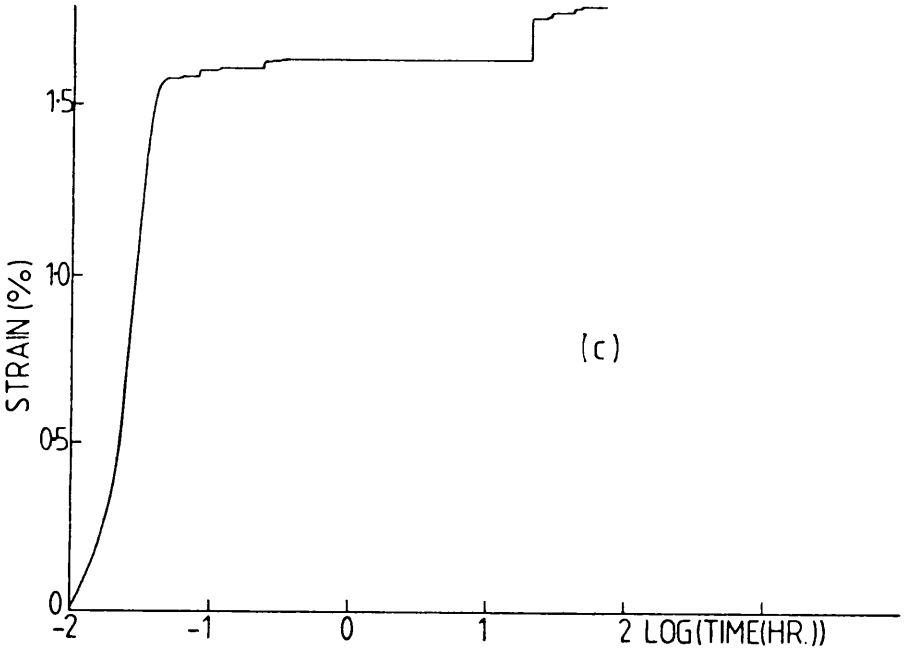
STRAIN (%)
1·5
1·0
0·5
0
-2
-1
0
1
2 LOG(TIME(HR.))
(c)

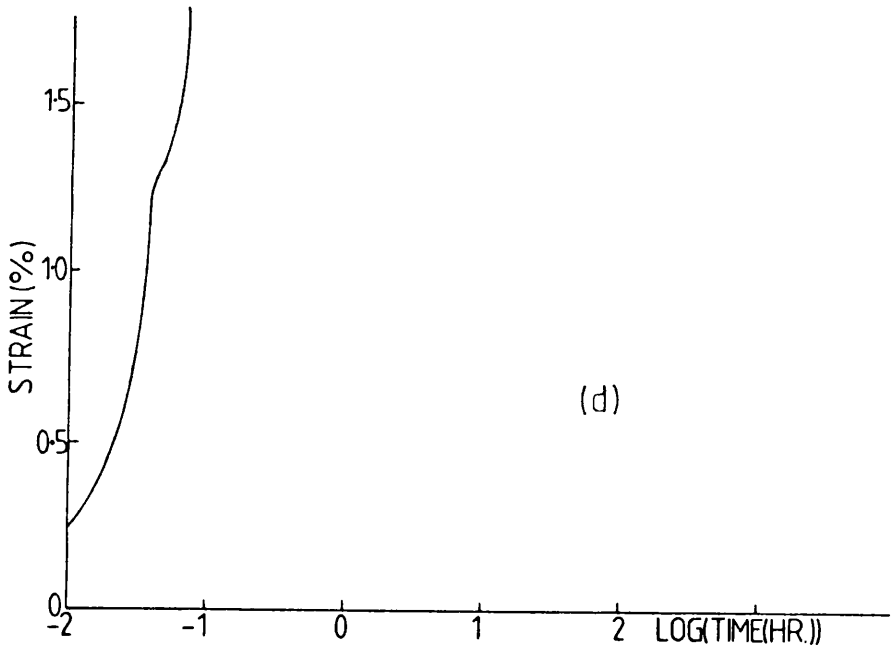
STRAIN (%)
1·5
1·0
0·5
0
-2
-1
0
1
2 LOG(TIME(HR.))
(d)

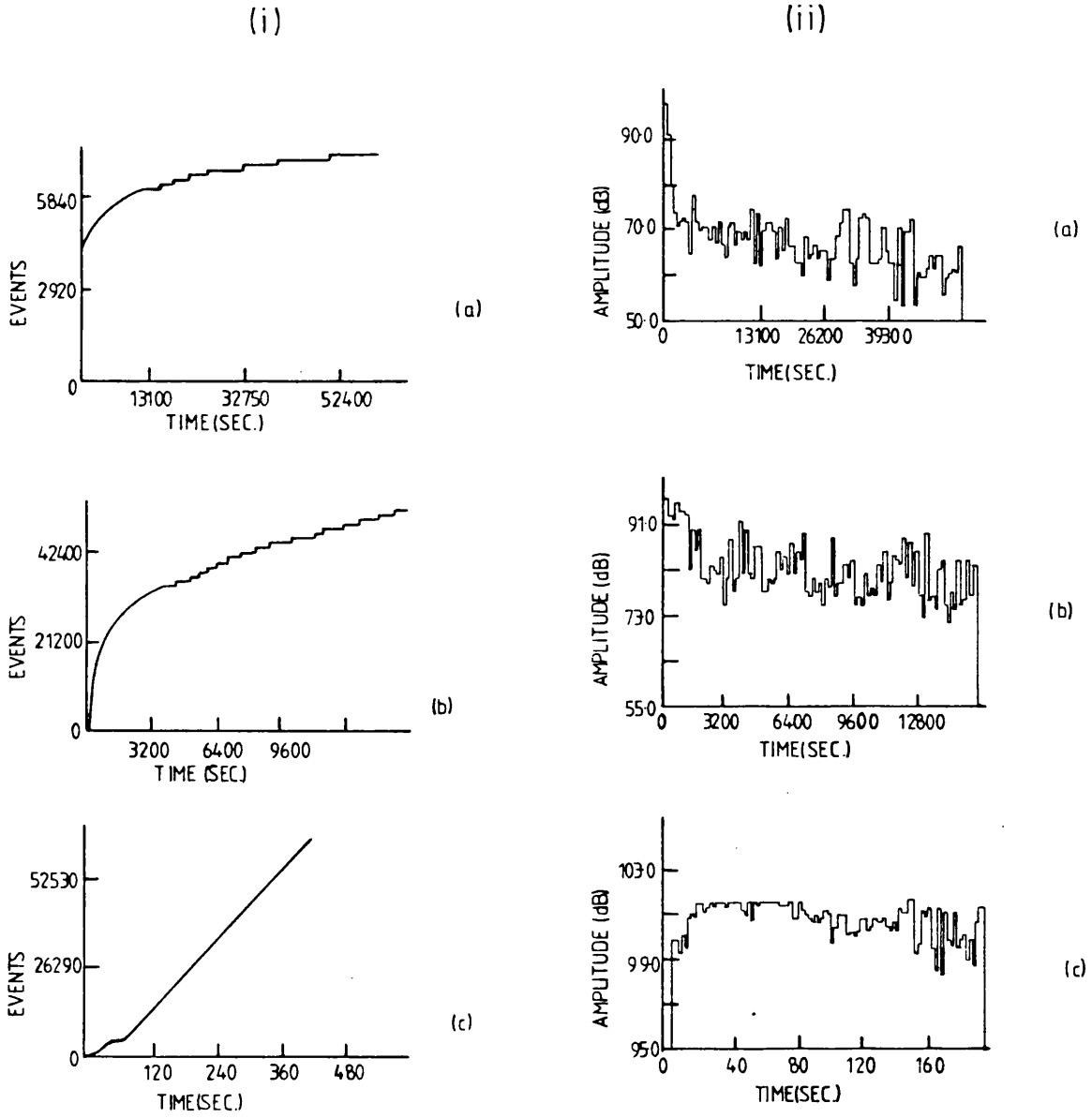

Figure 12.7

Acoustic emission plots for samples loaded in air for creep measurements. Two parameters are shown; (i) Events vs. time and (ii) Amplitude vs. time. Three typical lead levels are presented; (a) 60% UTUL, (b) 72% UTUL, and (c) 85% UTUL.

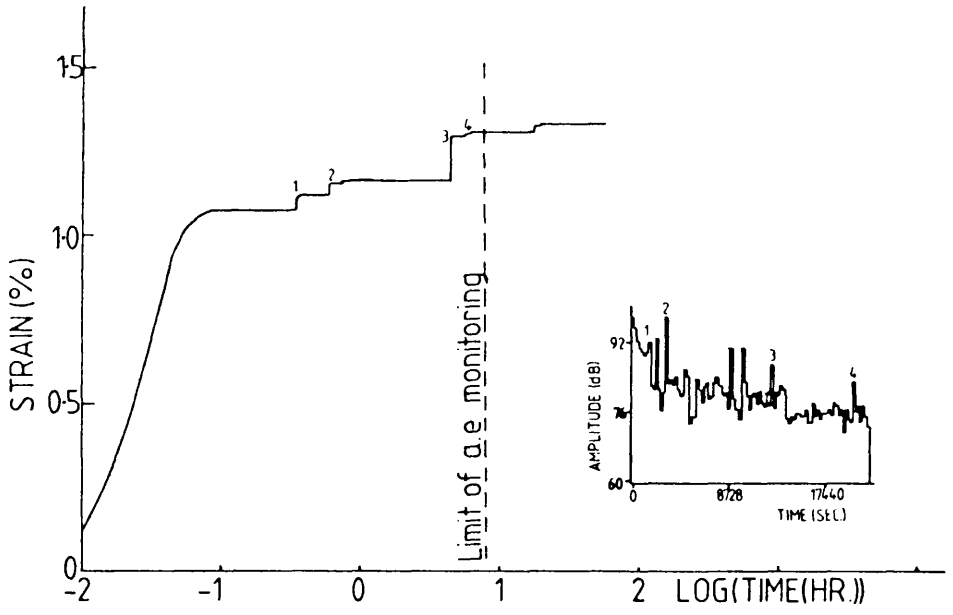

Figure 12.8.

Correlation between acoustic signal amplitude peaks, and secondary creep strain jumps, for a dry creep test.

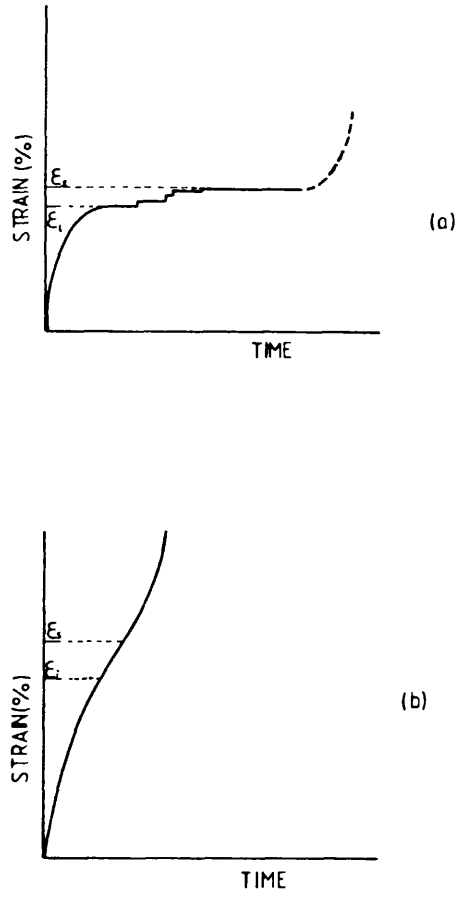

Figure 12.9

Definitions of creep strain parameters used for failure prediction. (a) below 80% UTUL (b) above 80% UTUL.

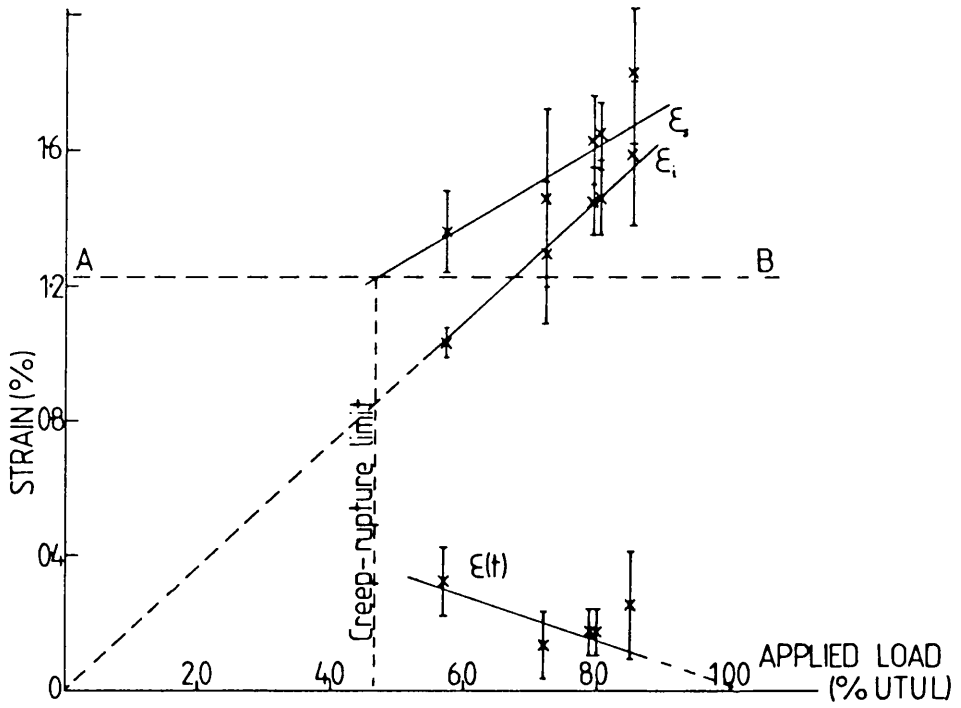

Figure 12.10

Maximum initial (ε_i), maximum secondary (ε_s), and total ($\pm\varepsilon(t)$, creep strains vs. applied load for samples tested in air. Error bars are $\pm$ 1 S.D. from a mean of 4 samples.

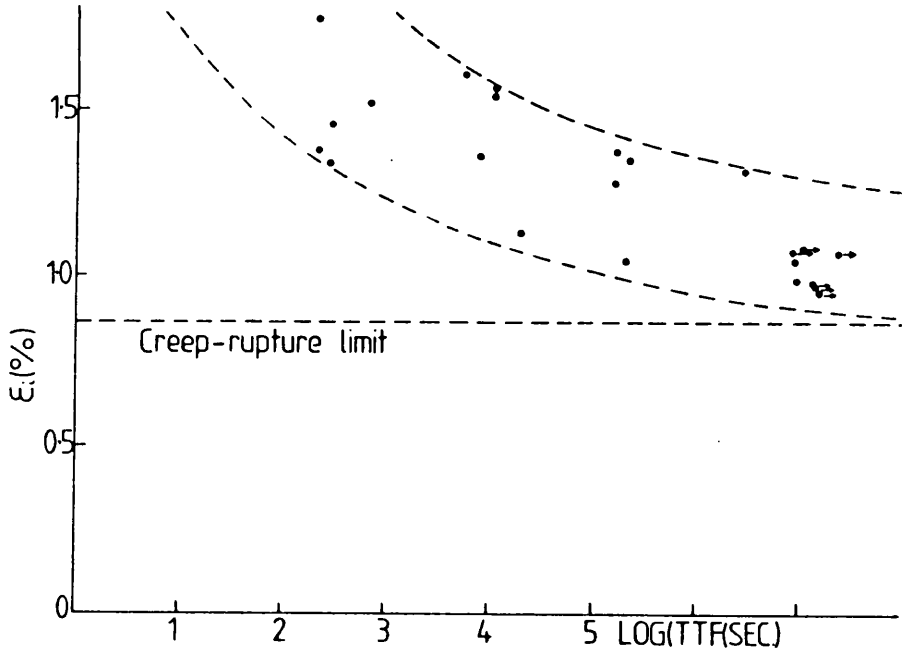

Figure 12.11

Maximum initial strain against time to failure for samples loaded to creep-rupture in air.

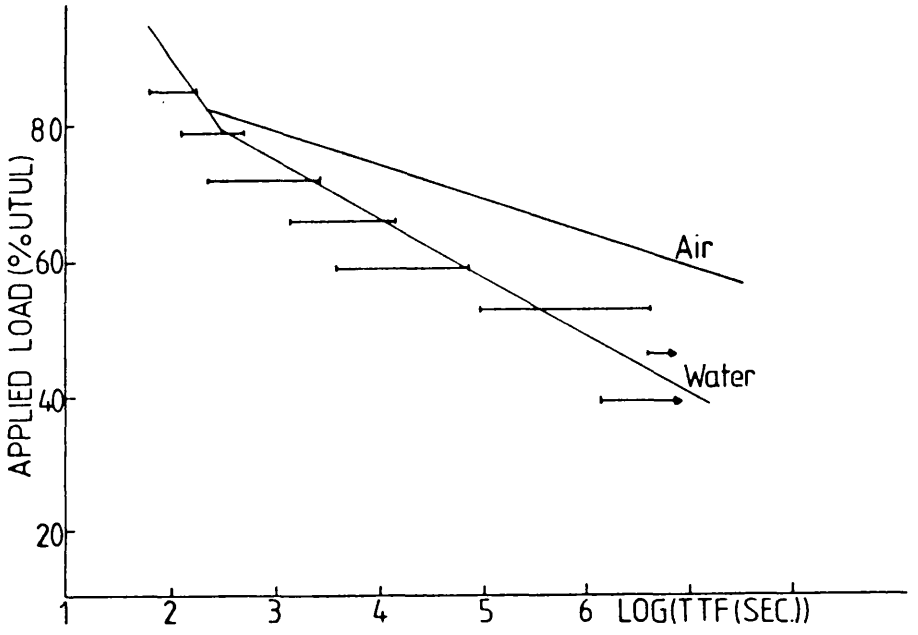

Figure 12. 12

Comparison of creep-rupture plots from immersed and dry creep test programmes.

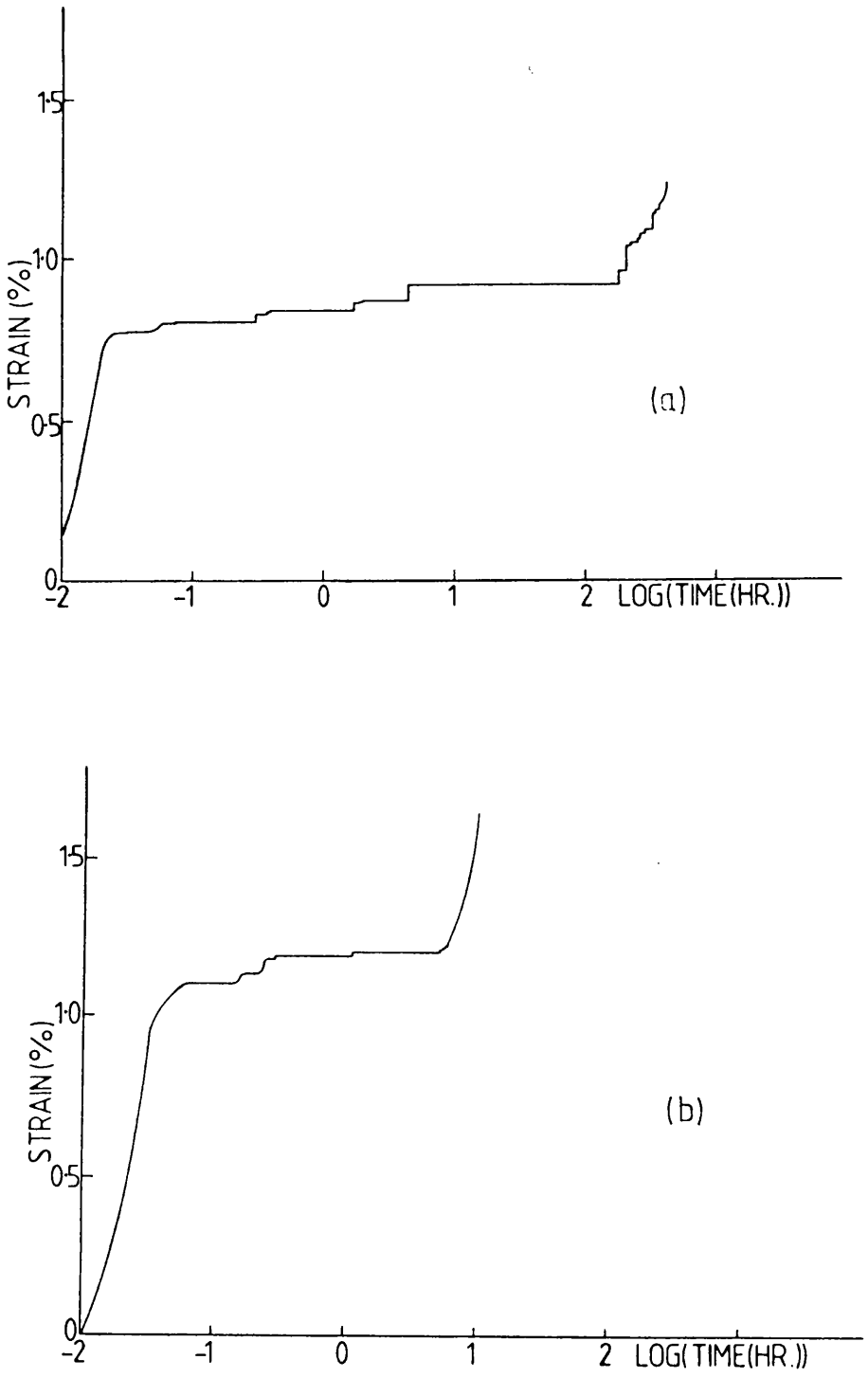

Figure 12.13

Typical creep curves from samples loaded in water at a variety of stress levels (a) 39% UTUL (b) 53% UTUL (c) 66% UTUL (d) 85% UTUL.

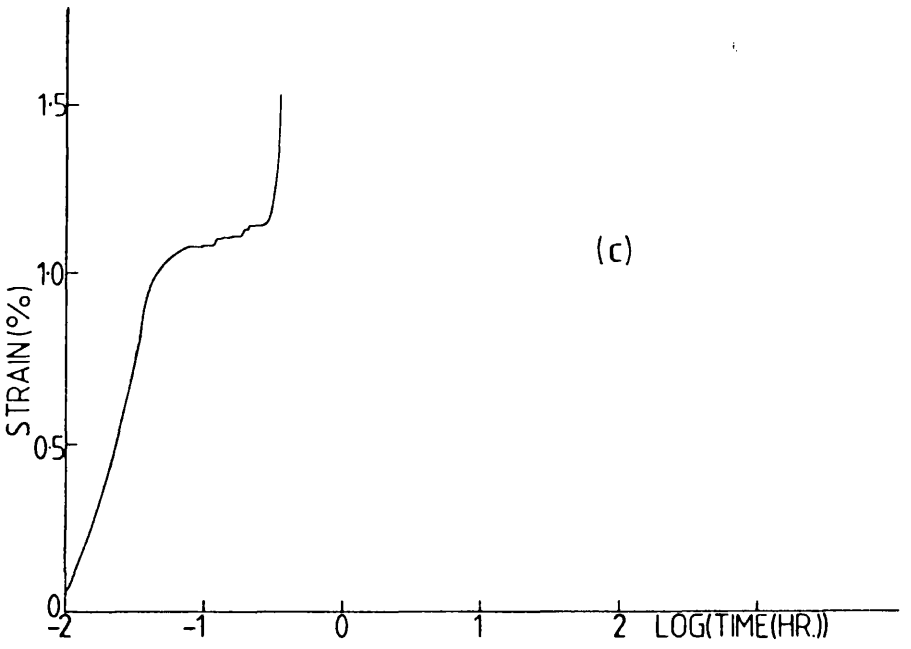
1·5
1·0
0·5
0
STRAIN(%)
-2
-1
0
1
2
LOG(TIME(HR.))

(c)

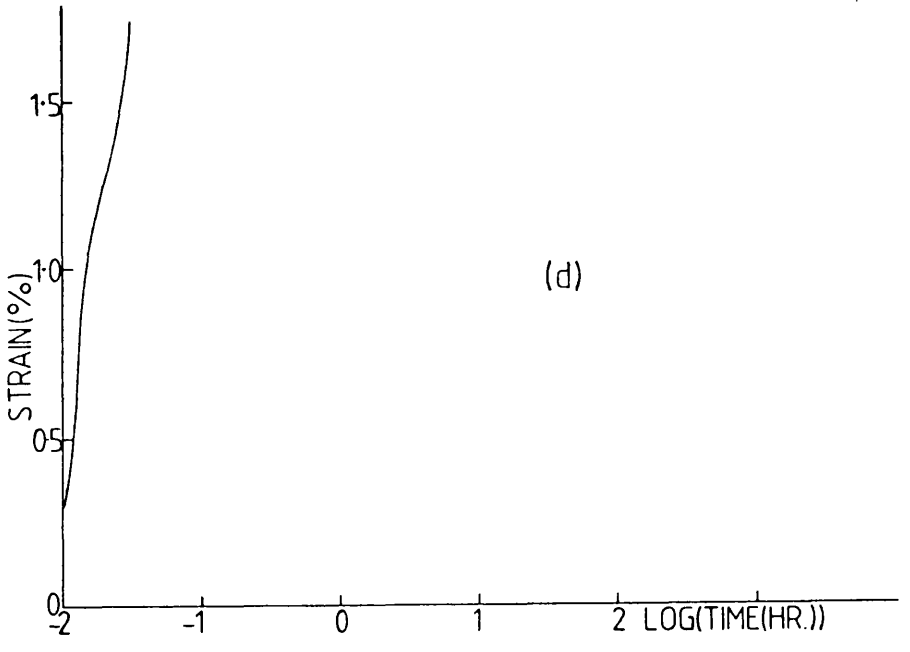
1·5
1·0
0·5
0
STRAIN(%)
-2
-1
0
1
2 LOG(TIME(HR.))

(d)

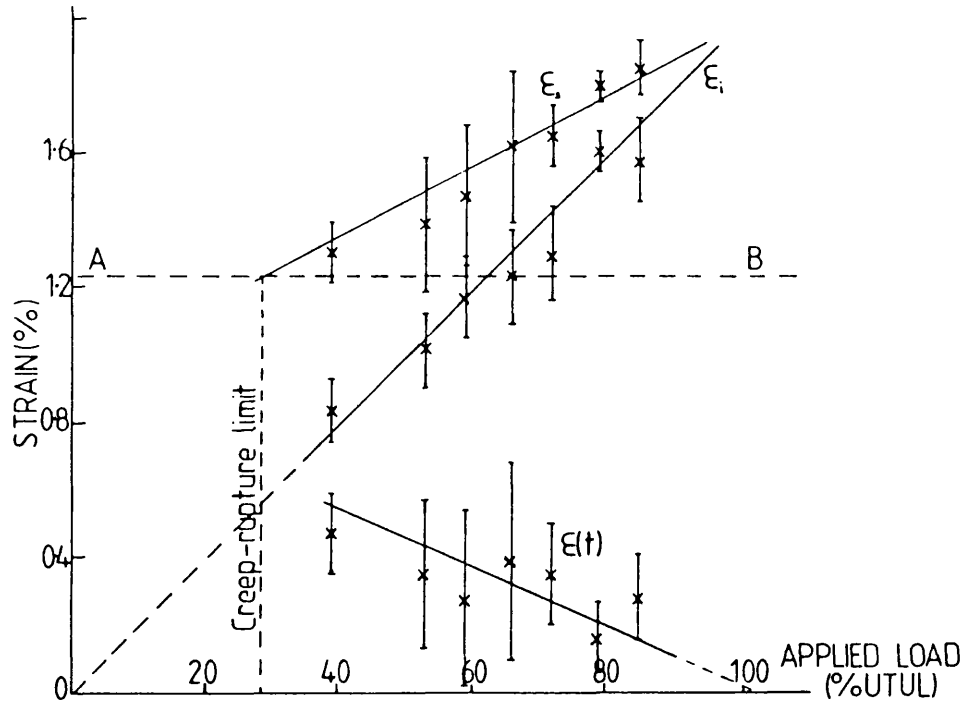

Figure 12.14

Maximum initial, maximum secondary, and total, creep strains vs. applied load for samples tested in water at 23°C. Error bars are ± 1 S.D. from a mean of 4 samples.

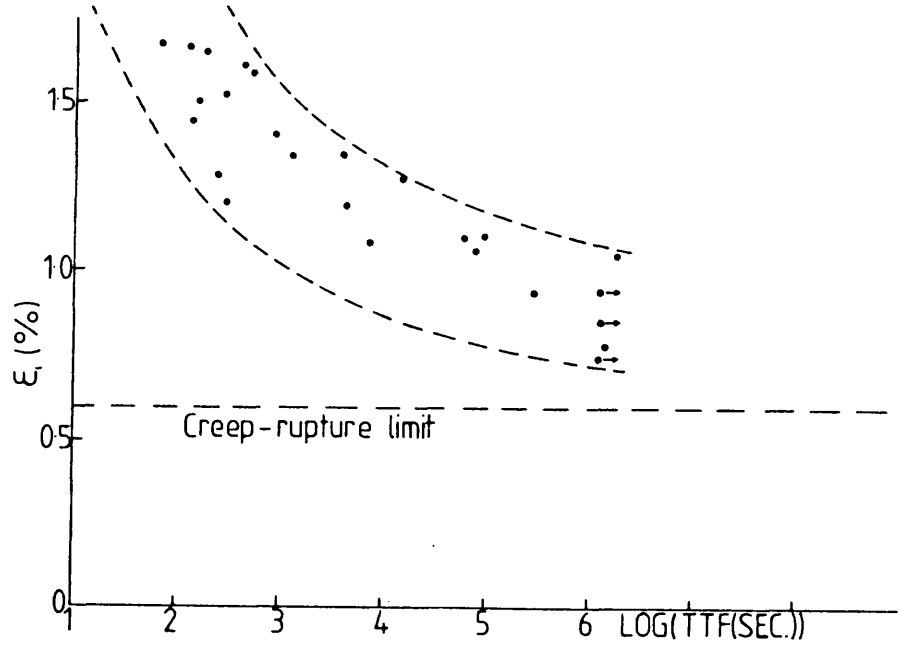

Figure 12.15

Maximum initial strain against time to failure for samples loaded to creep-rupture in water at 23°C.

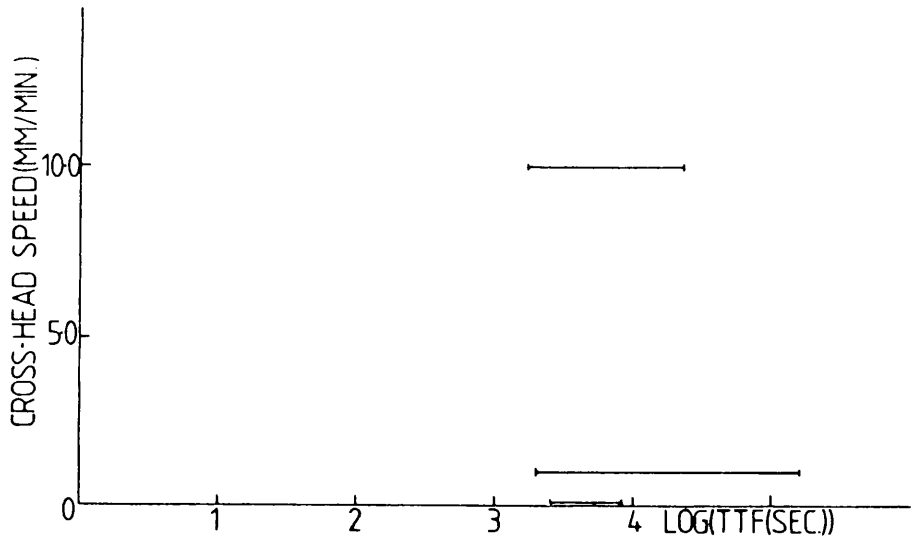

Figure 12.16

Initial loading rate against time to failure for creep tests in air at a load level of 80% UTUL.

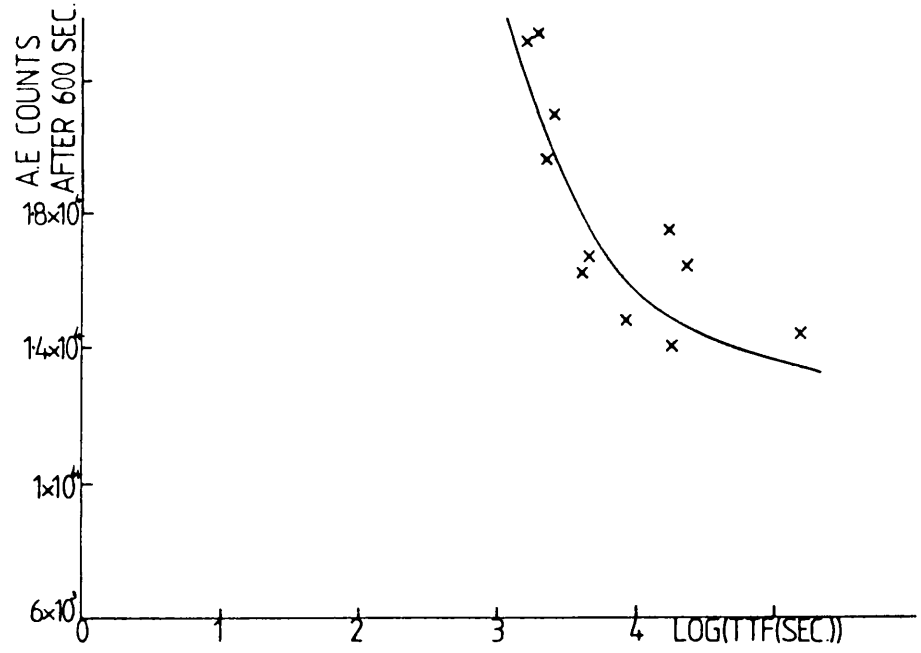

Figure 12.17

Initial acoustic activity vs. time to failure, for creep loading rate tests.

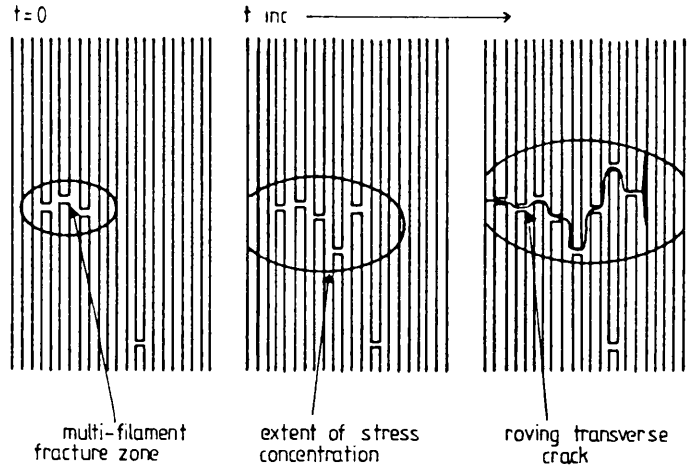

Figure 15.1

Schematic representation of the growth of multi-filament fracture zones during creep.

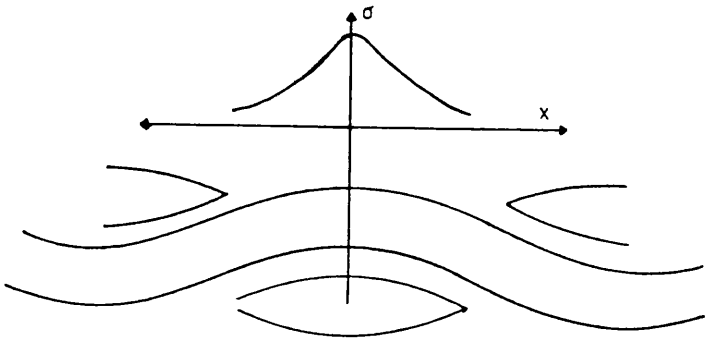

Figure 15.2

Schematic representation of fibre stress levels in a longitudinal woven roving in the cross-over region.

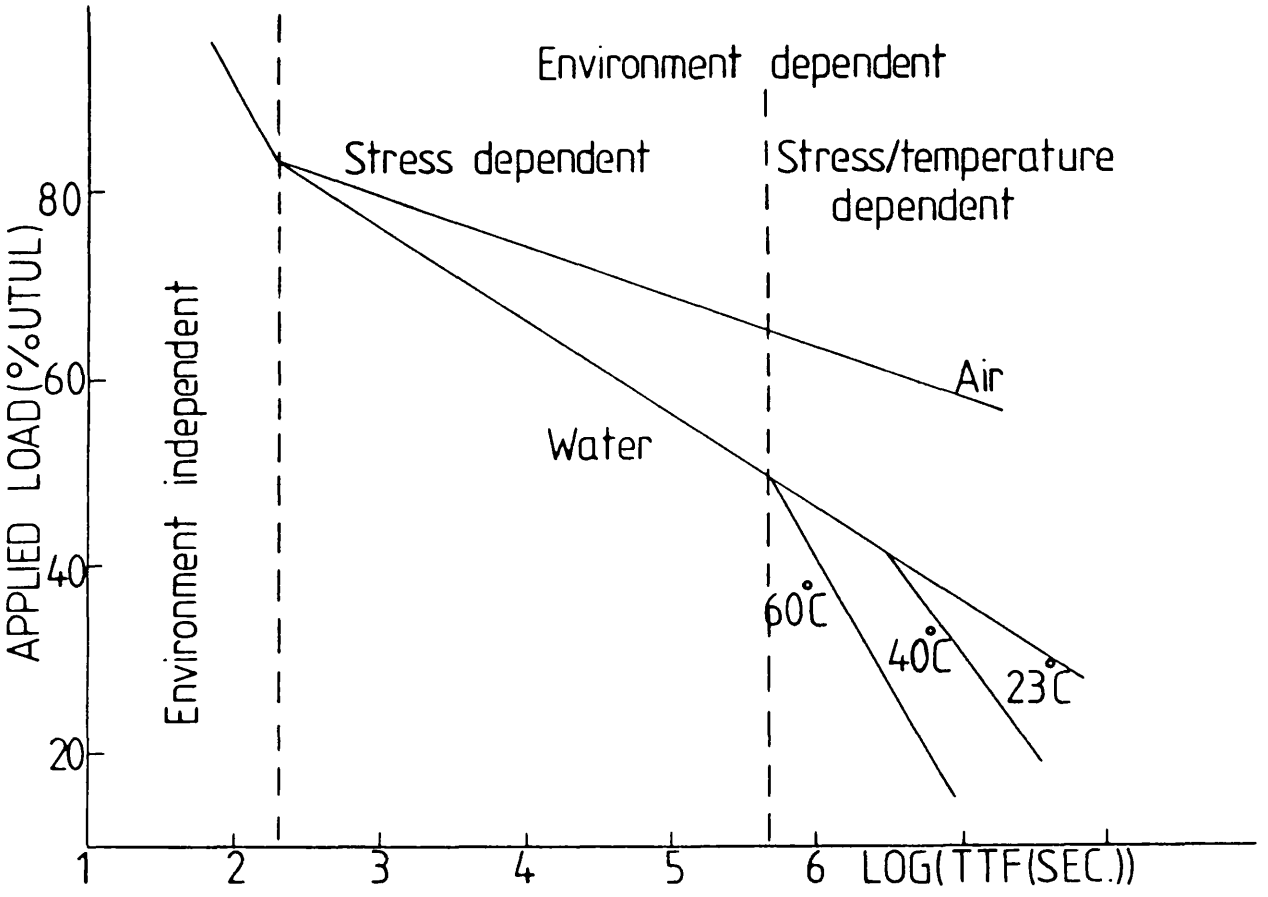

Figure 15.3

Creep-rupture plots showing the changes in creep behaviour that occur as the applied load varies.